THE UNIVERSITY OF QUEENSLAND

AUSTRALIA

The geometry, kinematics, and reactivation history of major fault systems in eastern Australia: Implications for deformation phases from the Permian to Cenozoic

Abbas Babaahmadi

MSc

A thesis submitted for the degree of Doctor of Philosophy at

The University of Queensland in 2015

School of Earth Sciences

Abstract

Eastern Australia has been affected by numerous fault systems, but their pattern, geometry, kinematics, and timing have hitherto remained relatively understudied. This thesis makes an effort to address this issue by investigating fault systems and their reactivation history. The results of this thesis shed new light on the tectonic history of eastern Australia since the Permian. The aim of this work is to unravel the role of major faults in the tectonic evolution of eastern Australia by studying geometry and kinematics of fault systems during the early Permian, Triassic to Jurassic, and late Mesozoic to Cenozoic.

The role of fault systems in the formation of the Texas and Coffs-Harbour oroclines in the southern New England Orogen has been studied. The results show that layer-parallel faults with a main strike-slip component occur parallel to the curved structure of the Texas and Coffs-Harbour oroclines. It indicates that a flexural slip mechanism may have operated during oroclinal bending in the early-mid Permian. The orocline-parallel faults were reactivated during the Mesozoic and Cenozoic, as indicated by the recognition of displaced Triassic granitoids, Mesozoic and Cenozoic sedimentary rocks, and Cenozoic basalts.

Structural analysis was conducted on faults in the Triassic-Jurassic sedimentary basins of eastern Australia. The results show that the intermittent phases of rifting events occurred during the Triassic. The early stage syn-sedimentary normal faults in the Nymboida Coal Measures suggest a rifting phase in the Early-Middle Triassic. This phase of rifting was followed by a contractional event that resulted in tilting, folding, and thrust faulting. Moreover, evidence of syn-sedimentary normal faults and bimodal volcanism during the early Late Triassic is indicative of another rifting phase, resulting in the development of the Ipswich Basin. The alternating episodes of rifting and contraction during the Triassic were possibly controlled by plate boundary migration and switches between trench retreat and advance.

The N-striking strike-slip Demon Fault is recognised as four steeply-dipping reverse dextral segments. It is interpreted to be a post-Late Triassic fault because it has displaced some Triassic NW-striking faults and Early to Late Triassic magmatic rocks. The amount of dextral offset along the different parts of the Demon Fault is decreased towards the south. The major activity of the Demon Fault is construed to have occurred contemporaneously with the development of the Clarence-Moreton Basin in the Jurassic. The recent reverse dextral activity of the Demon Fault could have possibly been related to either a mid-Cretaceous contractional deformation or Cenozoic deformation associated with collisional processes at the northern boundary of the Australian plate.

The NNW-striking North Pine Fault System (NPFS) has been studied. The NPFS has undergone sinistral reverse strike-slip movement with offsets ranging from ~3.4 to ~8.2 km. Based on a Triassic

granophyre dyke parallel to the southeastern NPFS, and the contribution of parallel NNW-striking strike-slip and normal faults in the development of the Late Triassic-Early Cretaceous Maryborough Basin, the NPFS has likely been active during the Mesozoic. The NPFS is interpreted to have been reactivated with oblique sinistral-normal kinematics during the Late Cretaceous-early Eocene in response to regional oblique extension associated with the opening of the Tasman and Coral seas. The recent strike-slip reverse movement was likely due to far-field contractional stresses from collisional tectonics at the eastern and northern boundaries of the Australian plate in the Cenozoic.

New evidence shows that numerous strike-slip faults with a reverse component have displaced Cenozoic volcanic rocks, ranging in ages from ~ 31 to ~21 Ma, in southeast Queensland. These ages point out that faulting must have occurred after the late Oligocene. The reactivation of major faults resulted in the occurrence of brittle subsidiary faults in Cenozoic volcanic rocks. Intraplate transpressional deformation resulted from far-field stresses transmitted from the collisional zones at the northeast and southeast boundaries of the Australian plate since the late Oligocene.

In summary, results of this thesis highlight the role of fault systems in the deformation of eastern Australia from the Permian to late Cenozoic. Layer-parallel faults around the Texas and Coffs-Harbour oroclines reflects a possible role of flexural slip mechanism during oroclinal bending in the early-mid Permian. Faults have intermittently been reactivated during the Mesozoic to early Cenozoic oblique extensional phases. The reactivation of faults has also occurred during the late Cenozoic in response to far-field stresses transmitted from the Australian plate boundaries.

Declaration by author

This thesis is composed of my original work, and contains no material previously published or written by another person except where due reference has been made in the text. I have clearly stated the contribution by others to jointly-authored works that I have included in my thesis.

I have clearly stated the contribution of others to my thesis as a whole, including statistical assistance, survey design, data analysis, significant technical procedures, professional editorial advice, and any other original research work used or reported in my thesis. The content of my thesis is the result of work I have carried out since the commencement of my research higher degree candidature and does not include a substantial part of work that has been submitted to qualify for the award of any other degree or diploma in any university or other tertiary institution. I have clearly stated which parts of my thesis, if any, have been submitted to qualify for another award.

I acknowledge that an electronic copy of my thesis must be lodged with the University Library and, subject to the policy and procedures of The University of Queensland, the thesis be made available for research and study in accordance with the Copyright Act 1968 unless a period of embargo has been approved by the Dean of the Graduate School.

I acknowledge that copyright of all material contained in my thesis resides with the copyright holder(s) of that material. Where appropriate I have obtained copyright permission from the copyright holder to reproduce material in this thesis.

Publications during candidature

Babaahmadi, A., Rosenbaum, G., 2015. Kinematics of orocline-parallel faults in the Texas and Coffs-Harbour oroclines (eastern Australia) and the possible role of flexural slip during oroclinal bending. Under review in Australian Journal of Earth Sciences.

Babaahmadi, A., Rosenbaum, G., Esterle, J., 2015. Alternating episodes of extension and contraction during the Triassic: Evidence from Mesozoic sedimentary basins in eastern Australia. Australian Journal of Earth Sciences, 62/5; DOI:10.1080/08120099.2015.1057864.

Babaahmadi, A., Rosenbaum, G. 2014. Late Cenozoic intraplate faulting in eastern Australia. Journal of Structural Geology, 69A, 59-74.

Babaahmadi, A., Rosenbaum, G. 2014. Late Mesozoic and Cenozoic wrench tectonics in eastern Australia: Insights from the North Pine Fault System (southeast Queensland). Journal of Geodynamics, 73, 83-99.

Babaahmadi, A., Rosenbaum, G. 2013. Kinematics of the Demon Fault: Implications for Mesozoic strike-slip faulting in eastern Australia. Australian Journal of Earth Sciences, 60, 255-269.

Publications included in this thesis

Babaahmadi, A., Rosenbaum, G., 2015. Kinematics of orocline-parallel faults in the Texas and Coffs-Harbour oroclines (eastern Australia) and the possible role of flexural slip during oroclinal bending. Under review in Australian Journal of Earth Sciences (Chapter 2).

Babaahmadi conducted the interpretation of pattern and kinematics of faults around the New England Oroclines. He wrote the paper and discussed the development of oroclines in the context of flexural slip mechanism during the early-mid Permian and the reactivation history of faults. Rosenbaum edited the paper and commented on the structural and tectonic models.

Babaahmadi, A., Rosenbaum, G., Esterle, J., 2015. Alternating episodes of extension and contraction during the Triassic: Evidence from Mesozoic sedimentary basins in eastern Australia. Australian Journal of Earth Sciences, 62/5; DOI:10.1080/08120099.2015.1057864 (Chapter 3).

Babaahmadi conducted the structural analysis of fault systems and wrote the paper and discussed the development of faults in Mesozoic basins and provided a tectonic model. Rosenbaum edited the

paper and commented on the structural and tectonic models. Esterle contributed in providing different seismic and well datasets and editing the paper. The earlier version of the paper benefited from comments by reviewers, Renate Sliwa and Chris Fergusson.

Babaahmadi, A., Rosenbaum, G. 2013. Kinematics of the Demon Fault: Implications for Mesozoic strike-slip faulting in eastern Australia. Australian Journal of Earth Sciences, 60, 255–269 (Chapter 4).

Babaahmadi conducted the field work and the interpretation of gridded aeromagnetic data in order to structural analysis of the Demon Fault and wrote the paper and discussed strike-slip faulting in the Mesozoic. Rosenbaum edited the paper and commented on the discussion. The earlier version of the paper benefited from comments by reviewers Russell Korsch and Dick Glen.

Babaahmadi, A., Rosenbaum, G. 2014. Late Mesozoic and Cenozoic wrench tectonics in eastern Australia: Insights from the North Pine Fault System (southeast Queensland). Journal of Geodynamics, 73, 83-99 (Chapter 5).

Babaahmadi conducted the field work and the interpretation of gridded aeromagnetic data in order to structural analysis of different segments of the North Pine Fault System (NPFS). He wrote the paper and discussed wrench tectonics in the late Mesozoic and Cenozoic. Rosenbaum edited the paper and commented on the structural and tectonic models. The earlier version of the paper benefited from comments by anonymous reviewers.

Babaahmadi, A., Rosenbaum, G. 2014. Late Cenozoic intraplate faulting in eastern Australia. Journal of Structural Geology, 69A, 59-74 (Chapter 6).

Babaahmadi conducted the field work and the interpretation of gridded aeromagnetic data in order to recognise faults in Cenozoic volcanic rocks. He wrote the paper and discussed possible tectonic origins of late Cenozoic faulting in eastern Australia. Rosenbaum edited the paper and commented on the structural and tectonic models. The earlier version of the paper benefited from comments by reviewers, Chris Fergusson and Rod Holcombe.

Contributions by others to the thesis

A/Professor Gideon Rosenbaum was the principal advisor of the project. He designed the thesis structure and edited and commented the thesis chapters.

Professor Joan Esterle was the associate advisor of the project. She provided different required datasets and software, and contributed in the conception and design of the chapter 3.

Statement of parts of the thesis submitted to qualify for the award of another degree

None

Acknowledgements

I would like to express my special appreciation to my principal supervisor A/Professor Gideon Rosenbaum who designed the project and helped me for being a successful researcher. His support has been priceless. I would like to thank deeply my associate supervisor Professor Joan Esterle for her invaluable support.

I would like to express gratitude to Professor Gregg Webb, RHD coordinator of the School of Earth Sciences for his advices. I want to thank Pamela Cooper, Tracy Paroz, Ashleigh Paroz, Frank Audsley, David McCarthy, Dario Hogg, Hannah Hartig, and Gerald Hertig for their help and support. I would like to acknowledge Dr Arne Scherrenberg, Scott Lyon, and Daniel Ashton for their kindly assistance in the field. I am grateful to Professor Paulo Vasconcelos, Dr Tonguc Uysal, Dr Kurt Knesel, Dr Charles Verdel, Dr Ben Cohen, Dr Pengfei Li, Dr Grant Dawson, Derek Hoy, and Uri Shaanan for their kindly comments and suggestions.

I am also deeply grateful for the International Postgraduate Research Scholarship (IPRS) and University of Queensland Centennial Scholarship (UQCent). I could not complete my PhD without these scholarships.

I would like to be deeply appreciative of my parents who have been supporting me in all my life especially during my tertiary education. Finally, I would like to express my deepest appreciation to my beloved wife, Atefeh, for her support and sacrifices. Her great patience, strong encouragement, and constant and gorgeous smiles always motivated me to work hard on my PhD project.

Keywords

New England Orogen, eastern Australia, fault systems, flexural slip mechanism, Mesozoic basins, Demon Fault, North Pine Fault System, late Cenozoic faulting, oroclines

Australian and New Zealand Standard Research Classifications (ANZSRC)

ANZSRC code: 040312 Structural Geology, 70%

ANZSRC code: 040313 Tectonics, 30%

Fields of Research (FoR) Classification

FoR code: 0403 Geology, 100%

Table of Contents

List of Figures

List of Tables

List of Abbreviations

DF-Demon Fault

MFS-Manning Fault System

NPFS-North Pine Fault System

PFS-Peel Fault System

RPF-Redbank Plains Fault

RTP-Reduced to pole

WIFS-West Ipswich Fault System

Chapter 1

Introduction

1.1. Introduction

Eastern Australia has abundant evidence for deformation along numerous fault systems, but the geometry, kinematics, and reactivation history of these faults is not well studied. Therefore, their tectonic significance has hitherto not been considered. This thesis presents studies of major fault systems within the Late Paleozoic to early Mesozoic New England Orogen and their reactivation history during the Mesozoic and Cenozoic. The outcomes of this thesis allow us to a better understanding of the nature of tectonic events that affected eastern Australia since the Permian. In fact, they propel us to appreciate the contribution of faults in the early-mid Permian oroclinal bending, the development of Mesozoic basins, the late Mesozoic-early Eocene fragmentation of eastern Australia, and intraplate deformation in response to the transmission of far-field stress fields in the late Cenozoic.

The approach is the investigation of geophysical data (aeromagnetic, gravity, and seismic reflection data), remote sensing, and field observations, which together provide constraints on the geometry, kinematics, and reactivation history of fault systems. Each chapter provides evidence for deformation along faults systems followed by a discussion on possible tectonic mechanisms responsible for this deformation.

In this chapter, I provide a geological background of the study area and information on the aims of this study, methods, and the layout of the thesis.

1.2. Geological Background

The geology of eastern Australia comprises rock units belonging to the New England Orogen, Mesozoic sedimentary basins, and Cenozoic volcanic rocks and sedimentary basins (Figures 1.1 and 1.2). The New England Orogen is the youngest and easternmost component of the Tasmanides, an assembly of orogenic belts that developed in eastern Australia since the Cambrian (Figure 1.1a) (Glen, 2005). The New England Orogen is normally subdivided into northern and southern parts, separated by the Mesozoic Clarence-Moreton Basin (Figure 1.2a). It is mostly composed of Paleozoic to early Mesozoic rock units, which include a Devonian-Carboniferous subduction complex, forearc basin, and magmatic arc (Leitch, 1975; Day et al., 1978; Henderson et al., 1993; Holcombe et al., 1997a), and Permo-Triassic sedimentary and magmatic rocks (Figure 1.2) (Shaw and Flood, 1981; Hensel et al., 1985; Leitch, 1988; Holcombe et al., 1997b).

During the early Permian, the New England Orogen was subjected to extensional tectonism, possibly in a backarc setting (Jenkins et al., 2002; Korsch and Totterdell, 2009; Rosenbaum et al., 2012; Shaanan et al., 2015). Extensional deformation involved the development of widespread rift basins

(Korsch and Totterdell, 2009) and the simultaneous emplacement of a large volume of S-type granitoids (Shaw and Flood, 1981; Hensel et al., 1985). Early Permian basins, filled by sedimentary and volcanic rocks, are represented by the Sydney, Gunnedah and Bowen Basins, and other early Permian successions (Leitch, 1988) (Figure 1.2a). These basins have been developed due to the activity of steep normal faults, mostly as half-grabens (Korsch et al., 2009a). Some authors have suggested that faults have also undergone strike-slip movement in the New England Orogen during the early Permian (Cawood, 1982; Offler and Williams, 1987). Curved orogenic belts (oroclines) in the southern New England Orogen, which include the Coffs-Harbour, Texas, Manning, and Nambucca oroclines, have formed during this period, possibly simultaneously with backarc extension (Li et al., 2012a; Rosenbaum, 2012; Rosenbaum et al., 2012).

During the late Permian to the Early Triassic, the New England Orogen was subjected to contractional deformation referred to as the Hunter-Bowen Orogeny (Collins, 1991; Jenkins et al., 2002). The Hunter-Bowen Orogeny was accompanied by calc-alkaline magmatism (Day et al., 1978; Shaw and Flood, 1981; Holcombe et al., 1997b; Korsch et al., 2009b; Shaw and Flood, 2009; Li et al., 2012b), and resulted in thrusting and folding of the Paleozoic rock units of the New England Orogen, as well as tectonic inversion in the Bowen-Gunnedah-Sydney Basins (Holcombe et al., 1997b; Korsch et al., 2009b). The Hunter-Bowen Orogeny was intermitted by an interval of extensional tectonics in the Early to Middle Triassic, resulting in the formation of the Esk Trough, likely in a backarc setting (Korsch et al., 1989; Li et al., 2012b). Alternatively, it has been suggested that the Esk Trough was a foreland basin in the Early-Middle Triassic (Elliott, 1993; Campbell, 2005). The Esk Trough has been subjected to folding and thrusting during the Middle Triassic, possibly during the last episode of the Hunter-Bowen Orogeny (Holcombe et al., 1997b).

Since the Late Triassic sedimentary basins have developed in two major episodes. The earlier episode, which occurred in the early Late Triassic, led to the development of sedimentary basins, such as the Ipswich Basin (Korsch et al., 1989; Holcombe et al., 1997b). The Ipswich Basin is located in southeast Queensland and northeast NSW (Figure 1.2b), and comprises sandstone, shale, conglomerate, coal seams, and basaltic volcanic rocks and rhyolitic tuff (Cranfield and Schwarzbock, 1976; Cranfield et al., 1976). The development of the Ipswich Basin involved bimodal volcanism in southeast Queensland (Roach, 1997) and was likely accompanied by oblique strike-slip normal faults (Babaahmadi and Rosenbaum, 2014b).

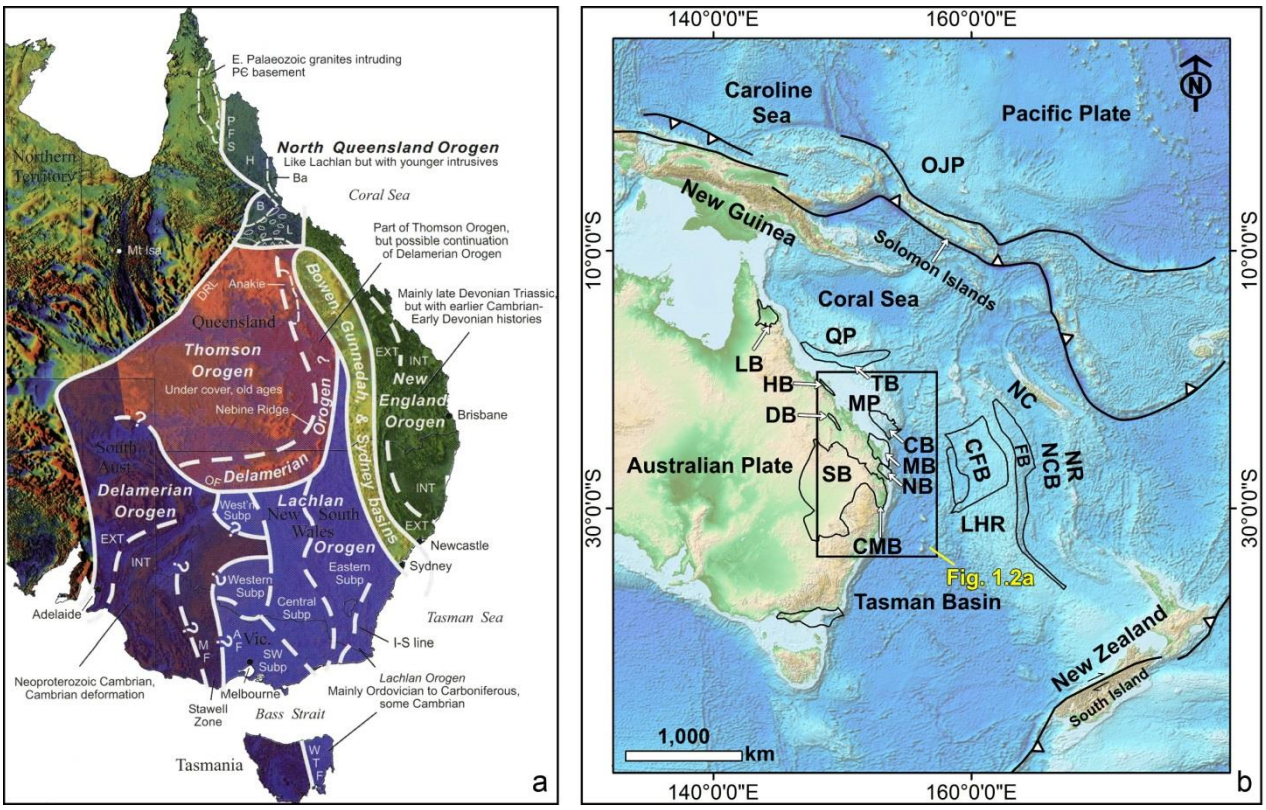

Figure 1.1. (a) Components of the Tasmanides in eastern Australia (Glen, 2005); (b) ETOPO1 digital elevation model of the Australian and Pacific plates (Amante and Eakins, 2009), and a simplified tectonic framework showing Mesozoic and Cenozoic sedimentary basins in eastern Australia. CMB, Clarence-Moreton Basin; CB, Capricorn Basin; CFB, Capel and Faust basins; DB; Duaringa Basin; HB, Hillsborough Basin; LB, Laura Basin; LHR, Lord Howe Rise; MB, Maryborough Basin; MP, Marion Plateau; NB, Nambour Basin; NCB, New Caledonia Basin; NC, New Caledonia; OJP, Ontong Java Plateau; QP, Queensland Plateau; SB, Surat Basin; TB, Townsville Basin.

The second episode of basin formation, from the latest Late Triassic to the Early Cretaceous, was associated with thermal relaxation subsidence that gave rise to the development of the Clarence-Moreton, Surat and Maryborough Basins (Figures 1.1 and 1.2b) (Korsch et al., 1989; Hill, 1994; Holcombe et al., 1997b; Korsch and Totterdell, 2009). Strike-slip faulting intermittently continued during the deposition of these basins in the Jurassic (Korsch et al., 1989; Babaahmadi and Rosenbaum, 2013).

From the Late Cretaceous to the early Eocene, the eastern Australian margin was subjected to continental fragmentation that accompanied the opening of the Tasman and Coral Seas (Weissel and Watts, 1979; Gaina et al., 1998a; Gaina et al., 1998b). It resulted in the development of a series of sedimentary basins such as the Townsville, Capricorn, Hillsborough, Duaringa, Capel and Faust Basins (Figure 1.1b) (Gray, 1976; Hill, 1994; Struckmeyer et al., 1994; Struckmeyer and Symonds, 1997; Gaina et al., 1998a; Gaina et al., 1998b; Korsch et al., 1998; Colwell et al., 2010). Some of these sedimentary basins have been folded and displaced by numerous strike-slip reverse faults during the Cenozoic (Gray, 1976; Hill, 1994; Struckmeyer and Symonds, 1997; Colwell et al., 2010).

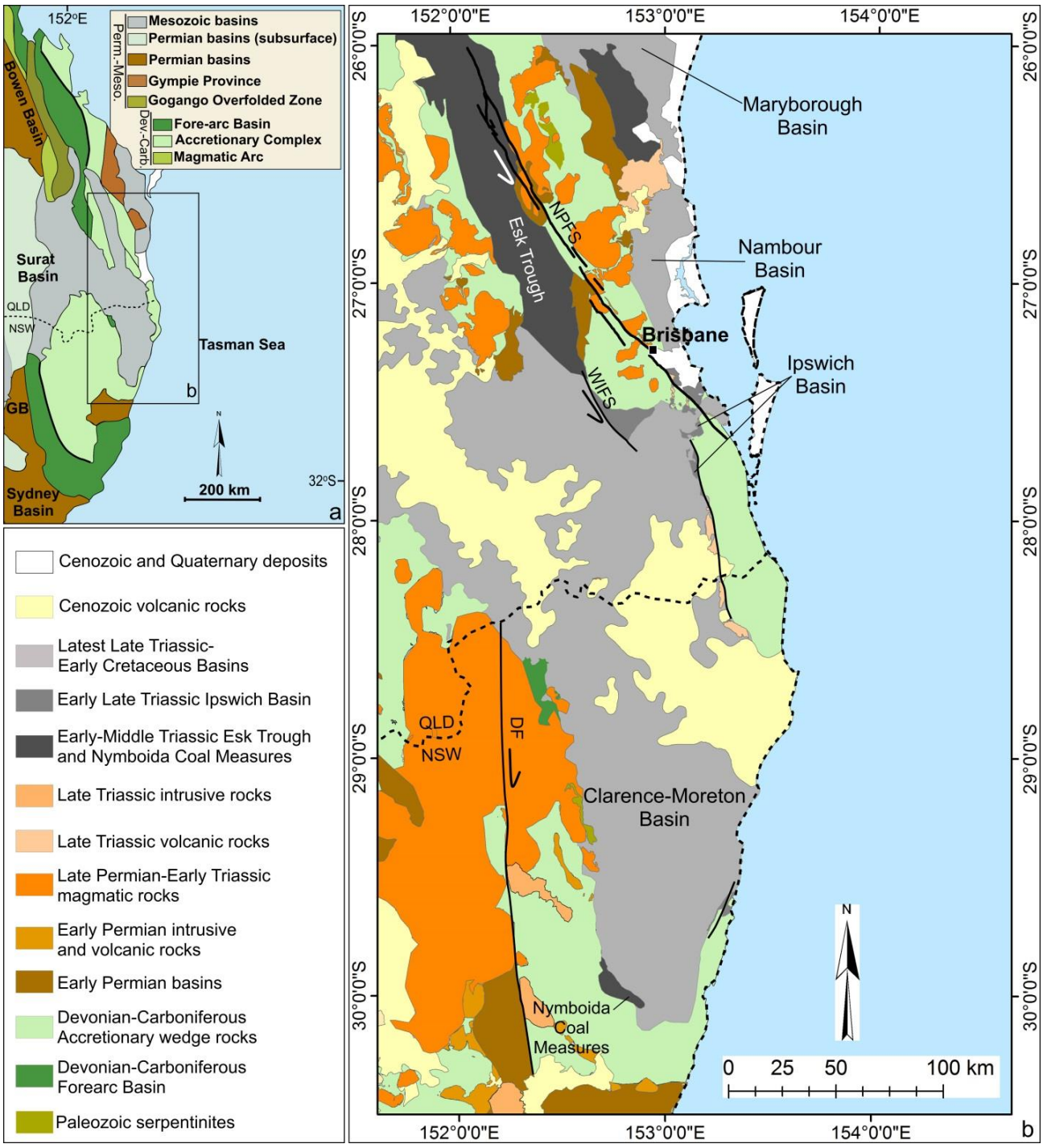

Figure 1.2. (a) Regional tectonic map of eastern Australia showing the components of the New England Orogen (see Figure 1.1 for location); GB, Gunnedah Basin; (b) Simplified geological map of eastern Australia; DF, Demon Fault ET, Esk Trough; NPFS, North Pine Fault System; WIFS, West Ipswich Fault System

Since the mid-Eocene, eastern Australia was subjected to a vast intraplate volcanism, which resulted in the formation of the voluminous amount of mafic and felsic volcanic rocks (Figure 1.2b) (Wellman and McDougall, 1974). Central volcanoes, lava field provinces, and high potassium mafic areas are three types of intraplate volcanism in eastern Australia (Wellman and McDougall, 1974). The central volcanoes are mostly basaltic but with some felsic lava flows and intrusions, such as Tweed and Main Range (Figure 2) (Wellman and McDougall, 1974; Johnson, 1989). They are interpreted to have

resulted from the northward motion of the Australian plate over a stationary hotspot(s) (Knesel et al., 2008). Lava field provinces are mostly composed of extensive and thin basaltic lavas, although in some locations their thickness reaches up to 1000 m (Wellman and McDougall, 1974). High potassium mafic areas are observed in central New South Wales as olivine leucitite (Wellman and McDougall, 1974).

1.3. Research aim

The main goal of this PhD project is to unravel the role of major faults during the tectonic evolution of eastern Australia by studying the geometry, kinematics and reactivation history of fault systems. The specific aims of the project are:

(1) *To understand the role of strike-slip faults in the formation of oroclines during the early Permian*

This work attempts to investigate the pattern, geometry, and kinematics of fault systems in the southern New England Orogen with the aim of unraveling their role during oroclinal bending. The study utilised aeromagnetic data and field measurements.

(2) *To determine the role of faults in the development and inversion of Mesozoic sedimentary basins*

This part of the thesis provides a detailed account on the structures associated with the Mesozoic basins (the Esk Trough, and the Nymboida, Ipswich, and Clarence-Moreton Basins) in southeast Queensland and northeast New South Wales. The study aims at understanding the origin and evolution of these basins in a regional geodynamic context.

(3) *To investigate the kinematics and timing of the Demon Fault*

This work presents a detailed structural analysis on the different segments of the Demon Fault with the aim of understanding the exact geometry and kinematics of each segment. The results are then discussed in the context of strike-slip faulting in eastern Australia and its relationship to the geodynamic evolution of eastern Australia during the Mesozoic.

(4) *To understand the kinematics and timing of the North Pine Fault System*

This part of the project describes the geometry and kinematics of the North Pine Fault System by presenting detailed structural analyses of the different fault segments. Then, the activity along this fault system is discussed in the context of the late Mesozoic and Cenozoic geodynamics of the eastern part of the Australian plate.

(5) *To provide evidence for late Cenozoic intraplate faulting in eastern Australia*

The aim of this work is to investigate whether evidence for intraplate transpressional deformation is recorded in deformational features within Cenozoic volcanic rocks in eastern Australia. The work is focused on a number of faults in southeast Queensland. Gridded aeromagnetic data and field observations are utilised to analyze the kinematics, magnitude, origin, and relative timing of deformation.

1.4. Methods

A combination of different methods, including geophysical methods, remote sensing, and field observations, were utilised in order to investigate fault systems in eastern Australia.

1.4.1. Geophysical methods

In this PhD project, I used aeromagnetic, gravity, and seismic reflection data to study the subsurface structures in eastern Australia. Aeromagnetic anomaly grid data with spatial resolution of 50, 80, and 250 m and gravity data with spatial resolution of 500 and 800 m, provided by Geoscience Australia (through "Geophysical Archive Data Delivery System" website) and the Geological Surveying of Queensland, were used to identify and interpret major faults.

I have conducted a series of image processing on potential fields data from eastern Queensland and NSW to produce filtered images. These filtered images are powerful tools for interpreting structures in both shallow and deep bodies. I used reduced-to-pole (RTP) gridded data, which locate anomalies directly above their sources (Swain, 2000; Cooper and Cowan, 2005), and operated a variety of filters in the Fourier domain to enhance both shallow and deep features. The first and second vertical derivatives were operated to sharpen short wavelength sources and especially fault lineaments (Blakely, 1995; Nabighian et al., 2005). These filters allow us to interpret faults acting in shallow sources. In particular, tilt angle derivative (the arc tangent of the ratio of the first vertical derivative to the absolute value of total horizontal derivatives) is a powerful filter for enhancing geological edges and fault lineaments from both shallow and regional sources equally (Miller and Singh, 1994). Total horizental derivative is another filter that enhances faults and boundaries. Tilt angle and total horizental derivatives are the most popular filters to map faults. Downward continuation is the process whereby potential field is measured over a plane closer to the sources in order to accentuate short wavelength and shallower sources (Blakely, 1995; Trompat et al., 2003). Upward continuation is the process whereby potential field is measured on a plane farther from all sources to highlight deeper sources and reduce shallower sources effects (Blakely, 1995). The gridded aeromagnetic data allowed us to recognise (1) offset and dragging of magnetic anomalies along faults; (2) pronounced structural lineaments; and (3) lensoid and en-echelon structures.

Seismic reflection method is another geophysical method that was utilised in this project. Practical application of the seismic reflection method is in the structural analysis of deformed belts and sedimentary basins. A number of new and old processed seismic reflection data were used to interpret stratigraphic horizons, faults and folds in the Mesozoic basins. Interpretation of seismic lines was complemented by field observations, potential field data, and stratigraphic columns to perceive deformation style of the basins. The seismic data used in this thesis have been provided by the Resources and Energy division of NSW Trade & Investment (Clarence-Moreton Basin Seismic Survey 2008 CD and Onshore Clarence-Moreton Basin Petroleum Data Package DVDs)

1.4.2. Remote Sensing

Remote sensing data that can be used for recognising fault lineaments are:

1) Multispectral images (e.g., ASTER with a spatial resolution of 15 m, and LANDSAT ETM+ images with a spatial resolution of 28.5 m) which are suitable for geological purposes.
2) ASTER digital elevation models

For better identification of rock units, faults and lineaments in larger scale, I used data fusion methods to merge multispectral images with high resolution panchromatic images (for example, merging multispectral ETM+ images with a 28.5m cell size and the panchromatic band of ETM+ image with a spatial resolution of 14.25m). Data fusion were performed by using the intensity–hue–saturation (IHS) method (Pohl and Van Genderen, 1998; Zhang, 2004). In this method, a multispectral image is transformed from Red-Green-Blue (RGB) into IHS space, and then the intensity component of the image is replaced by high resulotion panchromatic image. Finally, inverse transformation from IHS space into RGB space is carried out. ETM+ images are provided by Global Land Cover Facility (URL: <http://www.glcf.umd.edu>).

The digital elevation model is ASTER Global Digital Elevation Map version 2 (GDEM V2), produced by NASA and the Ministry of Economy, Trade and Industry of Japan. The 30m ASTER DEMs have been generated by bands 3N (nadir-viewing) and 3B (backward-viewing) of the ASTER Level-1A images, acquired by the Visible -Near Infrared (VNIR) sensor (ASTER-GDEM-Validation-Team, 2011). Combined with satellite images, they were utilised to interpret the surface expressions of faults.

1.4.3. Field Observations

Field trips were conducted in accessible exposures with the aim of finding faults and their related kinematic indicators. Kinematic indicators used in this project include slickenlines, offset and

dragged structures, and Riedel shears (R, P, and Y shears). In the absence of slickensides, the indicators, used to determine the hanging-wall movement in cataclastic fault zones, were P-Y shears, which are equivalent to S-C fabrics in ductile shear zones.

1.5. Thesis layout

The PhD thesis has seven chapters, including an introduction (Chapter 1), main body (Chapters 2-6), and conclusions and suggestions for future works (Chapter 7). The main body is presented in five chapters organised based on a chronological order. These chapters have been written in the format of journal articles and have been already published (Chapters 3, 4, 5, and 6) or submitted (Chapter 2) for publication. The presentation of each chapter as a "stand alone" journal article means that there is a fair bit of repetition in the geological background sections. The five chapters include:

Chapter 2- Kinematics of orocline-parallel faults in the Texas and Coffs-Harbour oroclines (eastern Australia) and the possible role of flexural slip during oroclinal bending

Chapter 3- Alternating episodes of extension and contraction during the Triassic: Evidence from Mesozoic sedimentary basins in eastern Australia

Chapter 4- Kinematics of the Demon Fault: Implications for Mesozoic strike-slip faulting in eastern Australia

Chapter 5- Late Mesozoic and Cenozoic wrench tectonics in eastern Australia: Insights from the North Pine Fault System (southeast Queensland)

Chapter 6- Late Cenozoic intraplate faulting in eastern Australia

Chapter 2

Kinematics of orocline-parallel faults in the Texas and Coffs-Harbour oroclines (eastern Australia) and the possible role of flexural slip during oroclinal bending

Kinematics of orocline-parallel faults in the Texas and Coffs-Harbour oroclines (eastern Australia) and the possible role of flexural slip during oroclinal bending

Abstract

The Texas and Coffs-Harbour oroclines are defined by a Z-shaped curvature in the southern New England Orogen (eastern Australia), but the geometry and kinematics of faults around these oroclines, as well as their possible role during oroclinal bending has hitherto not been understood. Using aeromagnetic and radiometric data, as well as field observations, the pattern, geometry, and kinematics of fault systems have been investigated. Fault traces with a strike-slip component are oriented parallel to the curved magnetic and structural fabrics of the Texas and Coffs-Harbour oroclines. The observed kinematics of NW-striking faults is sinistral or sinistral-reverse, whereas NNE- and NE-striking faults indicate dextral or dextral-reverse kinematics. The timing(s) of faulting are not well constrained, but the ubiquitous recognition of orocline-parallel faults may suggest that a flexural slip mechanism operated during oroclinal bending in the Early-Middle Permian (~299-265 Ma). Observations from this work and recent studies show that many of the orocline-parallel strike-slip faults were reactivated during the Mesozoic and Cenozoic, as indicated by the recognition of displaced Triassic granitoids, Mesozoic and Cenozoic sedimentary rocks, and Cenozoic basalts.

Key words: Texas Orocline, Coffs-Harbor Orocline, southern New England Orogen, faults, flexural slip, eastern Australia

2.1. Introduction

Flexural slip is a common folding mechanism that involves slip on foliation/bedding-parallel shear surfaces (Tanner, 1989). It can accommodate buckling (Ramsay and Huber, 1987) and bending (Gross et al., 1997; Twiss and Moores, 2007), and is characterised by slip towards the hinge on the convex side of the structure (Twiss and Moores, 2007). Most observations for flexural slip mechanism are from meso- and macro-scale folds (Fowler, 1996; Fowler and Winsor, 1997; Gross et al., 1997; Horne and Culshaw, 2001; Perritt and Roberts, 2007), with only few orogenic-scale examples (Faure and Lalevée, 1987; Kranendonk and Wardle, 1997; Gutierrez-Alonso et al., 2008). In particular, it is still unclear how flexural slip plays a role during the formation of curved orogenic belts (oroclines).

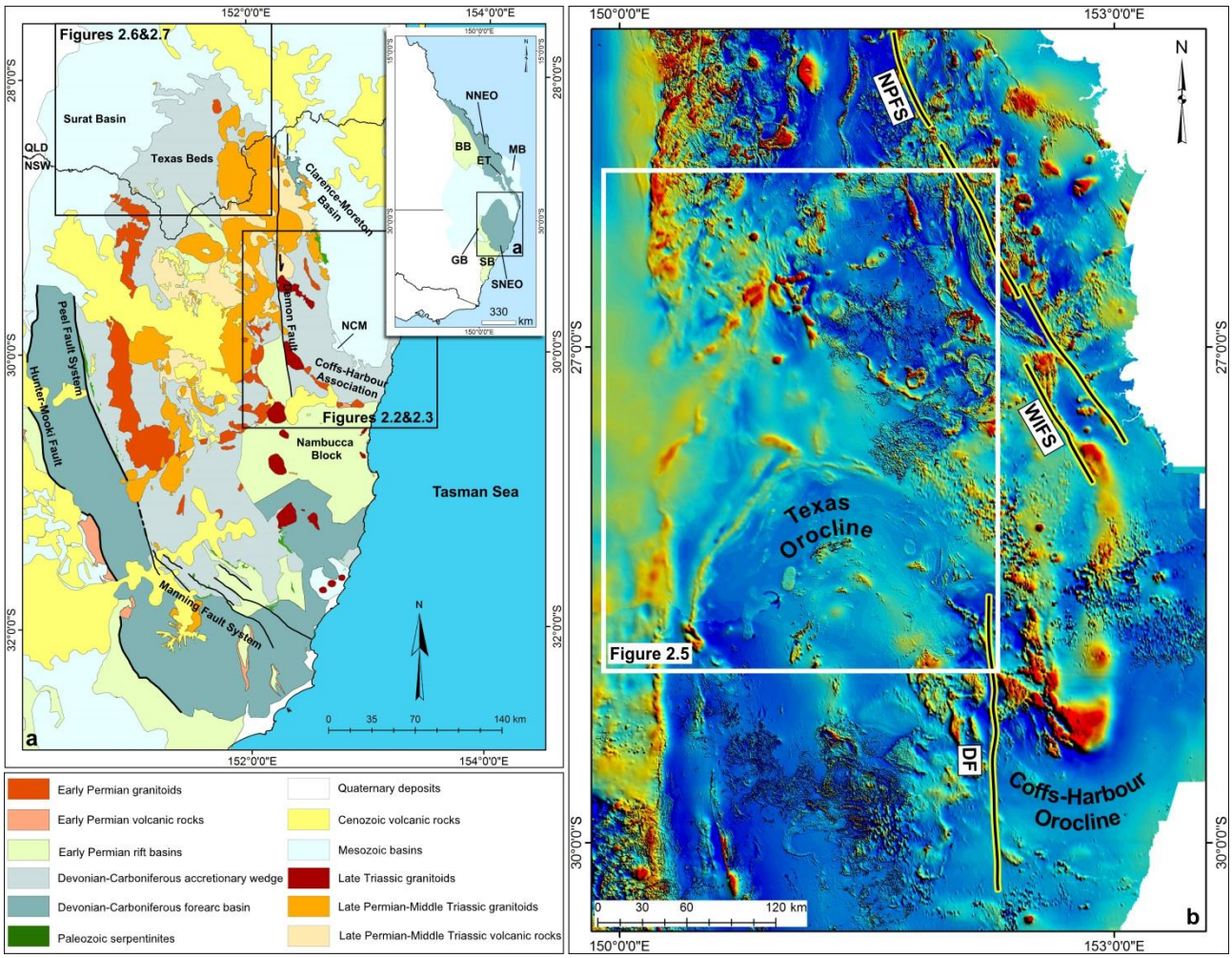

Figure 2.1. (a) Simplified geological map of the southern New England Orogen based on 1:250,000 (Singleton, Newcastle, Tamworth, Hastings, Manilla, Dorrigo-Coffs Harbour, Goondiwindi, and Grafton) and 1:500,000 (Moreton) geological maps (Rose et al., 1966; Mond et al., 1968; Rasmus et al., 1969; Brunker et al., 1970; Offenberg, 1971; Green et al., 1980; Brown et al., 1990; Gilligan et al., 1992; Henley et al., 2001). BB, Bowen Basin; ET, Esk Tough; GB, Gunnedah Basin; MB, Maryborough Basin; NCM, Nymboida Coal Measures; NNEO, Northern New England Orogen; SB; Sydney Basin; SNEO; Southern New England Orogen (b) Reduced to Pole (RTP) image of total magnetic intensity map showing the Texas and Coffs-Harbour orclines. DF, Demon Fault; NPFS, North Pine Fault System; WIFS; West Ipswich Fault System.

The southern part of the New England Orogen in eastern Australia is characterised by the Texas and Coffs-Harbour oroclines, which are clearly observed in gridded aeromagnetic images (Figure 2.1b) (Cawood et al., 2011b; Glen and Roberts, 2012). A number of fault systems (Figure 2.1a) seem to be parallel to the limbs of the oroclines. However, the geometry and kinematics of these faults, as well as their possible relationships with the formation of the oroclines have hitherto not been studied in detail.

The aims of this paper are to investigate the kinematics of orocline-parallel faults in the southern New England Orogen and the possibility that these faults have accommodated flexural slip during oroclinal

bending. Using aeromagnetic and radiometric data, as well as field observations, I present an analysis of the geometry and kinematics of faulting, which allow us to test whether the pattern of faults is consistent with a flexural slip mechanism.

2.2. Geological Setting

The New England Orogen evolved during the Paleozoic and early Mesozoic when eastern Australia, which was part of eastern Gondwana, was positioned in a convergent plate boundary setting against the paleo-Pacific plate. The orogen is subdivided into southern and northern segments, separated by Mesozoic basins (Figure 2.1a). A large component of the exposed rocks belongs to Devonian-Carboniferous subduction-related units (accretionary complex, forearc basin and magmatic arc) (Leitch, 1975; Day et al., 1978; Henderson et al., 1993; Holcombe et al., 1997a) (Figure 2.1a). These rocks are intruded by Early Permian S-type granitoids (298-288 Ma) (Shaw and Flood, 1981; Cawood et al., 2011b; Rosenbaum et al., 2012), and locally overlain by Early Permian clastic sedimentary successions (e.g., Nambucca Block; Figure 2.1a). The latter basins have likely formed in a backarc extensional setting (Shaanan et al., 2015) that was also responsible for rifting in the Sydney, Bowen, and Gunnedah basins (Korsch et al., 2009a). The Sydney, Bowen, and Gunnedah basins were subsequently transformed into foreland basins and continued to receive sediments until the Middle Triassic (Glen and Beckett, 1997; Glen, 2013).

From the Middle Permian to the early Late Triassic (265-230 Ma), the New England Orogen was subjected to contractional deformation, commonly referred to as the Hunter-Bowen Orogeny (Collins, 1991; Korsch et al., 2009b; Li et al., 2012b). Deformation is assumed to have been associated with E-W shortening and was accompanied by the emplacement of widespread I-type granitoids and calc-alkaline volcanic rocks (Day et al., 1978; Shaw and Flood, 1981; Collins, 1991; Holcombe et al., 1997b; Shaw and Flood, 2009). Younger rocks in the southern New England Orogen are associated with Late Triassic to Early Cretaceous sedimentary basins and Cenozoic volcanic and sedimentary rocks (Figure 2.1a).

The geometry and timing of deformation in the Texas and Coffs-Harbour oroclines have been discussed in previous publications (Lennox and Flood, 1997; Offler and Foster, 2008; Cawood et al., 2011b; Glen and Roberts, 2012; Li et al., 2012a; Rosenbaum, 2012; Rosenbaum et al., 2012). The shape of the orocline is recognised by the curvature of structural fabrics (Korsch, 1981; Fergusson, 1982; Lennox and Flood, 1997; Li et al., 2012a), the pattern of paleomagnetic fabrics (Aubourg et al., 2004; Mochales et al., 2014), the repetition of forearc units on both limbs of the orocline (Hoy et

al., 2014), and the curved shape of magnetic anomalies in gridded aeromagnetic data (Cawood et al., 2011b; Glen and Roberts, 2012) (Figure 2.1b).

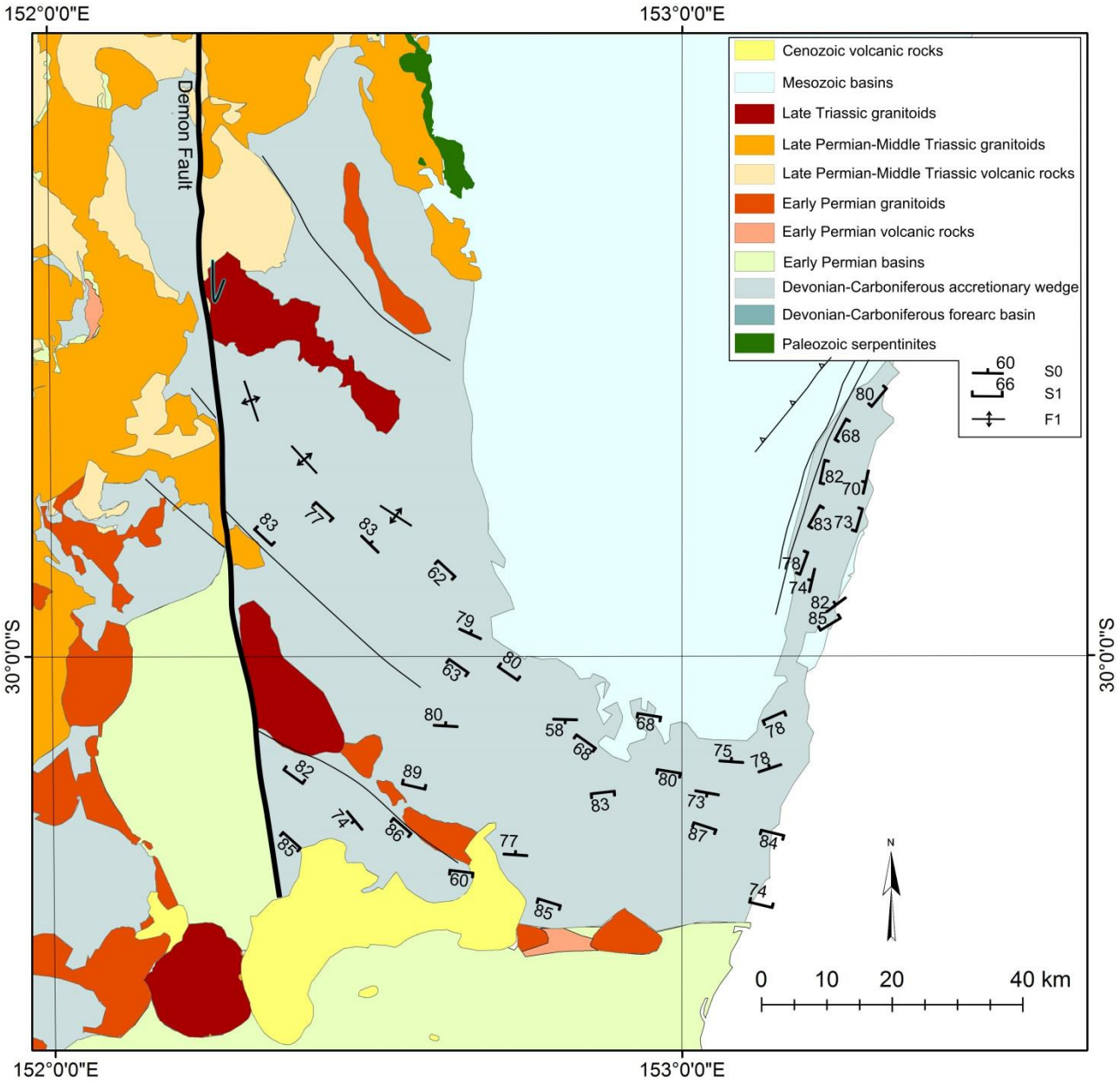

Figure 2.2. (a) Geological map of the Coffs-Harbour Orocline (based on 1:250,000 Grafton and Dorrigo-Coffs Harbour geological maps (Gilligan et al., 1992; Henley et al., 2001)), showing the axial surface foliations (S1) and primary beddings (S0) (see Figure 2.1a for location). Structural data are from Korsch (1981) and Fergusson (1982).

The timing of oroclinal bending has been constrained to the Early-Middle Permian (299-260 Ma) based on the observation that Early Permian granitoids (298-288 Ma) are curved parallel to the oroclinal structure and are crosscut by Late Permian to Triassic (260-230 Ma) magmatic rocks (Korsch and Harrington, 1987; Rosenbaum et al., 2012). Based on paleomagnetic data, Aubourg et al. (2004) have suggested that the initiation of oroclinal bending may have already commenced in the latest Carboniferous.

2.3. Methods

Faults in the area of the Texas and Coffs-Harbour oroclines were studied by using gridded aeromagnetic and radiometric data, and field observations. Owing to the limited number of well-preserved outcrops in the study area, the gridded aeromagnetic data are the main tool used for the recognition of geological structures. I used gridded aeromagnetic data with spatial resolution of 50 and 80 m, provided by Geoscience Australia and the Resources and Energy division of NSW Trade & Investment. For better recognition of magnetic bodies and faults in Paleozoic-Mesozoic rocks, I utilised a tilt angle derivative map of reduced-to-pole (RTP) gridded aeromagnetic data. Tilt angle derivative is a filter that enhances edges of magnetic sources from both shallow and deep sources, and is calculated as the arc tangent of the ratio of the first vertical derivative to the absolute value of the total horizontal derivatives (Miller and Singh, 1994). The first vertical derivative (1VD) was also operated to sharpen short-wavelength sources (Nabighian et al., 2005). Upper continuation is another process whereby the potential field is measured on a plane farther from all sources to highlight deeper sources and reduce the effects of shallower sources (Blakely, 1995). The gridded aeromagnetic data allowed us to recognise (1) offset and dragging of magnetic anomalies along faults; (2) pronounced structural lineaments; and (3) lensoid and *en-echelon* structures. The interpretation of aeromagnetic data was complemented by field observations in accessible areas and interpretation of gridded radiometric data provided by Geoscience Australia.

2.4. Structure

A summary of previously published structural information, combined with new observations of fault systems around the Texas and Coffs-Harbour oroclines, is provided below.

2.4.1. Coffs-Harbour Orocline

From interpretation of gridded aeromagnetic data, the Coffs-Harbour Orocline appears as an asymmetric bend with its eastern limb striking NNE and its western limb striking NW (Figure 2.1b). The trend of the dominant structural fabrics defines the limbs of the orocline. Field data by Korsch (1981) and Fergusson (1982) show that both bedding (S_0) and pre-oroclinal axial surface foliations (S_1) are folded, with steeply dipping S_1 fabric oriented NNE to NE in the eastern limb and WNW to NW in the western limb (Korsch, 1981) (Figure 2.2). The orientation of bedding is sub-parallel or parallel to S_1 (Korsch, 1981) (Figure 2.2). In the western limb, Fergusson (1982) has documented tight to isoclinal pre-oroclinal folds (F_1) with steeply dipping axial surface foliations (S_1) with a variable strike orientation of NNW in the west and WNW toward the hinge (the east) (Figure 2.2a).

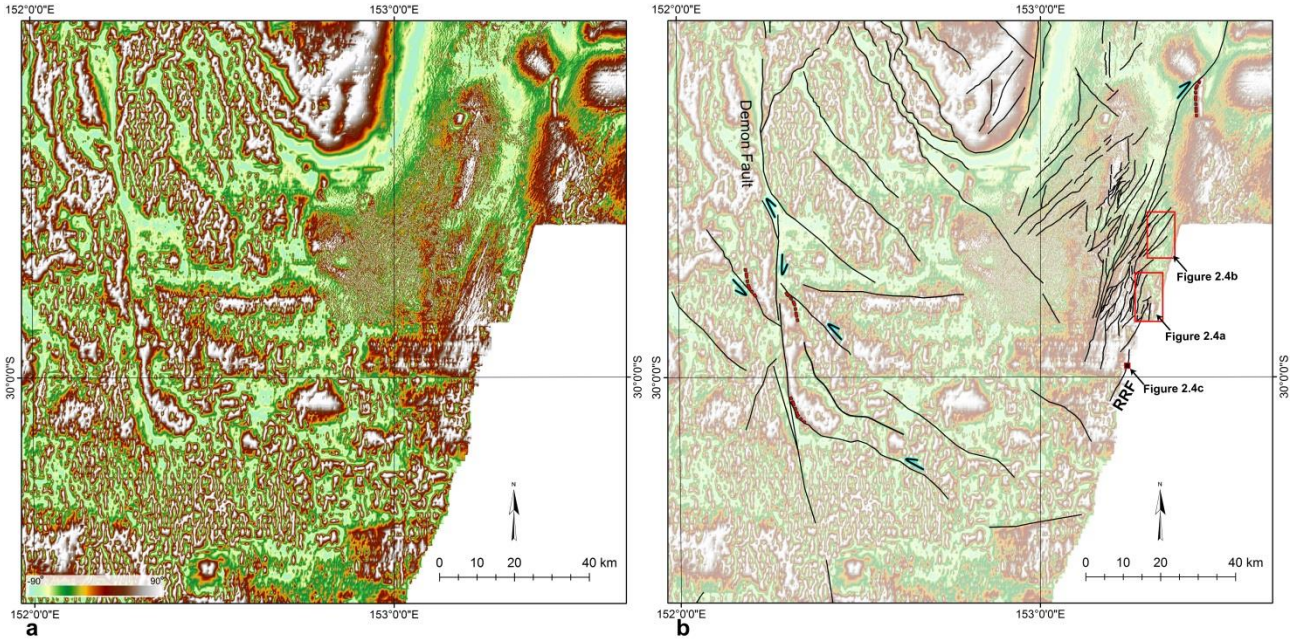

Figure 2.3. (a) Tilt map of gridded aeromagnetic data of the Coffs-Harbour Orocline, and (b) interpreted faults in the eastern and western limbs (see Figures 2.1a for location). NNE- to NE-striking fault lineaments are dominant in the eastern limb, whereas NW-striking fault lineaments are abundant in the western limb. Red dashed lines highlight deflected magnetic bodies along faults. RRF; Red Rock Fault.

Interpretations of the tilt map of gridded aeromagnetic data shows that some faults have displaced different rock units around the Coffs-Harbour Orocline (Figure 2.3a, b). In the eastern limb, NNE- to NE-striking fault lineaments are dominant (Figure 2.3). These fault lineaments appear to have dextral strike-slip kinematics. Figure 2.4 shows that two magnetic bodies were displaced and dragged dextrally by NE-striking faults. Interpretation of seismic lines indicates that some of NNE-striking faults acted as reverse steep faults and have displaced the Late Triassic Ipswich and Late Triassic-Jurassic Clarence-Moreton Basins (Babaahmadi et al., 2015), thus implying that faults were subjected to oblique movements. A detailed field study on one of the NNE-striking faults, the Red Rock Fault Zone (Rosenbaum et al., 2015), indicated a dextral reverse kinematics on this structure (Figure 2.4c), further supporting the interpretation of the aeromagnetic data.

The western limb of the Coffs-Harbour Orocline was mainly affected by NW-striking faults. I did not find convincing kinematic indicators for these faults due to the low resolution gridded aeromagnetic data in this area. However, based on dragging some magnetic bodies, (Figure 2.3) (Babaahmadi and Rosenbaum, 2013), information from the eastern part of the Texas Orocline (Figures 2.7 and 2.9, see next section), and southeastern Queensland (Babaahmadi and Rosenbaum, 2014b, a; Babaahmadi et al., 2015), I infer that most of these faults are most likely characterised by sinistral kinematics (Figures 2.2, 2.3). Two NW-striking sinistral faults have been displaced dextrally by the N-striking Demon Fault (Figure 2.3).

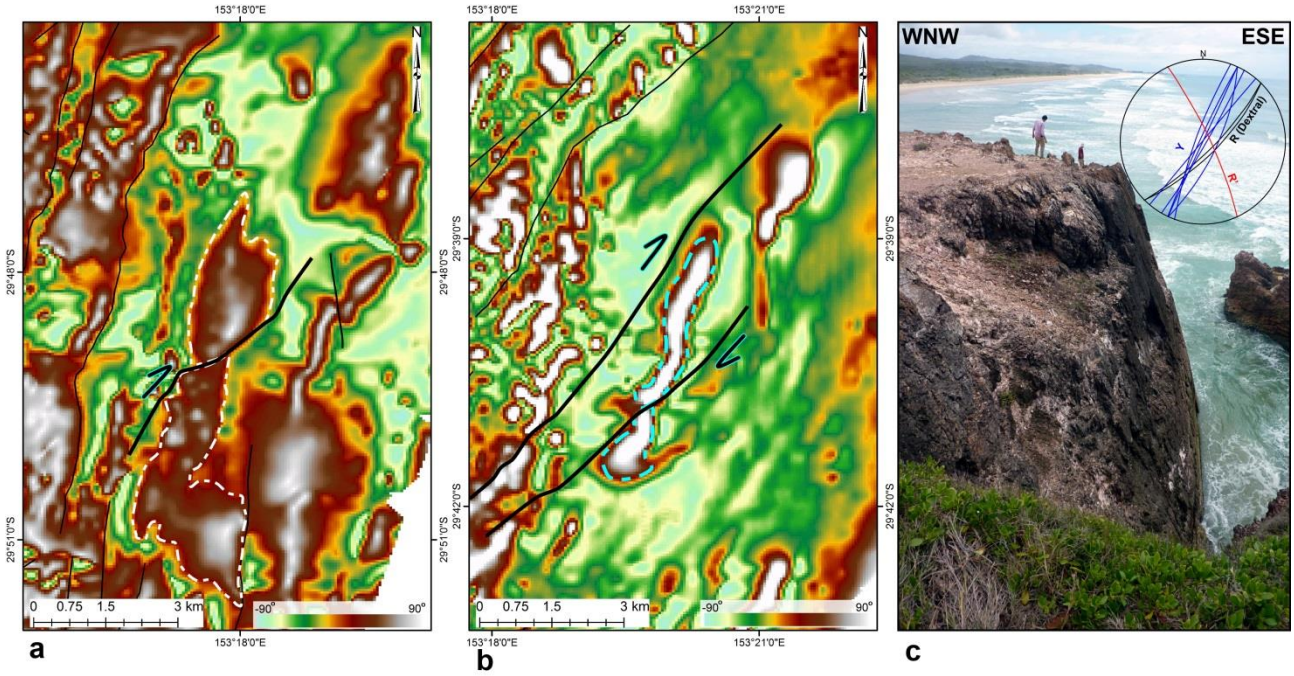

Figure 2.4. (a) Dextral dragging and offset of magnetic bodies along a NE-striking fault in the eastern limb of the Coffs-Harbour Orocline (see Figure 2.3b for location). (b) Another NE-striking fault has dragged and displaced a magnetic body dextrally (see Figure 2.3b for location). (c) A field photo from the sub-vertical Red Rock Fault surface and a stereonet showing the Riedel shears indicating dextral kinematics of the fault (after Rosenbaum et al. 2015) (see Figure 2.3b for location).

2.4.2. Texas Orocline

From aeromagnetic data, the Texas Orocline appears as a symmetrical curved structure with NW- and NE-striking limbs (Figures 2.1b, 2.5). Field mapping shows changes in the strike orientation of the dominant axial surface foliation (S1) (Lennox and Flood, 1997; Li et al., 2012a). In the eastern limb of the orocline, steeply dipping to sub-vertical S1 foliation strikes NW, whereas in the western limb, the strike is NE (Figure 2.6) (Li et al., 2012a). In the hinge zone of the orocline, the orientation of S1 is ~E-W (Figure 2.6). The orientation of bedding is steeply dipping sub-parallel or parallel to S1 (Figure 2.6). F1 folds are mostly tight to isoclinal with steeply dipping axial surfaces parallel to S1 orientation (Li et al., 2012a). Syn-oroclinal F2 structures are rare (Li et al., 2012a).

Similarly to the Coffs-Harbour Orocline, numerous lineaments, interpreted as faults, are observed around the Texas Orocline (Figures 2.5, 2.7). Interpretation of the tilt map of gridded aeromagnetic data indicates that NW- and NE-striking fault lineaments converge at an intersection point to the north in the outer hinge of the Texas Orocline (Figure 2.5) (Brooke-Barnett and Rosenbaum, 2015).

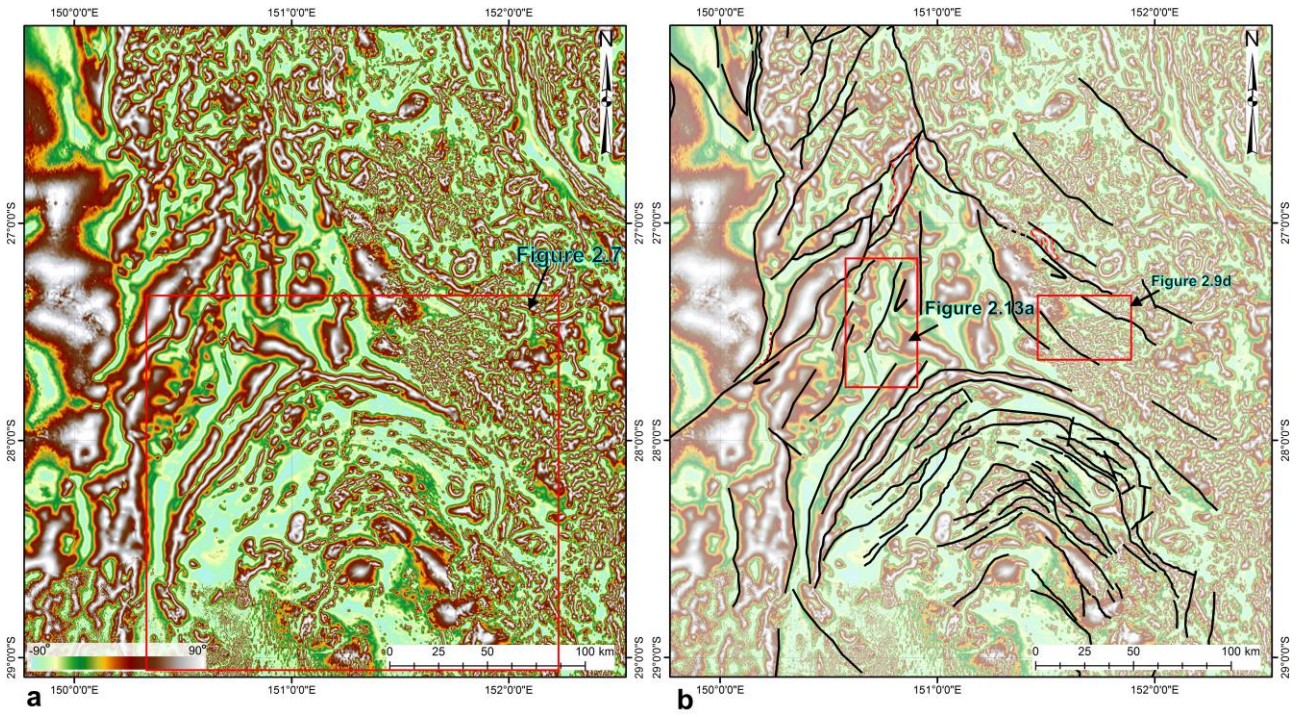

Figure 2.5. (a-b) Tilt angle map of (600m) Upper Continuation of the Reduced to pole aeromagnetic data of the Texas Orocline showing the outer and inner hinges of the Teas Orocline (see Figures 2.1b for location). NW- and NE-striking fault lineaments reach sharply an intersection point to the north in the outer hinge of the Texas Orocline.

The inner hinge of the Texas Orocline is defined by a number of curved continuous fault lineaments and several discontinuous ones (Figure 2.7). In the eastern limb, NW-striking fault lineaments are common, and are predominantly interpreted to have sinistral kinematics based on dragging and offset of magnetic bodies (Figures 2.7, 2.8, 2.9). Interpretation of faults from a radiometric image, overlaying the tilt map of aeromagnetic data, shows that a series of sinistral NW-striking faults that displaced rock units (Figure 2.8, 2.9), including the ~280 Ma (Donchak et al., 2007a) Greymare Granodiorite (Figure 2.8b). This granodiorite shows an inconsistent sinistral separation in its southeastern and northwestern contacts, indicating that it was likely offset by an oblique-slip fault rather than a pure strike-slip fault. A NW-striking sinistral fault was also responsible for dragging the southern part of the ~252 Ma (Li et al., 2012b) Herries Granite (HG) and the offset of the northwestern edge of the ~247 Ma (Donchak et al., 2007b) Stanthorpe Granite (SG) (Figure 2.8b). Indeed, a series of NW-striking faults were mapped in this area that displaced the western edge of the Stanthorpe Granite sinistrally (Figure 2.9a,b). Early Permian clastic sedimentary rocks (e.g., Bondonga Basin; Figure 2.6) are bounded by NW-striking faults that possibly represent syn-sedimentary boundary faults (Lennox and Flood, 1997). The reactivation of some NW-striking faults led to the sinistral separation of the contacts of Cenozoic volcanic rocks (Figure 2.9d, e).

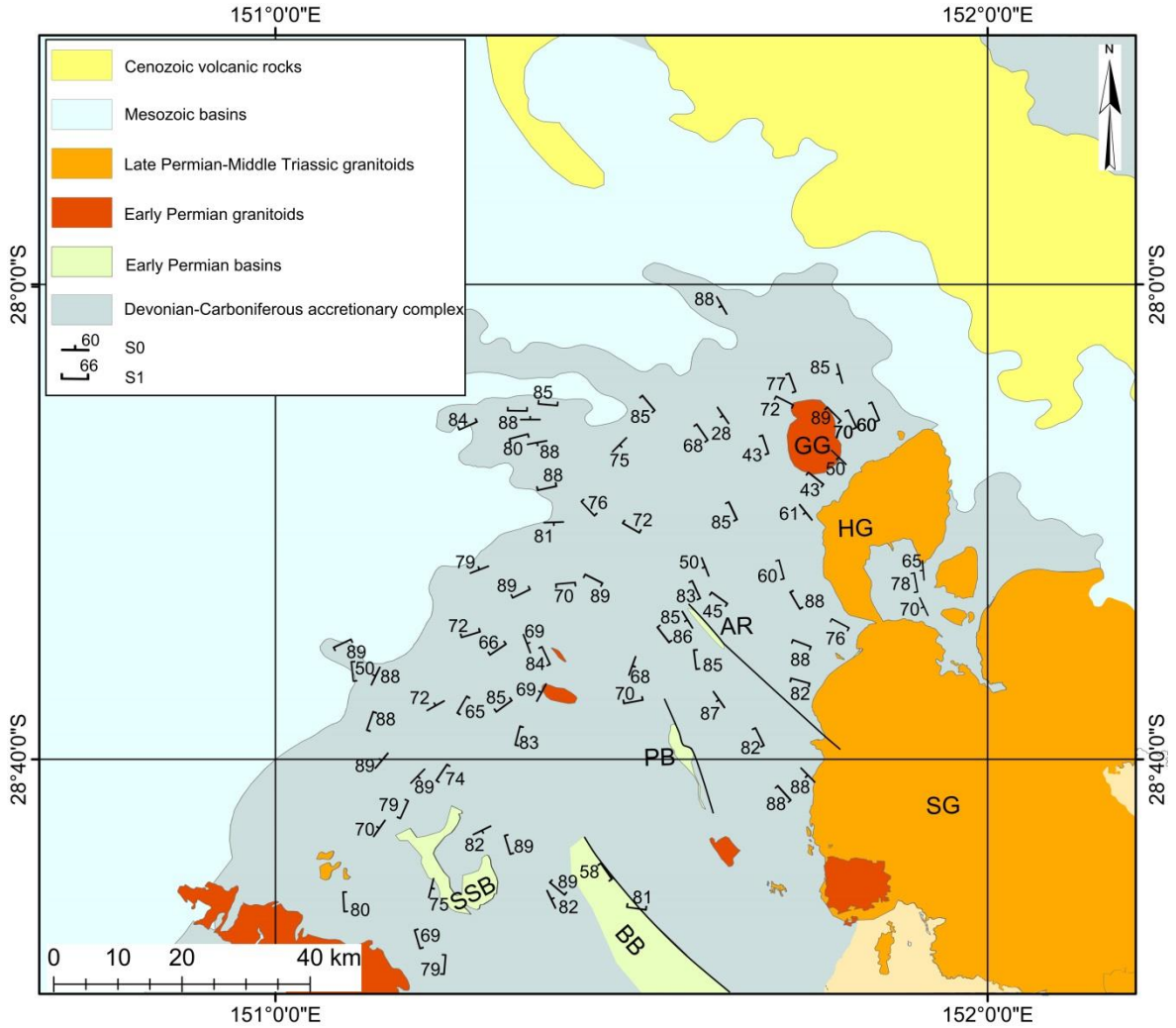

Figure 2.6. Geological map of the Texas Orocline showing the structural fabrics and beddings (based on 1:250,000 Goondiwindi and 1:500,000 Moreton geological maps (Mond et al., 1968; Green et al., 1980)) (see Figure 2.1a for location). Structural field data are from Li et al. (2012a). AR, Alum Rock; BB, Bondonga Basin; GG, Greymare Granodiorite; HG, Herries Granite; PB, Pikedale Basin; SG; Stanthorpe Granite; SSB, Silver Spur Basin.

Field observations indicate that most of NW-striking faults are high-angle faults (≥60°) (Figure 2.9c). Detailed kinematic analyses of many of these faults were not possible due to the scarcity of well-preserved kinematic indicators, such as slickenlines and Riedel shears. However, I observed kinematic indicators in a fault zone in the middle of the Texas Orocline (fault no. 1 in Figure 2.7 and 2.10b) that displaced Devonian-Carboniferous metasedimentary rocks of the Texas beds (Figure 2.10a,b). This fault zone is characterised by two steeply SW-dipping cataclastic zones (Figure 2.10a,b). The geometry and kinematics of Riedel shears (Y-R) in both map and cross-section views are indicative of oblique reverse-dextral movement (Figure 2.11). Younger E-W thrust faults placed older undeformed Carboniferous rock units over one of the cataclastic zones (faults no. 2 in Figure 2.10a,b). This thrust zone was also displaced by a younger NE-dipping fault with unknown kinematics (faults no. 3 in Figure 2.10a,b).

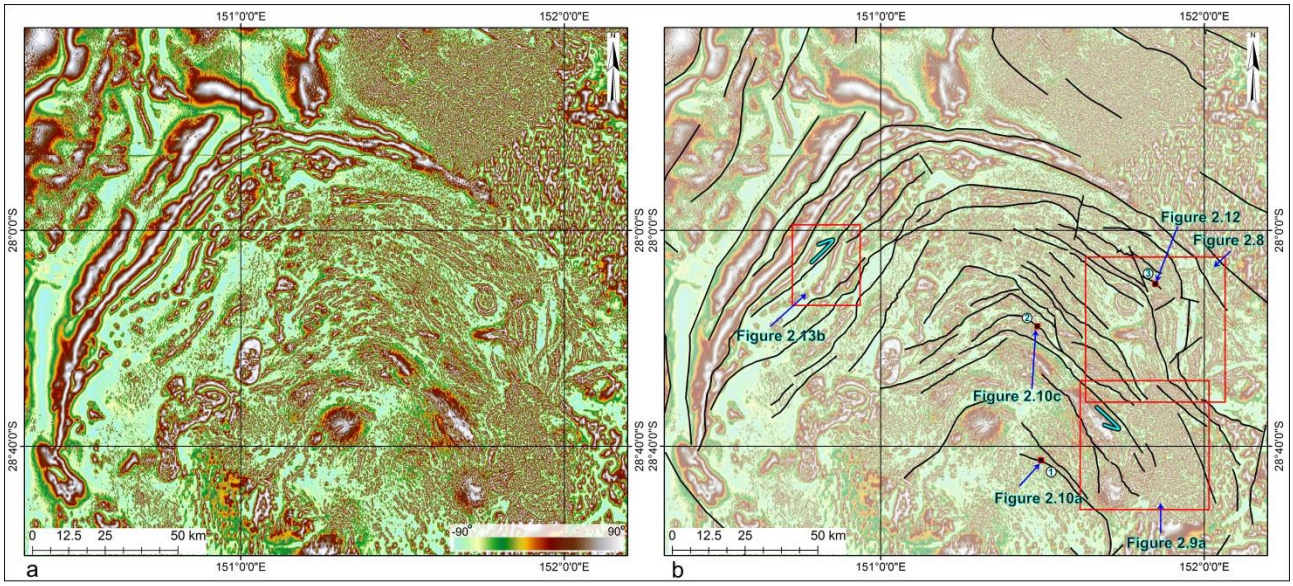

Figure 2.7. (a) Tilt angle map of the Texas Orocline, and (b) interpreted faults in the eastern and western limbs (see Figures 1a, 5a for location). NE-striking and NW-striking fault lineaments are dominant in the western and eastern limbs, respectively. Numbers are mapped faults in the field in Figures 2.10-2.12.

A NW-striking fault (fault no.2 in Figure 2.7) was also observed closer to the hinge of the Texas Orocline. In this locality, the Devonian-Carboniferous rocks of the Texas beds are displaced by a steep normal fault, and two antithetic normal faults, which branch off this fault, displace an overlying sandstone layer (Figure 2.10c, d). The age of the sandstone is unknown, but could be Jurassic (the Surat Basin). A wedge-shaped thickening of the sandstone in the hanging-wall of one of the antithetic faults may indicate syn-tectonic deposition (Figure 2.10c, d). Another example of a steeply-dipping NW-striking fault (fault no.3 in Figure 2.7) was observed in the eastern part of the Texas Orocline (Figure 2.12). The kinematics of this fault seems to be dextral, based on the recognition of dextral Riedel (Y-R) shears (Figure 2.12b). Outcrop-scale releasing bends along a Y shear further support a dextral strike-slip movement of this fault (Figures 2.12c-e). From the interpretation of aeromagnetic data, it appears that this fault was displaced sinistrally by a younger NNW-striking fault (Figure 2.8b). In the western limb of the Texas Orocline, NE-striking lineaments are dominant (Figures 2.4b, c). Some of these lineaments are interpreted as faults with a dextral strike-slip component based on the dragging and offset of magnetic bodies (Figure 2.13). One of these NE-striking faults in the outer hinge of the orocline displaced low and high magnetic anomalies dextrally (Figure 2.13a). The *en-echelon* pattern of NE-striking faults produced a duplex structure within a restraining step-over zone (Figure 2.13a). Figure 2.13b shows magnetic bodies between NE-striking faults in the inner hinge of the Texas Orocline that seem to be shearband boudins, showing synthetic dragging and displacement

by minor ENE-striking dextral faults, indicating a general dextral movement along the NE-striking faults.

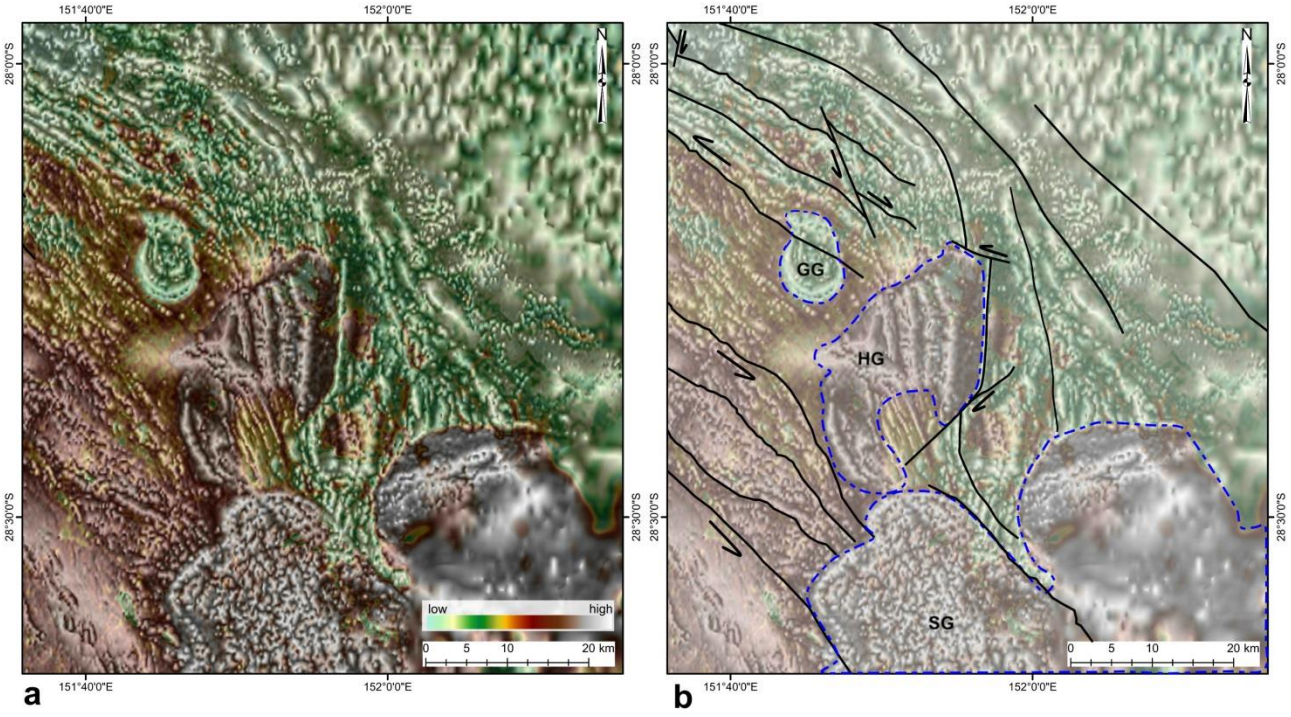

Figure 2.8. (a-b) Potassium radiometric image overlaying tilt angle map of eastern part of the Texas Orocline shows orocline-parallel NW-striking faults displaced by younger faults (see Figure 2.7b for location). One of the NW-striking faults displaces the ~280 Ma Greymare Granodiorite (GG) (Donchak et al., 2007a) sinistrally. A NW-striking fault sinistrally dragged the southern part of the ~252 Ma Herries Granite (HG) (Li et al., 2012b) and separated the northwestern edge of the ~247 Stanthorpe Granite (SG) (Donchak et al., 2007b).

2.5. Discussion

2.5.1. Kinematics and timing of faulting

Results of this study demonstrate that a network of NNE-, NE-, and NW-striking faults occur parallel to the limbs of the Coffs-Harbour and Texas oroclines. The interpretation of aeromagnetic data and field observations reveals that many of these faults are steep with a major strike-slip component. In most cases, the two limbs of the oroclines show opposite sense of kinematics. Along the eastern limb of the Coffs-Harbour Orocline and the western limb of the Texas Orocline, most of NNE- and NE-striking faults show dextral or reverse-dextral kinematics (see also Rosenbaum et al., 2015), whereas along the eastern limb of the Texas Orocline (which is also the western limb of the Coffs-Harbour Orocline), NW-striking faults predominantly show sinistral kinematics (Figures 2.4, 2.9, 2.10). This pattern of fault kinematics is not restricted to the proximity of the oroclines and is observed in other parts of southeast Queensland and northern New South Wales. For example, sinistral-reverse sense

of movement has been recognised along the NNW-striking North Pine Fault System (NPFS) and West Ipswich Fault System (WIFS) (Figure 2.1b) (Babaahmadi and Rosenbaum, 2014b, a; Babaahmadi et al., 2015).

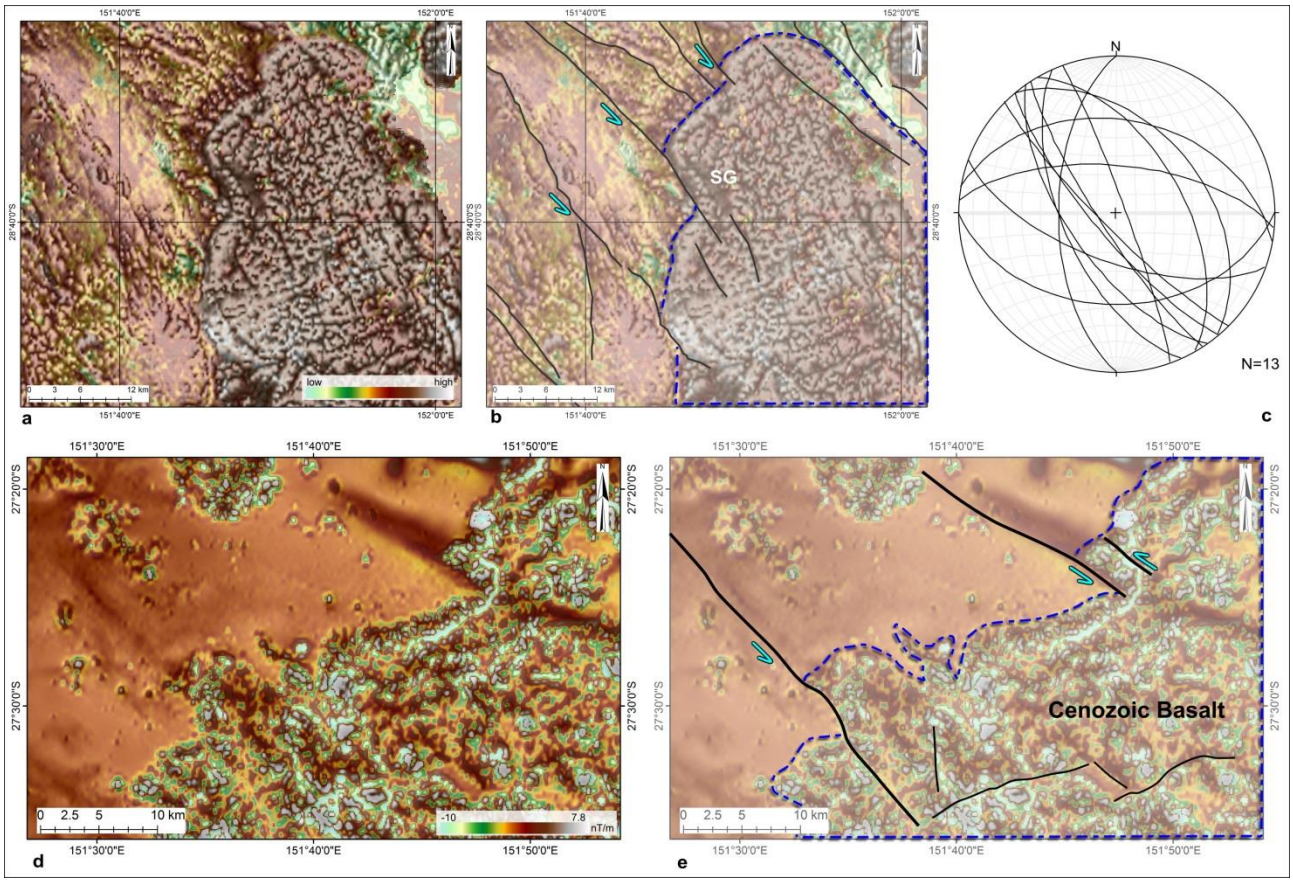

Figure 2.9. (a-b) Potassium radiometric image overlaying tilt angle map of eastern part of the Texas Orocline indicates that a series of parallel NW-striking faults sinistrally displaced the western margins of the Stanthorpe Granite (SG) (see Figure 2.7b for location). (c) Lower hemisphere stereographic projection of fault planes in eastern part of the Texas Orocline. (d-e) Interpretation of the first vertical derivative map of aeromagnetic data shows the sinistral separation of the contacts of the Cenozoic volcanic rocks, expressed by small curvy short-wavelength magnetic bodies, by NW-striking faults in the eastern limb of the Texas Orocline (see Figure 2.5b for location).

Unfortunately, the timing of sinistral movement along NW-striking faults and dextral movement along NNE- and NE-striking faults is not well constrained. However, the results of this study, together with observations from recent studies, indicate that these faults displaced Mesozoic and Cenozoic rock units (Figures 2.2, 2.3, 2.9, 2.10c-d) (Babaahmadi and Rosenbaum, 2013, 2014b, a; Babaahmadi et al., 2015). Based on these observations, Babaahmadi and Rosenbaum (2014a,b) suggested that NW- and NNW-striking sinistral faults, and NE- and NNE-striking dextral faults have intermittently been reactivated since the Late Cretaceous.

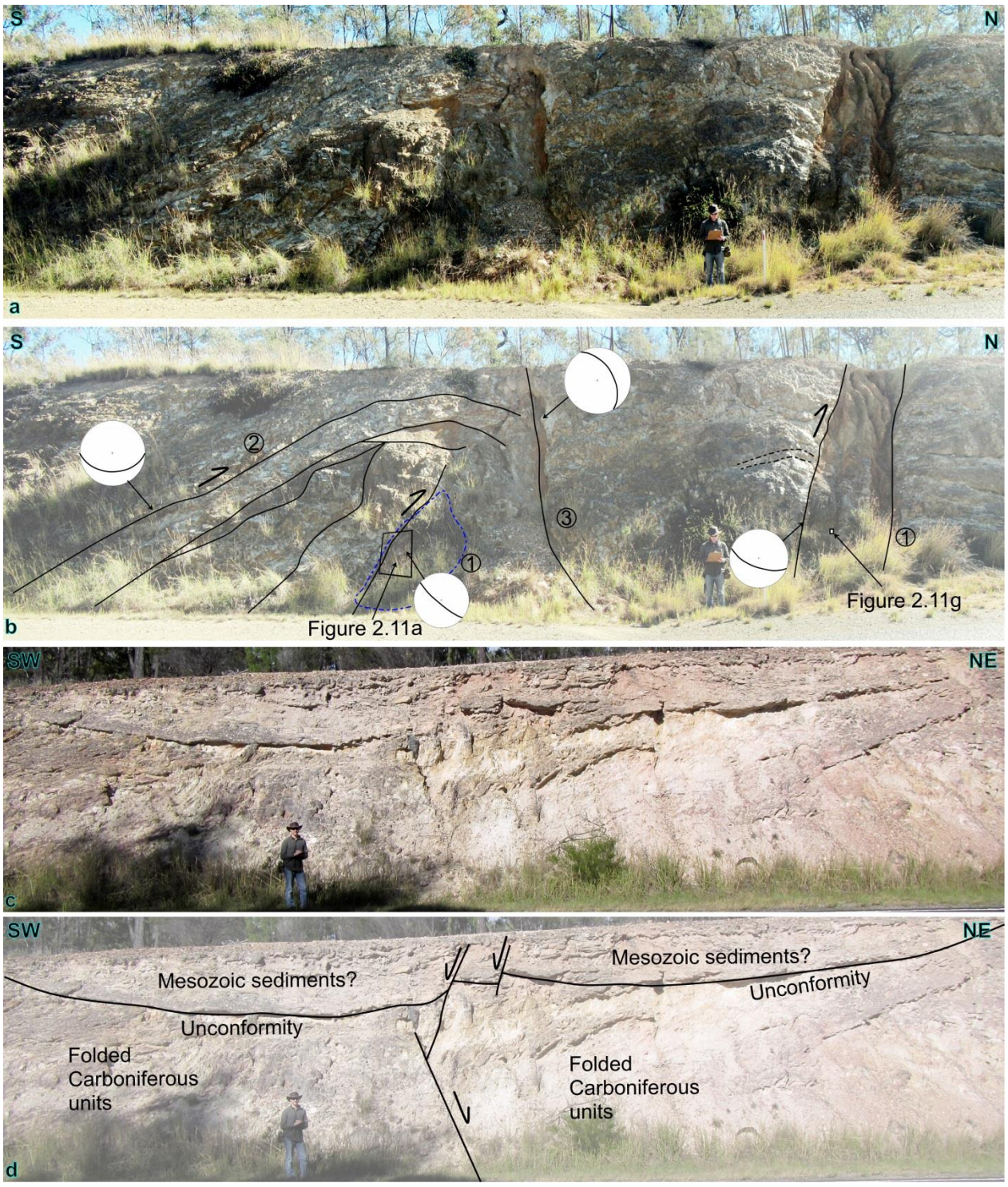

Figure 2.10. (a-b) Field photo of a NW-striking fault cataclastic zone (fault no.1 in Figure 2.7b) overprinted by a brittle E-W thrust (2) and a NW-striking fault (3). Blue dashed line is one of the cataclastic zones. (c-d) NW-striking steep fault (fault no.3 in Figure 2.7b) in the Texas beds, and antithetic normal faults that displaced the overlying (Mesozoic?) sandstone. The wedge-shaped thickening of the sandstone layers in the hanging-wall of one of antithetic faults suggests syn-tectonic deposition.

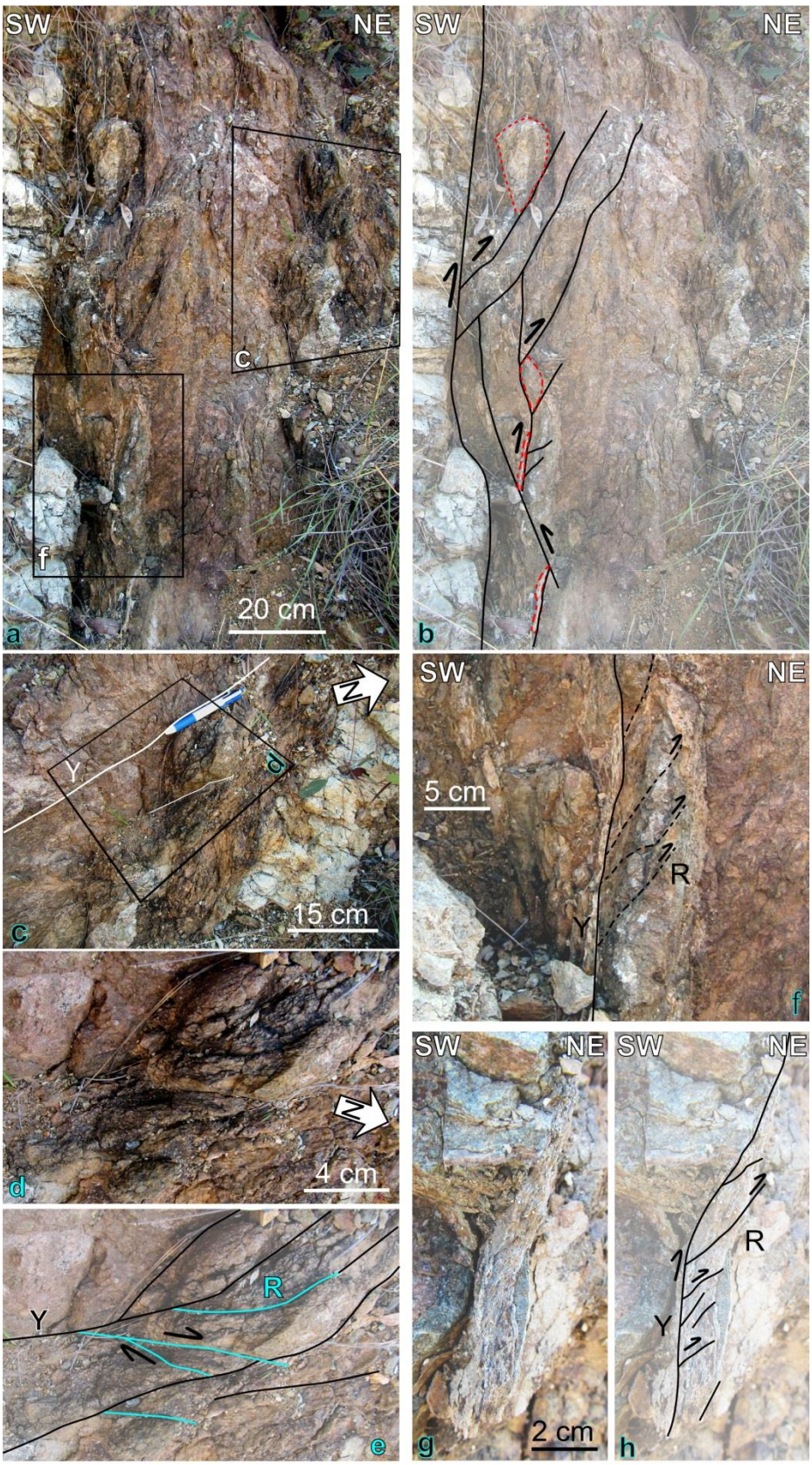

Figure 2.11. (a-b) A cataclastic zone associated with fault no.1 (cross-section view), showing synthetic reverse shears (R) indicative of a reverse kinematics (see Figure 2.10 for location). (c-e) Dextral Y-R shears (map view). (f-h) Synthetic reverse faults (R) (cross-section view) (see Figure 2.10 for location).

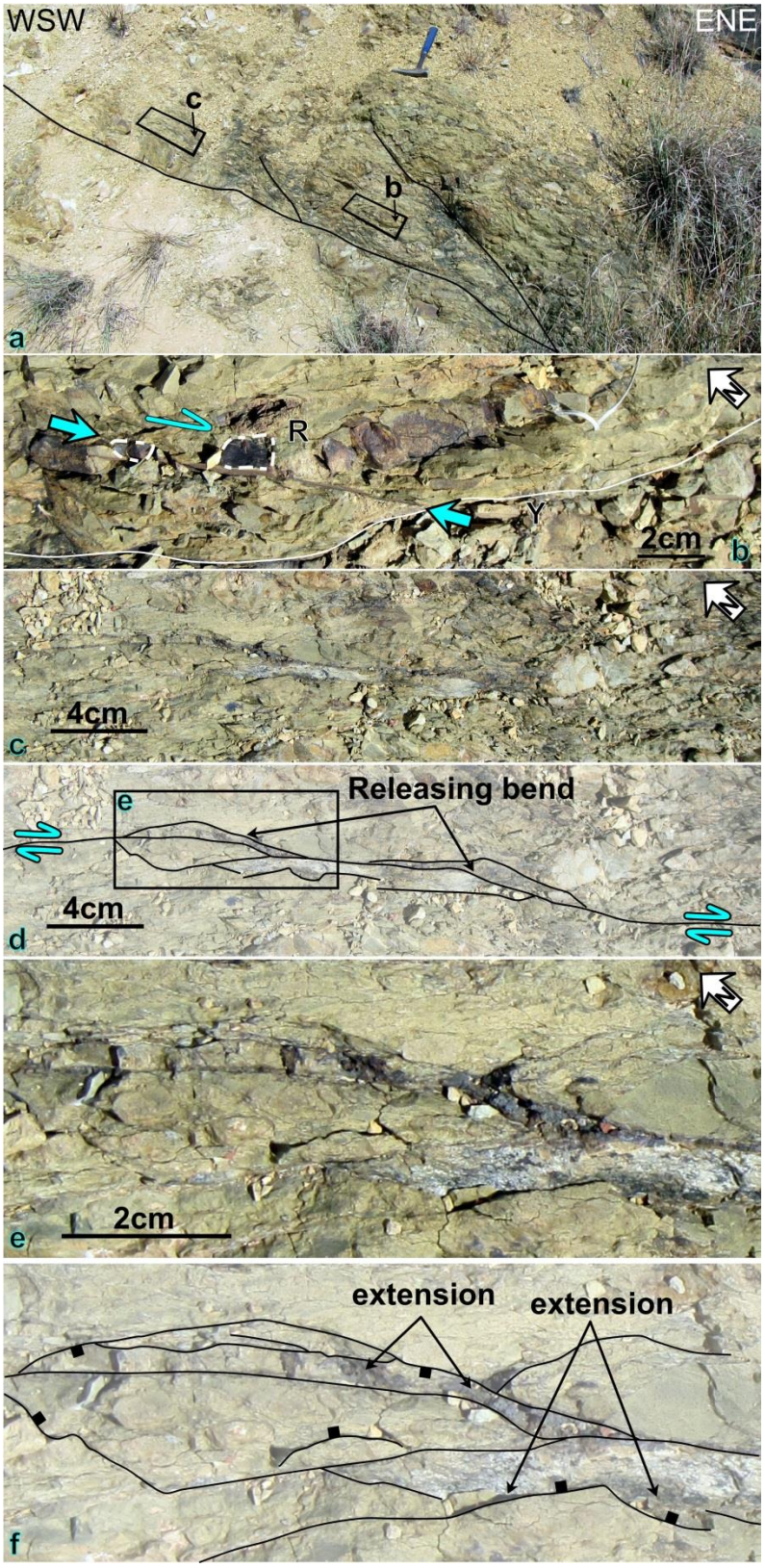

Figure 2.12. (a) A NW-striking fault zone (fault no.2 in Figure 2.7b) within the Texas beds. (b) A dextral Riedel shear (R). (c-f) An outcrop-scale dextral fault (Y) with releasing bends that produced pull-apart basins.

Specifically, fault reactivation may have occurred due to (1) oblique extensional episodes during the NNE-SSW opening of the Tasman and Coral Seas from the Late Cretaceous to early Eocene (~84-65 Ma) (Weissel and Watts, 1979; Gaina et al., 1998a; Gaina et al., 1998b; Dyksterhuis et al., 2005b)

(Figure 2.14a); and (2) compressional far-field stresses transmitted from the northeastern, eastern, and southeastern boundaries of the Australian Plate during the late Eocene-early Oligocene, late Oligocene-early Miocene, and possibly Pliocene-Quaternary (Babaahmadi and Rosenbaum, 2014b, a) (Figure 2.14b-c).

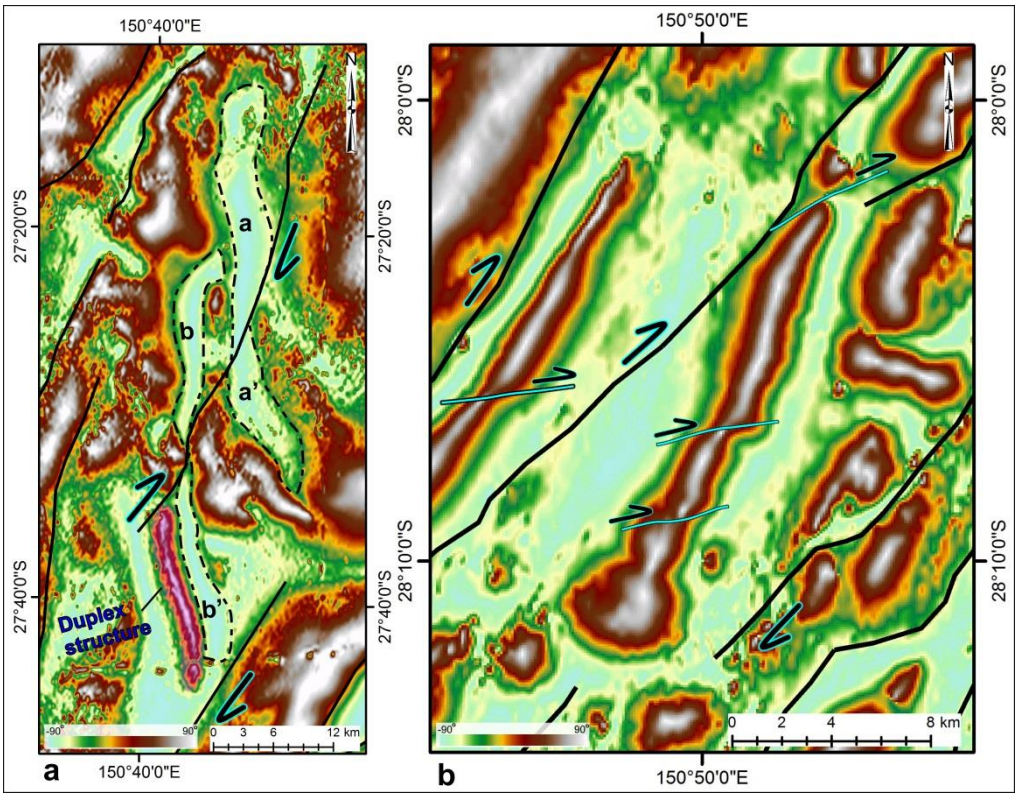

Figure 2.13. (a) A NE-striking fault that displaces low magnetised bodies dextrally. (see Figures 5b for location). (b) Dextral shearband boudins in the western limb of the Texas Orocline are indicative of dextral movement along NE-striking faults (see Figure 7b for location).

Two NW-striking sinistral faults, which displaced Triassic granitoids, in the western limb of the Coffs-Harbour Orocline were displaced by the southern segment of the N-striking dextral Demon Fault (Figure 2.3) (Babaahmadi and Rosenbaum, 2013). Babaahmadi and Rosenbaum (2013) suggested that the Demon Fault was active during the Mesozoic, possibly during the Late Triassic to Jurassic development of sedimentary basins in eastern Australia. They also suggested that the latest component of the dextral movement (with a reverse component) along the Demon Fault could be due to the far-field stress fields from the oblique collisional event at the northern margin of New Guinea possibly during the Miocene with a possible ENE-WSW maximum horizontal stress (Muller et al., 2012), possibly led to the southward development of the southern segment of the Demon Fault (Figure 2.14c). Given these facts, the sinistral movement along the NW-striking faults, which have been offset by the Demon Fault, possibly occurred before the activity of the Demon Fault either in the Mesozoic or Miocene. If I assume that these NW-striking sinistral faults have been offset by the Demon Fault during the Mesozoic, it would imply that these faults were active sometimes in the early Mesozoic,

but the exact timing of faulting remains unknown. Alternatively, if they have been offset by the Demon Fault during the Miocene, the sinistral movement of these faults was probably due to Late Cretaceous-early Eocene extensional events. The latter interpretation seems to be more reasonable, as most of other NW-striking sinistral faults are younger than early Mesozoic as discussed above.

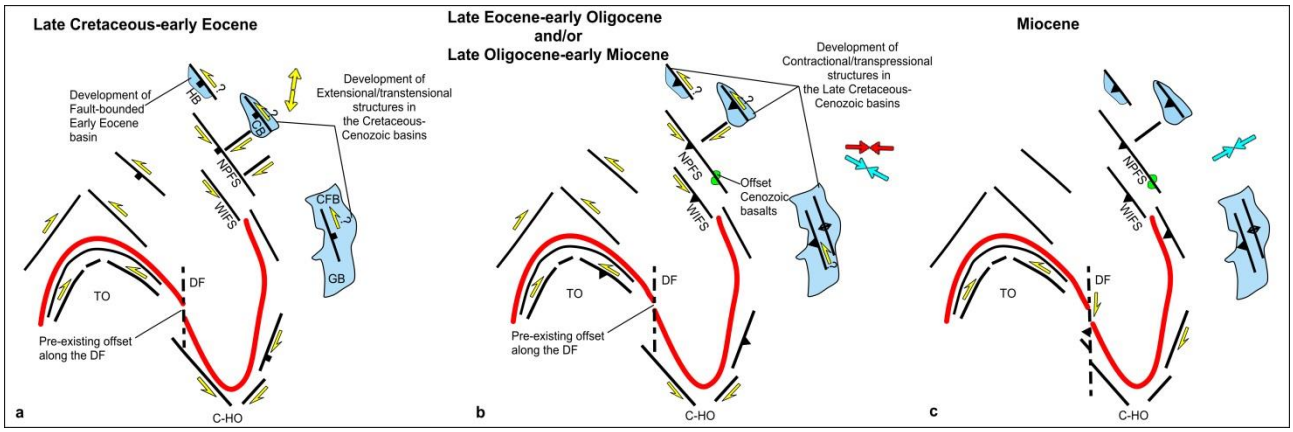

Figure 2.14. (a-c) Schematic structural model showing possible tectonic causes of the NW-striking sinistral faults and NNE- and NE-striking dextral faults around the Texas and Coffs-Harbour oroclines from the Late Cretaceous-early Eocene oblique extensional tectonics to Cenozoic contractional events (not to scale). Large yellow arrows show the average horizontal tensional stress direction during the Late Cretaceous to Eocene (Gaina et al., 1998a; Gaina et al., 1998b; Dyksterhuis et al., 2005b), blue and red arrows show the maximum horizontal compressive stress (Dyksterhuis et al., 2005b; Muller et al., 2012; Babaahmadi and Rosenbaum, 2014a). Note that a component of dextral movement could occur along the Demon Fault during the Miocene (Babaahmadi and Rosenbaum, 2013) in response to ENE-trending maximum horizontal compressive stress (Muller et al., 2012) displacing some NW-striking sinistral faults. Contractional or extensional events in sedimentary basins have been provided by different authors (Clarke et al., 1971; Gray, 1976; Willcox and Sayers, 2002; Colwell et al., 2010). CB, Capricorn Basin; CFB, Capel and Faust Basins, C-HO, Coffs-Harbour Orocline; DF, Demon Fault; GB, Gower Basin; NPFS, North Pine Fault System; TO, Texas Orocline; WIFS; West Ipswich Fault System.

In contrast to the dominant sinistral kinematics that is recognised along the NW-striking faults, two of the field localities (faults no.1, 3) in the Texas Orocline indicate dextral strike-slip and oblique reverse-dextral movement, respectively (Figures 2.10-2.12). Field observations of fault no.1 show that this fault was displaced by younger faults (Figure 2.10). Furthermore, interpretation of aeromagnetic data show that fault no.3 was displaced by a NNW-striking sinistral fault (Figure 2.8). These observations may suggest that the dextral movement along some of NW-striking faults predated the dominant sinistral kinematics. The fact that fault no.1 was active as an oblique reverse-dextral fault may suggest contractional faulting prior to the Late Cretaceous-early Eocene oblique extensional events. There are two possible tectonic causes for this oblique reverse dextral movement along NW-striking faults. The first possibility is that this kinematics could be related to a contractional event in the early Late Cretaceous, which supposedly reactivated basement faults in the

Bowen and Surat basins (Moonie event) (Korsch et al., 2009b; Raza et al., 2009) and the Maryborough Basin (Hill, 1994). Alternatively, the reverse-dextral movement along these NW-striking faults could be related to the last phase of Hunter-Bowen contractional deformation in the early Late Triassic (Holcombe et al., 1997b; Korsch et al., 2009b; Babaahmadi et al., 2015). This event is expressed by reverse faults in the youngest units of the Bowen Basin (Goondiwindi event) (Korsch et al., 2009b), the deformation of the Kin Kin beds in the Gympie Terrane, and folding and thrusting in the Early-Middle Triassic rock units of the Esk Trough and the Nymboida Coal Measures (Holcombe et al., 1997b; Babaahmadi et al., 2015). Holcombe et al. (1997b) provided evidence of dextral movement along NNW-striking faults during this event based on the angular relationships between fold axial traces and faults in the Esk Trough.

2.5.2. Faulting during Early to Middle Permian oroclinal bending

Based on the results of this study, I cannot unambiguously conclude that faults were active during the development of the oroclines in the Early-Middle Permian. Nevertheless, a number of lines of evidence support this idea (Figure 2.15). Firstly, in a recent paper on the Red Rock Fault Zone (Rosenbaum et al., 2015), Rb-Sr and ^{40}Ar-^{39}Ar geochronological data from fault gouge illites were presented that support an Early-Middle Permian (288-264 Ma) age of deformation. Secondly, NW-striking Early Permian basins in the eastern limb of the Texas Orocline are bounded by steep orocline-parallel faults (Figure 2.6), indicating that these faults have potentially been active during the Early Permian with an extensional component (Lennox and Flood, 1997; Campbell, 2014). Similar faults that bound subsurface Early Permian basins have also been recognised in the western limb of the Texas Orocline beneath younger sedimentary cover (Brooke-Barnett and Rosenbaum, 2015).

The pattern of faults parallel to the Texas and Coffs-Harbour oroclines suggests that flexural slip was likely one of the structural mechanisms that allowed oroclinal bending (Figure 2.15). Some fault lineaments seem to be curved around the hinges of the Texas and Coffs-Harbour oroclines (Figures 2.3, 2.5, 2.7), indicating that they originated prior to the development of the oroclines. These orogen-parallel faults were likely rotated and underwent some slip during oroclinal bending.

The kinematics of faults during the Early-Middle Permian is unknown. However, the flexural slip model would imply dextral kinematics along NNE- and NE-striking faults, and sinistral kinematics along NW-striking faults (Figure 2.15). This kinematic pattern is similar to the dominant kinematics associated with fault reactivation, as discussed in the previous section, as well as with the expected kinematics associated with ~E-W contraction during the Late Permian Hunter-Bowen Orogeny.

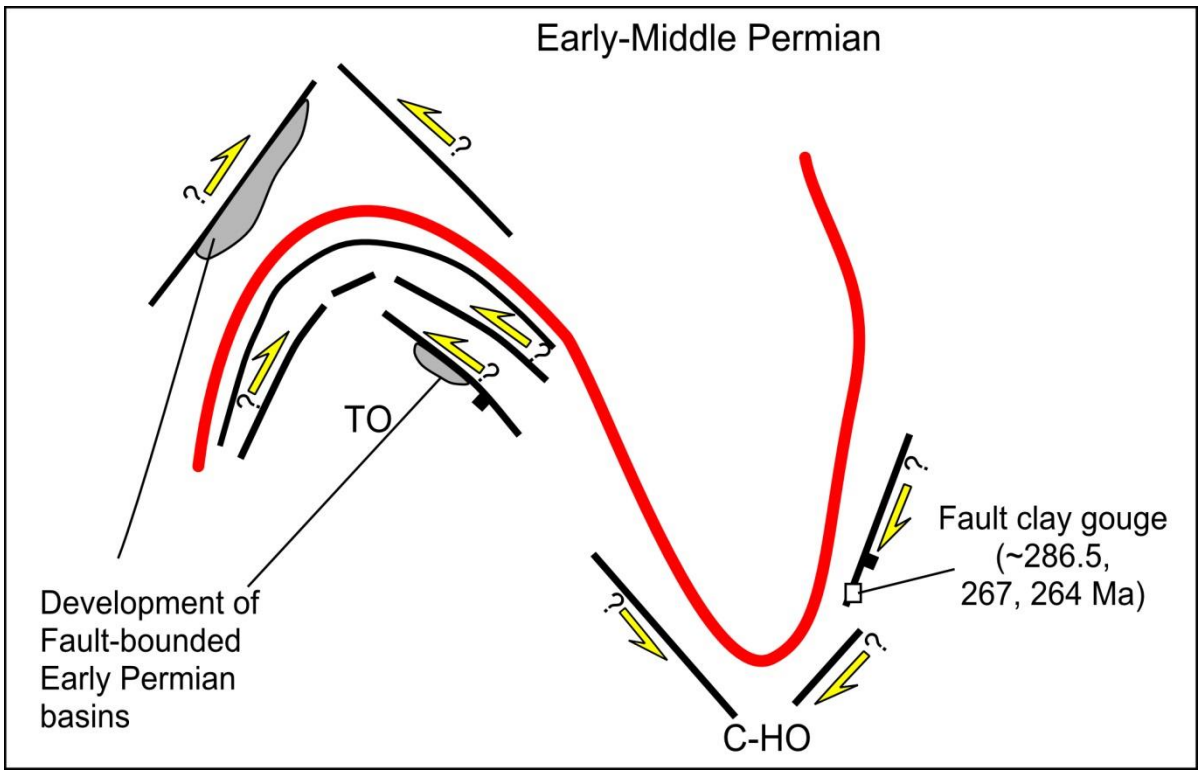

Figure 2.15. Schematic structural model showing the possible role of flexural slip during Early-Middle Permian oroclinal bending (not to scale). The evidence of Early Permian fault bounded basins is discussed in Lennox and Flood (1997), Campbell (2014) and Brooke-Barnett and Rosenbaum (2015). The geochronological data of a NNE-striking fault clay gouge in the eastern limb of the Coffs-Harbour Orocline is after Rosenbaum et al. (2015).

2.6. Conclusions

The results show that fault systems with a strike-slip separation are parallel to the Texas and Coffs-Harbour oroclines. The observation of orocline-parallel high-angle faults is consistent with the idea that oroclinal bending was at least partly facilitated by a flexural slip mechanism. The observed dominant kinematics along the orocline-parallel faults is younger, and was likely associated with reactivation episodes during the Mesozoic and Cenozoic.

Chapter 3

Alternating episodes of extension and contraction during the Triassic: Evidence from Mesozoic sedimentary basins in eastern Australia

Alternating episodes of extension and contraction during the Triassic: Evidence from Mesozoic sedimentary basins in eastern Australia

Abstract

Triassic to Early Cretaceous continental sedimentary basins occur in eastern Australia, but the tectonic and structural evolution of these basins is not fully understood. Using gridded aeromagnetic data, seismic reflection data, and field observations, I conducted a structural analysis aimed at characterising major faults and deformation style in these sedimentary basins. The results show evidence for two alternating episodes of rifting during the Triassic. An earlier episode of rifting, that took place in the Early Triassic to early Late Triassic, is inferred based on synsedimentary normal faults in the Nymboida Coal Measures and the boundary West Ipswich Fault System in the Esk Trough. This phase of rifting was followed by a contractional event that resulted in tilting, folding, and thrust faulting. Evidence of synsedimentary normal faults and bimodal volcanism indicates that another rifting phase occurred during the Late Triassic and resulted in the development of the Ipswich Basin. From the latest Late Triassic to the Early Cretaceous, the accumulation of continental sediments in the Clarence-Moreton Basin was accompanied by subsidence. I suggest that the alternating rifting episodes and contraction were ultimately controlled by plate boundary migration and switches between trench retreat and advance during the Triassic.

Keywords: Mesozoic, eastern Australia, Esk Trough, Nymboida Coal Measures, syn-sedimentary normal faults, Ipswich Basin, Clarence-Moreton Basin

3.1. Introduction

Sedimentary basins that developed from the Early Triassic to Early Cretaceous occupy a large portion of eastern Australia (Figure 3.1a) (Cranfield et al., 1976; Harrington and Korsch, 1985; Korsch et al., 1989; Hill, 1994; Campbell, 2005). The development of these basins has been attributed to extensional and/or transtensional deformation (Evans and Roberts, 1980; Korsch et al., 1989; O'Brien et al., 1994). However, the nature and origin of this deformation is not fully understood and warrants further investigation of the structures associated with the sedimentary basins.

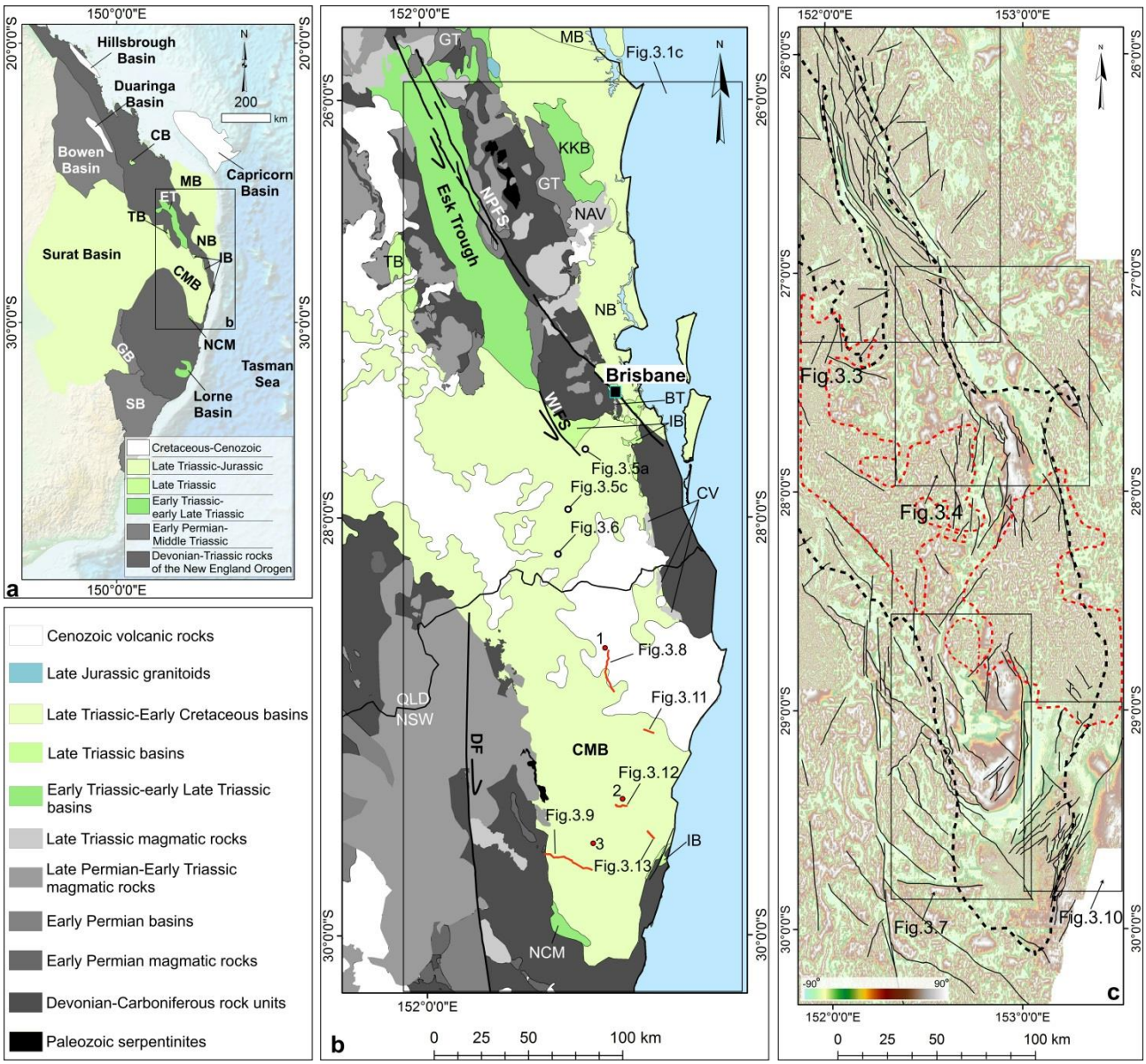

Figure 3.1. ETOPO1 digital elevation model of the Australian and Pacific plates (Amante and Eakins, 2009), and a simplified tectonic framework showing Mesozoic sedimentary basins in eastern Australia. CB, Callide Basin; CMB, Clarence-Moreton Basin; ET, Esk Trough; GB, Gunnedah Basin; IB, Ipswich Basin; MB, Maryborough Basin; NB, Nambour Basin; NCM, Nymboida Coal Measures; SB, Sydney Basin; TB, Tarong Basin. (b) Simplified geological map of southeast Queensland and northeast NSW (see Figure 3.1a for location) based on 1:250,000 (Maryborough, Dorrigo–Coffs Harbour, and Grafton–Maclean) and 1:500,000 (Moreton) geological maps (Ellis, 1968; Green et al., 1980; Gilligan et al., 1992; Henley et al., 2001). Red lines are seismic lines used in this study, and red points are deep petroleum well data: (1) Kyogle-1, (2) Tullymorgan-1, and (3) Clifden-3. BT, Brisbane Tuff; CV, Chillingham Volcanics; DF, Demon Fault; GT, Gympie Terrane; IB, Ipswich Basin; KKB, Kin Kin beds; MB, Maryborough Basin; NAV, North Arm Volcanics; NB, Nambour Basin; NCM, Nymboida Coal Measures; NPFS, North Pine Fault System; TB, Tarong Basin; WIFS, West Ipswich Fault System. (c) Tilt map of gridded aeromagnetic data (see Figure 3.1b for location). The boundary of the Mesozoic sedimentary basins is indicated by a black dashed line. The red dashed line outlines short-wavelength magnetic bodies related to Cenozoic volcanic rocks

This paper focuses on the Mesozoic Esk Trough, Nymboida Coal Measures, Ipswich Basin, and Clarence-Moreton Basin (Figure 3.1a, b). The development of these basins initiated in the Early Triassic (Esk Trough), Middle Triassic to early Late Triassic (Nymboida Coal Measures) and Late Triassic (Ipswich and Clarence-Moreton basins), in a tectonic setting that was relatively proximal to the west-dipping subduction boundary (unlike the larger foreland basins farther west; Figure 3.1a). As such, structures associated with these basins may provide a record of overriding-plate deformation that could underpin spatial and temporal changes in the geodynamics of the convergent boundary.

Here, I present results from an investigation of fault systems in the Mesozoic basins of southeast Queensland and northeast New South Wales (NSW). I conducted a structural synthesis by utilising gridded aeromagnetic data, seismic reflection data, and field observations. The results, which show evidence for at least two periods of extension during basin formation in the Triassic, are then discussed in the context of the structural and tectonic evolution of eastern Australia during the Mesozoic.

3.2. Geological setting and stratigraphy

The study area comprises a series of sedimentary basins overlying older Paleozoic and early Mesozoic rocks of the New England Orogen (Figure 3.1b). The New England Orogen includes Devonian–Carboniferous subduction-related units, some older remnant of early Paleozoic ophiolitic assemblages, and Permo-Triassic magmatic rocks and sedimentary basins (Figure 3.1b) (Leitch, 1975; Day et al., 1978; Henderson et al., 1993; Holcombe et al., 1997a).

The early Permian rocks in the New England Orogen supposedly originated in an extensional setting, possibly a backarc environment. Backarc extension resulted in the development of widespread sedimentary basins (Sydney, Gunnedah and Bowen basins; Figure 3.1a) that continued to receive sediments until the Middle Triassic (Kassan, 1994; Korsch et al., 2009a). The episode of early Permian extension was accompanied by the emplacement of S-type granitoids (298–288 Ma) and involved oroclinal bending in the southern New England Orogen (Cawood et al., 2011b; Glen and Roberts, 2012; Rosenbaum, 2012; Rosenbaum et al., 2012). The geodynamic setting that controlled oroclinal bending was possibly associated with a combination of trench retreat, subduction segmentation and wrench faulting (Rosenbaum et al., 2012; Shaanan et al., 2014). Following the period of extension, from the late Permian to early Late Triassic (270–235 Ma), the New England Orogen was subjected to pronounced phases of contractional deformation, commonly referred to as the Hunter-Bowen Orogeny (Holcombe et al., 1997b; Korsch et al., 2009b). This deformation was accompanied, at 260–230 Ma, by widespread calc-alkaline magmatism (Day et al., 1978; Shaw and Flood, 1981; Holcombe et al., 1997b; Korsch et al., 2009b; Shaw and Flood, 2009; Li et al., 2012b).

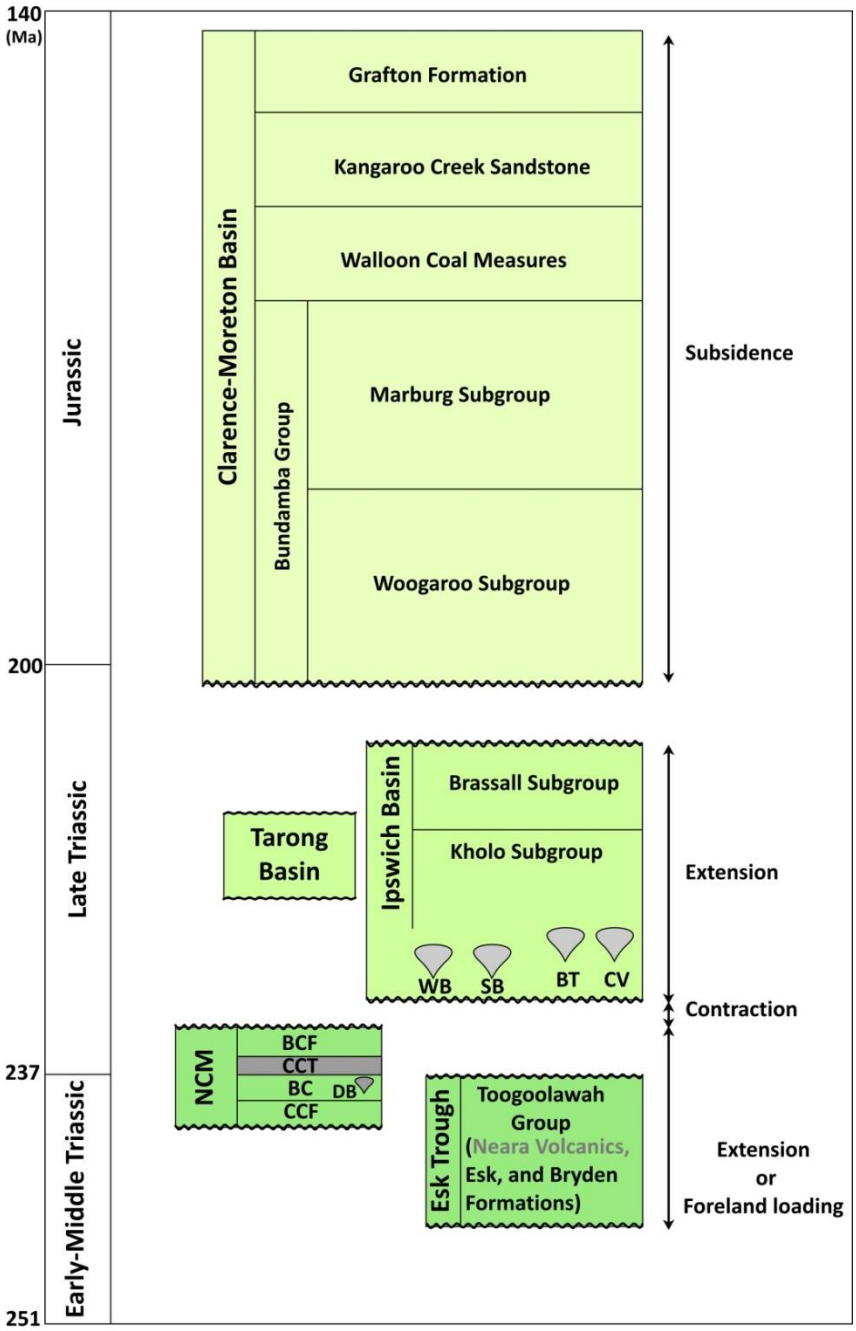

Figure 3.2. A schematic time–space chart showing main Triassic–Jurassic stratigraphic units and unconformities in the study area (McElroy, 1975; Cranfield and Schwarzbock, 1976; Cranfield et al., 1976; Wells and O'Brien, 1994), as well as major deformation phases (Evans and Roberts, 1980; Korsch et al., 1989; Holcombe et al., 1997b; Campbell, 2005), and magmatic events in the basins (McElroy, 1975; Cranfield and Schwarzbock, 1976; Purdy and Cranfield, 2013; Purdy and Cross, 2013). BC, Bardool Conglomerate; BCF, Basin Creek Formation; BT, Brisbane Tuff; CCF, Cloughers Creek Formation; CCT, Copes Creek Tuff; CV, Chillingham Volcanics; DB, Dalmally Basalt; NCM, Nymboida Coal Measures; SB, Sugars Basalt; WB, Weir Basalt.

The Paleozoic rocks of the New England Orogen are overlain by Early Triassic to Early Cretaceous sedimentary basins, which are predominantly composed of continental detrital sediments. One of the Triassic basins is the NNW-striking Esk Trough in southeast Queensland (Cranfield et al., 1976;

Campbell et al., 1998), which extends over a distance of ~260 km and has a maximum width of ~35 km (Figure 3.1b). The Triassic sedimentary fill of the Esk Trough belongs to the Toogoolawah Group, which includes continental volcaniclastic conglomerate, sandstone, and shale (the Bryden and Esk formations), and intermediate volcanic rocks (the Neara Volcanics) (Figures 3.1b,3. 2) (Cranfield et al., 1976; Campbell, 2005). The exact age of the Toogoolawah Group is not well constrained. Based on the study of miospore fossils in the Toogoolawah Group, and the correlation of miospore assemblages with those in the Moolayember Formation of the Bowen Basin, the age of the Toogoolawah Group has been interpreted to be the Middle Triassic (de Jersey, 1972, 1973). However, Cranfield et al. (1976) suggested an Early–Middle Triassic age for the Toogoolawah Group, as the age of the basal part of the Bryden Formation is unknown. A recalculated age of the Neara Volcanics is ca 242 Ma (Campbell, 2005), also implying a Middle Triassic age.

The Nymboida Coal Measures is interpreted to be a Middle Triassic stratigraphic succession with a maximum thickness of ~1000 m in northeast NSW (Figure 3.1b,3.2) (McElroy, 1975; Webb, 2001). The succession includes the Coughers Creek Formation, Bardool Conglomerate, Copes Creek Tuff, and Basin Creek Formation (Figure 3.2) (McElroy, 1962, 1975; Webb, 2001). The correlation of macroflora in the Nymboida Coal Measures with that in the Esk Trough implies a Middle Triassic age for the Nymboida Coal Measures (Flint and Gould, 1975; Webb, 2001). However, an $^{40}Ar/^{39}Ar$ radiometric age of the Dalmally Basalt Member of the Bardool Conglomerate (Figure 3.2) indicates an age of ca 237 Ma (Middle–Late Triassic boundary) (Retallack et al., 1993), implying that deposition continued in the early Late Triassic. Therefore, I assume that the age of the Nymboida Coal Measures is the Middle Triassic to early Late Triassic.

The Ipswich Basin is a Late Triassic succession with an equivalent age as the Tarong and Callide basins (Figure 3.1a, b) (Wilson, 1975; Cranfield and Schwarzbock, 1976; Jorgensen, 1997). The Ipswich Basin is located in southeast Queensland and northeast NSW (Figure 3.1b) and composed of the Kholo and Brassall subgroups (Figure 3.2), which include sandstone, shale, conglomerate, coal seams, and basal basaltic volcanic rocks and rhyolitic tuff (Cranfield and Schwarzbock, 1976; Cranfield et al., 1976). The basaltic rocks belong to the Weir and Sugars basalts (Purdy and Cranfield, 2013). The age of the Sugars Basalt, based on a recalculation of previously published K–Ar ages (Webb and McNaughton, 1978) is ca 232–229 Ma (Purdy and Cross, 2013).

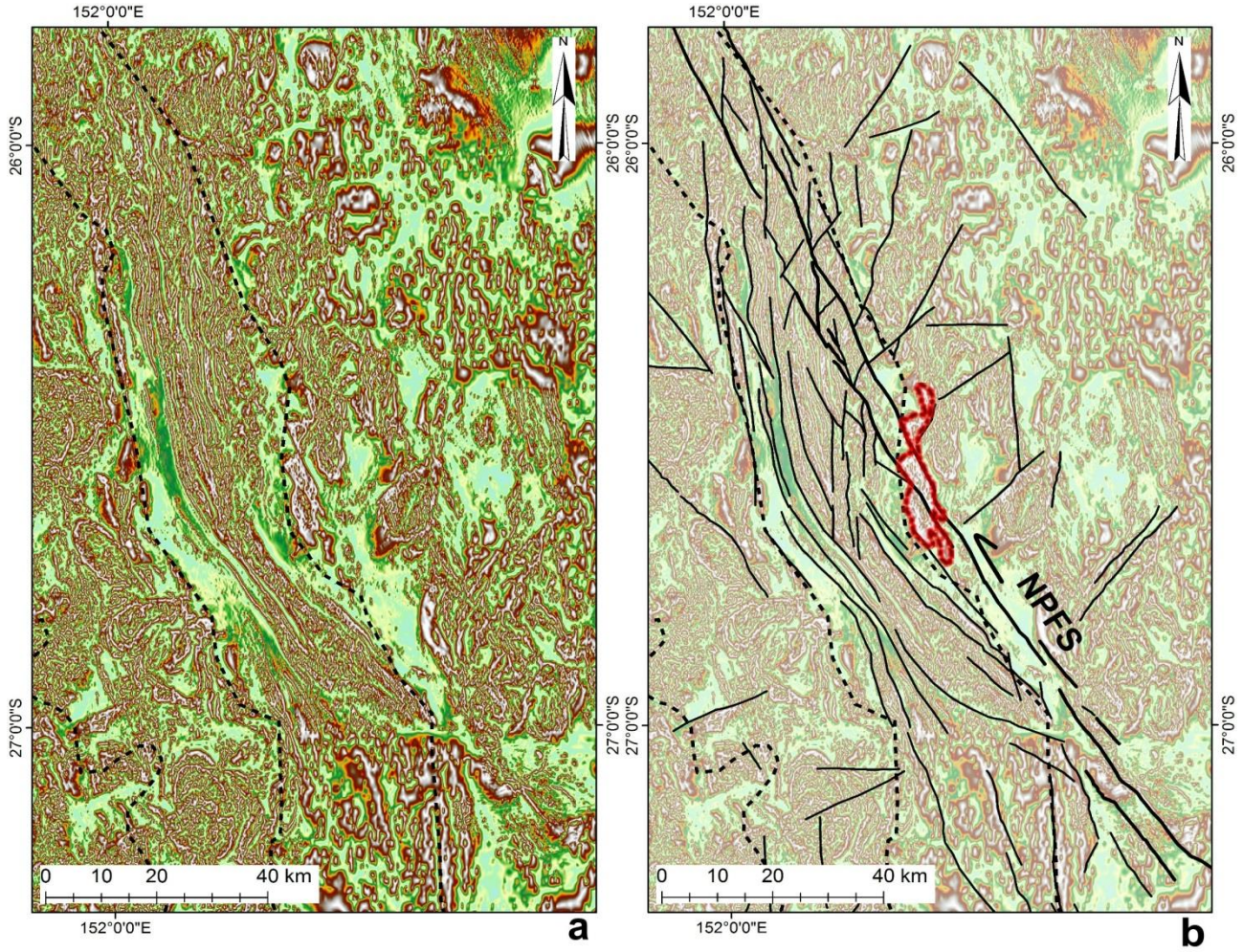

Figure 3.3. (a) Tilt map of gridded aeromagnetic data in the Esk Trough (see Figure 3.1c for location). Dashed line indicates the boundary of the sedimentary basin. (b) Interpretation of the gridded aeromagnetic data showing dominant NNW- to N-striking faults displaced sinistrally by the NPFS.

The sedimentary rocks of the Ipswich Basin unconformably overlie the Late Triassic Chillingham Volcanics (a thick sequence of rhyolite and tuff), which are likely equivalent to the Brisbane tuff (Cranfield et al., 1976; Korsch et al., 1989) (Figures 3.1b, 3.2). The Brisbane Tuff is mainly composed of rhyolitic tuff and is overlain by the Brassall Subgroup of the Ipswich Basin (Cranfield et al., 1976). The Clarence-Moreton Basin in southeast Queensland and northeast NSW overlies the sediments of the Ipswich Basin and Esk Trough (Figure 3.1b) (Wells and O'Brien, 1994; Ingram and Robinson, 1996; Cadman et al., 1998). It is filled with up to 3 km of continental sedimentary rocks (Wells and O'Brien, 1994). Major stratigraphic units in the Clarence-Moreton Basin are presented in Figure 3.2 (Wells and O'Brien, 1994; Ingram and Robinson, 1996).

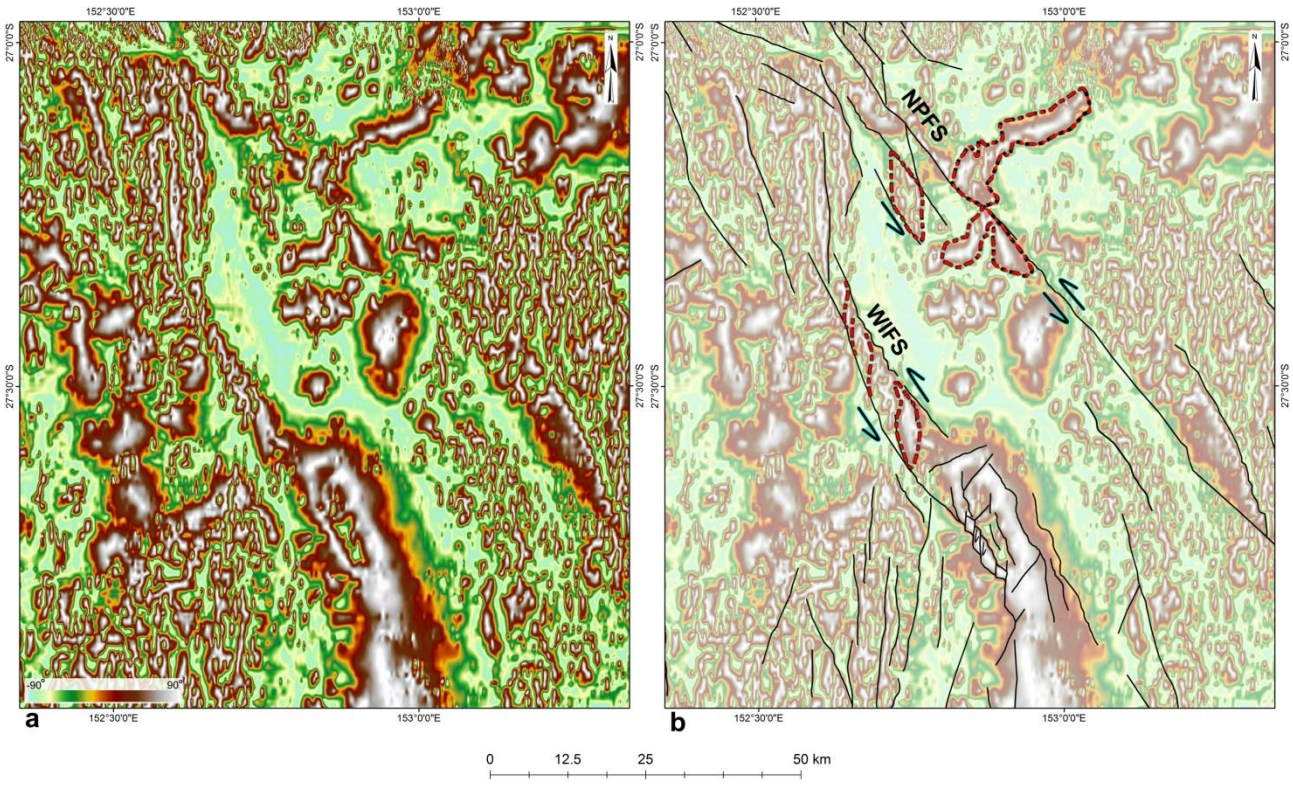

Figure 3.4. (a) Tilt map of gridded aeromagnetic data of the Ipswich and Clarence-Moreton basins (see Figure 3.1c for location). (b) Interpretation of the gridded aeromagnetic data showing NNW-striking faults, such as the NPFS and WIFS, and NNE-striking faults. A sinistral strike-slip kinematics is inferred based on dragging and separation of magnetic bodies (red dashed lines) for NNW-striking faults.

3.3. Methods

I used gridded aeromagnetic data, seismic reflection data, geological maps, and field observations to map faults in selected Mesozoic basins in southeast Queensland and northeast NSW. Due to the limited number of well-preserved outcrops in the study area, gridded aeromagnetic data are the most valuable tools for the recognition of geological structures. In this study, I used gridded aeromagnetic data with spatial resolution of 50 and 80 m, provided by Geoscience Australia and the Resources and Energy division of NSW Trade & Investment. For better recognition of magnetic bodies and faults in Paleozoic basement, I utilised a tilt angle derivative map of reduced-to-pole (RTP) gridded data. Tilt angle derivative is a filter that enhances edges of magnetic sources from both shallow and deep sources, and is calculated as the arc tangent of the ratio of the first vertical derivative to the absolute value of the total horizontal derivatives (Miller and Singh, 1994). The filtered image includes the positive values over magnetic sources, zero values over the edges, and negative values elsewhere (Miller and Singh, 1994). The tilt angle derivative of gridded aeromagnetic data allows us to recognise faults based on: (1) offset and dragging of magnetic anomalies along faults, (2) pronounced structural lineaments, and (3) lensoid and en-echelon structures.

A number of seismic reflection data were utilised to interpret structures in the basins. The seismic data used in this study include DPICM08-03 and DPICM08-05 (Clarence-Moreton Basin Seismic Survey 2008, CD), 84-C3, C90-406, and C90-410 (Onshore Clarence-Moreton Basin Petroleum Data Package, DVDs). Seismic data were provided by the Resources and Energy division of NSW Trade & Investment.

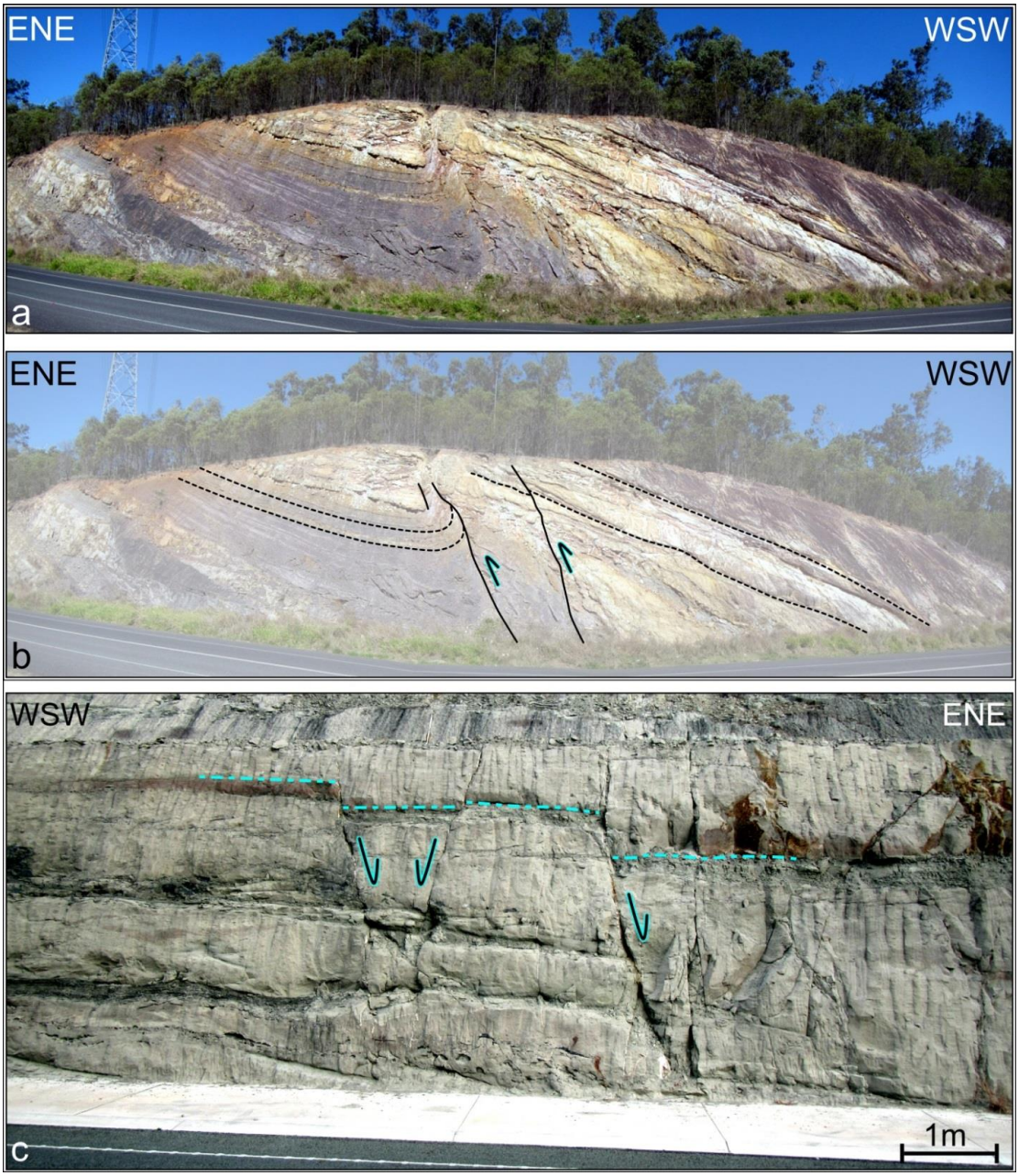

Figure 3.5. (a–b) Field photograph of steep reverse faults associated with the WIFS, which displace rocks of the Woogaroo Subgroup (Clarence-Moreton Basin) (latitude: 27° 40’ 29”S, longitude: 152° 50’ 39”E). (c) Normal faults in the Marburg Subgroup (Clarence-Moreton Basin) (latitude: 27° 55’ 41”S, longitude: 152° 47’ 21”E). The outcrop locations are shown in Figure 3.1b.

3.4. Structure

Structural observations from key localities are presented below. The term “basement faults” is referred to faults that affected Paleozoic rocks of the New England Orogen.

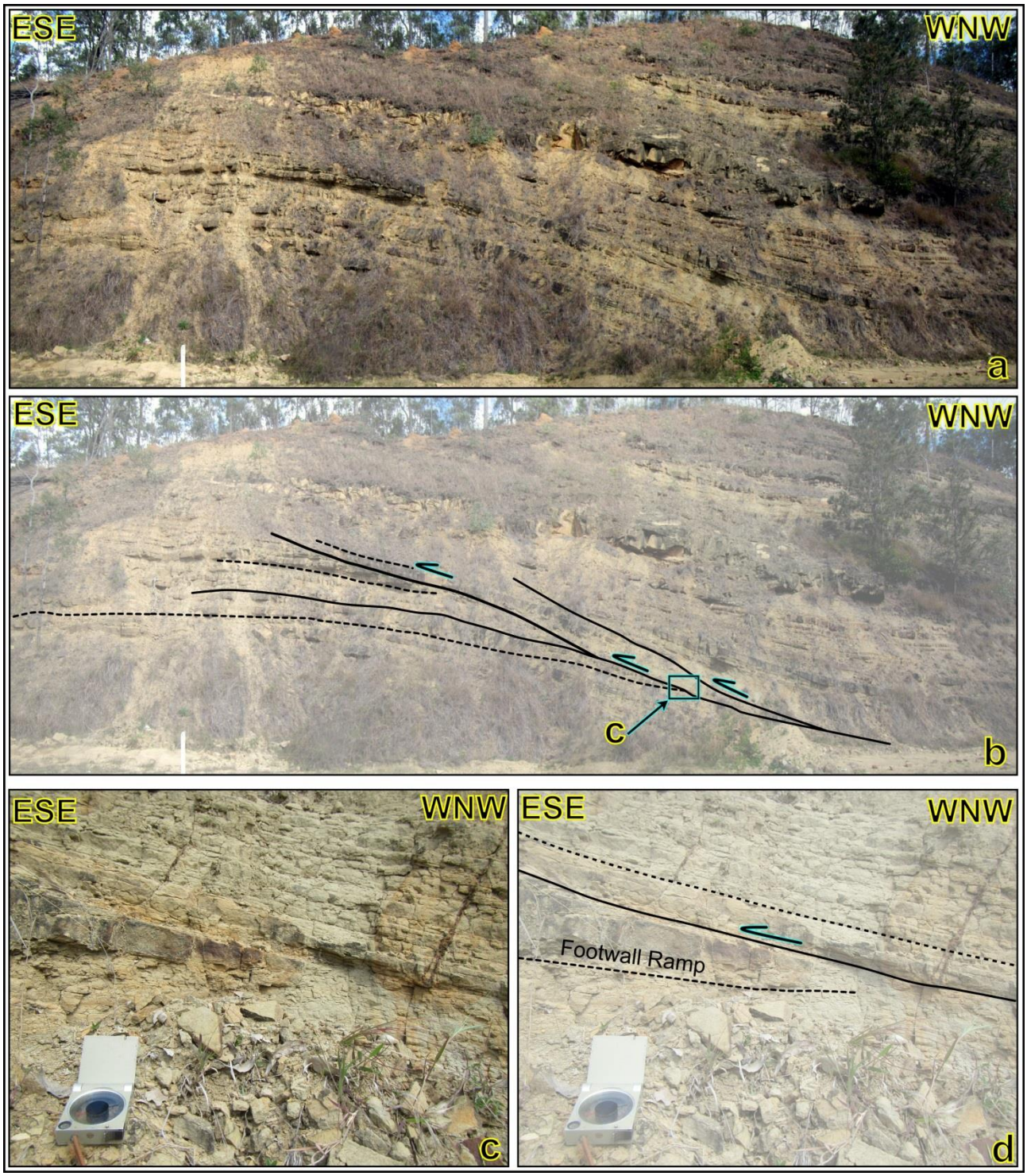

Figure 3.6. (a, b) Shallow thrusts and fault-related fold in the Marburg Subgroup (Clarence-Moreton Basin) (latitude: 28° 12’ 34”S, longitude: 152° 48’ 21”E); (c, d) Discordant bedding planes on both sides of the fault. The outcrop location is shown in Figure 3.1b.

3.4.1. Southeast Queensland

The interpretation of the tilt map shows that the Esk Trough was mainly affected by NW- to N-striking faults (Figure 3.3). These faults were displaced by the post-Triassic sinistral NNW-striking North Pine Fault System (NPFS) (Babaahmadi and Rosenbaum, 2014b). The interpretation of the tilt map indicates that the dominant structures in southeast Queensland are NNE-, NE-, and NNW-striking faults (Figures 3.1c, 3.4). One of the NNW-striking structures is the West Ipswich Fault System (WIFS), which is composed of a broad zone of parallel and subparallel faults (Figure 3.4). Similarly to the NPFS, the tilt map shows that the WIFS sinistrally displaced high-amplitude magnetic bodies that appear as dragged lensoid structures (red lines in Figure 3.4b). The interpretation of the deep seismic section "BMR Traverse 16" by Korsch et al. (1989) indicates that the WIFS is a west-dipping steep fault that controlled the development of the Esk Trough and the Clarence-Moreton Basin. Well data and seismic reflection data indicate that the Esk Trough does not exist east of the fault, and there is no evidence for the Ipswich Basin rocks west of the WIFS (Cranfield et al., 1976; Korsch et al., 1989). Field observations of one branch of the WIFS indicate that steep SW-dipping reverse faults displaced the Woogaroo Subgroup (Figure 3.5a, b).

Other faults in southeast Queensland are NNE- and NE-striking faults, displacing magnetic bodies (Figures 3.1c,3.4). Some faults are young and affected Cenozoic volcanic rocks (Babaahmadi and Rosenbaum, 2014a) (red dashed lines in Figure 3.1c). Field observations show that shallow thrust faults displaced rocks of the Clarence-Moreton Basin. An example of shallow thrusts faults that displaced layers and produced a fault-related fold is presented in Figure 3.6. Several minor normal faults that displaced the Marburg Subgroup are presented in Figure 3.5c.

3.4.2. Northeast NSW

The northeast of NSW is composed of the Nymboida Coal Measures to the south, the Ipswich Basin, and all stratigraphic successions of the Clarence-Moreton Basin (Figures 3.1, 3.2).

3.4.2.1. Western and central parts

The main basement structural features in the western and central parts are N-, NE-, and NW-striking fault lineaments (Figure 3.7). In this area, there are no reliable kinematic indicators, such as dragged and offset features, for N- and NE-striking faults (Figure 3.7). However, these faults are most likely characterised by dextral kinematics, based on information from the eastern part of the Clarence-Moreton Basin (Figure 3.10, see next section), and other parts of northeastern NSW (Babaahmadi and Rosenbaum, 2013; Rosenbaum et al., 2015) and southeastern Queensland (Babaahmadi and

Rosenbaum, 2014b, a). The NW-striking faults have sinistral kinematics, as indicated by the dragging and displacement of magnetic bodies (Figure 3.7b).

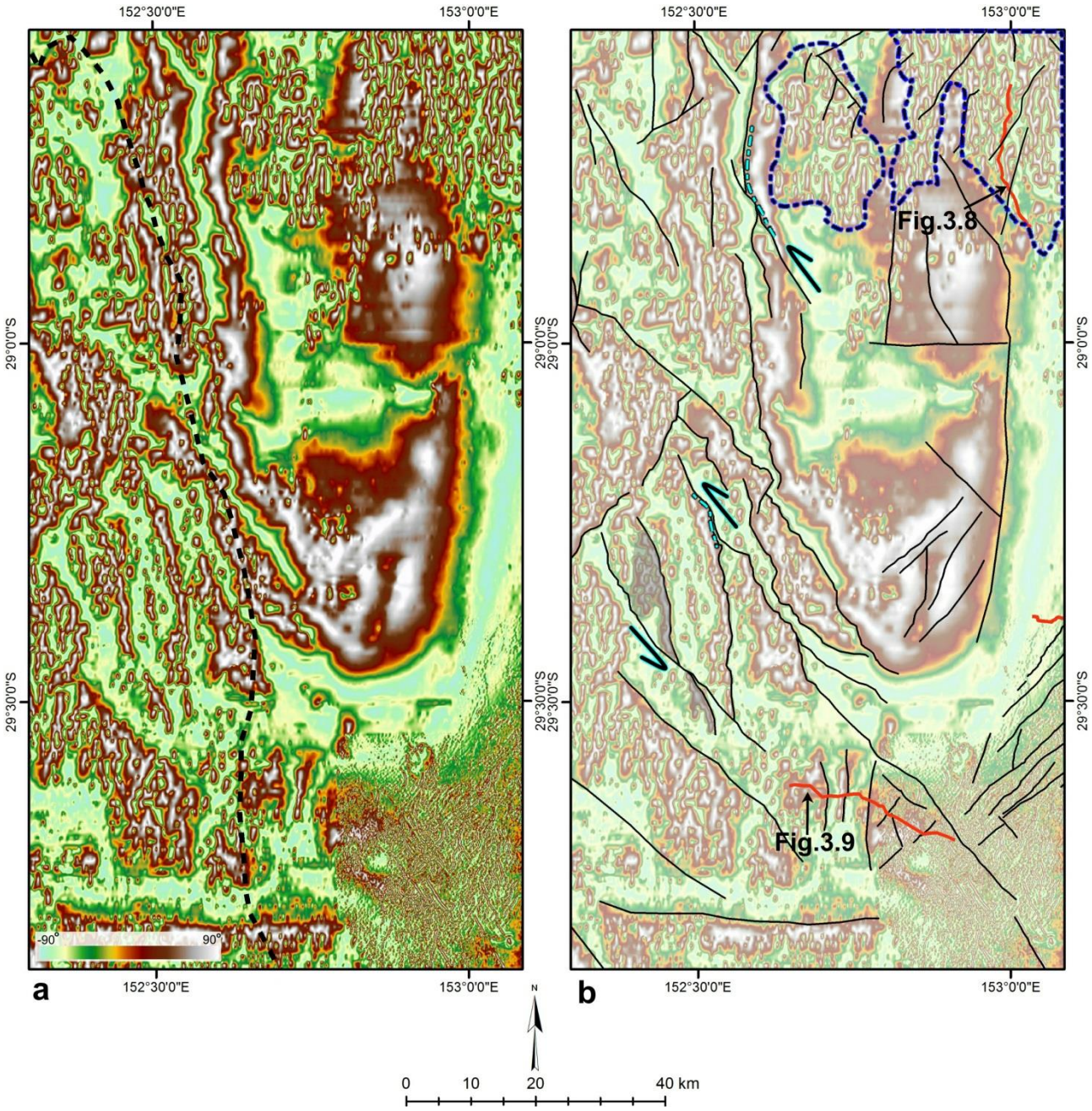

Figure 3.7. (a) Tilt map of gridded aeromagnetic data of the western Clarence-Moreton Basin (see Figure 3.1c for location). Black dashed line indicates the western boundary of the basin. (b) Interpretation of the gridded aeromagnetic data showing sinistral NW-striking faults. Dragged and offset features are shown by light blue dashed lines and grey areas, respectively. Dark blue dashed lines are short-wavelength magnetic sources related to shallow Cenozoic volcanic rocks. Red lines are the locations of seismic lines.

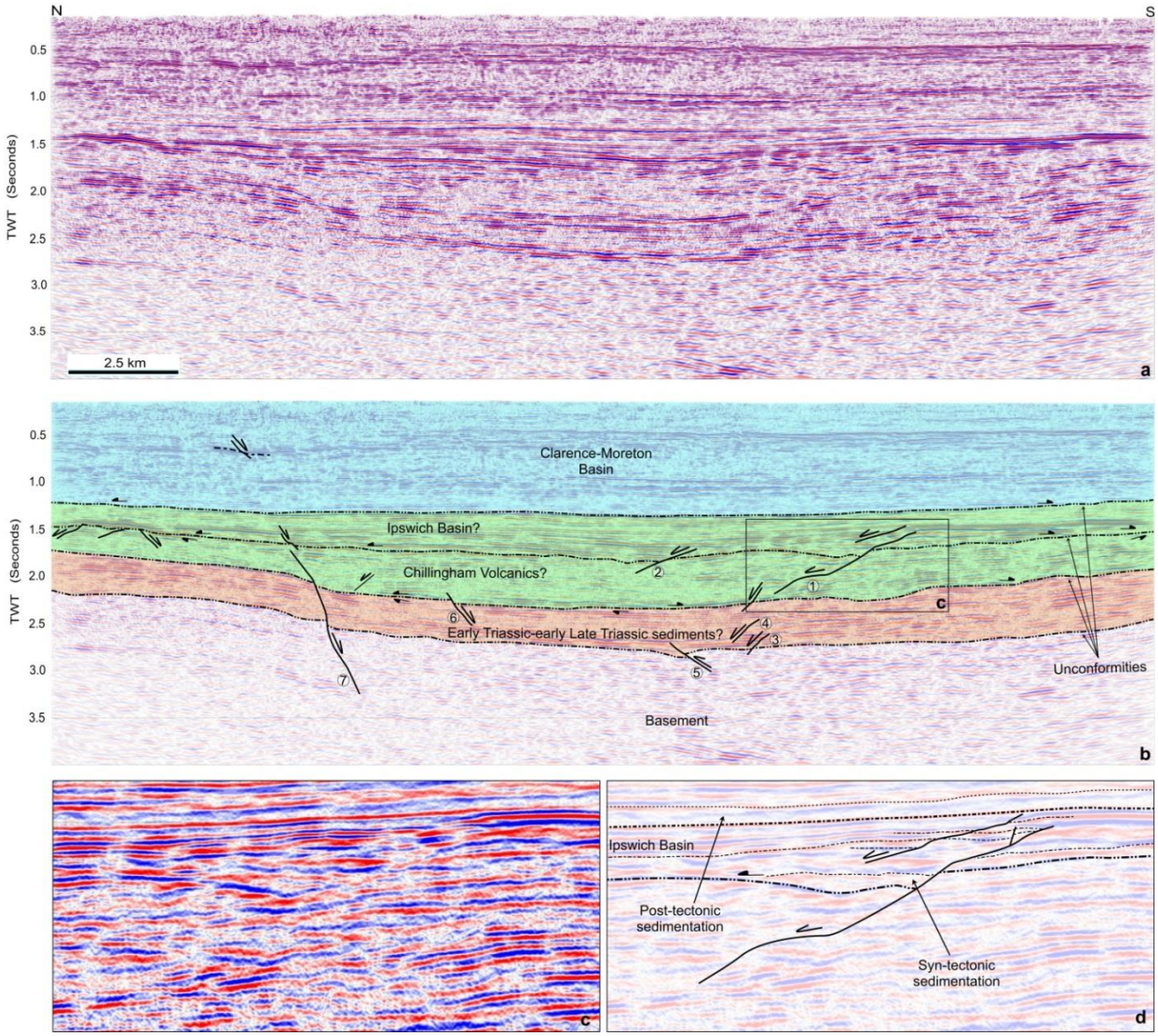

Figure 3.8. (a) Migrated seismic section DPICM08-03 (see Figures 3.1b, 3.7b for location). The time–depth curve of the Kyogle-1 well data (Ingram and Robinson, 1996) was used to estimate the depth of the seismic line, indicating that the vertical to horizontal scale is almost 1:1. (b) Structural interpretation of the seismic section showing normal faults within the Early to Late Triassic successions. The estimated throw (T) and heave (H) are: fault no. 1 (T = 170 m, H = 225 m), fault no. 2 (T = 80 m, H = 250 m), fault no. 6 (T = 115 m, H = 80m), fault no. 7 (T = 100 m, H = 40 m). (c–d) A close-up of a local wedge-shaped stratigraphic thickening in the hanging-wall of the growth fault no. 1, implying syntectonic sedimentation in the Ipswich Basin.

Field evidence of faulting is scarce due to the lack of well-preserved outcrops, but some information on the fault kinematics can be obtained from two seismic reflection data (DPICM08-03 and DPICM08-05). Depositional sequences were defined based on the recognition of four unconformities in the migrated seismic line DPICM08-03 (Figure 3.8b), indicated by discordant relationships between reflectors (Badley, 1985). The horizontal reflectors at the top of the section are interpreted to be sedimentary layers of the Clarence-Moreton Basin (Figure 3.8). These layers unconformably

overlie a succession, which is interpreted as the Ipswich Basin, and is unconformably underlain by two other successions (Figure 3.8). The upper part is characterised by poor data quality zones that may correspond to the Late Triassic Chillingham Volcanics, whereas the lower part possibly represents Early Triassic to early Late Triassic sedimentary units (Figure 3.8). A stratigraphic log from the Kyogle-1 well data (Relph, 1963) (Table 1), which is located ~3 km from the northern end of the DPICM08-03 seismic line, validates the subsurface presence of the Clarence-Moreton Basin, Ipswich Basin, and Chillingham Volcanics. The seismic profile shows that the inferred Ipswich Basin, Chillingham Volcanics, and the Early Triassic to early Late Triassic sedimentary units were displaced by a number of normal faults (Figure 3.8). Faults no. 1 and 2 mainly displaced the Ipswich Basin, whereas Faults no. 3, 4, and 6 displaced the Chillingham Volcanics and the Early Triassic to early Late Triassic sedimentary units (Figures 3.8b–d). Fault no. 7 displaced all Early to Late Triassic units. Fault no. 1 is a listric growth fault, which shows a local wedge-shaped stratigraphic thickening in its hanging-wall, indicating syntectonic sedimentation (Figures 3.8b–d). Fault no. 5 is a reverse fault, displacing the contact between the Early Triassic to early Late Triassic sedimentary units and the basement rocks (Figure 3.8). A small normal fault displaced the Clarence-Moreton Basin units (Figure 3.8b).

The interpretation of the migrated seismic line DPICM08-05 shows two major unconformities that are recognised based on incongruous relationships between reflectors (Figure 3.9). The first unconformity is inferred to be between the Nymboida Coal Measures and the underlying basement rocks of the New England Orogen. A second unconformity is interpreted between the Nymboida Coal Measures and Clarence-Moreton Basin (or Ipswich Basin) (Figure 3.9). The lithological units of the Nymboida Coal Measures and Clarence-Moreton Basin have been documented in the Clifden-3 well data, ~5 km to the north of the seismic line (Figure 3.1b; Table 3.1) (Burmah-Oil, 1963). The reflectors in the inferred Nymboida Coal Measures are tilted, and appear to be displaced by a number of normal faults (e.g. faults no. 1, 2 and 3 in Figure 3.9b). In the hanging-wall of faults no. 1, 2 and 3, the sedimentary units thicken towards the faults, indicating syntectonic sedimentation of the Nymboida Coal Measures (Figures 3.9b–d). The next phase of normal faulting can be inferred from fault no. 3, which shows an upward continuation that also displaces the Clarence-Moreton Basin (or the Ipswich Basin) (Figure 3.9b). A shallow thrust fault is observed in the upper eastern part of the Nymboida Coal Measures (fault no. 4 in Figure 3.9), as well as a number of other minor normal faults.

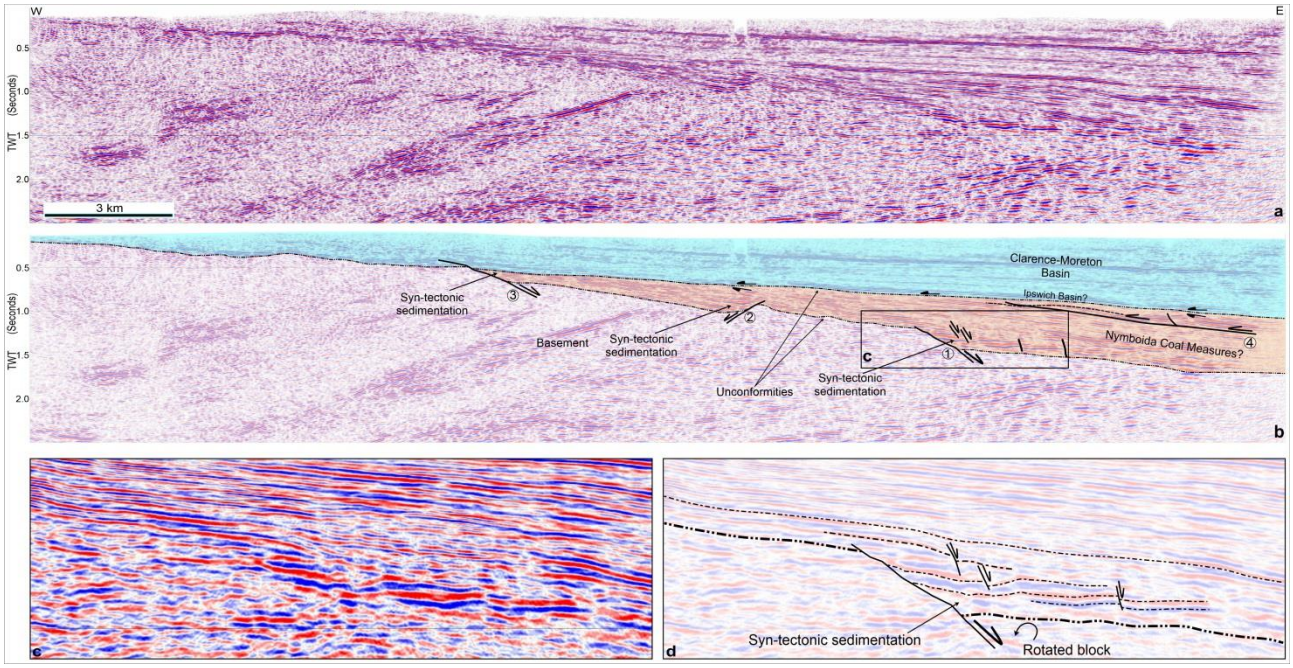

Figure 3.9. (a) Migrated seismic section DPICM08-05 (see Figures 3.1b, 3.7b for location). The time–depth curve of the Clifden-3 well data (Ingram and Robinson, 1996) was used to estimate the depth for the seismic section, indicating that the vertical to horizontal scale is almost 1:1. (b) Structural interpretation of the seismic section, showing normal faults in the inferred Nymboida Coal Measures. The estimated throw (T) and heave (H) of the faults are: fault no. 1 (T = 480 m, H = 900 m), fault no. 2 (T = 120 m, H = 200 m), fault no. 3 (T = 350 m, H = 900 m). (c–d) A close-up of a local wedge-shaped stratigraphic thickening in the hanging-wall of fault no. 1, implying syntectonic sedimentation in the Nymboida Coal Measures.

3.4.2.2. Eastern Part

The tilt map of gridded aeromagnetic data shows dextral displacement of magnetic anomalies by NNE- and NE-striking basement faults (Figure 3.10). A number of N-striking faults are also observed. I interpreted three seismic lines in the eastern part of the area in order to obtain further constraints on how these faults affected the basins. The interpretation of seismic line 84-C3 indicates that one of the NNE-striking steep faults displaced the Ipswich and Clarence-Moreton basins (fault no. 1 in Figures 3.10b, 3.11). Reverse movement along this fault resulted in folding of the Clarence-Moreton succession in the hanging-wall (Figure 3.11). A shallow thrust fault that only displaced the sedimentary rocks of the Clarence-Moreton Basin is recognised in the eastern part of the profile (fault no. 2 in Figure 3.11).

Interpretation of seismic line C90-406 indicates that the succession of the Clarence-Moreton Basin overlies the Ipswich Basin with the boundary located at ~1.00 sec two-way time (Figure 3.12). Interpretation of well data from the Tullymorgan well, approximately 3 km north of the seismic line (Boisvert, 1965; Ingram and Robinson, 1996), are approximately consistent with this interpretation (Table 3.1).

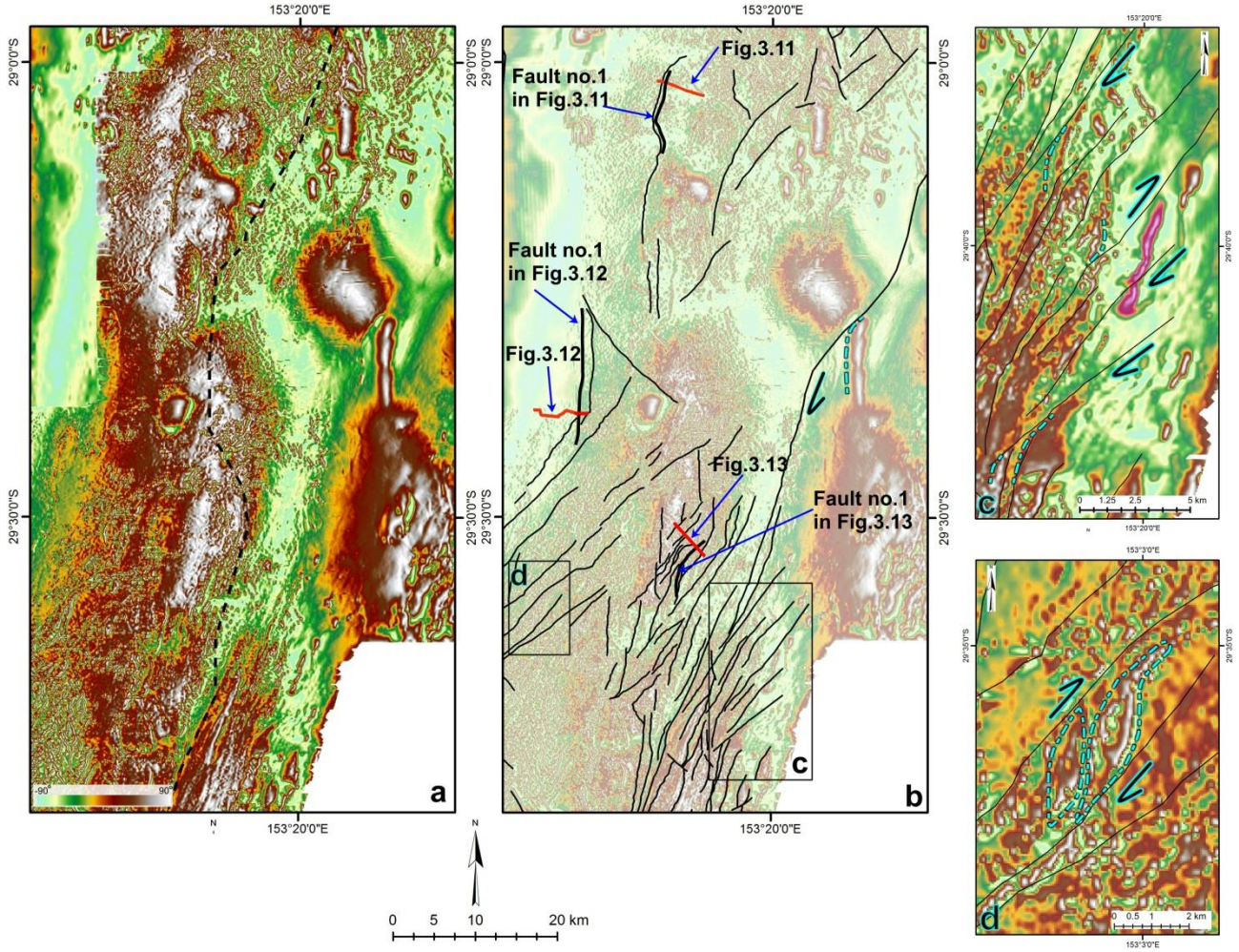

Figure 3.10. (a) Tilt map of gridded aeromagnetic data of the eastern Clarence-Moreton Basin (provided by Clarence-Moreton SEEBASE and Structural GIS Project, the Resources and Energy division of NSW Trade & Investment) (see Figure 3.1c for location). Black dashed line is the eastern boundary of the basin. (b) Interpretation of the gridded aeromagnetic data showing dominant NNE- and NE-striking faults. Red lines are the locations of the seismic lines, and bold lines are faults that are also interpreted in seismic lines. (c–d) Dextral NNE- and NE-striking faults. Dragged and offset features are shown by light blue dashed lines and purple areas, respectively.

To the east of the seismic line, all units were displaced by a N-striking subvertical reverse fault that created a hanging-wall anticline (fault no. 1 in Figures 3.10b, 3.12). The rocks of the Clarence-Moreton Basin were also affected by a back-thrust (fault no. 2 in Figure 3.12) and a normal fault (fault no. 3 in Figure 3.12).

Interpretation of seismic line C90-410 (Figure 3.13) indicates that a NW-dipping steep reverse basement fault (fault no. 1) and a back-thrust (fault no. 2) displaced the Ipswich and Clarence-Moreton basins. The possible trace of the fault is observed in the tilt map of gridded aeromagnetic data (Figure 3.10b). A minor thrust fault affected the upper part of the Ipswich Basin (Figure 3.13).

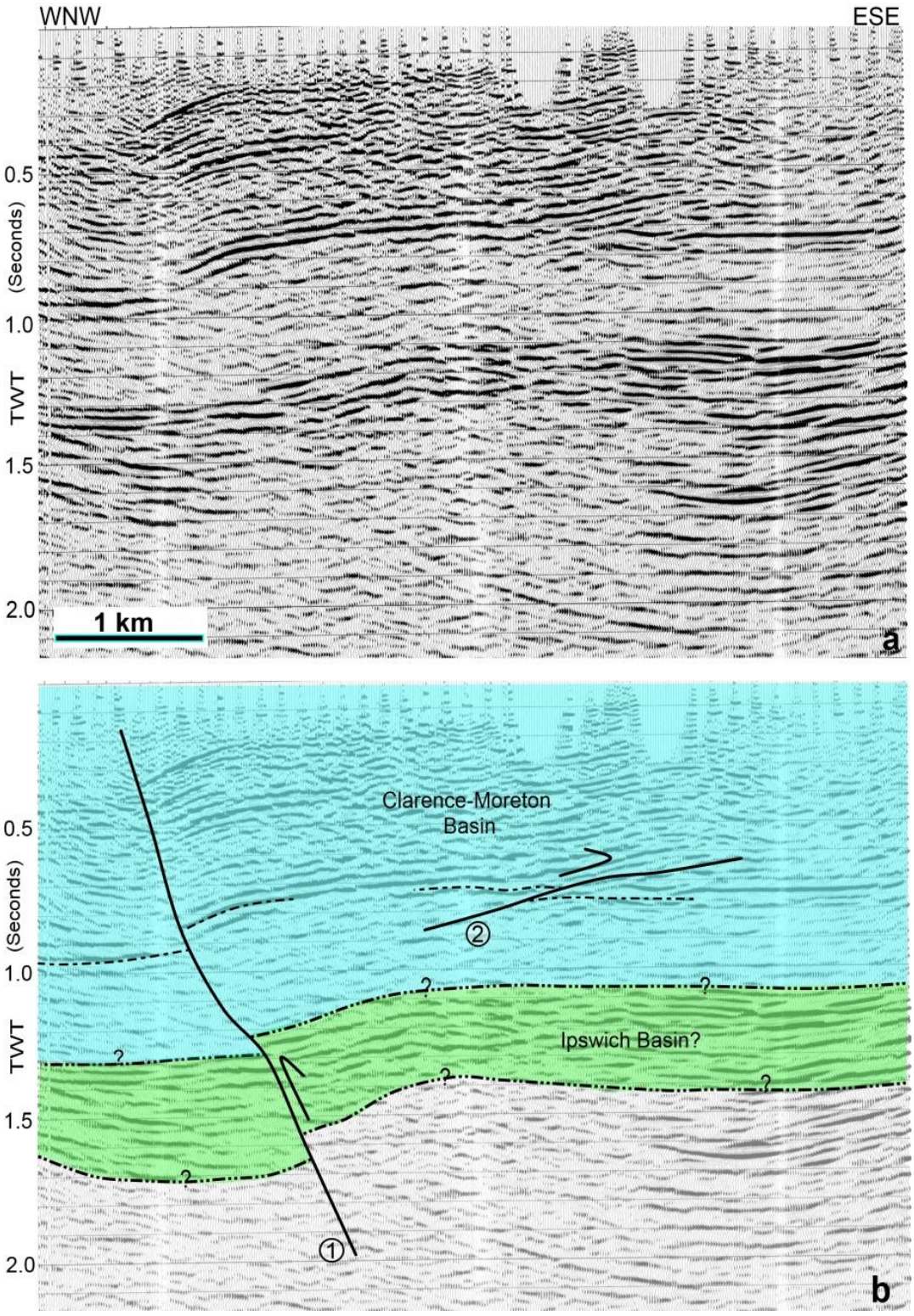

Figure 3.11. (a) Migrated seismic section 84-C3 (see Figures 3.1b, 3.10b for location). The time–depth curve of the Tullymorgan-1 well data (Ingram and Robinson, 1996) was used to estimate depth for this seismic line, indicating that the vertical to horizontal scale is almost 1:1. (b) Structural interpretation of the seismic section. The boundary between the Ipswich and Clarence-Moreton Basin is based on the interpretation by Shaw (1987). A reverse basement fault (no. 1) and a shallow intrabasin thrust (no. 2) displaced the Ipswich and Clarence-Moreton basins. The estimated throw (T) of fault no. 1 is ~140 m.

Table 3.1. Interpretation of three deep petroleum well data in the vicinity of seismic lines in the Clarence-Moreton Basin

Kyogle-1 (Total Depth: 2474.4 m)		
Reference	(Relph, 1963)	
Formation	**Top Fm (m)**	**Thickness**
Kangaroo Creek Sandstone	9	125
Wallon Coal Measures	134	551
Bundamba Group	685	1445
Ipswich Basin	2130	301
Chillingham Volcanics	2431	>43
Tullymorgan-1 (Total Depth: 2310.99 m)		
Reference	(Boisvert, 1965)	
Formation	**Top Fm (m)**	**Thickness**
Kangaroo Creek Sandstone	0	309
Wallon Coal Measures	309	368
Bundamba Group	677	1607
Ipswich Basin	2284	>26
Clifden-3 (Total Depth: 2288.13 m)		
Reference	(Burmah-Oil, 1963)	
Formation	**Top Fm (m)**	**Thickness**
Wallon Coal Measures	0	219
Bundamba Group	219	1492
Nymboida Coal Measures	1710	796

3.5. Discussion

3.5.1. Kinematics of faults in the Mesozoic basins

Results of this study show that faults played an important role in the development of Mesozoic basins in southeast Queensland and northwest NSW. Based on the aeromagnetic data, I recognised three dominant sets of faults, which are: (1) sinistral NW- to NNW-striking faults, (2) dextral NE- to NNE-striking faults, and (3) N-striking faults (Figures 3.3, 3.4, 3.7, 3.10). Observations show that some of these faults, such as the NPFS and WIFS, were reactivated as steep strike-slip reverse faults during the Cenozoic (Babaahmadi and Rosenbaum, 2014b, a). Interpretation of seismic reflection data indicates that some of these faults accommodated normal movements during the development of the Nymboida Coal Measures and Ipswich Basin in the Triassic, and were not reactivated during the later post-Triassic deformational phases (Figures 3.8, 3.9). Other observed structures in the Jurassic rocks of the Clarence-Moreton Basin are shallow thrusts and fault-related folds (Figures 3.6, 3.11, 3.12), which are interpreted to be related to thin-skinned deformation.

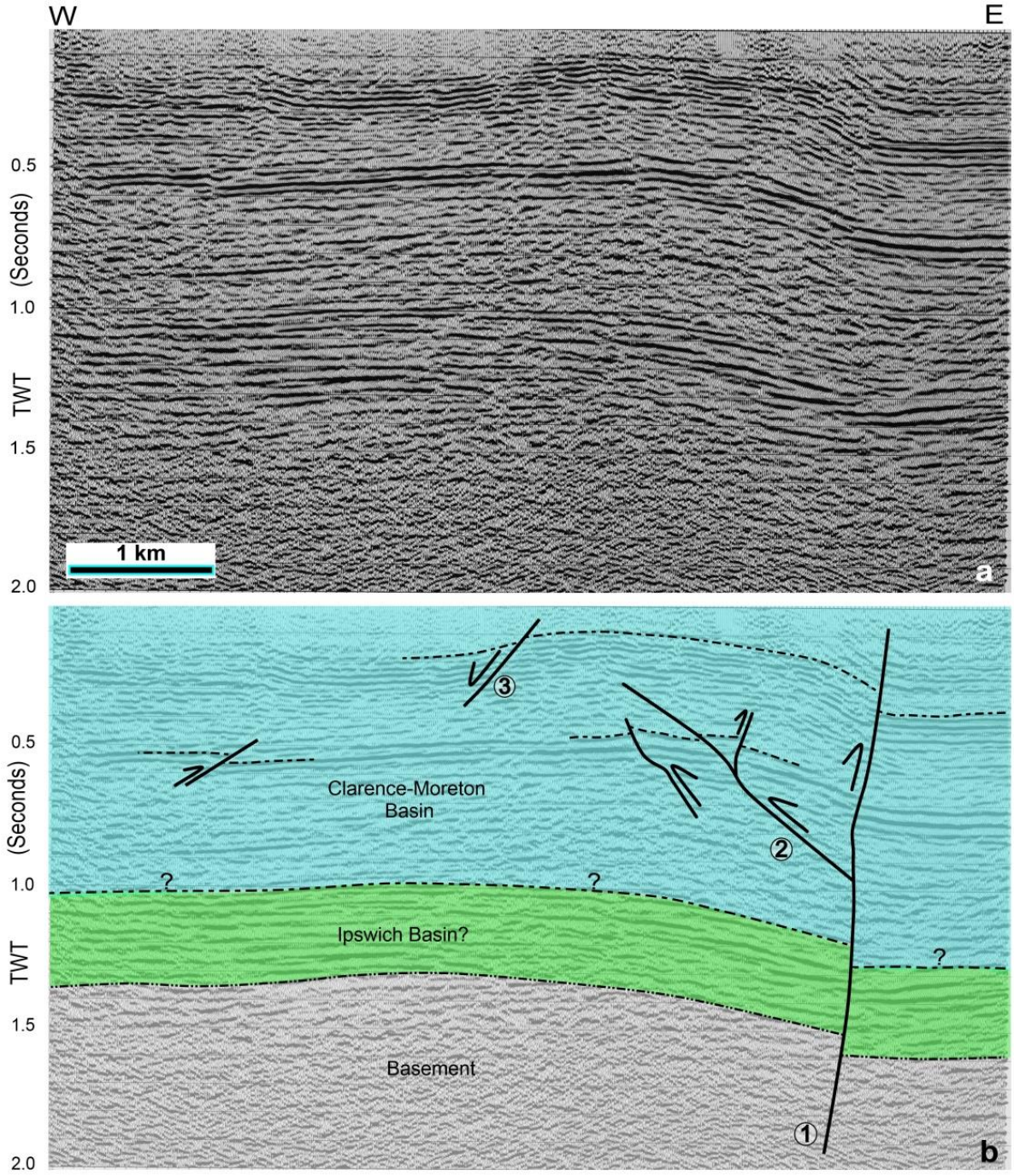

Figure 3.12. (a) Migrated seismic section C90-406 (see Figures 3.1b, 3.10b for location). The time–depth curve of the Tullymorgan-1 well data (Ingram and Robinson, 1996) was used to estimate depth, indicating that vertical to horizontal scale is almost 1:1. (b) Structural interpretation of the seismic section. The boundary between the Ipswich and Clarence-Moreton basins is similar to the interpretation of the Tullymorgan-1 well data (Ingram and Robinson, 1996). In the east part of the seismic section, a subvertical reverse basement fault (no. 1) and its splay faults displaced the Ipswich and Clarence-Moreton basins. The estimated throw (T) of fault no. 1 is ~140 m.

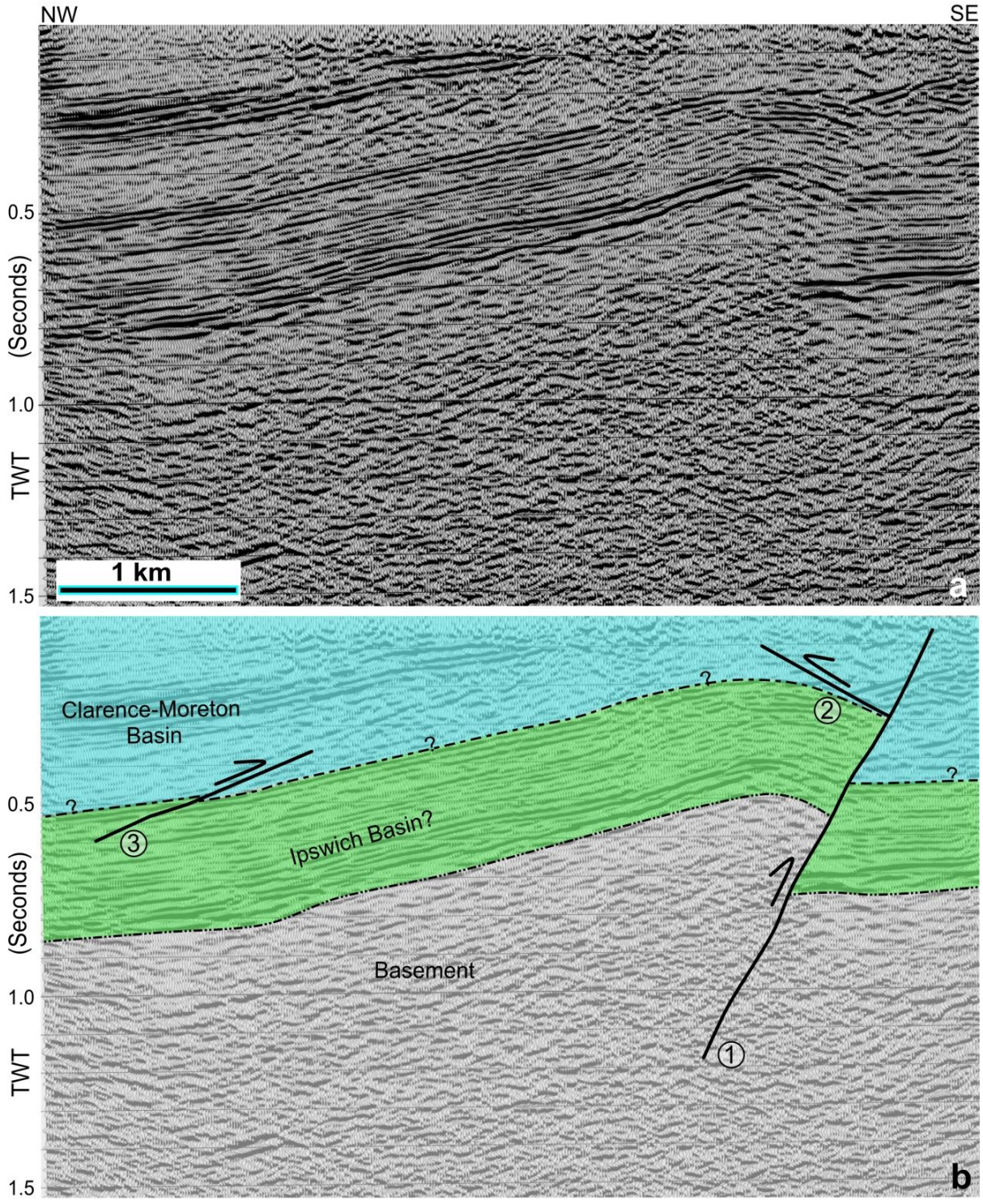

Figure 3.13. (a) Migrated seismic line C90-410 (see Figures 3.1b, 3.10b for location) The time–depth curve of the Pillar Valley-2 well data (Ingram and Robinson, 1996) was used to estimate depth, indicating that the vertical to horizontal scale is almost 1:1. (b) Structural interpretation of the seismic section. The boundary between the Ipswich and Clarence-Moreton basins was validated by the interpretation of a parallel seismic line C90-412 (Ingram and Robinson, 1996). A steep reverse basement fault (no. 1) and a shallow thrust (no. 2) displaced the Ipswich and Clarence-Moreton basins. The estimated throw (T) of fault no. 1 is ~350 m.

I suggest that the contractional structures (thrusts and steep reverse faults) in the Ipswich and Clarence-Moreton basins (Figures 3.5a-b, 3.6, 3.11, 3.12, 3.13), could possibly resulted from deformational phases during the Cenozoic (Babaahmadi and Rosenbaum, 2013, 2014b). These episodes of deformation were likely due to far-field stresses transmitted from collisional zones at the northeastern and southeastern boundaries of the Australian Plate during the late Eocene–early Oligocene, late Oligocene–early Miocene and late Miocene–Pliocene (Babaahmadi and Rosenbaum, 2014b, a). Alternatively, some authors have suggested that reverse faulting in the Ipswich and Clarence-Moreton basins developed in the mid-Cretaceous, during a contractional event that also led to thrusting in the Bowen, Surat and Maryborough basins (Hill, 1994; Korsch et al., 2009b).

3.5.2. Origin of the Triassic sedimentary basins

3.5.2.1. Early to early Late Triassic basins

Early Triassic to early Late Triassic basins in eastern Australia include the Esk Trough in southeast Queensland and the Nymboida Coal Measures in northeast NSW (Figure 3.1). The tectonic origin of the Esk Trough is controversial. Some authors proposed that the Esk Trough was a foreland basin in the Early–Middle Triassic (Holcombe et al., 1997b; Campbell, 2005). This suggestion was explained based on (1) the interpretation of unconformable contacts between the Esk Trough sedimentary rocks and the older Paleozoic rock units; and (2) the recognition of thickening to the west and the westerly to southerly movement of paleocurrents across the Esk Trough, which have been interpreted as indicators that the basin was fed by a highland to the east (Campbell, 2005).

An alternative explanation for the origin of the Esk Trough is that basin formation was controlled by extensional and/or transtensional tectonics (Evans and Roberts, 1980; Korsch et al., 1989; O'Brien et al., 1994). The interpretation of Early Triassic to early Late Triassic extension in the Esk Trough and Nymboida Coal Measures is supported by the following consequential interpretations of structures. Firstly, sedimentation in the Nymboida Coal Measures occurred contemporaneously with normal faulting (Figure 3.9), and this is further supported by the interpretation of the WIFS as a boundary fault that played an important role in the development of the Esk Trough (Korsch et al. 1989). Secondly, N- and NNW-striking basement faults around and within the Esk Trough could have been active as controlling basement normal and strike-slip faults during the Early Triassic and early Late Triassic (Figures 3.1c, 3.3). Thirdly, the inferred unconformities, rather than boundary faults, between the Toogoolawah Group and the late Paleozoic rocks (Campbell, 2005) may have resulted from synformal depressions that developed in the early stage of extension and prior to the development of a boundary fault(s). Similar features were observed, for example, in the East African Rift System

(Usangu Flats, Tanzania) (Morley, 2002), where a dominant controlling boundary fault is lacking, possibly because this area represents the first stage of the basin development. Fourthly, the thickening of the Bryden and Esk formations to the west (Campbell, 2005) could have been originated from an east-dipping blind boundary fault.

The interpretation of seismic line DPICM08-05 indicates that the earlier stage of rifting in the Nymboida Coal Measures was coincident with the activity of synsedimentary normal faults (Figure 3.9). Following this phase of faulting, deposition continued in the Nymboida Coal Measures, possibly in a period of subsidence.

Following the Early Triassic to early Late Triassic extensional phase, a contractional event, associated with the last episode of the Hunter-Bowen Orogeny (Holcombe et al., 1997b), gave rise to thrusting, folding, and tilting of bedding in the Esk Trough and Nymboida Coal Measures. The interpretation of the seismic reflection data supports the occurrence of this (relatively weak) contractional event, as indicated by tilted succession and a shallow thrust faulting in the Nymboida Coal Measures (Figure 3.9). Outcrop-scale folding and tilting of the Nymboida Coal Measures have also been reported by McElroy (1975). Other evidence for this contractional phase is observed in the Esk Trough, where east-verging low- to moderate-amplitude folds are associated with thrusts and strike-slip faulting (Holcombe et al., 1997b). The exact timing of this deformation is not well constrained. Holcombe et al. (1997b) reported that volcanic rocks dated at ca 228 Ma overlie folds in the Esk Trough, and thus indicate that folding occurred before this age and within the interval of 241–228 Ma. Based on the following reasons, I propose that the contractional event took place in a shorter interval of 237–232 Ma. Firstly, the maximum K–Ar age of the Sugars Basalt at the base of the Ipswich Basin, which may represent the initial stage of rifting in the Ipswich Basin, is 232 Ma (Purdy and Cross, 2013). This indicates that contractional deformation had likely occurred prior to this age. Secondly, an $^{40}Ar/^{39}Ar$ radiometric age of a basalt member from the Bardool Conglomerate of the Nymboida Coal Measures (Figure 3.2) indicates an age of ca 237 Ma (Retallack et al., 1993), implying that deposition of sediments in the Nymboida Coal Measures continued through the early Late Triassic and that contractional deformation occurred after this age. The exact timing of deposition cessation in the Nymboida Coal Measures remains unknown.

Evidence for contractional deformation can also be observed in the Early–Middle Triassic Kin Kin beds of the Gympie Terrane, which is composed of strongly deformed phyllites and slates (Cranfield et al., 1997). The Kin Kin beds are unconformably overlain by the North Arm Volcanics (Murphy et al., 1976), which have been dated at ca 213 Ma (Late Triassic) by K–Ar geochronology (Green and Webb, 1974). Detrital zircons from the Kin Kin beds have recently been shown to be as young as ca

240 Ma (Li et al., 2015), indicating that deformation must have occurred after ca 240 Ma but before the initiation of Late Triassic volcanism. I suggest that this deformation was likely contemporaneous with the observed contractional deformation in the Esk Trough and Nymboida Coal Measures.

3.5.2.2. Late Triassic to Early Cretaceous basins

Following the early Late Triassic contractional phase, a second phase of Triassic sedimentation occurred during the Late Triassic, resulting in the deposition of coal-bearing clastic sediments in the Ipswich Basin. Early synsedimentary normal faults in the Ipswich Basin indicate that sedimentation was ultimately controlled by rifting (Figure 3.8). Early rifting phase is further supported by the occurrence of Late Triassic bimodal volcanic rocks at the base of the Ipswich Basin (Holcombe et al., 1997b; Roach, 1997; Purdy and Cranfield, 2013). Strike-slip normal faults, such as the NPFS and WIFS, were likely active during the development of the Ipswich Basin in the Late Triassic (Korsch et al., 1989; O'Brien et al., 1994; Babaahmadi and Rosenbaum, 2014b). Once the activity of the synsedimentary faults ceased, a subsidence phase likely led to the continuation of deposition in the Ipswich Basin (post-rift sediments in Figure 3.8d).

The unconformity between the Ipswich Basin and the overlying Clarence-Moreton Basin (Figure 3.8) could possibly be related to an uplift phase that occurred after the deposition of the Ipswich Basin, but this suggestion remains speculative. The Clarence-Moreton Basin is assumed to have developed in a period of thermal subsidence from the latest Late Triassic to Jurassic (Korsch et al., 1989). The observations do not show evidence of faulting during deposition, and the presence of normal faults with minor separations in the different units of the Clarence-Moreton Basin implies that faulting occurred after lithification, and possibly during later deformational phases (Figures 3.5c, 3.8).

3.5.3. A geodynamic model for the development of the eastern Australian Triassic basins

The results indicate that two episodes of extension occurred in the Triassic, intermitted by a phase of contraction. The first extensional episode occurred in the Early Triassic to early Late Triassic and gave rise to the development of the Esk Trough and the Nymboida Coal Measures. A possible origin of this event is the steepening of the subducting slab and/or trench retreat.

The origin of the early Late Triassic contractional episode, which represents the last phase of the Hunter-Bowen Orogeny, has previously been attributed to the final docking of the Gympie Terrane with the Australian continent (Cranfield et al., 1997; Li et al., 2012b). However, this idea seems inconsistent with the relatively low contractional strain in the Esk Trough and the Nymboida Coal Measures. In addition, recent detrital zircon provenance data by Li et al. (2015) cast doubt on the assumption that the Gympie Terrane was accreted to the Australian continent as an allochtonous

terrane (e.g. (Harrington, 1983). Thus, the point whether the Gympie Terrane played an important role driving the Hunter-Bowen deformation remains an open question. Some authors have suggested that the Hunter-Bowen deformation, in general, was driven by trench advance (Jenkins et al. 2002), which may imply that the first episode of Triassic extension was triggered by a switch from trench advance to a transient period of trench retreat. The second extensional phase occurred in the Late Triassic and gave rise to bimodal volcanism and the development of the Ipswich Basin. The driving mechanism of this extensional phase was likely associated with the recommencement of trench retreat following the termination of the Hunter-Bowen Orogeny.

3.6. Conclusions

New observations support the idea that the Triassic tectonic activity in eastern Australia was characterised by two episodes of extension intermitted by a phase of contraction possibly in response to switches between trench retreat and advance, respectively. The results indicate that the Esk Trough in southeast Queensland and the Nymboida Coal Measures in northeast NSW developed during the Early Triassic to early Late Triassic as a result of an extensional regime. Following this episode of rifting, a contractional event that was possibly triggered by trench advance affected the Esk Trough and the Nymboida Coal Measures in the early Late Triassic, resulting in tilting, thrusting, and mild folding. After this contractional event, eastward trench retreat resumed, giving rise to the development of the Ipswich Basin during the Late Triassic.

Chapter 4

Kinematics of the Demon Fault: Implications for Mesozoic strike-slip faulting in eastern Australia

Kinematics of the Demon Fault: Implications for Mesozoic strike-slip faulting in eastern Australia

Absract

The Demon Fault is a N-striking, dextral strike-slip fault that displaces Carboniferous to Middle Triassic rock units in eastern Australia. I present results from aeromagnetic gridded data, satellite images, digital elevation models, and field observations, which provide constraints on the geometry and kinematics of the Demon Fault. The fault can be subdivided into four steeply-dipping segments (DF1 to DF4) with oblique reverse-dextral kinematics. Earlier NW-striking faults, which affected Early and Middle Triassic magmatic rocks, are displaced by the Demon Fault, implying that activity along the Demon Fault has occurred during the latest Middle Triassic or later. The amount of dextral offset along the different parts of the Demon Fault is decreased towards the south. This suggests that different segments have experienced different histories of reactivation, or that deformation toward the south has partitioned into minor splays, which operated as reverse faults and resulted in a lesser dextral displacement. I propose that the Demon Fault and other sub-parallel faults operated in conjunction with the development of basins in eastern Australia from the Late Triassic to Early Cretaceous. The pattern of minor faults and their kinematics indicate that recent activity along the Demon Fault has occurred during dextral transpression, which I attribute to mid-Cretaceous contractional deformation, or possibly even Cenozoic deformation associated with collisional processes at the northern boundary of the Australian plate.

Key words: Demon Fault, New England Orogen, eastern Australian sedimentary basins, strike-slip faults, transpression, Mesozoic basins

4.1. Introduction

A series of strike-slip faults with different trends are recognised in eastern Australia, but their exact geometry, kinematics and relationship to the regional tectonics are relatively poorly understood. For example, the Demon, West Ipswich and East Richmond faults are strike-slip faults that affected Paleozoic to early Mesozoic lithological units of the New England Orogen (Figure 4.1). These faults were active during the Mesozoic and have likely played an important role in the development of sedimentary, extension-related, basins (Korsch et al., 1989). The N-striking dextral Demon Fault,

which is located in northeastern New South Wales (Figure 4.1), affected Paleozoic to Jurassic lithological units, and has particularly pronounced morphological and geophysical expressions.

The Demon Fault was first recognised as a major strike-slip fault by Shaw (1969), who based on the apparent offset of the Stanthorpe Monzogranite, estimated that 30 km of dextral displacement has occurred along this structure (Figure 4.2a). In a subsequent study, Korsch *et al.* (1978) restored late Permian–Early Triassic contacts (the Dundee Rhyodacite and the Bungulla Monzogranite) on both sides of the Demon Fault and estimated only 17 km of dextral displacement. McPhie & Fergusson (1983) proposed a ~23 km dextral offset of the Coombadjha Volcanic Complex along the Demon Fault. Although these studies provided relatively robust constraints on the amount of dextral offset along the Demon Fault, they recognised the fault as a continuous fault and did not include detailed analysis of the geometry and kinematics of the different fault segments.

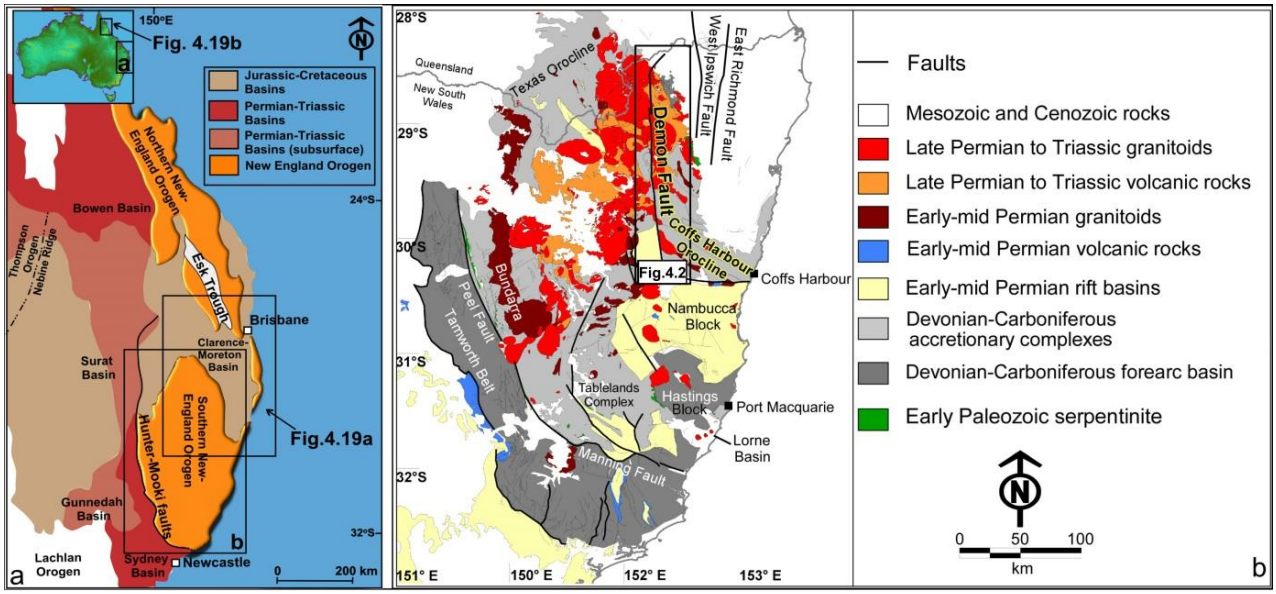

Figure 4.1. (a) Tectonic units of eastern Australia (Korsch et al. 2009b). (b) Regional Geological Map of the southern New England Orogen (Rosenbaum et al., 2012).

In this paper, I present a detailed structural analysis on the different segments of the Demon Fault with the aim of understanding the exact geometry and kinematics of each segment. The analysis is done by utilising different datasets, including Landsat ETM+ satellite images, ASTER digital elevation models, aeromagnetic anomaly gridded data, geological maps and field observations. The results are then discussed in the context of strike-slip faulting in eastern Australia and its relationship to the geodynamic evolution of eastern Australia since the Mesozoic.

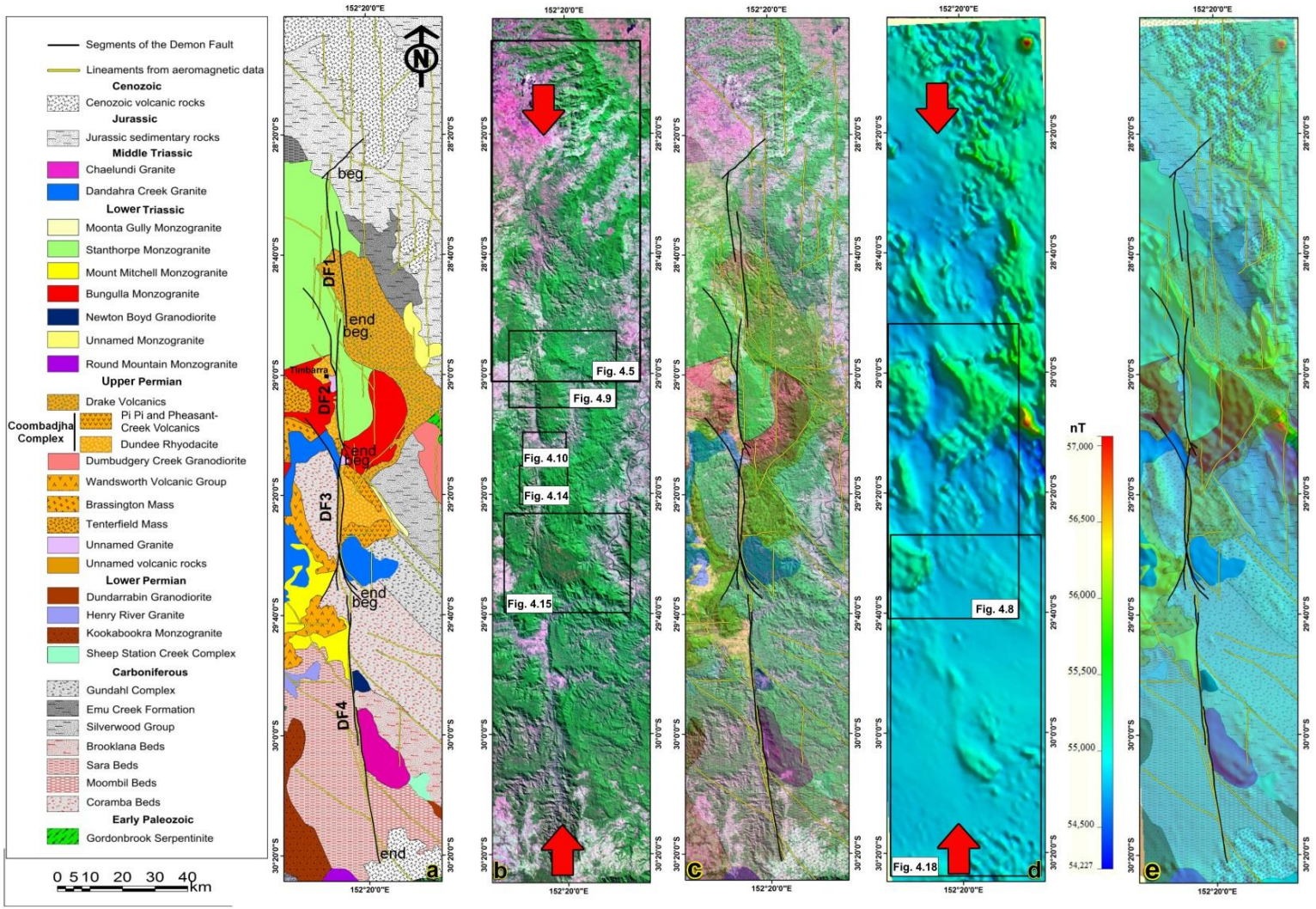

Figure 4.2. (a) Geological map of the study area and the Demon Fault segments (after Green et al. (1980), Gillgan et al. (1992) and Henley et al. (2001)). The words “beg” and “end” indicate the beginning and end of each segment. (b) Landsat ETM+ image (spatial resolution 14.25 m) of the Demon Fault. (c) Transparent geological map overprinted on the Landsat ETM+ image. (d) Aeromagnetic gridded data of the Demon Fault. (e) Transparent geological map overprinted on aeromagnetic gridded data.

4.2. Geological Setting

The geology of the study area involves Paleozoic to early Mesozoic rocks of the New England Orogen (Leitch, 1974; Glen, 2005), as well as younger rocks associated with Mesozoic sedimentary basins and Cenozoic volcanism. The study area is located in the southern New England Orogen, which is characterised by a complex oroclinal geometry, possibly associated with alternating extensional and contractional deformation phases from the Devonian to the Middle Triassic (Jenkins et al., 2002; Rosenbaum, 2012; Rosenbaum et al., 2012). Devonian–Carboniferous rocks mainly include remnants of the accretionary complex (Tablelands Complex) and forearc basin (Tamworth Belt) (Crook, 1964; Leitch, 1974; Cawood and Leitch, 1985; Roberts and Engel, 1987; Glen and Roberts, 2012).

During the early Permian (300–280 Ma), the New England Orogen was subjected to extensional tectonism, possibly in a backarc setting (Leitch, 1988; Korsch et al., 2009a). Extensional deformation involved the development of widespread rift basins (Korsch et al., 2009a) and the simultaneous emplacement of a large volume of S-type granitoids, which are intruded into the Tablelands Complex (Shaw and Flood, 1981; Hensel et al., 1985; Cawood et al., 2011a; Rosenbaum, 2012; Rosenbaum et al., 2012). Early Permian basins, filled by sedimentary and volcanic rocks, are represented by the Sydney, Gunnedah and Bowen Basins, and in other early Permian successions east of the Peel Fault (Leitch, 1988) (Figure 4.1). Early Permian magmatism and rift basins have been inferred to have resulted from extensional tectonics (Caprarelli and Leitch, 1998; Korsch et al., 2009a), possibly in response to subduction rollback (Jenkins et al., 2002; Rosenbaum, 2012; Rosenbaum et al., 2012).

From the mid-Permian to the Middle Triassic, the southern New England Orogen was subjected to contractional deformation, known as the Hunter-Bowen Orogeny. This contractional phase was characterised by folding and thrusting within the New England Orogen and in its peripheral early Permian basins (Collins 1991; Korsch *et al.* 2009b), and was accompanied by calc-alkaline magmatism and the emplacement of voluminous I-type granitic intrusions (Shaw & Flood 1981; Collins 1991; Offler & Foster 2008; Korsch et al. 2009b; Shaw & Flood 2009; Li et al. 2012b). Oroclinal bending in the southern New England Orogen, which commenced at *ca* 300 Ma, has been concluded prior to the initiation of the second magmatic episode at *ca* 260 Ma (Glen and Roberts, 2012; Li et al., 2012a; Rosenbaum et al., 2012).

From the Early–Middle Triassic, a series of sedimentary basins developed in eastern Australia, such as the Early–Middle Triassic Esk Trough and the Late Triassic to Jurassic Clarence-Moreton and Surat Basins (Korsch et al., 1989) (Figure 4.1). The Esk Trough and Ipswich Basin may have initiated as extensional (or transtensional) sedimentary basins, in a backarc position relative to a retreating subduction zone (Korsch et al., 1989; Li et al., 2012b). This subduction setting has probably existed offshore of eastern Australia until the middle Cretaceous (Korsch and Totterdell, 2009; Waschbusch

et al., 2009), giving rise to episodic transitions from overriding-plate extension/transtension deformation to contraction/transpression deformation (Korsch et al., 1989; Li et al., 2012b).

In the area affected by the Demon Fault, in the eastern part of the southern New England Orogen (Figures 4.1, 4.2a), the oldest rocks are deformed metasedimentary rocks of the Tablelands Complex and early Permian magmatic rocks of the Hillgrove granitic suite (e.g. Dundurrabin Granodiorite and the Henry River Granite; Figure 4.2a). Late Permian–Middle Triassic units are volcanic and intrusive rocks, including the Coombadjha Volcanic Complex, Wandsworth Volcanic Group, Stanthorpe Monzogranite, Mount Mitchell Monzogranite, Bungulla Monzogranite, Newton Boyd Granodiorite and Dandahra Creek Granite (Figure 4.2a). The Jurassic rocks belong to the Clarence-Moreton Basin and consist mainly of sandstone, shale, siltstone and conglomerate, covering the older rocks unconformably in the northern part of the study area (Figure 4.2a). The youngest rocks in the study area are Cenozoic basalts (Figure 4.1), which are widespread in the northern and southern parts of the Demon Fault.

4.3. Methods

I used remote sensing data, aeromagnetic images, geological maps and field observations to map the Demon Fault and related structures. Remote sensing is beneficial for recognising fault lineaments in a number of ways (Prost, 2001; Babaahmadi et al., 2012). It allows the recognition of (1) offset and dragging of rock units, geological structures and geomorphic features, (2) structural lineaments with pronounced traces and marked topographic expression, and (3) lensoid and en-echelon structures indicating the presence of hidden faults.

Satellite images used in this study are Landsat ETM+ images with 7-4-2 composite bands, which are suitable for geological purposes (Figure 4.2b, c). For better identification of rock units and larger scale faults and lineaments, I used data fusion methods (Pohl and Van Genderen, 1998; Zhang, 2004) to merge multispectral ETM+ images with a 28.5 m cell size and the panchromatic band of the ETM+ image with a spatial resolution of 14.25 m. Contrast stretching, such as linear contrast stretching and histogram equalization, was performed on the resulting image of data fusion.

The digital elevation model is ASTER Global Digital Elevation Map version 2 (GDEM V2), produced by NASA and the Ministry of Economy, Trade and Industry of Japan. The 30 m ASTER DEMs has been generated by bands 3N (nadir-viewing) and 3B (backward-viewing) of the ASTER Level-1A images, acquired by the Visible-Near Infrared (VNIR) sensor (ASTER-GDEM-Validation-Team, 2011).

Aeromagnetic anomaly gridded data with spatial resolution of 250 m were used to identify and interpret subsurface fault traces (Figure 4.2d, e). I located anomalies directly above their sources on

reduced-to-pole (RTP) aeromagnetic images (Swain, 2000; Cooper and Cowan, 2005), and operated a variety of filters in the Fourier domain to enhance both shallow and deep features. The first and second vertical derivatives were operated to sharpen short wavelength sources, and especially fault lineaments (Blakely, 1995). In particular, tilt angle derivative (the arc tangent of the ratio of the first vertical derivative to total horizontal derivatives) is a powerful filter for enhancing geological edges and fault lineaments from both shallow and regional sources (Miller and Singh, 1994). Total horizontal derivative is another filter that enhances faults and boundaries. Downward continuation is the process whereby potential field is measured over a plane closer to the sources in order to highlight short wavelengths and shallower sources (Blakely, 1995; Trompat et al., 2003). Upward continuation is the process whereby potential field is measured on a plane farther from all sources to highlight deeper sources and to reduce the effects of shallower sources (Gibert and Galdeano, 1985; Blakely, 1995). I used the software Intrepid to process aeromagnetic data. Aeromagnetic gridded data were used to recognise faults in similar ways to those mentioned for the remote sensing interpretation.

Geological maps were utilised to recognise strike-slip displacements of rock units. This was complemented by field observations at a number of locations, where fault-related structures and kinematic indicators (such as slickenlines and Riedel shears) were found. In brittle fault zones, the deflection of older Riedel shears by younger shears can be used to define shear sense (Passchier and Trouw, 2006). Riedel structures documented here as shear sense indicators are mostly P–Y shears, which are equivalent to S–C fabrics in ductile deformation (Doblas, 1998; Passchier and Trouw, 2006). P–Y shears can be used to determine movement direction of hanging-wall by using stereographic projections (e.g.,(Yassaghi and Madanipour, 2008; Babaahmadi et al., 2012). The intersection line of Y shears, which are parallel to the fault boundary, and the deflected P shears, is normal to slickensides on the Y surfaces (Figure 4.3a). Therefore, the hanging-wall movement direction can be determined by projecting the average orientations of P and Y surfaces on the stereonet and then move 90° from the P–Y intersection along the Y great circle (Figure 4.3b). Hanging-wall movement direction of the fault is updip (towards the stereonet centre) in reverse faults (Figure 4.3b) and downdip in normal faults (Figure 4.3c).

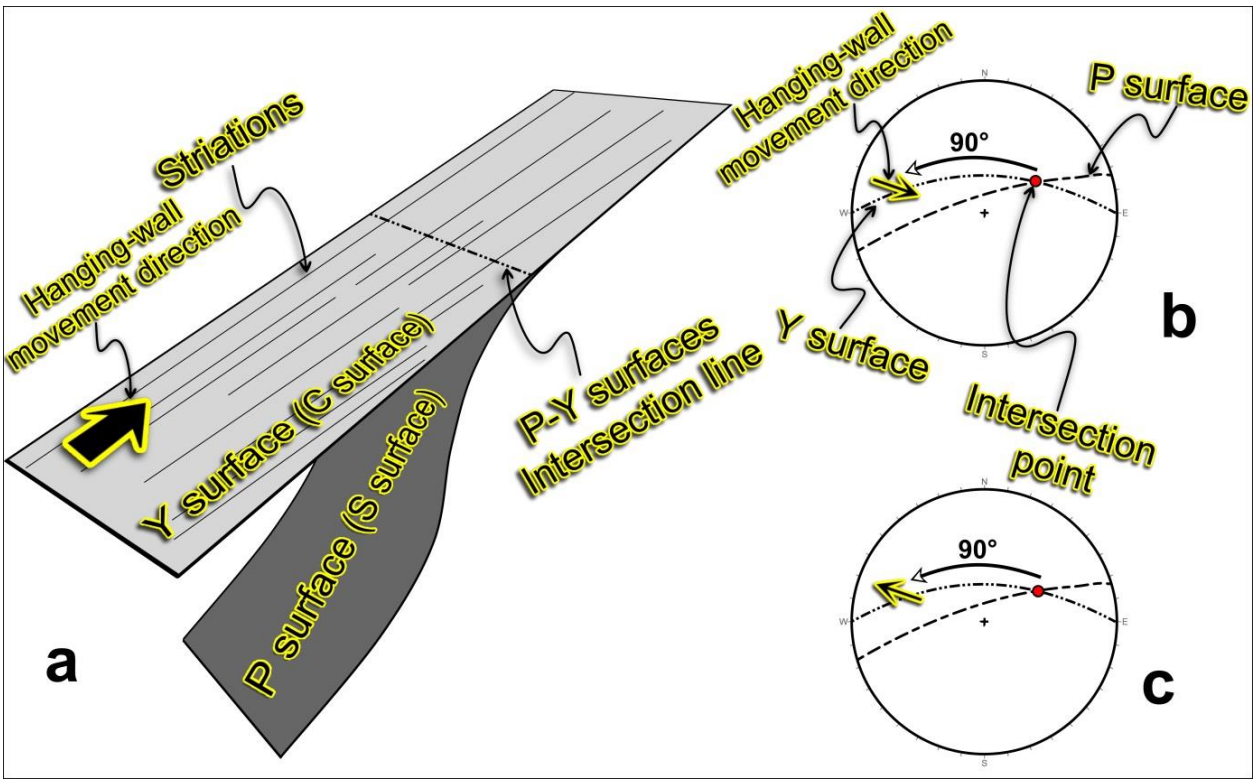

Figure 4.3. (a) A sketch of P and Y surfaces (or S and C surfaces in ductile deformation) shows that their intersection line is normal to slickenside on the Y surface. (b, c) Stereonet analysis of hanging-wall movement direction in reverse and normal faults (see text).

4.4. Magnetic response

The northern part of the study area is mainly dominated by short wavelength, high amplitude magnetic anomalies while the southern part is mainly dominated by long wavelength, low amplitude anomalies (Figure 4.4). In the northernmost study area, short wavelength, high amplitude anomalies have propagated as small irregular and curved bodies with high amplitude in profile indicating very shallow bodies (Figures 4.4b, d). By comparison with geological maps (Figure 4.4a), these anomalies are probably related to Cenozoic basaltic volcanic rocks. Farther south, there is a low amplitude body, possibly indicating late Permian felsic volcanic rocks or Carboniferous metasedimentary rocks (Figure 4.4a–e). This low anomaly body reaches high amplitude bodies with a more regular pattern, which gradually change to a longer wavelength, low amplitude anomaly southward. By comparison with geological maps (Figure 4.4a), these different anomalies are interpreted to be Early–Middle Triassic intermediate to felsic intrusive rocks (Figures 4.4a–e). Farther south, there is a constant long wavelength, low amplitude anomaly, possibly associated with Carboniferous metasedimentary rocks (Figure 4.4).

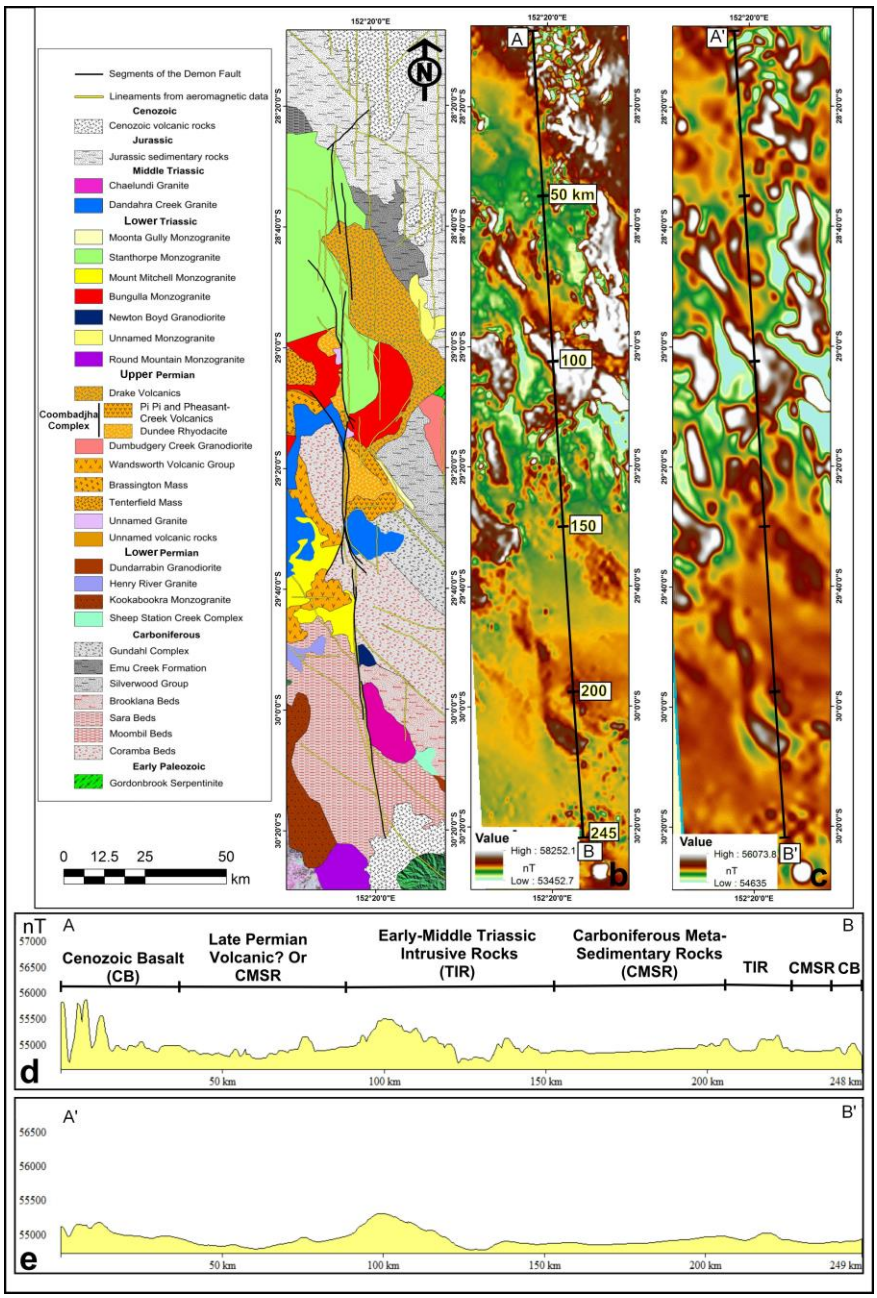

Figure 4.4. (a) Geological map of the study area. (b) Downward continuation aeromagnetic image of the study area. Line A–B shows cross section of magnetic response in Figure 4.4d. (c) Upward continuation aeromagnetic image of the study area. Line A'–B' shows cross section of magnetic response in Figure 4.4e. (d, e) Profiles of magnetic anomaly in the Demon Fault area.

4.5. The Demon Fault

The Demon Fault is observed on the satellite images as a pronounced ~215 km long N–S lineament, displacing Paleozoic and Mesozoic rocks (Figure 4.2). From the interpretation of satellite images and aeromagnetic gridded data, the Demon Fault is a segmented fault with some parallel faults around it. Following the interpretation of satellite images, I describe the Demon Fault in three parts: northern, central, and southern.

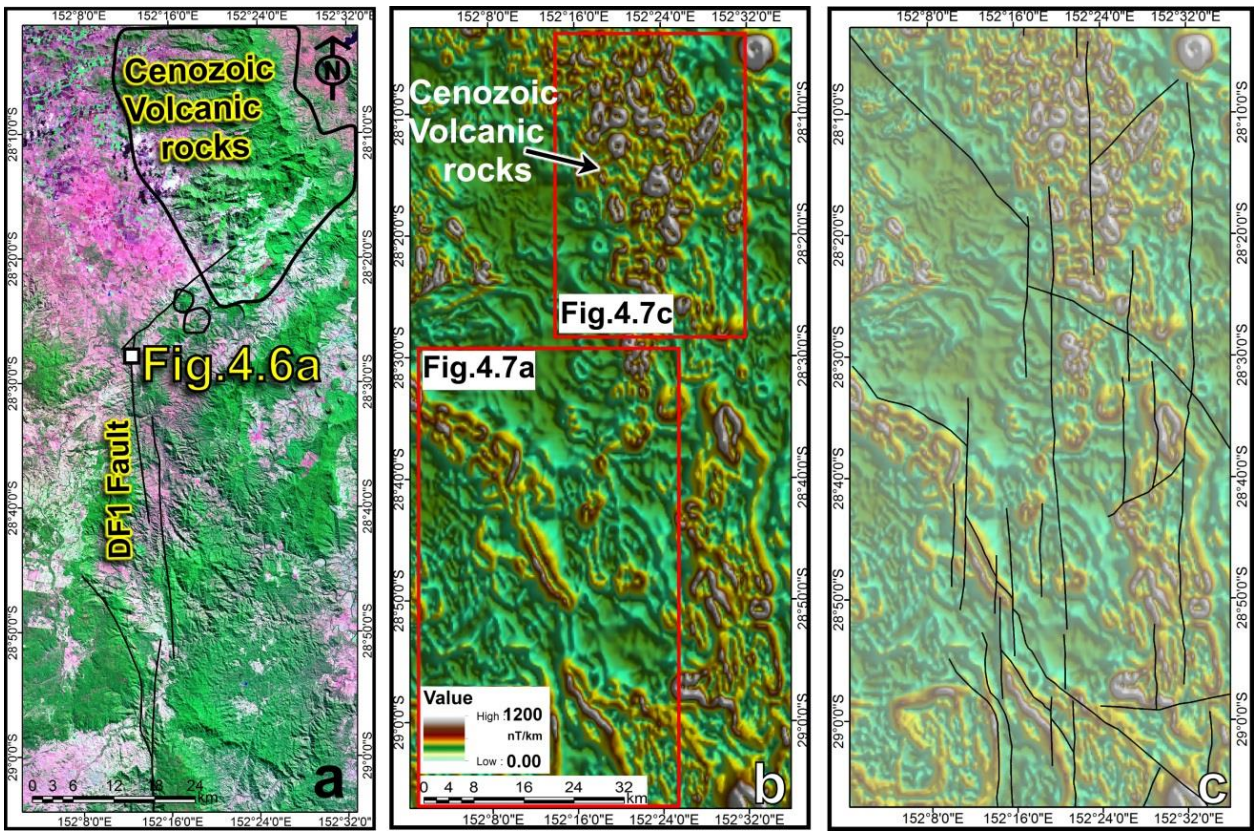

Figure 4.5. (a) The DF1 fault traces on Landsat ETM+ image (see Figure 4.2b for location). (b, c) the total horizontal derivative image indicates displacement of high anomaly units by the N-striking, NW-striking, and NE-striking faults.

4.5.1. The northern part

The northern part of the Demon Fault (DF1 segment) is ~47 km long and includes two parallel faults, recognised from satellite images (Figures 4.2, 4.5a). The DF1 faults have mainly affected the Stanthorpe Monzogranite and the Drake Volcanic rocks, but from satellite images, Jurassic units also seem to be deformed by these structures (Figures 4.2a–c).

Riedel shears (Y and P shears) in the Stanthorpe Monzogranite indicate that the DF1 is a reverse dextral strike-slip fault (Figure 4.6). Interpretation of the total horizontal and tilt derivative aeromagnetic images shows that the northern part of the Demon Fault is composed of a series of parallel faults, which displaced high amplitude anomalies in an en-echelon pattern (Figures 4.5b, c, 4.7a, b). The satellite images and digital elevation models show a NE-striking fault lineament in the northern part of the DF1 faults in the Jurassic units (Figures 4.2a, 4.5a). From the second vertical derivative aeromagnetic image, Cenozoic volcanic rocks, which are widespread in the northeastern part of the DF1 fault area, appear to be truncated by the N-striking faults (Figures 4.5b, 4.7c). This implies that late reactivation along the DF1 segment was possibly younger than 24.5–22.5 Ma, which

is the K–Ar age of these volcanic rocks (Webb et al., 1967). Nevertheless, I could not find appropriate field observations that support this interpretation.

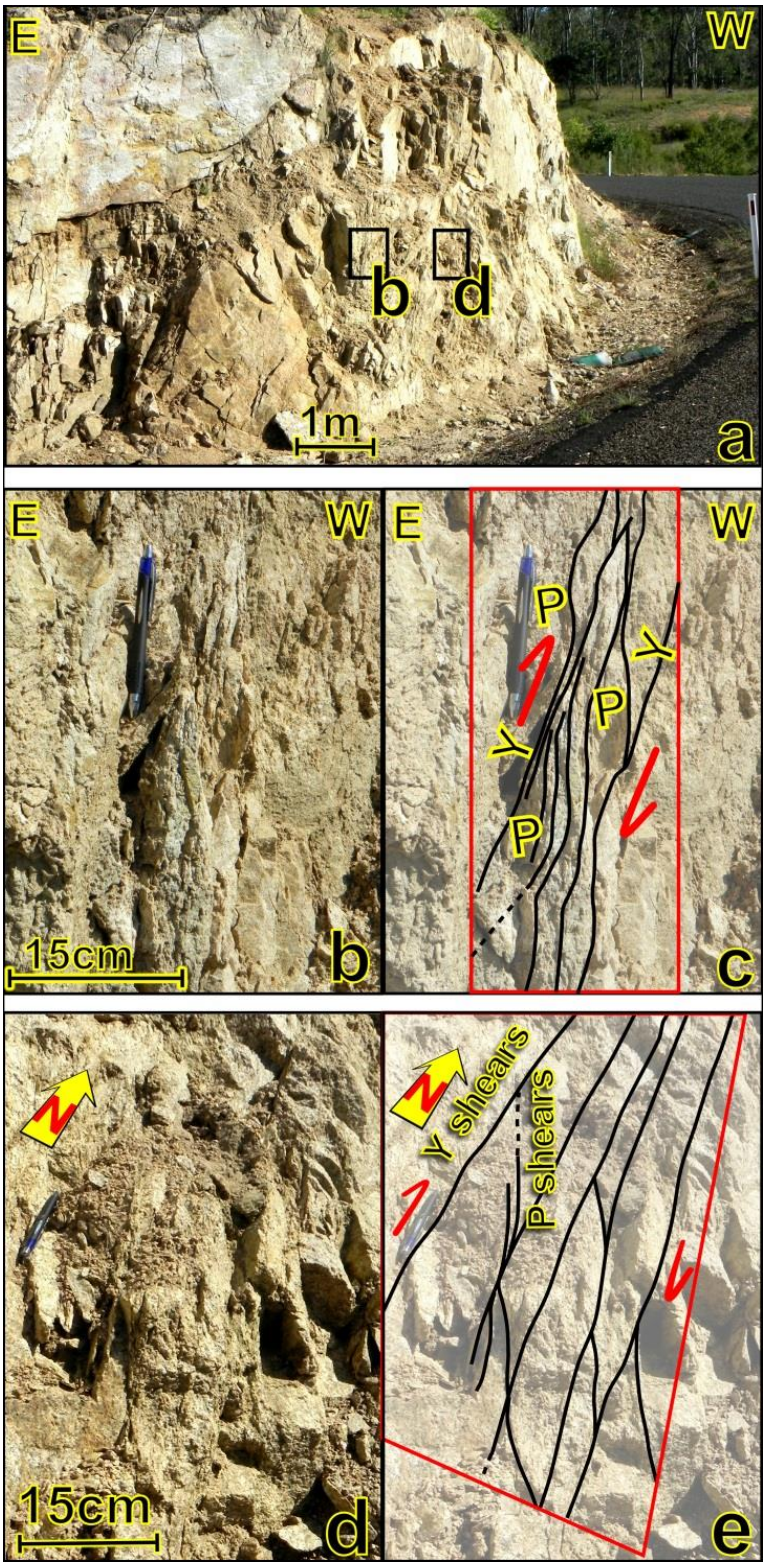

Figure 4.6. (a) Field photograph of the DF1 fault zone. (b, c) Riedel shears (P–Y shears) (section view) indicate reverse component of the DF1 fault. (d, e) Riedel shears (P–Y shears) in the DF1 fault zone, indicating dextral movement of the fault (map view). P shears have been deflected by Y shears dextrally.

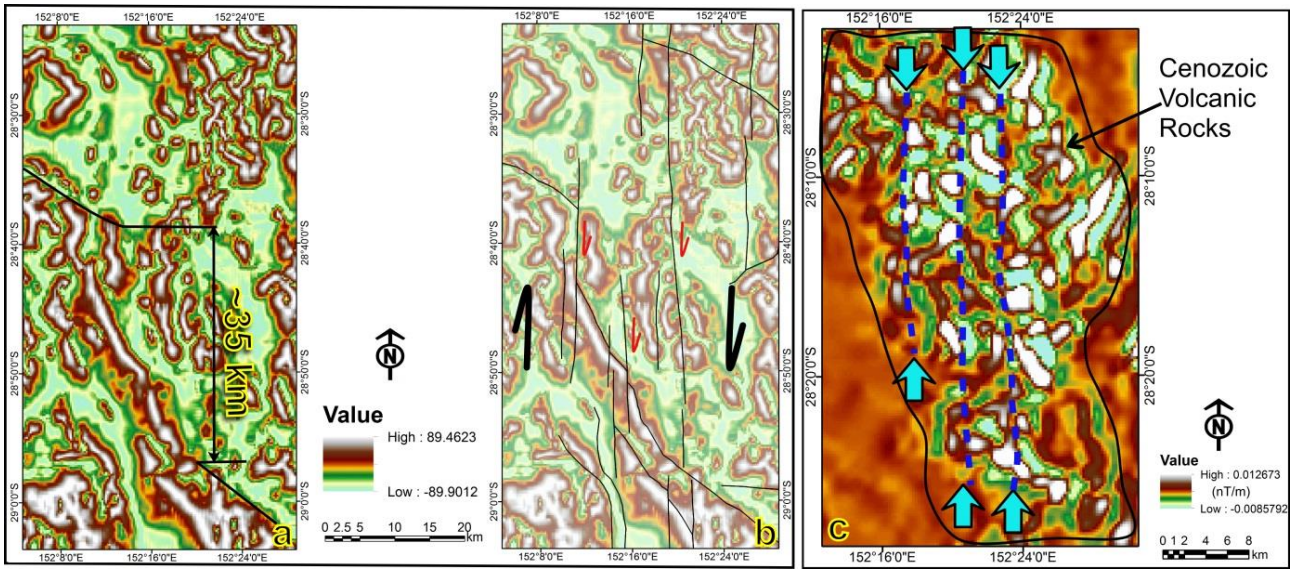

Figure 4.7. (a, b) Tilt angle derivative image of the Demon Fault Zone, displacing high amplitude Triassic magmatic rocks (see Figure 4.5b for location). (c) Second derivative image showing N-striking faults truncating short wavelength Cenozoic basalts.

4.5.2. The central part

From both satellite images and aeromagnetic data, it appears that the central part of the Demon Fault consists of two segments: DF2 and DF3 (Figures 4.2, 4.8). The tilt derivative aeromagnetic image shows that the central part of the Demon Fault has juxtaposed high amplitude anomalies against low amplitude anomalies (Figures 4.8a, b). Other faults cut magnetic anomalies on both sides of the Demon Fault (Figures 4.8a, b). Due to a lack of reliable markers on both sides of the fault, it is not possible to estimate the accurate displacement along the central part of the Demon Fault from remote sensing and aeromagnetic data.

4.5.2.1. The DF2 Fault

The DF2 fault, ~35 km in length, is a high angle (~75°) (dip) west-dipping oblique reverse dextral fault. It has mostly displaced the Stanthorpe Monzogranite, the Bungulla Monzogranite, and the Coombadjha Volcanic Complex (Figure 4.2a). The DF2 fault is observed as a sharp and linear trace on the satellite images and DEMs, creating a maximum elevation difference of 600 m in the middle of fault (Figure 4.2b). This elevation difference could have resulted from the juxtaposition of the Bungulla Monzogranite on west, with lower elevation, with the Stanthorpe Monzogranite on east with higher elevation (Figures 4.2a–c). In the Timbarra region (Figures 4.2a, 4.8a), the DF2 segment has some synthetic parallel faults, implying a wide (~1 km) fault zone (Figure 4.9). Some splays branch off the northern tip of the DF2 fault, creating a horsetail pattern of fractures with some minor antithetic

faults (Figures 4.2a, 4.9a–d, g). Based on field measurements, these NNW-striking splays have an average orientation of 57°/067° (dip/dip direction). Stereographic analysis of P–Y shears shows that the hanging-wall movement of these splays is toward the S to SSW, indicating a dextral-reverse component (Figures 4.9e, f). The northern part of the DF2 fault has been truncated by minor faults (Figure 4.9g).

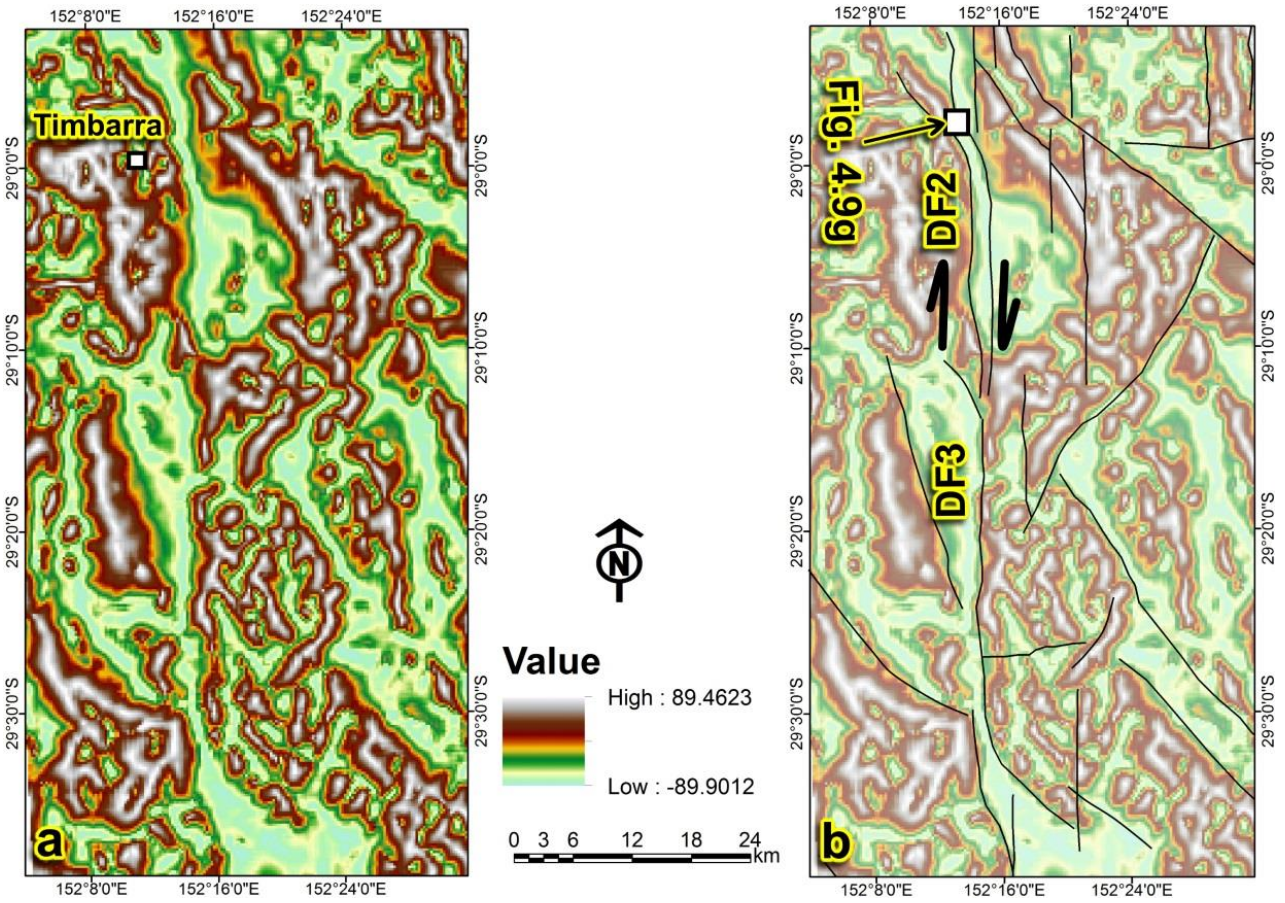

Figure 4.8. (a-b) Tilt angle derivative image of central part of the Demon Fault Zone, showing N-, NE- and NW-striking faults around the fault (see Figure 4.2d for location).

The trend of the southern part of the DF2 segment rotates eastward, reaching an azimuth trend of ~330° (Figure 4.10a–c). Field observations show a wide fault zone (~50 m) in the southern tip of the DF2 segment. The orientation of the southern DF2 segment is ~65°/242° (dip/dip direction). Stereographic analysis of slickensides and P–Y shears indicates that the DF2 fault is a reverse dextral fault (Figures 4.10c, d, 4.11a, b). Several medium-scale older Riedel shears, deflected by Y shears, are seen in the fault zone of the DF2 segment in the Bungulla Monzogranite, showing a dextral strike-slip movement (Figure 4.11c, d). Similarly to the northern tip, the southern part of the DF2 segment is observed as fault splays, branching off the main fault (Figures 4.2a, 4.10a, b). Brittle fault zones of these splays have developed in the Bungulla Monzogranite, resulting in the development of lensoid structures (Figure 4.12a). A dextral reverse movement of the hanging-wall is interpreted from analysis

of these structures (Figure 4.10e). Synthetic and antithetic fragmented grains are also indicative of dextral shearing in this zone (Figure 4.12b–d).

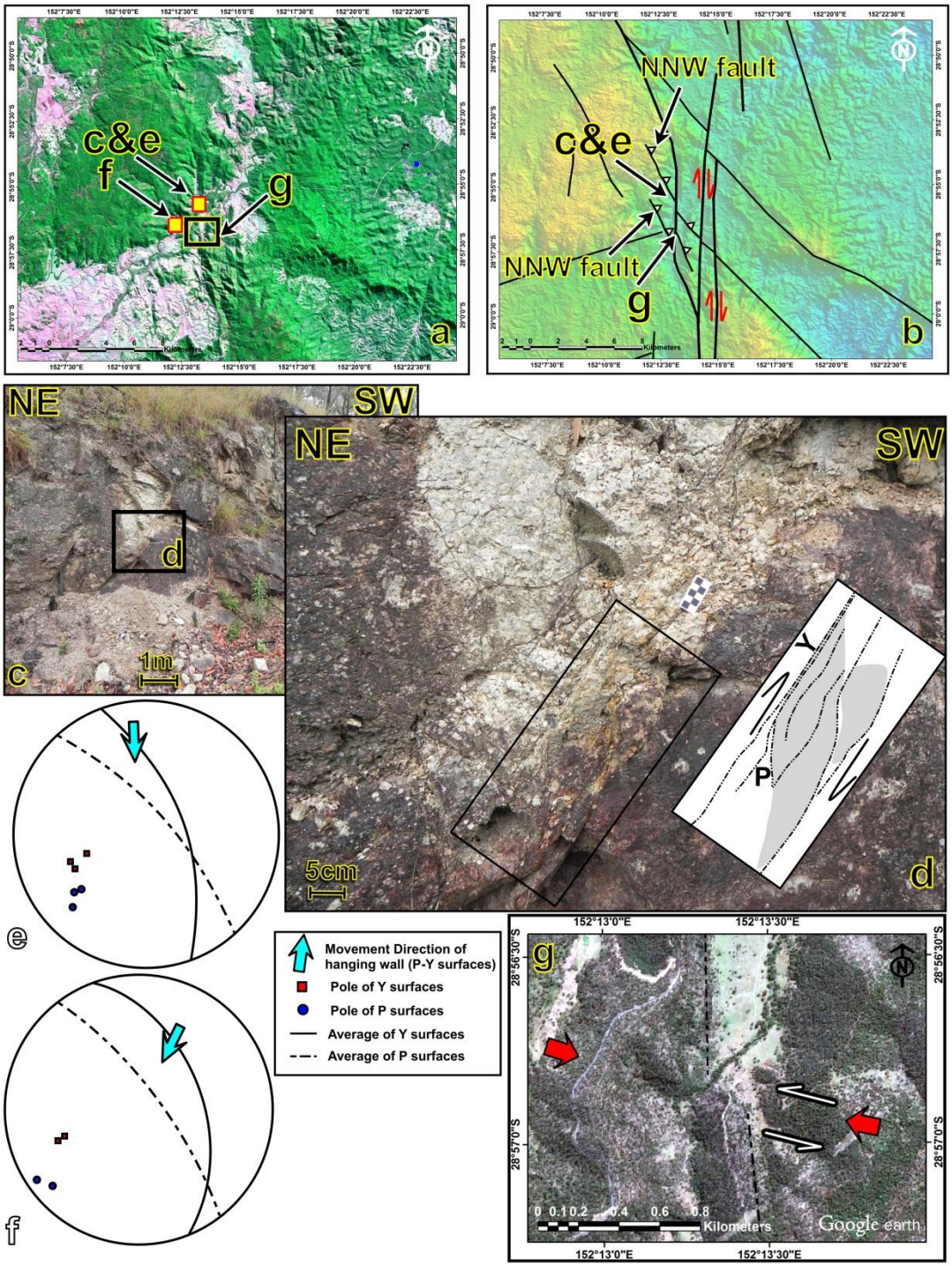

Figure 4.9. (a) Landsat ETM+ image of the northern part of the DF2 fault (see Figure 4.2b for location). (b) The northern part of the DF2 fault trace and its splays on ASTER digital elevation model. (c, d) Fault zone of a NNW-striking reverse splay of the DF2 fault. (e, f) Lower hemisphere equal angle stereographic projection of P–Y shears, indicating hanging-wall movement of the DF2 fault splays towards the ~S and SSW, respectively. (g) Google Earth image of an ESE-striking fault, sinistrally displacing the northern part of the DF2 fault.

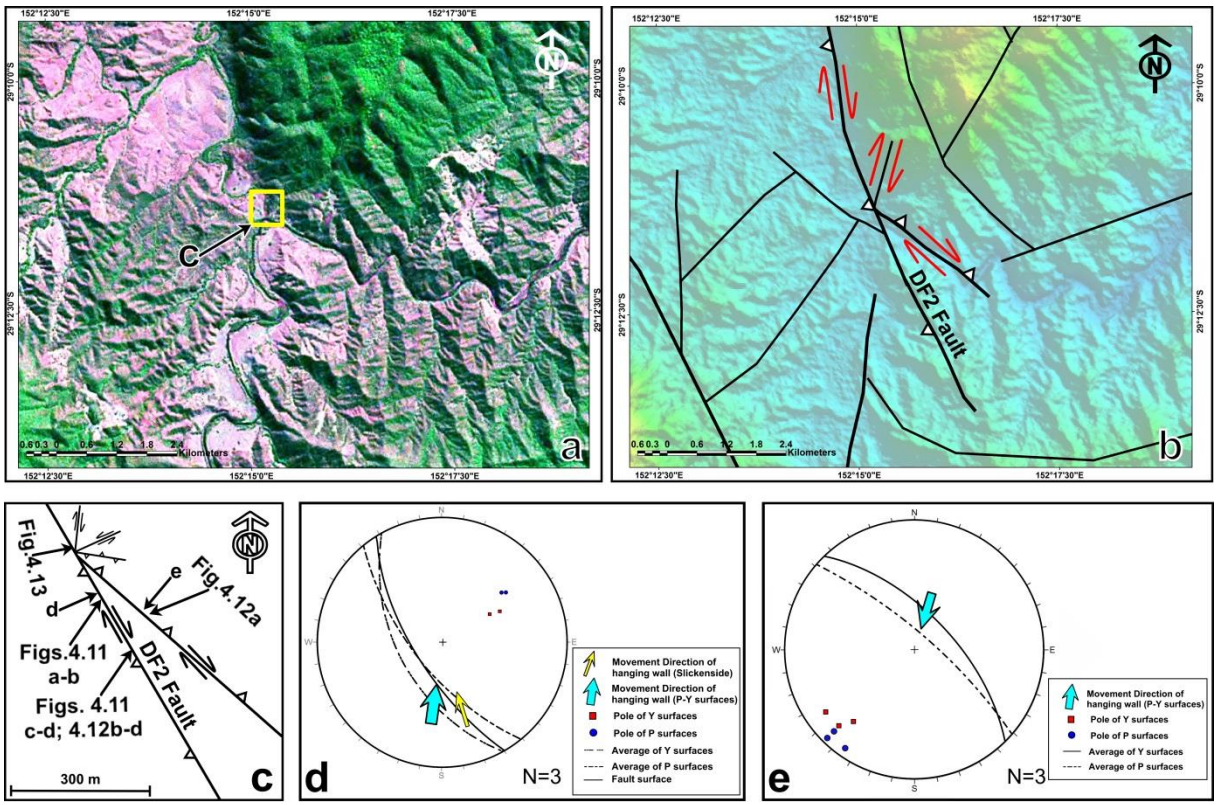

Figure 4.10. (a) Landsat ETM+ image of the southern part of the DF2 fault (see Figure 4.2b for location). (b) The southern part of the DF2 fault trace and its splays on ASTER digital elevation model. (c) A small part of the southern DF2 fault mapped in the field, showing its minor faults. (d) Lower hemisphere equal angle stereographic projection of P–Y shears, fault surface, and slickenside indicating reverse dextral movement of the DF2 fault. (e) Lower hemisphere equal angle stereographic projection of P–Y shears indicating the hanging-wall movement of a splay of DF2 fault toward the SSW.

Systematic small faults extend into the Bungulla Monzogranite in the DF1 fault zone. From mapping of these fractures, three fault systems with different orientations were recognised (Figure 4.13):

1. NNE-striking dextral faults with an average strike azimuth of 011°;
2. ENE-striking sinistral faults with an average strike azimuth of 065°; and
3. ESE-striking sinistral reverse faults with an average strike azimuth of 105°.

4.5.2.2. The DF3 Fault

The DF3 fault segment is ~44 km in length and displaces mostly the Coramba beds, the Dandahra Creek Granite and the Coombadjha Volcanic Complex (Figure 4.2a). From field observations, such as slickensides and lensoid structures, the DF3 fault is a high angle (~80°) W-dipping reverse dextral fault. Remote sensing data show that the width of the fault zone is up to a few hundred metres, including parallel N-striking faults and related minor faults (Figures 4.2a; 4.14a, b, 4.15a, b).

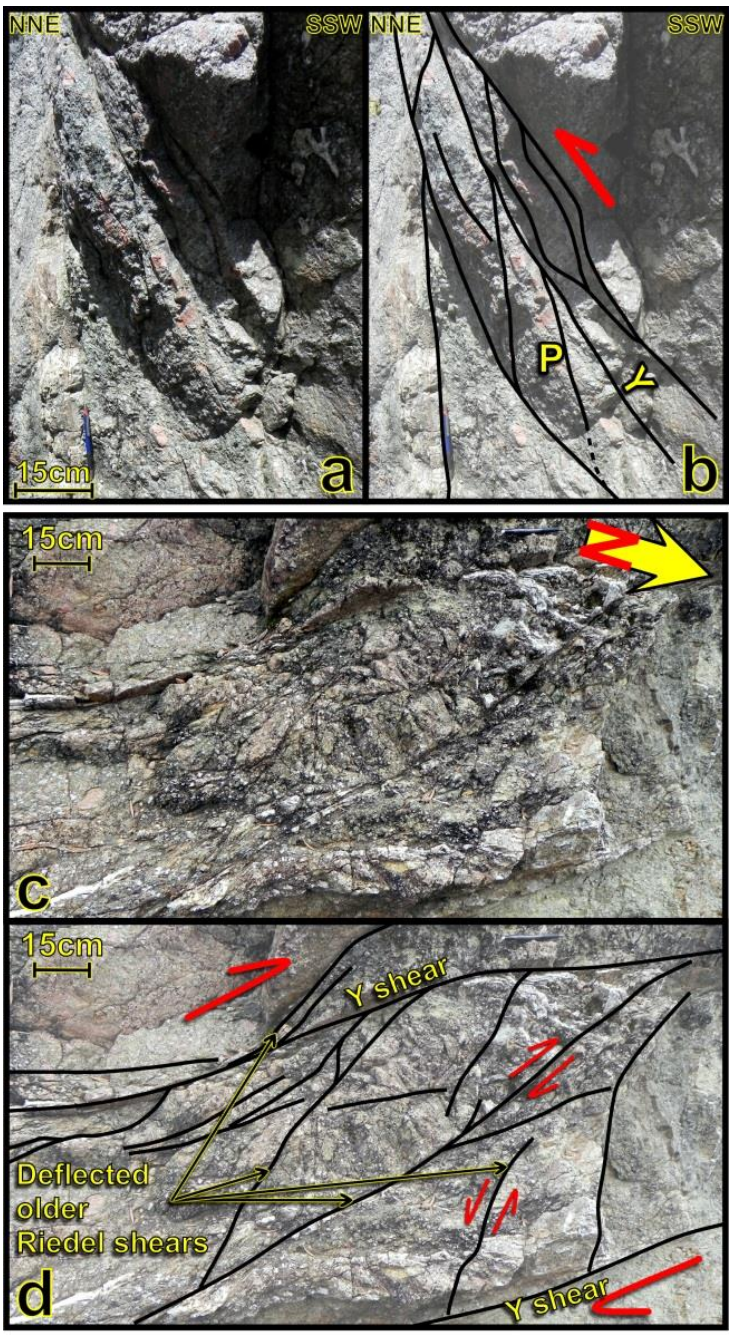

Figure 4.11. (a) Field photograph of the southern tip of the DF2 fault; and (b) a sketch of lensoid and Riedel shears (P–Y shears), indicating a reverse component of the fault. (c, d) Development of the dextral lensoids in the DF2 fault zone including deflected older Riedel shears by Y shears parallel to the DF2 fault. See Figure 4.9c for location.

Similarly to the DF2 fault, some synthetic faults splay off from the northern and southern parts of the DF3 segment to form horsetail and synthetic branch patterns, respectively (Figures 4.2a, 4.14a, b, 4.15a, b). The orientation of the northern part of the DF3 fault is 75°/265° (dip/dip direction). The trace of the northern part of the DF3 fault is mostly eroded by the Upper Rocky River; however, some brittle indicators, such as P–Y shears, parallel to the fault zone are consistent with dextral movement of the fault (Figure 4.14 c–g). Kinematic analysis of a strand of the DF3 fault confirms the reverse dextral movement in this area (Figure 4.14h).

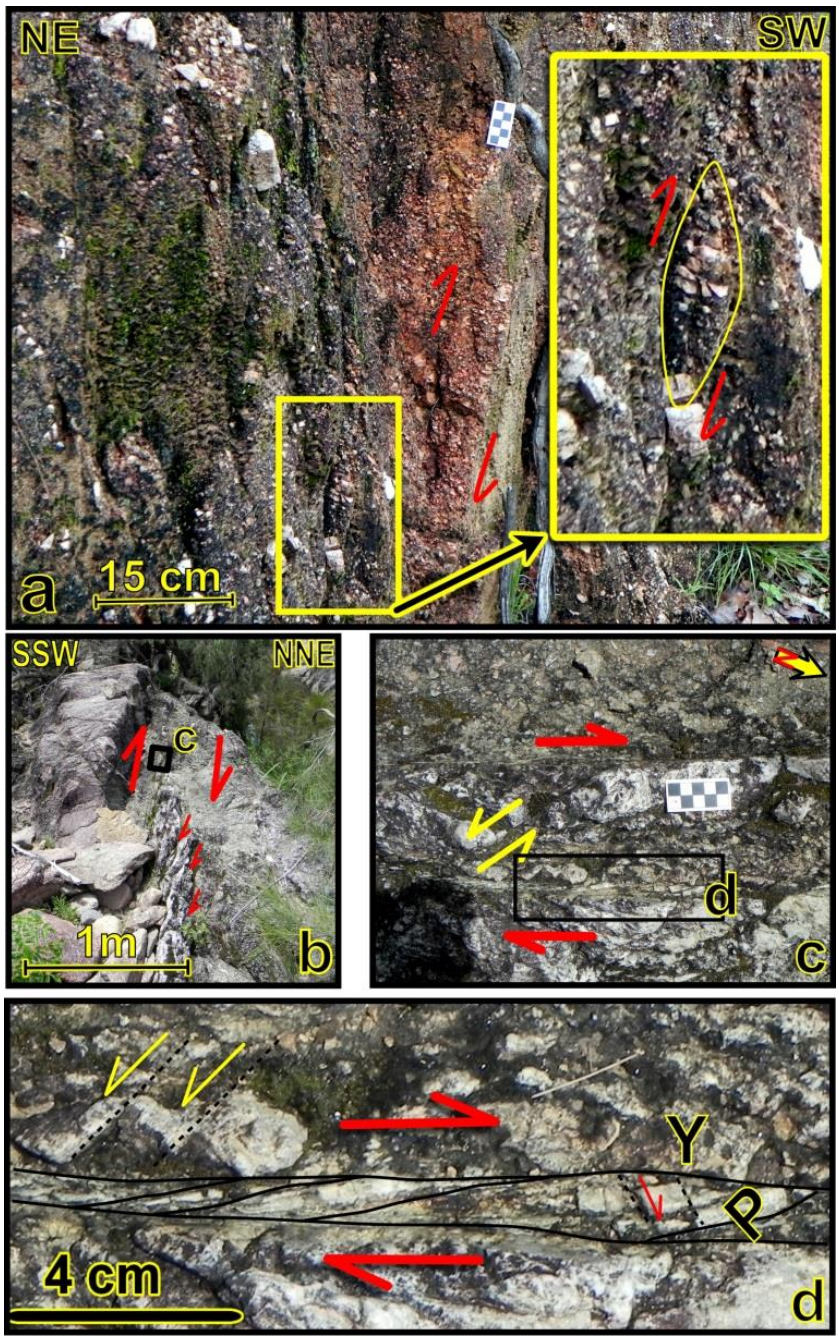

Figure 4.12. (a) Development of lensoid structures and P–Y shear in fault zone of a splay fault (see Figure 4.9c for location). (b) Fault zone of the southern part of the DF2 fault in the Bungulla Monzogranite (see Figure 4. 9c for location). Synthetic and (c) antithetic fragmented grains implying dextral movement of the DF2 fault (see Figure 4.9e for location). (d) P–Y shears and synthetic and antithetic fragmented grains implying dextral movement.

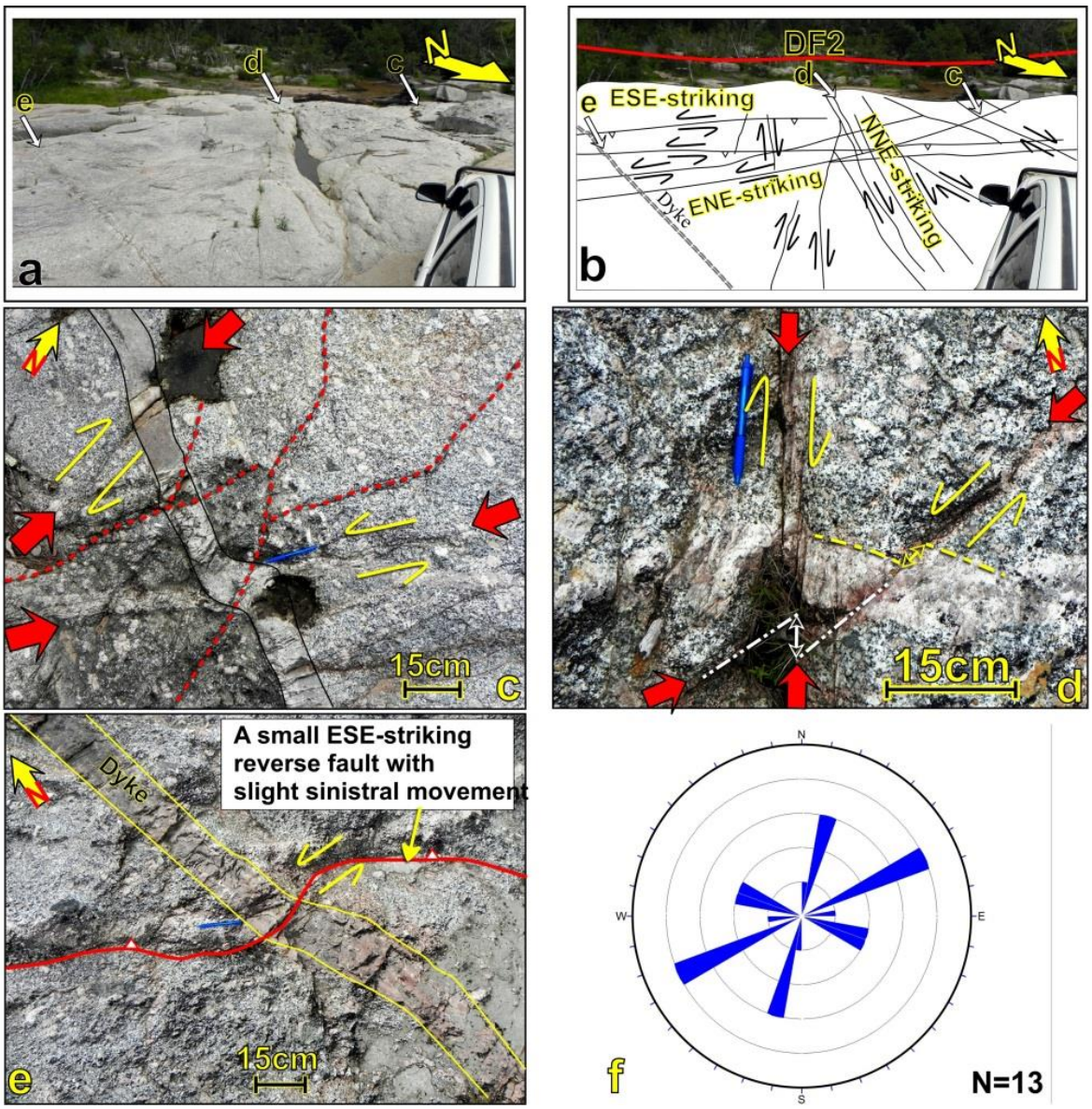

Figure 4.13. (a, b) A fracture system propagated in the DF2 fault zone indicating dextral movement of the main fault. (c, d) NNE-striking dextral and ENE-striking sinistral small faults developing in the dextral zone of the DF2 fault. Dash lines in (c) are fractures with no displacements. (e) A small ESE-striking reverse fault with slight sinistral movement, displacing a dyke. (f) Rose diagram of the small faults.

The azimuth trend of the DF3 fault changes to ~345° southward (Figure 4.15a, b). The southern part of the DF3 fault has a NNW-striking sharp vertical scarp between the Dandahra Creek Granite with higher elevation and the Coramba metasedimentary rocks, which have been eroded by a river (Figure 4.15c). Slickensides on the DF3 fault surface indicate a dextral strike-slip movement with a minor reverse component (Figure 4.15d–f). Fault splays, branching off the DF3 fault, have developed in the Dandahra Creek Granite and intensely deformed it (Figures 4.2a, 15b, 16a–c). These faults have orientation of 50–80°/050–080° east of the DF3 fault and 70°/105° west of the fault. A dextral reverse movement is inferred from these fault splays (Figure 4.16d).

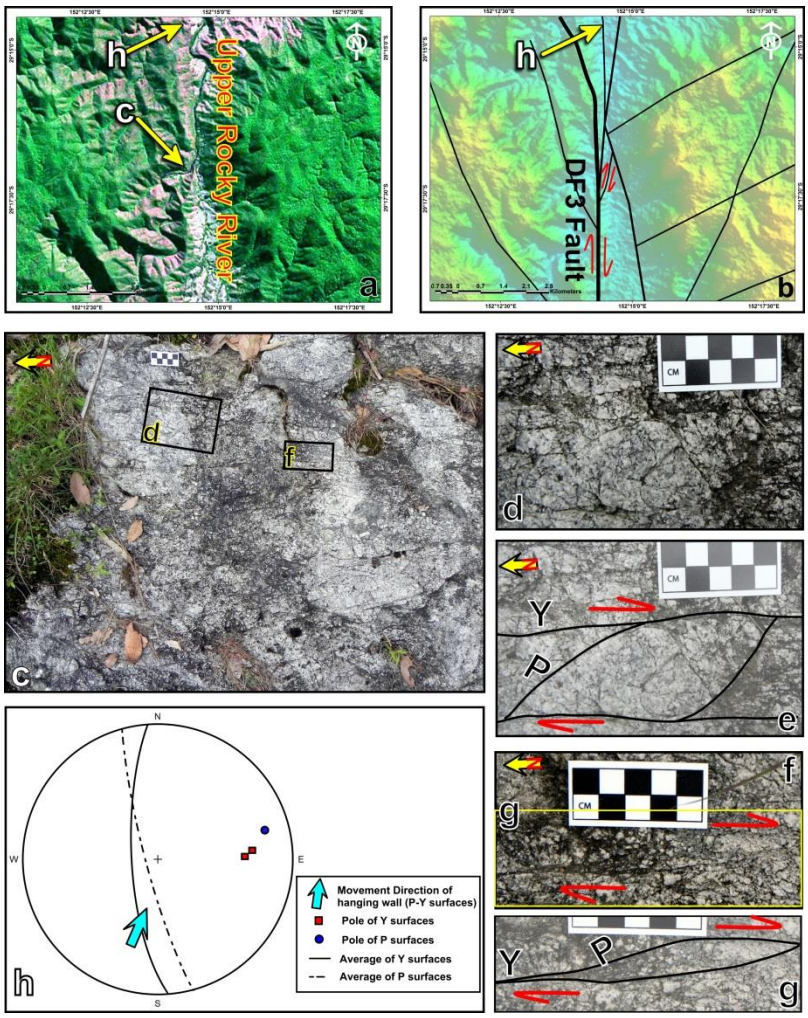

Figure 4.14. (a) Landsat ETM+ image of the northern part of the DF3 fault (see Figure 4.2b for location). (b) The northern part of the DF3 fault trace and its splays on ASTER digital elevation model. (c) N-striking brittle fabric in the DF3 fault zone. (d–g) lensoid and P–Y shears in the DF3 fault zone, showing dextral movement. (h) Lower hemisphere equal angle stereographic projection of P–Y shears indicates hanging-wall movement of the DF3 fault is toward the NNE.

4.5.3. The central part displacement

The restoration of geological units along the central part of the Demon Fault, with inferred steep boundaries, indicates that the Late Permian Granite, the Dandahra Creek Granite, and the Coombadjha Volcanic Complex have been displaced dextrally by ~25 km (A–A', B–B', and C–C', respectively in Figure 4.17). Figure 4.17 also indicates that the Demon Fault possibly displaced dextrally an older NNW-trending fault (juxtaposing D with D'). This result is approximately in agreement with the previous estimate of 23 km displacement by McPhie & Fergusson (1983) based on displacement of the Coombadjha Volcanic Complex.

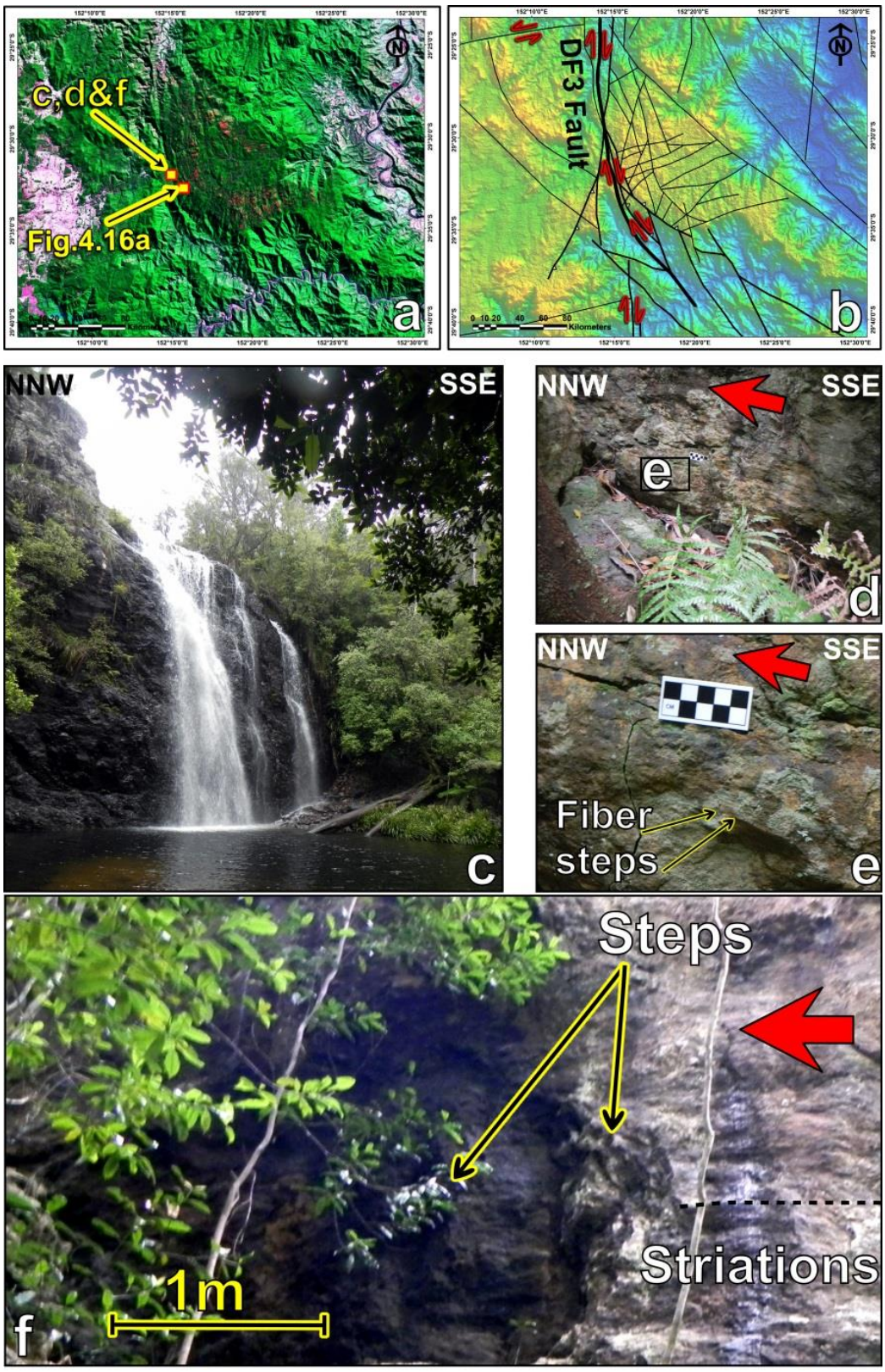

Figure 4.15. (a) Landsat ETM+ image of the southern part of the DF3 fault (see Figure 2b for location). (b) The southern part of the DF3 fault trace and its splays on ASTER digital elevation model. Note synthetic and antithetic faults reaching the DF3 fault. (c) Vertical fault scarp of the DF3 fault. (d, e) Slickenside on the DF3 fault surface with fiber steps shows a dextral strike slip movement with a minor reverse component. (f) Large steps on the DF2 fault surface indicating dextral movement of missing block.

4.5.4. The southern part (DF4)

The NW-striking dextral DF4 fault is ~87 km in length and is the longest and southernmost strand of the Demon Fault. It mainly deforms Carboniferous metasedimentary rocks, such as the Coramba and Brooklana beds, and Middle Triassic rocks, such as the Chaelundi Granite (Phillips et al., 2011) (Figure 4.2).

The DF4 fault produces a sharp linear scarp in the Newton Boyd area, up on the east, creating an elevation difference of more than 400 m (Figures 4.2a, b). This elevation difference may have resulted from the juxtaposition of the higher elevated Coramba beds and Chaelundi Granite, next to the lower elevated Mount Mitchell Monzogranite and Sara beds, respectively (Figure 4.2a, b).

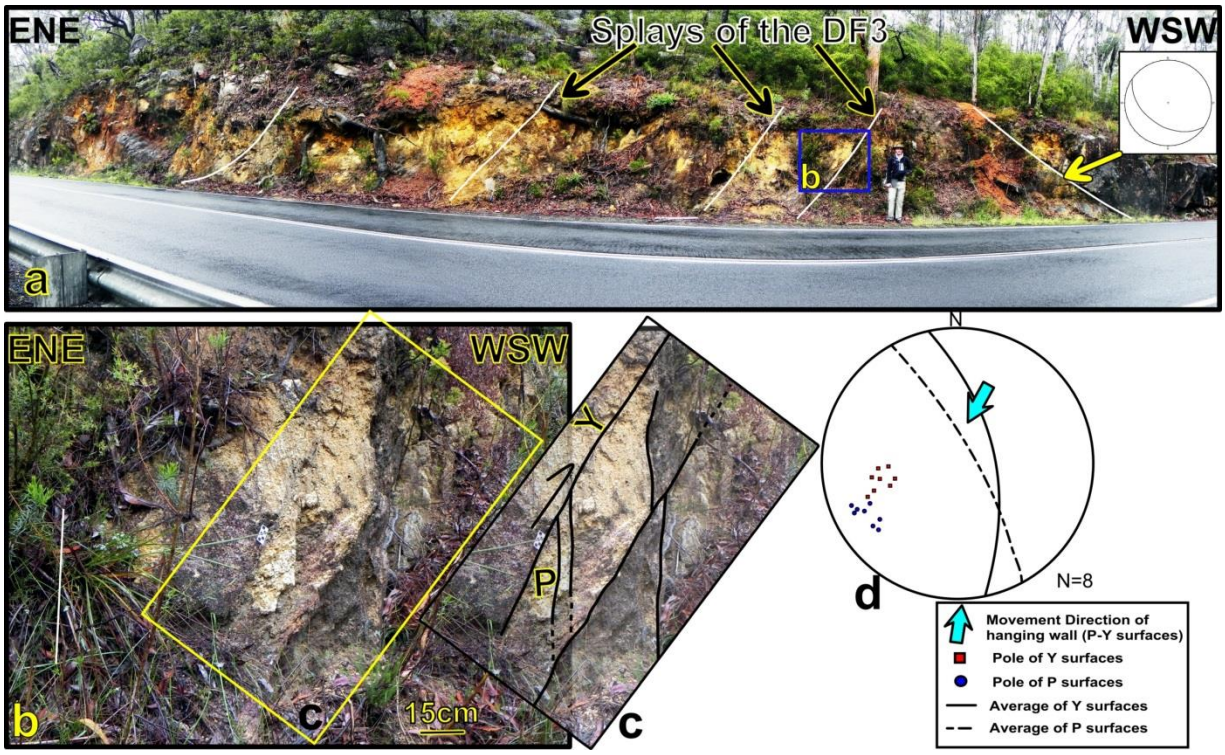

Figure 4.16 (a) A wide fault zone (~50 m) of splays branching off the DF3 fault in the Dandahra Creek Granite (see Figure 4.14a for location). (b, c) Riedel shears (P–Y shears) propagating in this fault zone. (d) Lower hemisphere equal angle stereographic projection of P–Y shears indicating a dextral reverse hanging-wall movement toward the SSW.

The interpretation of the second vertical derivative and tilt derivative aeromagnetic images reveals a series of the sinistral NW-striking faults that have been displaced by the DF4 fault (Figure 4.18a). These NW-striking faults have deformed and dragged high amplitude anomalies sinistrally and formed structural lensoid shapes, which have been displaced by the DF4 fault (Figures 4.18a–c). By comparison with geological maps (Figures 4.2a, d, e), these dragged anomalies correspond to the Chaelundi Granite, Newton Boyd Granodiorite, and Mount Mitchell Monzogranite. The restoration

of one of these displaced lensoid structures indicates ~19 km dextral displacement along the DF4 fault (Figures 4.18b, c).

4.6. Discussion

4.6.1. Kinematics of the Demon Fault

Kinematic indicators from the different segments indicate that the Demon Fault is not a pure strike-slip fault, but has a minor reverse component. This conclusion is in agreement with observation of slickensides by Korsch *et al.* (1978) in the Newton Boyd area.

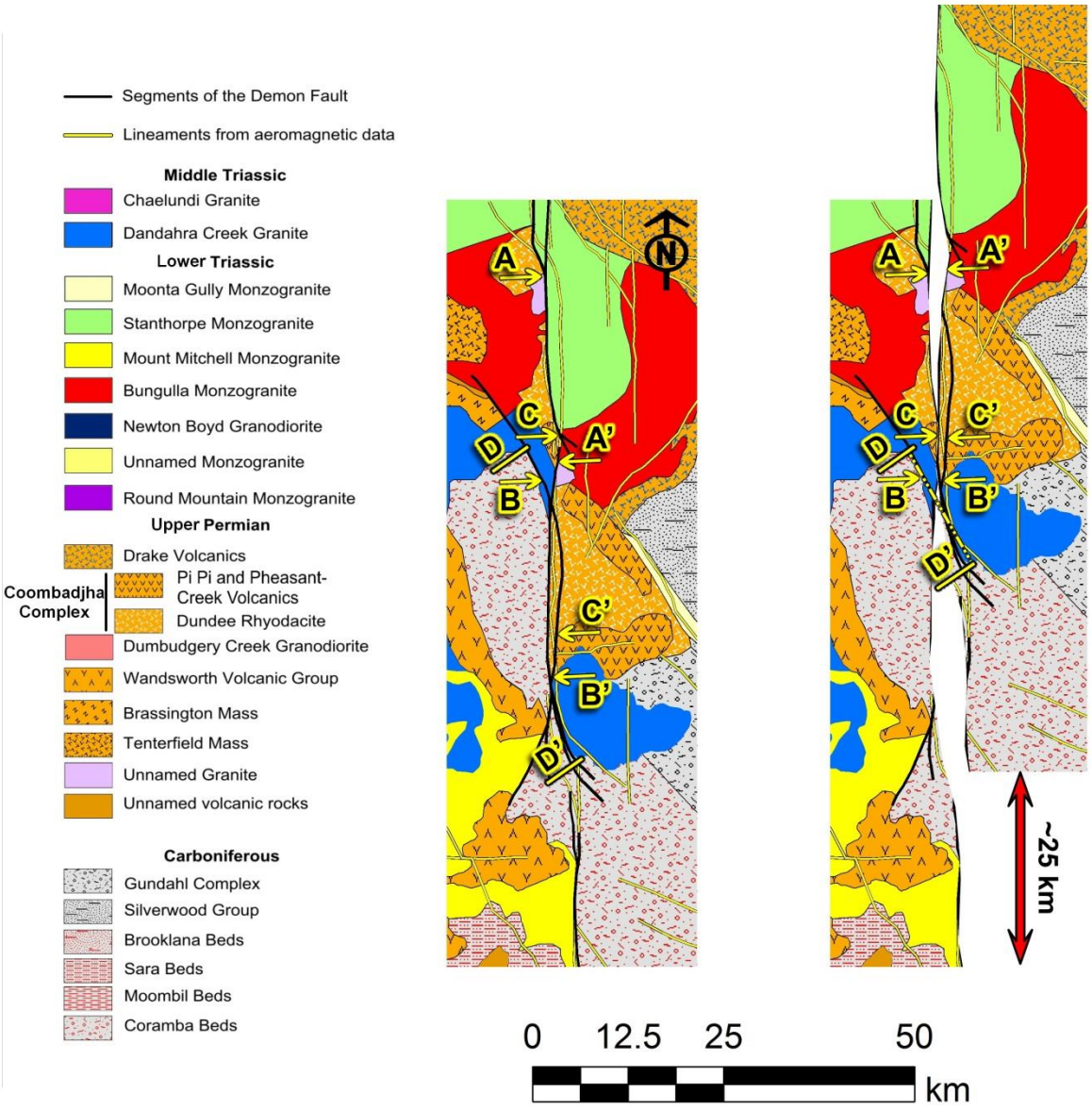

Figure 4.17. Restoration of the central part of the Demon Fault based on the offset of geological units, showing ~25 km of dextral displacement.

The dextral kinematics of the Demon Fault has been discussed in earlier studies, but the exact amount of displacement has been debated (30 km by Shaw 1969 in the Stanthorpe Monzogranite; 17 km by Korsch *et al.* 1978 in the Dundee Rhyodacite and the Bungulla Monzogranite; and 23 km by McPhie & Fergusson 1983 in the Coombadjha Volcanic Complex). The results indicate that different parts of the Demon Fault are characterised by different offsets. In the northern part, the Demon Fault has displaced a NW-striking high anomaly unit by ~35 km (Figure 4.7). In the central part, the restoration of geological maps shows ~25 km apparent dextral offset of late Permian and Triassic lithological units (Coombadjha Volcanic Complex, the Dandahra Creek Granite, and late Permian Granite; Figure 4.17), which is consistent with the estimation by McPhie & Fergusson (1983). In the southern part of the Demon Fault, NW-striking structures have been displaced by ~19 km (Figure 4.18).

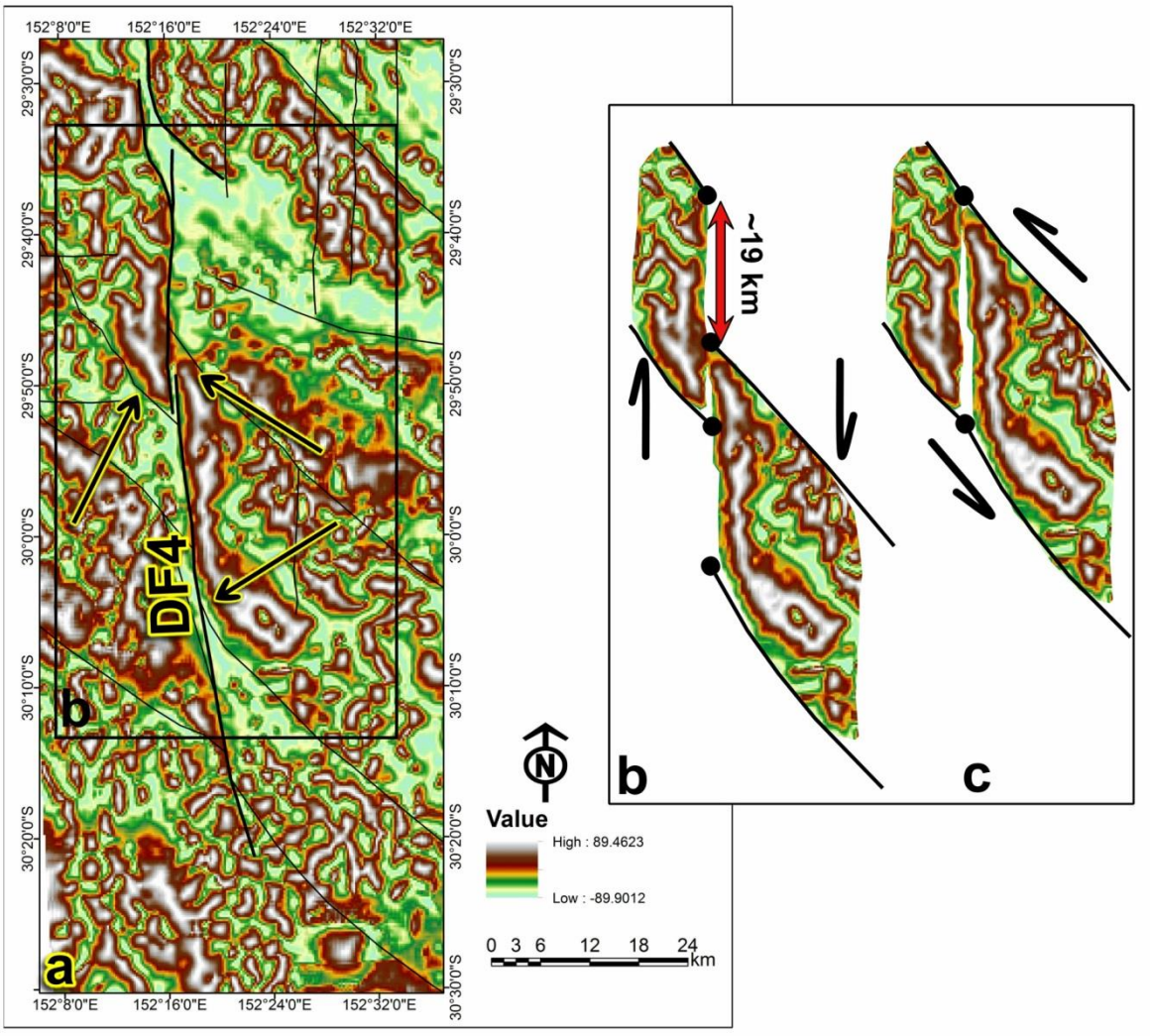

Figure 4.18. (a) Tilt angle derivative image of the southern part of the Demon Fault Zone, indicates NW-striking faults, sinistrally dragging magnetic anomalies and forming lensoid structures. Arrows show sinistrally dragged areas. The DF4 has displaced these faults. (b, c) displacement of an older sinistral NW-striking lensoid structure by the DF2 by ~19 km.

There are two possibilities for these different displacements in the northern, central, and southern parts of the Demon fault. Firstly, it is possible that the different segments have experienced different deformational histories. For example, the history of the northern part was perhaps more complex, and may have involved recent reactivations that have not affected the central and southern parts. Alternatively, it is possible that, towards the south, deformation was partitioned into minor reverse splays of the Demon Fault (e.g. Figures 4.10e, 4.16c), thus reducing the overall dextral displacement in comparison with the northern part.

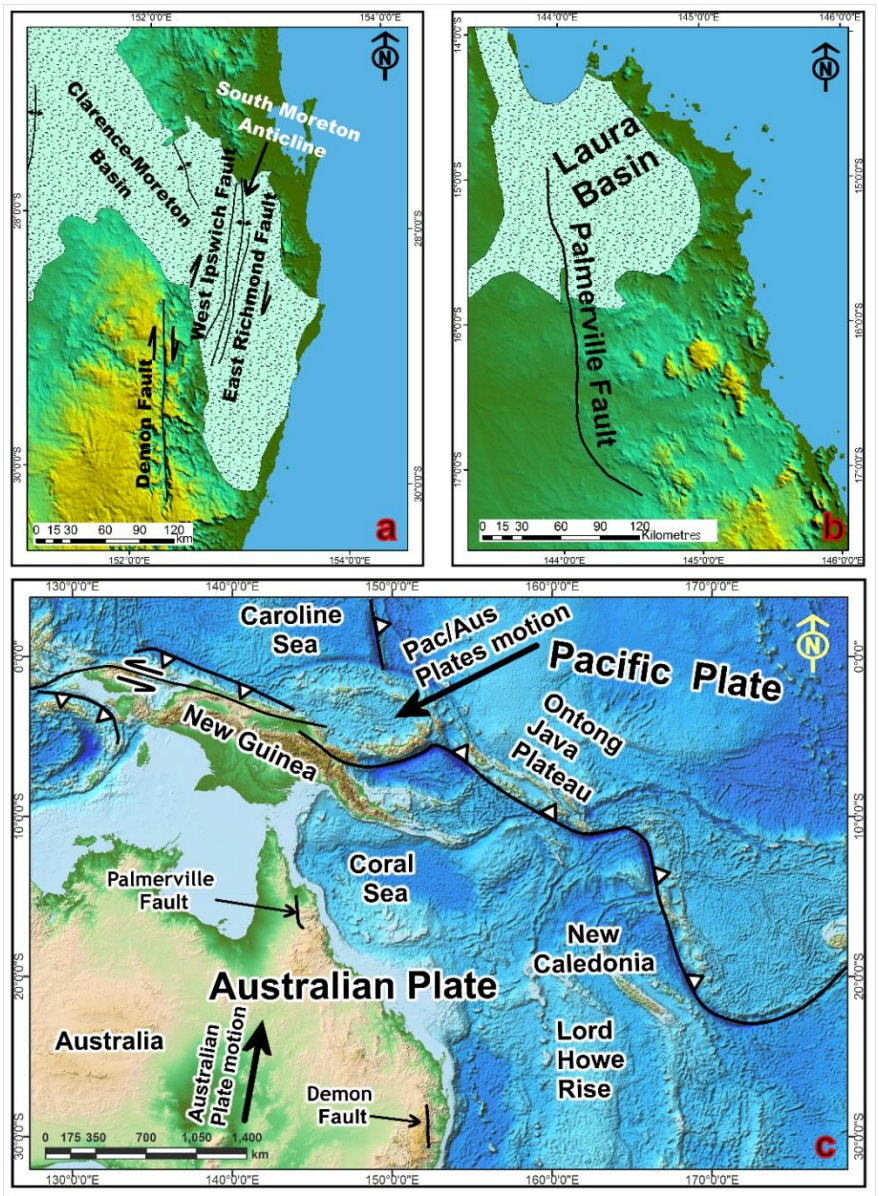

Figure 4.19. (a) The West Ipswich and East Richmond faults in the Clarence-Moreton Basin (see Figure 4.1a for location). (b) The Palmerville Fault in northern Queensland crossing the Jurassic–Cretaceous Laura Basin (see Figure 4.1a for location). (c) ETOPO1 digital elevation model of the Australian and Pacific plates (Amante and Eakins, 2009) and a simplified tectonic framework. The Pacific/Australia relative motion vector is from DeMets *et al.* (1994).

The aeromagnetic and remote sensing data show that the structure of the northern part of the Demon Fault involves a number of N-striking dextral faults, E-striking sinistral faults, and NE-striking faults. I interpret these faults as synthetic and antithetic faults in the tip of a northward propagating damage zone (Figure 4.5).

There are a large number of minor faults in the vicinity of the Demon Fault zone, mainly NNE-striking dextral faults, NE-striking sinistral faults and ESE-striking sinistral reverse faults. I interpret these structures as being generated in a brittle dextral shear zone during the recent activities of the Demon Fault.

4.6.2. Timing and possible tectonic causes of faulting

The Demon Fault has displaced Triassic magmatic rocks dated at 249–232 Ma (Shaw, 1994; Phillips et al., 2011), but whether it was active prior to the Triassic is unclear. Some authors have suggested that a continental-scale dextral strike-slip fault that accommodated ~500 km of dextral movement was active in eastern Australia during the Carboniferous and/or Permian, and was responsible for the formation of the Texas and Coffs Harbour oroclines (Evans and Roberts, 1980; Murray et al., 1987). This model, however, requires considerably larger displacements along N–S dextral strike-slip structures and higher strain in the surrounding area (Li et al. 2012a). I, therefore, think that the existence of a late Paleozoic transform boundary, as suggested by Murray *et al.* (1987), remains speculative and that the Demon Fault activity is not related to this inferred fault. The major activity of the Demon Fault is interpreted to be younger than 233 Ma, based on the ~19 km displacement of the Chaelundi Granite (Phillips et al., 2011), and most likely did not play a major role in the formation of the New England oroclines. The Demon Fault, however, has displaced and dragged the shared limb of the Texas and Coffs Harbour oroclines and accentuated the curvature of the Coffs Harbour Orocline (Rosenbaum 2012).

Early and Middle Triassic magmatic rocks have been displaced by NW-striking sinistral faults, which were active either synchronously with magmatism or subsequently (Figures 4.2a, 4.7, 4.18). The results show that these faults are displaced by both northern and southern parts of the Demon Fault (see Figures 4.7, 4.17, 4.18). Therefore, the initiation of the Demon Fault must have occurred after the emplacement of the Middle Triassic magmatic rocks and activity of the NW-striking faults.

I speculate that the initiation of the Demon Fault was associated with the development of Late Triassic–Jurassic basins in eastern Australia. Tectonic activity during this period involved the formation of sedimentary basins in a transtensional regime dominated by strike-slip faulting (Korsch et al., 1989). Strike-slip faults, which include the West Ipswich and East Richmond faults in the Clarence-Moreton Basin, are sub-parallel to the Demon Fault (Figure 4.19a). These faults are steep

reverse dextral strike-slip faults, which form the western and eastern borders of the South Moreton Anticline, respectively (Korsch et al., 1989; O'Brien et al., 1994) (Figures 4.1a, 4.19a). The faults were active from the Early Triassic to Early Jurassic (or possibly during all of the Jurassic), in a transtensional regime as important structures in the development of the Esk Trough, the Ipswich and Clarence-Moreton basins (Korsch et al., 1989; O'Brien et al., 1994). Strike-slip movement possibly continued intermittently into the Jurassic and Early Cretaceous (Korsch et al., 1989). In the last stage of faulting, these faults were inverted in a transpressional regime and accommodated the deformation of the Triassic–Jurassic basins (Korsch et al., 1989; O'Brien et al., 1994).

Similarly to the West Ipswich and East Richmond faults, the most recent activity of the Demon Fault was likely associated with contractional deformation, giving rise to its dextral strike-slip movement with minor reverse kinematics (e.g. Figures 4.10d, 4.14h, 4.15d–e). In addition, the pattern of fractures in the vicinity of the Demon Fault indicates a dextral transpressional movement (Figure 4.13). This more recent activity has displaced Jurassic strata and possibly Cenozoic basalts, for example, in the splays of the northern strand of the Demon Fault (the DF1 fault) (Figures 4.2a, 4.5, 4.7). There are a number of possible tectonic causes for this dextral transpression. The first possibility is that deformation occurred in a mid-Cretaceous contractional event, which also resulted in thrust faults in the Bowen and Surat basins (Korsch *et al.* 2009b). Alternatively, it is possible that this activity may have occurred in the latest Cretaceous (from 67.7 to 64 Ma), when northeastern Australia was subjected to transpression (Gaina et al., 1998a). Nevertheless, there is no detailed structural evidence supporting this transpressional event.

Another possibility is that the latest dextral transpressional movement of the Demon Fault was related to far-field compressional stresses transmitted from the convergent boundary at the northern margin of Australia. This convergent plate boundary, associated with the rapid northward motion of Australia, has involved significant collisional events in northern New Guinea during the late Cenozoic, for example in the late Oligocene and late Miocene (e.g., the Melanesian arc collision and the collision of Ontong Java) (Hill and Hall, 2003; Quarles van Ufford and Cloos, 2005; Knesel et al., 2008; Baldwin et al., 2012). The vector of convergence was oblique, resulting in an ESE-striking sinistral oblique deformation in New Guinea (DeMets et al., 1994; McCaffrey, 1996; Davies, 2012) (Figure 4.19c). This oblique convergence gave rise to strain partitioning in New Guinea, producing sinistral strike slip faults along the northern accreted arcs and fold-and-thrust belt to the south (McCaffrey, 1996). This oblique convergence could have resulted in sporadic reactivation of some structures in northern and eastern Australia during the late Cenozoic. For example, the Palmerville Fault, which affected the Jurassic–Cretaceous Laura Basin, in northern Queensland has been active intermittently since the Paleozoic (De Keyser, 1963; Shaw et al., 1987) (Figure 4.19b), and was still

active during the Cenozoic, as indicated by the deformation of Cenozoic rocks (De Keyser, 1963; De Keyser and Lucas, 1968).

4.7. Conclusions

Aeromagnetic gridded data, satellite images, digital elevation models and field observations were utilised to investigate the dextral Demon Fault in eastern Australia. I show that the Demon Fault is not a pure strike-slip fault, but has a minor component of high-angle reverse movement. The estimation of displacement from aeromagnetic data and geological map indicates that different offsets occurred along different parts of the Demon Fault, with a general decrease in displacement towards the south. This observation may suggest that different segments have experienced different histories of reactivation, or that deformation was partitioned into minor reverse splays toward the south. The Demon Fault has displaced NW-striking faults, which deformed Early to Middle Triassic magmatic rocks, indicating that the initiation of Demon Fault has occurred after the emplacement of the magmatic rocks and activity of the NW-striking faults. The presence of sub-parallel structures in Late Triassic to Cretaceous basins in eastern Australia suggests that the Demon Fault has been active during the Mesozoic. The last activity of the Demon Fault has been associated with a transpressional regime, which is interpreted to be related to a mid-Cretaceous contractional event or to Cenozoic collisional processes at the northern Australian margin.

Chapter 5

Late Mesozoic and Cenozoic wrench tectonics in eastern Australia: Insights from the North Pine Fault System (southeast Queensland)

Late Mesozoic and Cenozoic wrench tectonics in eastern Australia: Insights from the North Pine Fault System (southeast Queensland)

Abstract

The North Pine Fault System (NPFS) in SE Queensland belongs to a series of NNW-striking sinistral faults that displaced Paleozoic to Cenozoic rock units in eastern Australia. I have studied the geometry and kinematics of the NPFS by utilizing gridded aeromagnetic data, digital elevation models, and field observations. The results indicate that all segments of the NPFS were subjected to sinistral reverse strike-slip faulting. Restorations of displaced magnetic anomalies indicate sinistral offsets ranging from 3.4 to 8.2 km. The existence of a (possibly) Late Triassic granophyre dyke parallel to one of the fault segments, and the occurrence of NNW-striking steeply dipping strike-slip and normal faults in the Late Triassic-Early Cretaceous Maryborough Basin, indicate that the NPFS has likely been active during the Mesozoic. I propose that from the Late Cretaceous to early Eocene, NNW-striking faults in eastern Australia, including the NPFS, were reactivated with oblique sinistral-normal kinematics in response to regional oblique extension associated with the opening of the Tasman and Coral Seas. This interpretation is line with the modeled dominant NNE- to NNW-directed horizontal tensional stress in the Eocene. The latest movements along the NPFS involved sinistral transpressional kinematics, which was possibly related to far-field contractional stresses from collisional tectonics at the eastern and northern boundaries of the Australian plate in the Cenozoic. This sinistral-reverse oblique kinematics of the NPFS in the Cenozoic is in line with ESE to ENE orientations of the modeled maximum horizontal stress in SE Queensland.

Key words: North Pine Fault System, eastern Australian sedimentary basins, Late Cretaceous-early Cenozoic extension, strike-slip faults, transtension, transpression

5.1. Introduction

The tectonic evolution of eastern Australia since the Late Triassic has involved three important stages: (1) the development of Late Triassic to Early Cretaceous sedimentary basins, possibly in a back-arc setting associated with trench retreat (Korsch et al., 1989; Li et al., 2012b); (2) Late Cretaceous to early Eocene continental fragmentation during the opening of the Tasman and Coral Seas (Gaina et al., 1998a; Gaina et al., 1999); and (3) mid-Eocene to recent volcanism and minor deformation

accompanied by a fast northward motion of the Australian plate over a hotspot track (Veevers, 2000; Knesel et al., 2008; Vasconcelos et al., 2008). Although these processes have played a major role in the evolution of the Australian continent since 200 Ma, there is only limited information on the exact geodynamic setting associated with each stage of deformation, and the expression of such deformation in the regional geology. One way to address this shortcoming is by studying fault systems in eastern Australia, including their reactivation history, kinematics, style and intensity of deformation.

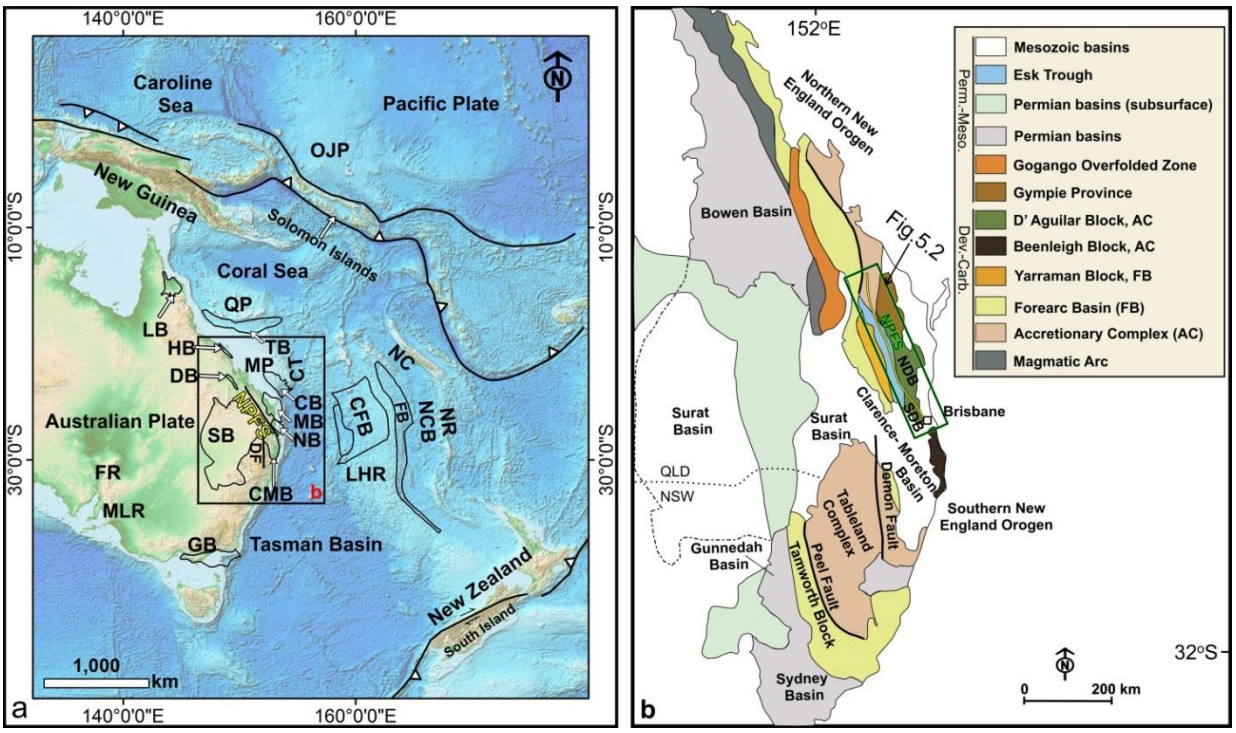

Figure 5.1. (a) ETOPO1 digital elevation model of the Australian and Pacific plates (Amante and Eakins, 2009), and a simplified tectonic framework and Mesozoic sedimentary basins at eastern Australia. CMB, Clarence-Moreton Basin; CB, Caledonia Basin; CB, Capricorn Basin; CFB, Capel and Faust basins; CT, Cato Trough; DB, Duaringa Basin; DF, Demon Fault; FB, Fairway Basin; FR, Flinders Ranges; GB, Gippsland Basin; HB, Hillsborough Basin; LB, Laura Basin; LHR, Lord How Rise; MB, Maryborough Basin; MLR, Mt Lofty Ranges; MP, Marion Plateau; NB, Nambour Basin; NCB, New Caledonia Basin; NC, New Caledonia; NR, Norfolk Ridge; OJP, Ontong Java Plateau; QP, Queensland Plateau; SB, Surat Basin; TB, Townsville Basin. (b) Regional tectonic elements of eastern Australia. SDB, South D'Aguilar Block; NDB, North D'Aguilar Block.

The major fault systems in eastern Australia are thought to be associated with the late Paleozoic to early Mesozoic New England Orogen (Murray et al., 1987; Holcombe et al., 1997b; Li et al., 2012b). These fault systems may have been reactivated as strike-slip and normal faults during the Late Triassic-Early Cretaceous and played a role in the development of Mesozoic sedimentary basins (Korsch et al., 1989; Babaahmadi and Rosenbaum, 2013). Such structures could have also been active as strike-slip or normal faults during the Late Cretaceous opening of the Tasman Sea (Gaina et al.,

1998a; Gaina et al., 1998b). The North Pine Fault System (NPFS) in southeastern Queensland (Figure 5.1) is one of these faults. It comprises several parallel and *en echelon* NNW-striking sinistral segments, but so far there is no detailed documentation of the geometry and kinematics of each segment within the fault system.

In this paper, I describe the geometry and kinematics of the NPFS by presenting detailed structural analysis of the different fault segments. Using information from field observations, digital elevation models, gridded aeromagnetic data, and geological maps, I demonstrate that activity along this fault system may have been related to the Mesozoic and Cenozoic geodynamics of the eastern part of the Australian Plate.

5.2. Geological Setting

The geology of eastern Australia is characterised by Paleozoic to early Mesozoic rocks of the New England Orogen, early Permian to Mesozoic sedimentary basins, and Cenozoic volcanic rocks. The New England Orogen is the youngest component in the Tasmanides orogenic collage of eastern Australia (Leitch, 1974; Glen, 2005), and is normally subdivided into northern and southern parts, which are separated by the Mesozoic Clarence-Moreton Basin (Figure 5.1b). The northern part of the orogen, from Brisbane northwards, follows a gently curved NNW-trending structural grain along the Queensland coast (Figure 5.1b). It is composed of a Devonian-Carboniferous subduction complex, forearc basin, and magmatic arc (Leitch et al., 1992; Henderson et al., 1993; Holcombe et al., 1997a). The southern New England Orogen also includes a Devonian-Carboniferous subduction complex, but its structural grain is more complex and is characterised by four tight curves (oroclines) (Rosenbaum et al., 2012).

During the early Permian, eastern Australia was affected by extensional deformation that resulted in the development of widespread sedimentary basins, including the Sydney, Gunnedah, and Bowen Basins (Leitch, 1988l Korsch et al., 2009a). Basin formation took place simultaneously with the emplacement of S-type granitoids (Shaw and Flood, 1981; Hensel et al., 1985) and oroclinal bending (Rosenbaum et al., 2012), and may have been controlled by extensional backarc deformation (Korsch et al., 2009a; Rosenbaum et al., 2012).

Following the period of extensional tectonism, eastern Australia was affected, from ~260 to ~230 Ma, by folding and thrusting normally referred to as the Hunter-Bowen phase (Day et al., 1978; Holcombe et al., 1997b; Korsch et al., 2009b; Li et al., 2012b). Contractional deformation was accompanied by calc-alkaline magmatism and the emplacement of voluminous I-type granitic intrusions (Shaw and Flood, 1981, 2009), possibly indicating an origin in an Andean-type supra-subduction margin.

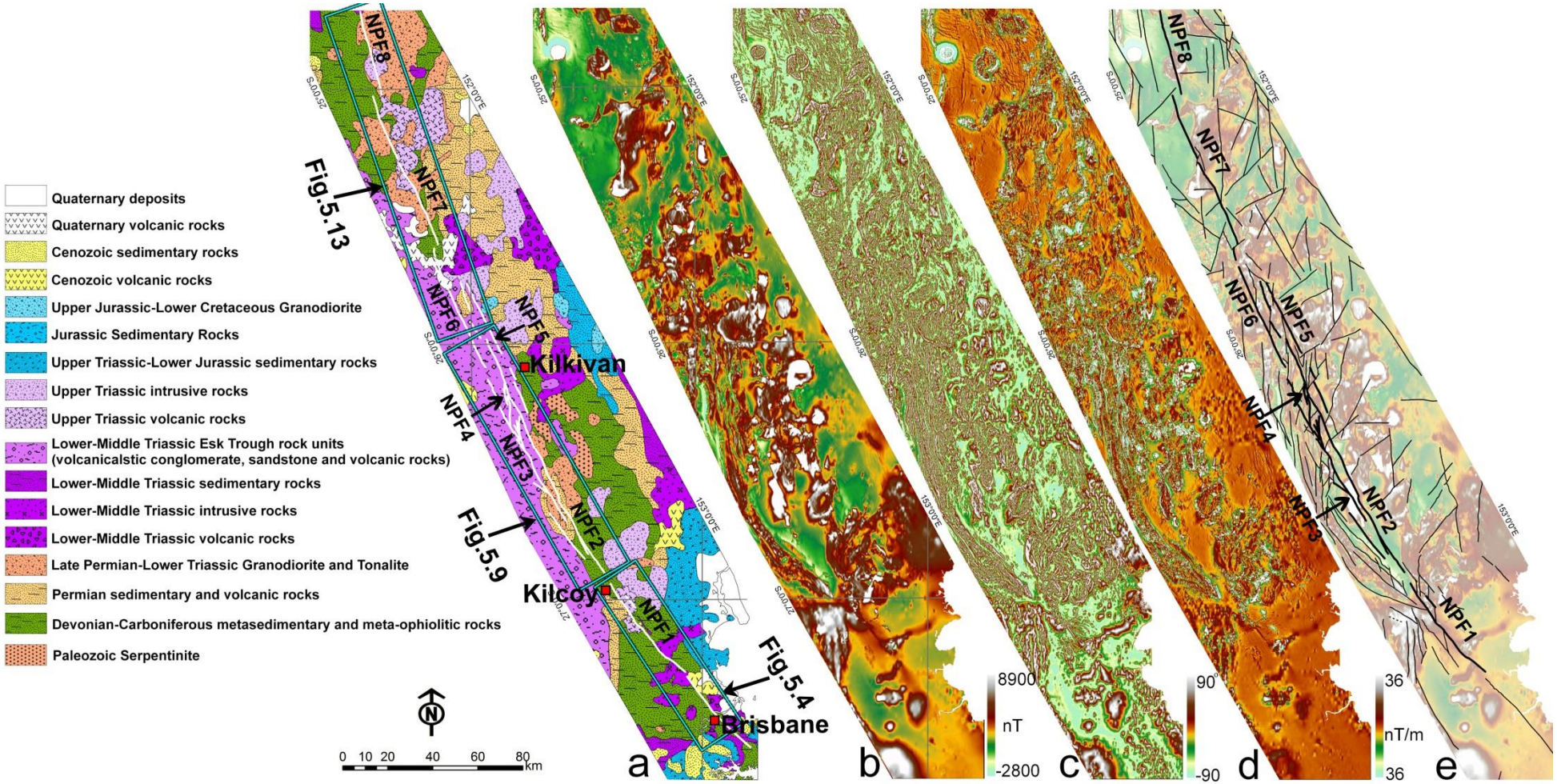

Figure 5.2. (a) Geological map of the study area. Modified after Ellis (1968), Ellis and Whitaker (1976), Green et al., (1980) and corrections based on field observations and interpretation of aeromagnetic data. (b) Reduced to pole (RTP) gridded aeromagnetic data of the study area. (c) Tilt angle derivative of RTP gridded data. (d) First vertical derivative of RTP gridded data. (e) Interpreted fault lineaments.

Sedimentary basins, such as the Esk Trough, Clarence-Moreton, Maryborough, Nambour and Surat Basins, developed in eastern Australia from Early Triassic to Early Cretaceous (Figures 5.1a, b). The development of these Mesozoic basins was possibly associated with subduction retreat, which recommenced in the Early Triassic following the end of the Hunter-Bowen phase (Li et al., 2012b). Korsch et al., (1989) have suggested that thermal relaxation subsidence, accompanied with strike-slip faulting, have also played a role in the development of the Late Triassic to Early Cretaceous sedimentary basins (Korsch et al., 1989). From the Late Cretaceous to the early Eocene, additional basins developed in eastern Australia, including the Townsville, Capricorn, Hillsborough, Duaringa, Capel and Faust Basins, accompanying the opening of the Tasman and Coral Seas (Figure 5.1a) (Gray, 1976; Hill, 1994; Struckmeyer et al., 1994; Struckmeyer and Symonds, 1997; Gaina et al., 1998a; Gaina et al., 1998b; Korsch et al., 1998; Colwell et al., 2010). The development of these basins has also been interpreted as resulting from E- to NE-directed slab rollback of the Pacific slab (Schellart et al., 2006).

The area affected by the NPFS is composed of Paleozoic to Cenozoic rocks. Rock units include deformed Devonian-Carboniferous metasedimentary and meta-ophiolitic rocks, late Permian–Middle Triassic volcanic and intrusive rocks, Early-Middle Triassic sedimentary rocks of the Esk Trough, Late Triassic volcanic and intrusive rocks, Late Triassic to Jurassic continental sedimentary rocks, and Cenozoic volcanic and sedimentary rocks (Figure 5.2a).

5.3. Methods

I used remote sensing data, gridded potential field data, geological maps and field observations to map the NPFS and related structures. Remote sensing data utilised in this study to trace fault lineaments are ASTER Global Digital Elevation Map version 2 (GDEM V2), produced by NASA and the Ministry of Economy, Trade and Industry of Japan. The 30 m ASTER DEMs have been generated by bands 3N (nadir-viewing) and 3B (backward-viewing) of the ASTER Level-1A images, acquired by the Visible -Near Infrared (VNIR) sensor (ASTER-GDEM-Validation-Team, 2011).

The reduced-to-pole gridded aeromagnetic anomaly data with spatial resolution of 80 m, provided by Geoscience Australia, were used to identify and interpret subsurface fault traces (Figures 5.2b, e). I operated the first vertical derivative and tilt angle derivative filters in the Fourier domain to enhance magnetic features and lineaments (Figure 5.2d). The first vertical derivative was operated to sharpen short wavelength sources, especially fault lineaments (Blakely, 1995). In particular, tilt angle derivative (the arc tangent of the ratio of the first vertical derivative to total horizontal derivatives) is a powerful filter for enhancing edges of magnetic sources and fault lineaments from both shallow and regional sources (Miller and Singh, 1994) (Figure 5.2c). I used the software Intrepid to process

aeromagnetic data. The gridded aeromagnetic data and remote sensing data allowed us to recognise (1) offset and dragging of rock units, magnetic anomalies and geological structures along faults; (2) pronounced structural lineaments; and (3) lensoid and *en-echelon* structures. I also used gridded onshore Bouguer and offshore free-air gravity data provided by Geoscience Australia to extract the main lineaments of eastern Australia.

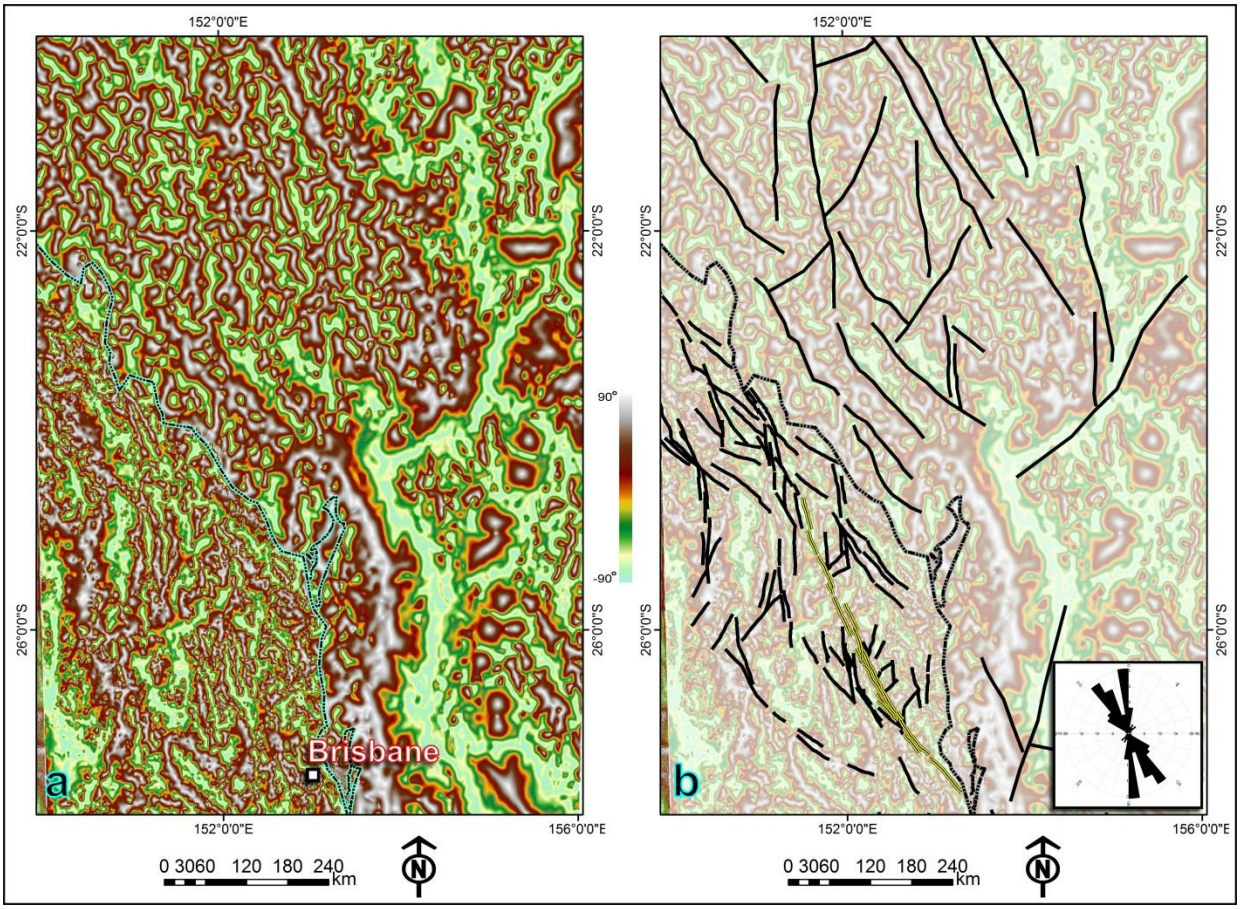

Figure 5.3. (a) Tilt angle map of gridded onshore Bouguer and offshore free-air gravity data of eastern Australia. (b) Interpreted main lineaments from these data indicate that NNW-striking lineaments are predominant in both offshore and onshore eastern Australia.

Field work has been conducted along all NPFS segments in accessible areas with the aim of observing fault-related structures and kinematic indicators. Kinematic indicators used in this study included drag folds, Riedel shears (R, P, and Y shears), and slickensides with fractured steps (Petit, 1987; Doblas, 1998). In the absence of slickensides, the indicators used to determine the hanging-wall movement in cataclastic fault zones were P-Y shears, which are equivalent to S-C fabrics in ductile shear zones (Doblas, 1998; Passchier and Trouw, 2006; Babaahmadi and Rosenbaum, 2013). I used the FaultKin v.5 program for stereonet analysis of fault slip data (Marrett and Allmendinger, 1990)

5.4. The North Pine Fault System

Interpretation of offshore and onshore gravity and aeromagnetic data shows that NNW-striking sinistral faults are predominant structures in eastern Australia (Figure 5.3). The North Pine Fault System (NPFS) is one of these NNW-striking faults. Its total length is ~380 km, and it is observed in the digital elevation models and aeromagnetic data as a series of parallel segments (Figures 5.2a, e). Here, the North Pine Fault System is described in three parts: southeastern, central, and northwestern.

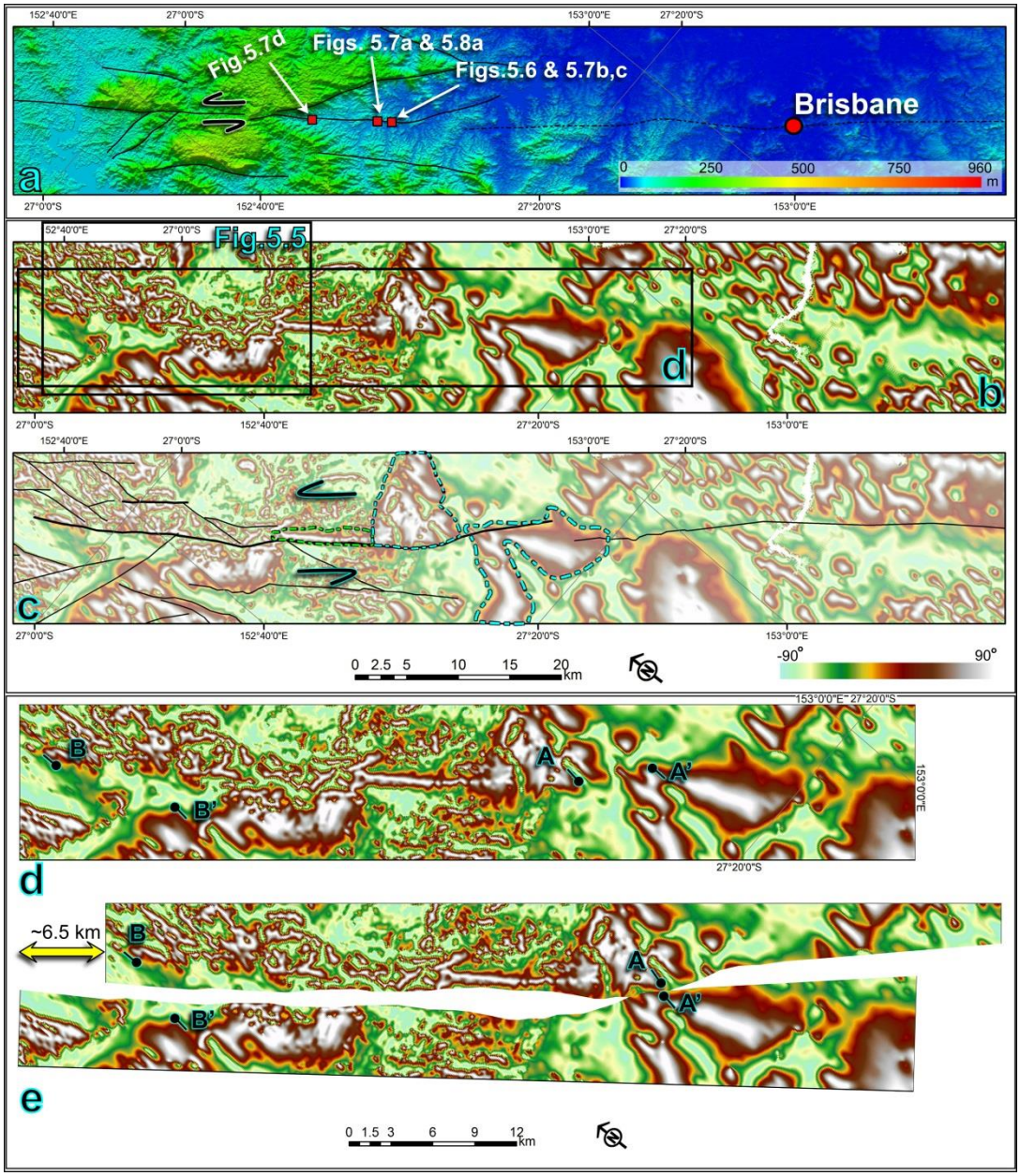

Figure 5.4. (a) ASTER digital elevation model of the NPF1 segment (see Figure 5.2a for location). (b, c) Tilt angle derivative image of the NPF1. Blue lines show displaced Triassic intrusive rocks and green lines show a dyke (possibly Late Triassic) parallel to the NPF1. (d, e) Restoration of the high anomaly bodies showing ~6.5 km sinistral offset.

5.4.1. Southeastern part

The southeastern part of the NPFS (NPF1) includes at least three parallel faults that can be recognised in the gridded aeromagnetic data (Figures 5.2, 5.4a-c). The NPF1 have mainly displaced Devonian-Carboniferous metasedimentary and meta-ophiolite rocks, and Triassic volcanic and intrusive rocks (Figure 5.2a). Interpretation of the tilt derivative of gridded aeromagnetic data shows that the NPF1 has displaced high amplitude anomalies (Figures 5.4b, c), which correspond to Triassic intrusive rocks (blue line in Figure 5.4c) and Late Triassic volcanic rocks (Figure 5.5). A NNW-striking dyke (Mt Mee Granophyre), ~11 km long and ~1.5 km wide, of a possible Late Triassic age, is situated parallel to the NPF1 fault zone (Figures 5.4b, c and 5.5). By reconstructing the displacement of Late Triassic volcanic and intrusive rocks, a sinistral offset of ~6.5 km is estimated (Figures 5.4d, e). Some of these rocks are covered by Cenozoic volcanic rocks (Figures 5.2a, 5.4b, c, 5.5), which appear as small irregular and curved high amplitude bodies in aeromagnetic data (Figure 5.5). The NPF1 has displaced these younger volcanic rocks by ~1.5 km (Figures 5.4b, c, 5.5).

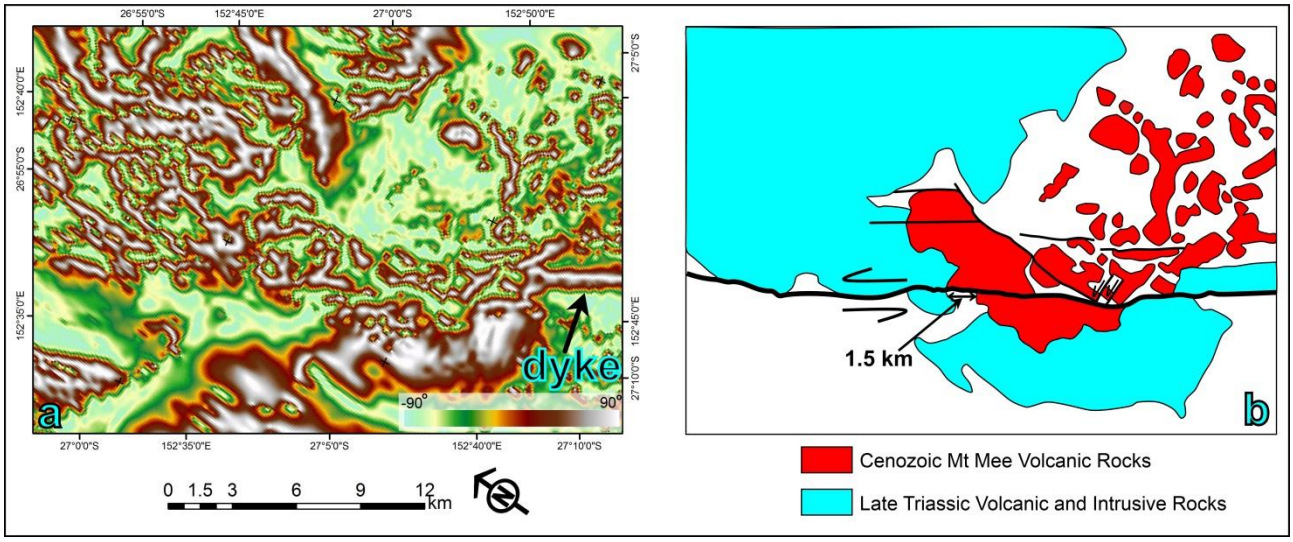

Figure 5.5. (a) Tilt angle derivative image of the NPF1. (b) Geological interpretation of this part of the NPF1 indicates Late Triassic igneous rocks and Cenozoic basalts, displaced by the NPF1 (see Figure 5.4b for location).

Different strands of the southeastern part of the NPFS are observed in the Devonian-Carboniferous metasedimentary rocks with an average fault dip orientation of 68/234 (dip/dip direction) (Figures 5.6, 5.7, 5.8). Stereographic analyses of kinematic indicators, such as P-Y shears and slickenlines, show a SW-dipping reverse sinistral kinematics of the NPF1 (Figures 5.7a, b,d,e; 5.8a). A sinistral movement is also indicated by R shears with sinistral kinematics (Figures 5.6 d, e). Field observations indicate that the NPF1 has been cut by NE-striking faults (Figures 5.6b, c), which based on stereographic analysis of dragged folds, are interpreted as reverse dextral faults (Figure 5.7c).

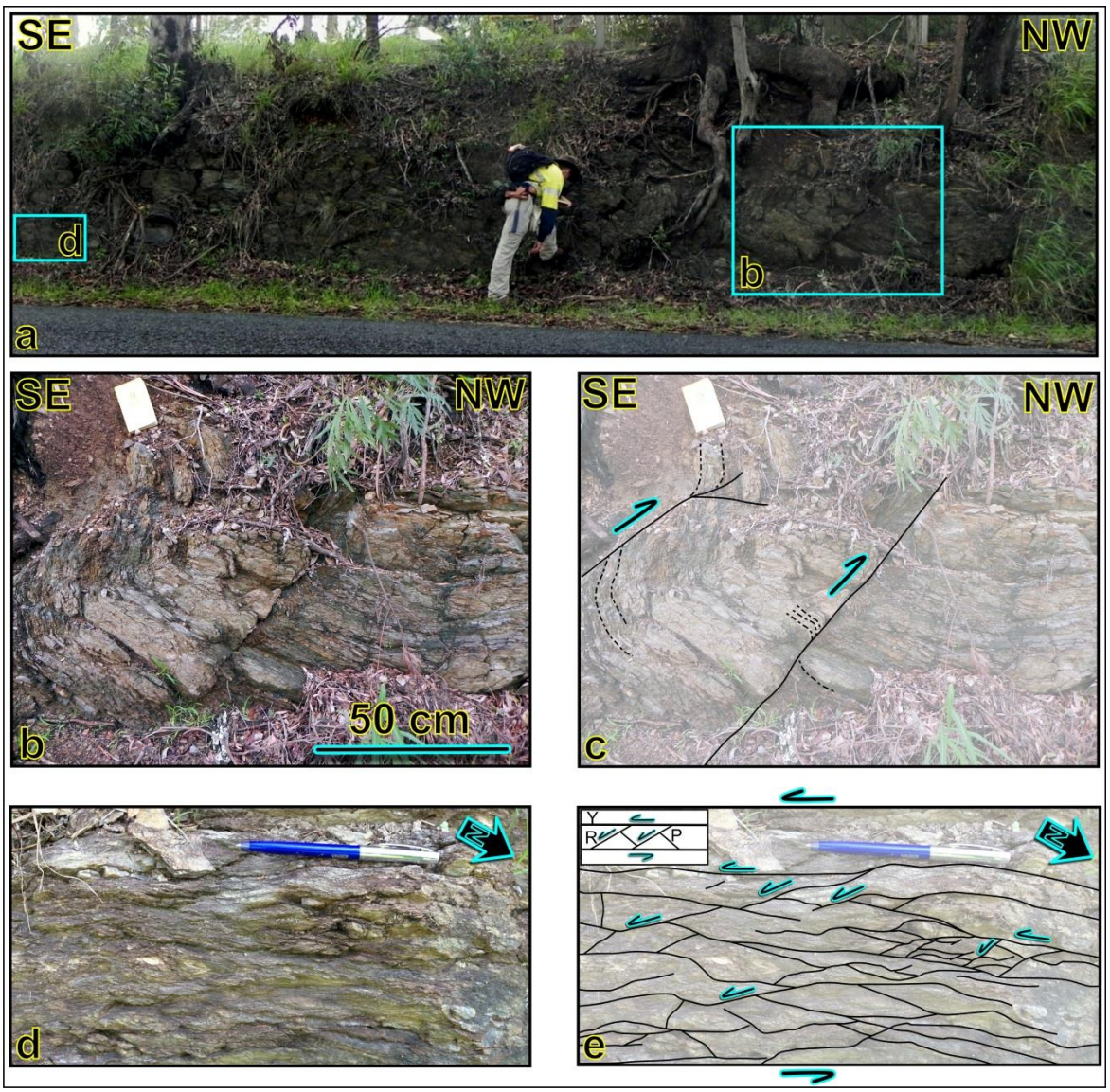

Figure 5.6. (a) The NPF1 fault zone (see Figure 5.4a for location). (b, c) NE-striking dextral reverse faults displaced Devonian-Carboniferous rocks in the fault zone (see Figure 5.4a for location) (d, e) Propagation of sinistral Riedel shears in the NPF1 fault zone, indicating sinistral fault kinematics.

5.4.2. Central Part

From both digital elevation models and aeromagnetic data, it appears that the central part of the NPFS consists of a number of parallel faults (indicated as NPF2, NPF3, NPF4 and NPF5 in Figure 5.9). The central part of the NPFS has sinistrally displaced Devonian-Carboniferous metasedimentary rocks, Permian sedimentary and volcanic rocks, Early-Middle Triassic rock units of the Esk Trough, and late Permian- Triassic intrusive rocks (Figure 5.2a). The tilt angle derivative of gridded aeromagnetic data shows that the NPF2 and NPF3 have displaced some high amplitude anomalies. I interpret these round shaped anomalies as late Permian-Early Triassic granodiorite (blue line in Figure 5.9c) and

Paleozoic serpentinite with a NE linear trend (yellow line in Figure 5.9c). Some older folds in the Esk Trough have also been sinistrally displaced by the NPFS (green lines in Figure 5.9c). The restoration of these high amplitude anomalies along the NPF2 and NPF3 (Figure 5.10) indicates sinistral displacements of ~6.6 km and ~3.8 km, respectively. Some NE-striking faults with minor dextral displacements are observed in aeromagnetic data (Figures 5.9b, c).

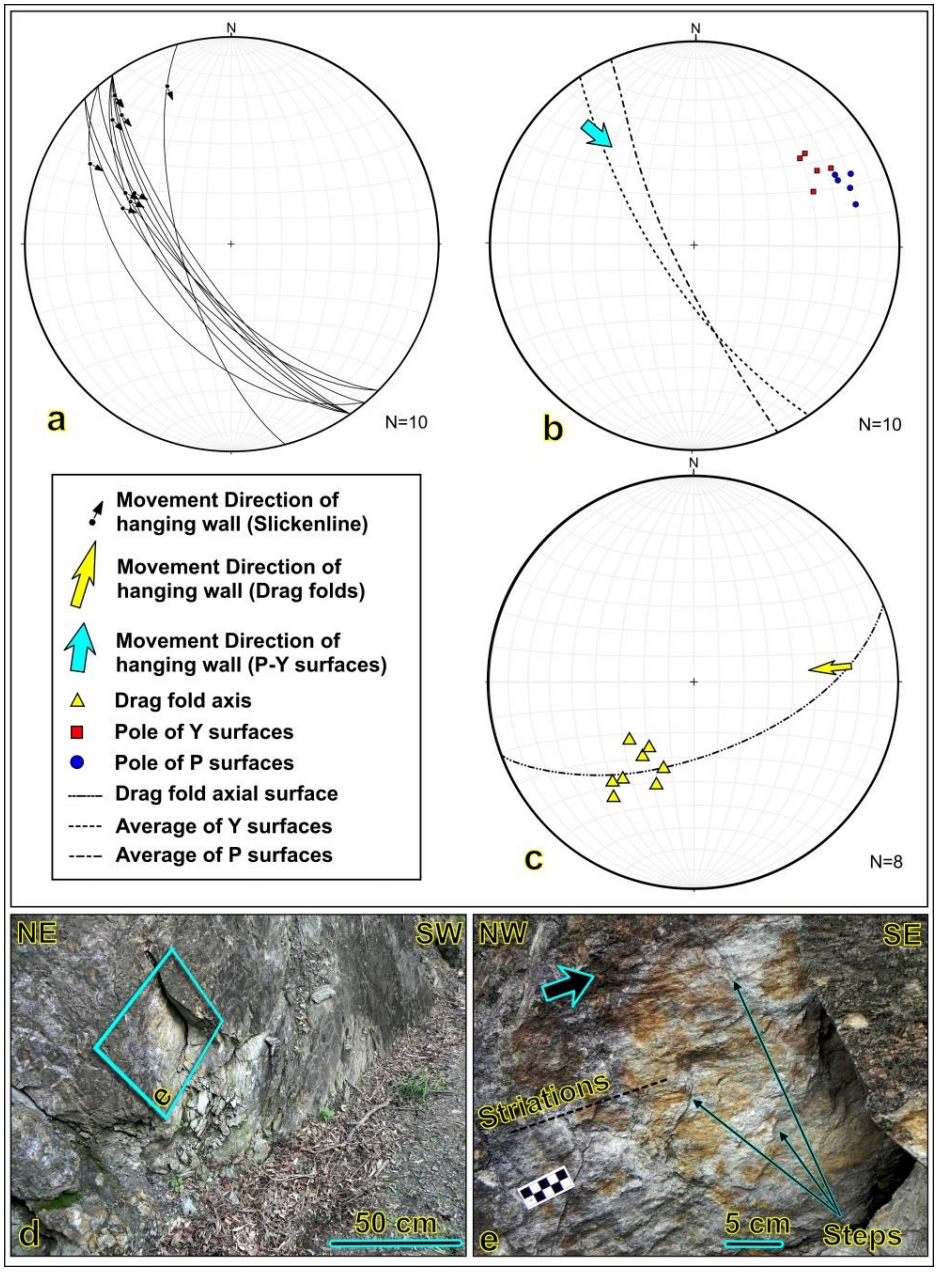

Figure 5.7. (a) Lower-hemisphere equal-area stereographic projection of fault surfaces and their kinematics, indicating reverse sinistral kinematics of the NPF1 segment (see Figure 5.4a for location). (b) Lower-hemisphere equal-area stereographic projection of P-Y surfaces in NPF1 cataclastic zone (see Figure 5.4a for location). (c) Lower-hemisphere equal-area stereographic projection of drag fold axes along a NE-striking fault. (d, e) Slickenlines with congruous fractured steps on one of the NPF1 strands, showing a reverse sinistral movement of the missing block (see Figure 5.4a for location).

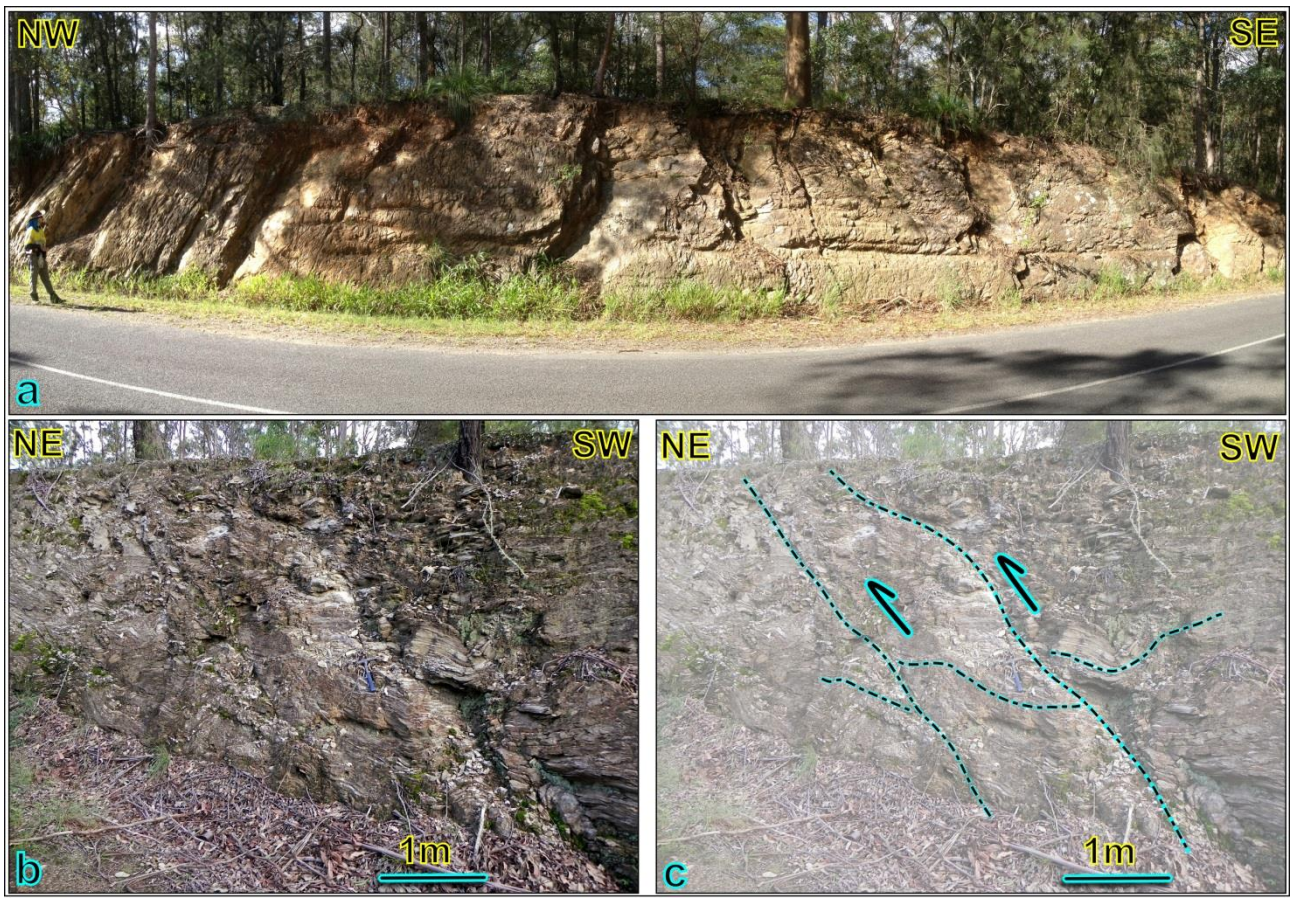

Figure 5.8. (a) Devonian-Carboniferous rocks displaced by NNW-striking reverse sinistral strands of the NPF1 (see Figure 5.4a for location). (b, c) Displaced folds in Carboniferous metasedimentary rocks (see Figure 5.9a for location).

I measured in the field different strands of the NPFS in the Devonian-Carboniferous rocks and the Early-Middle Triassic volcaniclastic conglomerate of the Esk Trough. The SW-dipping reverse sinistral NPF2 has displaced folded Carboniferous phyllite (Figures 5.8b, c). The SW-dipping NPF4 fault zone has displaced volcaniclastic conglomerate of the Esk Trough, forming cataclastic fault rocks (Figure 5.11). Sinistral R shears have developed in the NPF4 fault rocks and displaced older Y shears and P fabrics sinistrally (Figures 5.11a-c, e). Stereographic analysis of slickenlines indicates a reverse sinistral hanging-wall movement of the NPF4. Some NE-striking faults displaced the NPF4 dextrally (Figures 5.11d, e). There are some minor dextral NW-striking faults, displacing the NPF4 (Figure 5.11e). They are interpreted to be older sinistral R shears of the NPF4, which have been reactivated as dextral R shears of younger NE-striking faults. The NE-dipping NPF5 fault zone has mainly deformed the Esk Trough volcaniclastic conglomerate (Figure 5.2a). Stereographic interpretation of kinematic indicators, such as R shears and congruous steps on slickensides, indicates a reverse sinistral movement of the NPF5 hanging-wall (Figure 5.12a-e). Sinistral R shears are widespread in the NPF5 fault zone with an average strike orientation of 120° (Figure 5.12e). Some NE-striking reverse faults are also observed in this fault zone (Figure 5.12f).

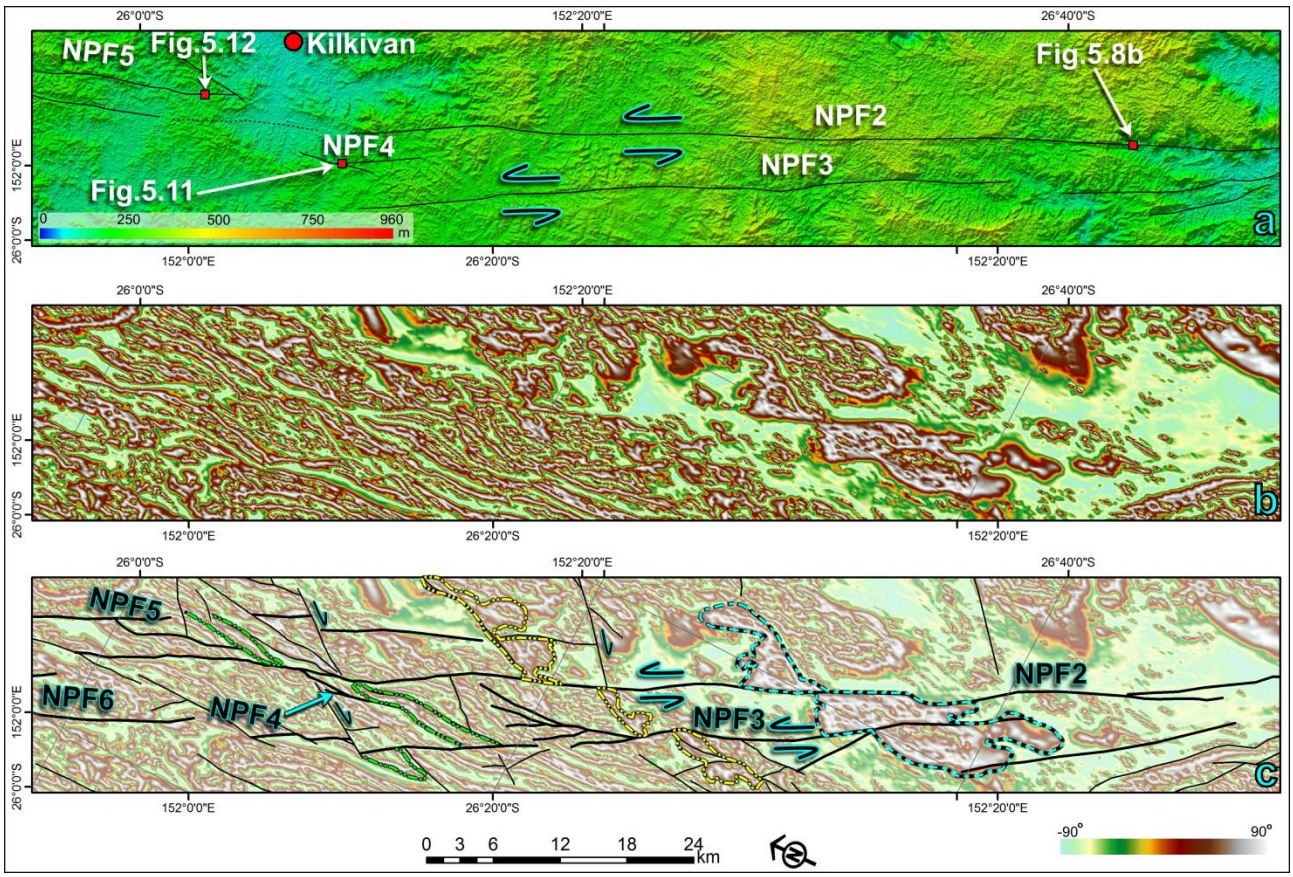

Figure 5.9. (a) ASTER digital elevation model of the central part of the NPFS (see Figure 5.2a for location). (b, c) Tilt angle derivative image of the central part of the NPFS. Blue, yellow and green lines indicate displaced late Permian-Triassic intrusive rocks, Paleozoic serpentinite, and folds in the Esk Trough, respectively.

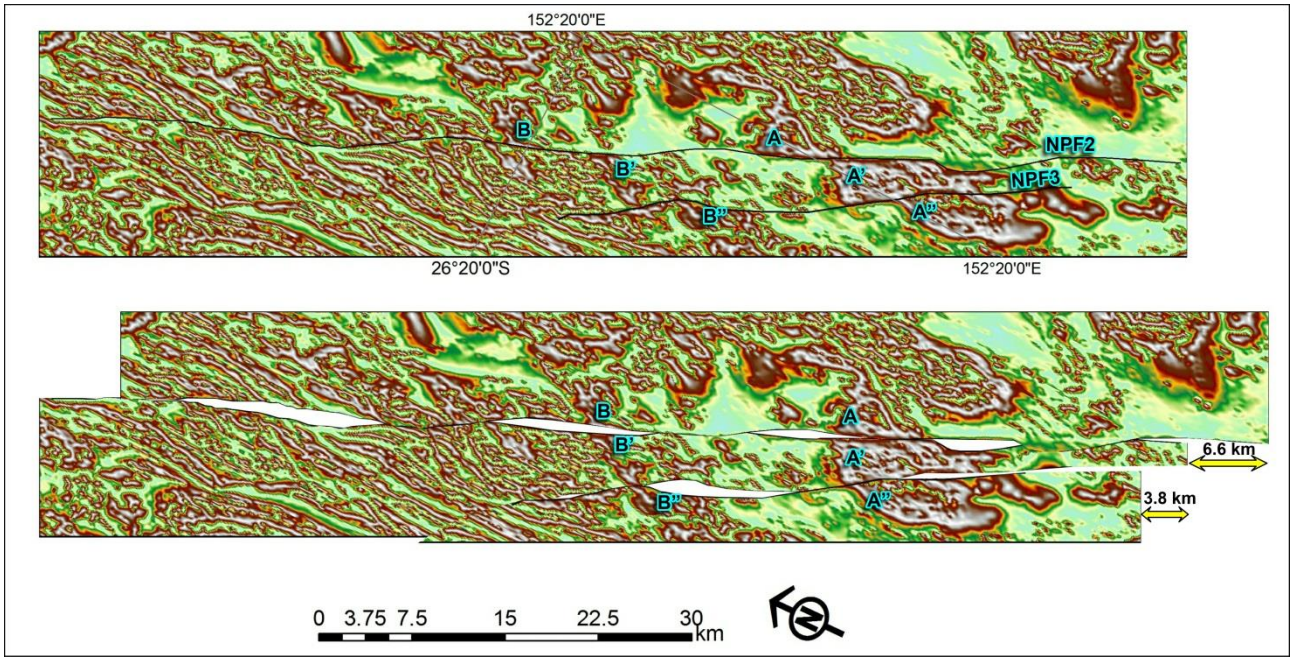

Figure 5.10. Restoration of high anomaly bodies showing ~6.6 and ~3.8 km sinistral offset along the NPF2 and NPF3, respectively. A, A', A"; and B, B', B"; indicate displaced boundaries of magnetic bodies affected by NPF2 and NPF3.

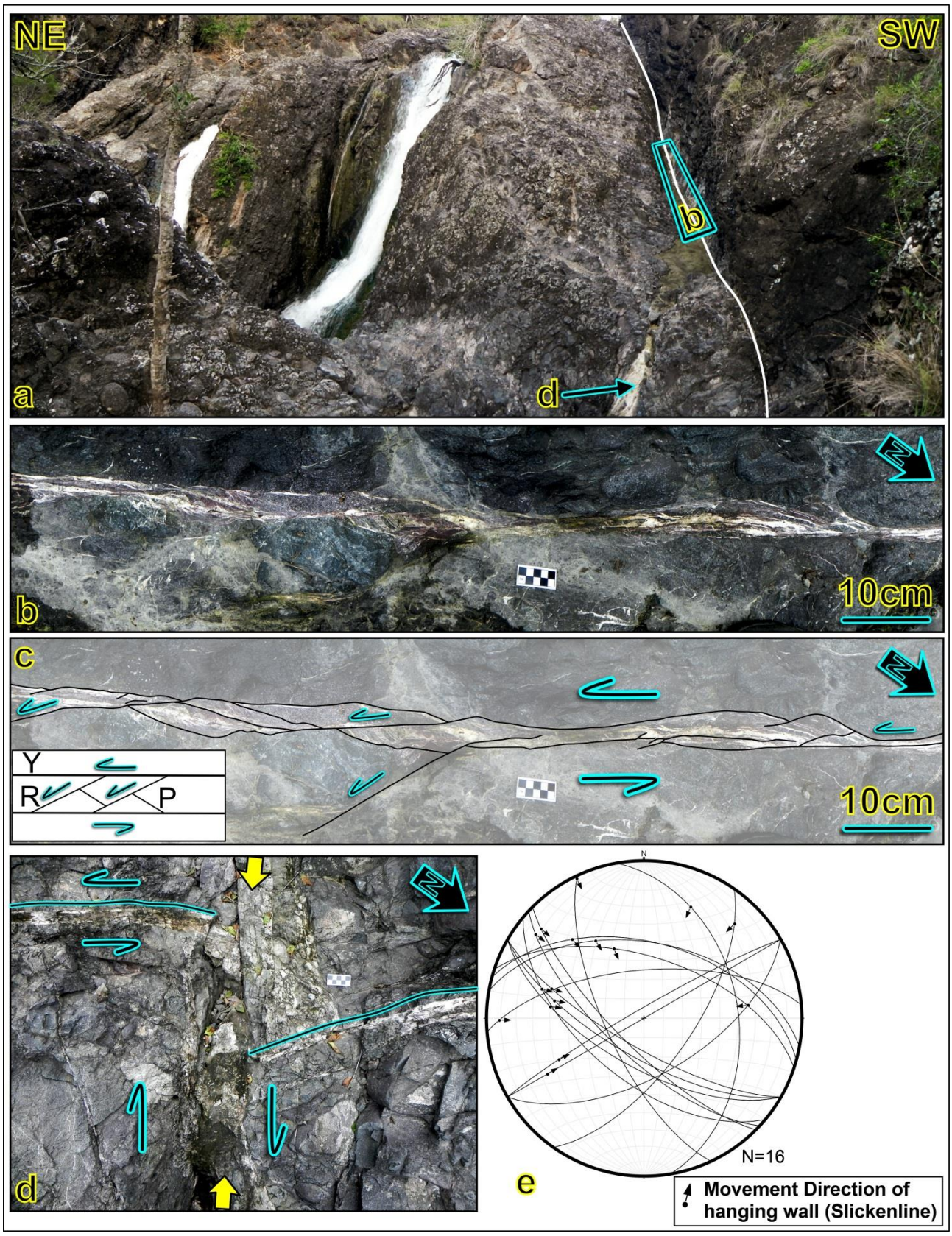

Figure 5.11. (a) The fault zone of NPF4, displacing Triassic conglomerate of the Esk Trough (see Figure 5.9a for location). (b-c) Propagation of sinistral Riedel shears in Fault cataclasite showing sinistral movement of NPF4. (d) A NE-striking dextral fault displaced one of the NPF4 strands dextrally. (e) Lower-hemisphere equal-area stereographic projection of faults and their kinematics.

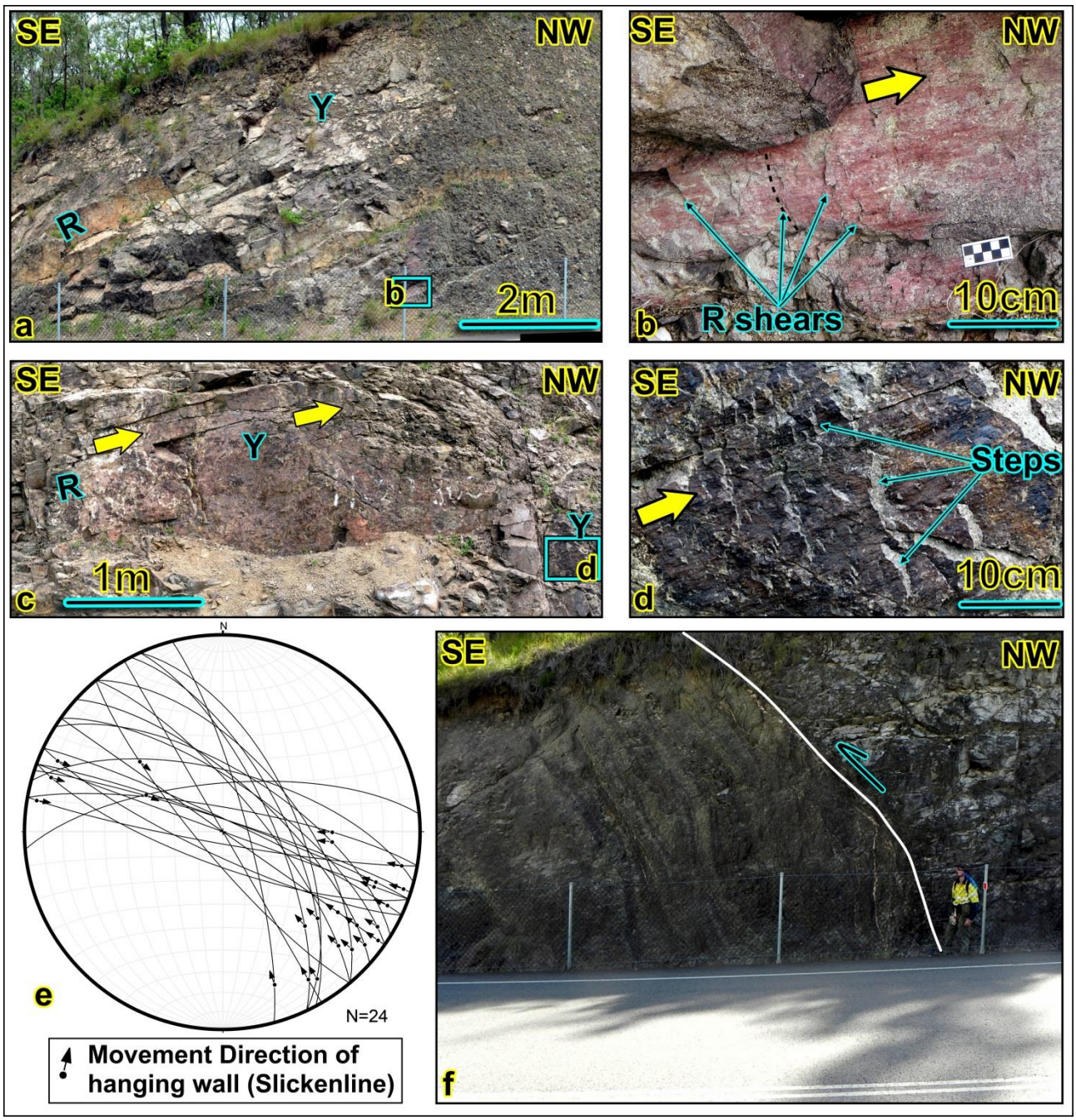

Figure 5.12. (a) The NPF5 surface in the Esk Trough conglomerate (see Figure 5.9a for location). (b) Slickenlines and Riedel shears on the NPF5 surface indicate reverse sinistral movement of the fault. (c, d) Slickenside of the NPF5 and a connected R shear; Slickenlines with congruous steps indicating reverse sinistral movement of the fault. (e) Lower-hemisphere equal-area stereographic projection of faults and their kinematics. (f) A steep reverse NE-striking fault, deforming the Esk Trough conglomerate.

5.4.3. The Northwestern Part

The northwestern part of the NPFS consists of a few parallel faults, including NPF6, NPF7 (previously termed Perry Fault by Ellis (1968)), and NPF8 (Figure 5.13). The northwestern part of the NPFS has displaced Paleozoic to Late Triassic rock units sinistrally (Figure 5.2a). Interpretation

of the tilt derivative of gridded aeromagnetic data shows that the NPFS has displaced some moderate to high amplitude magnetic anomalies (Figure 5.13). By comparison with geological maps, I infer these magnetic anomalies as possibly early Permian basic meta-volcanic rocks (yellow lines in Figure 5.13c), a set of late Permian to Late Triassic volcanic and intrusive rocks (blue lines in Figure 5.13c) and a Late Triassic circular monzogranite (green lines in Figure 5.13c). The red lines in Figure 5.13c indicate the area covered by Quaternary volcanic rocks that have not been truncated by the NPF6 (Figure 5.2a). The restoration of gridded aeromagnetic data indicates that the NPF7 and NPF8 displaced different magnetic bodies by ~8.2 and ~3.4 km, respectively (Figure 5.14). A series of dextral NE-striking faults are observed east of the NPFS (Figures 5.13b, c and 5.15e).

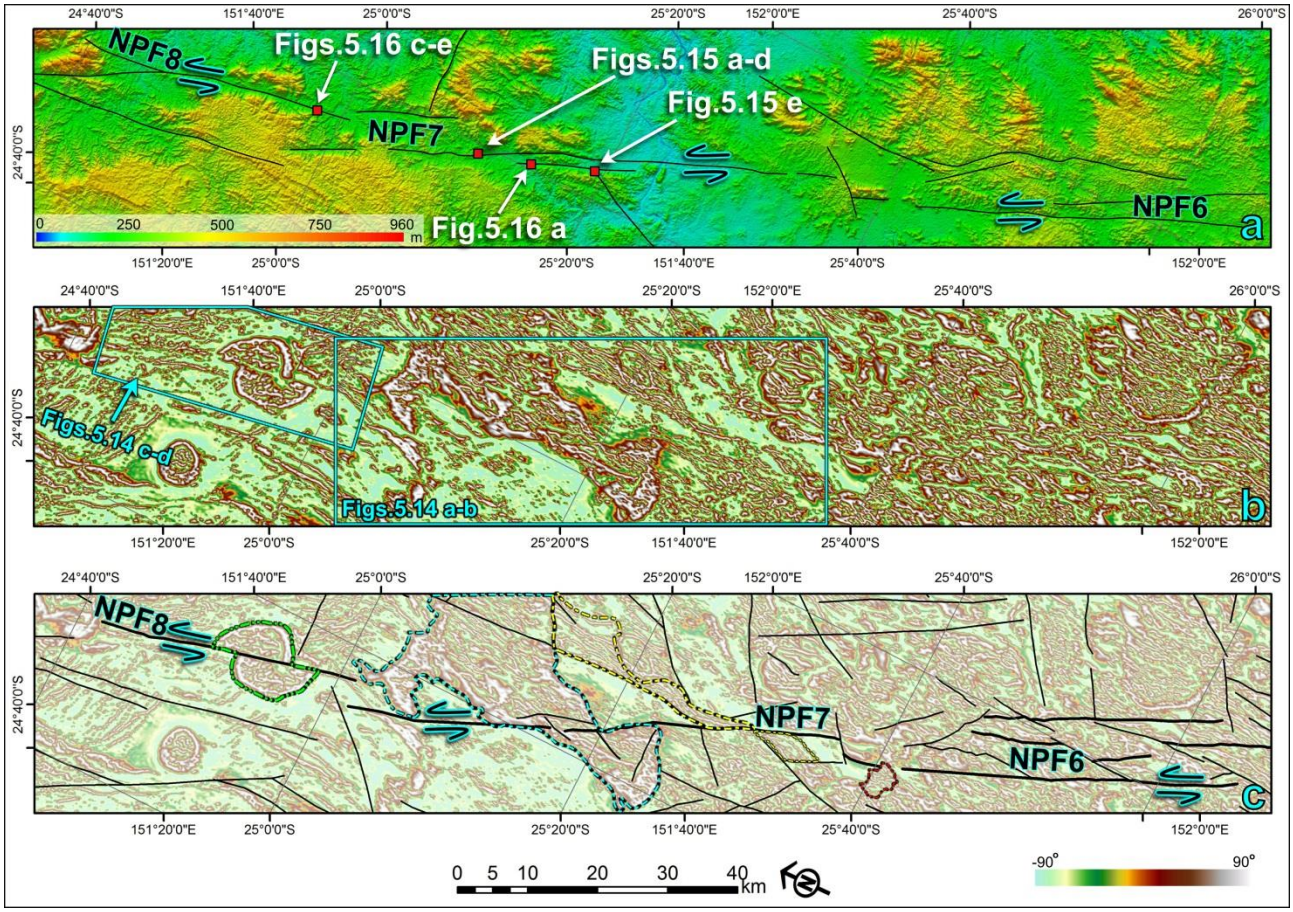

Figure 5.13. ASTER digital elevation model of the northwestern part of the NPFS (see Figure 5.2a for location). (b, c) Tilt angle derivative image of the northwestern part of the NPFS. Yellow, blue and green lines indicate displaced Permian basic metavolcanics, a set of late Permian to Late Triassic volcanic and intrusive rocks, and Late Triassic monzogranite, respectively. Red line shows Quaternary basaltic rocks, which have not been affected by the NPF6.

The area of the northwestern part of the NPFS is mostly covered by forest. I traced the NPF7 fault plane, which is dipping 65/245 (dip/dip direction), in folded Paleozoic metasedimentary rocks. The slickenlines on the fault surface indicate sinistral reverse kinematics of the fault (Figures 5.16a, b). I

measured a splay of the NPF7 in a road quarry which cuts strongly folded Carboniferous metasedimentary rocks (Figures 5.15a-c). Stereographic analysis of P-Y shears indicates reverse sinistral kinematics of the fault (Figure 5.15d). Steep NPF8 fault surfaces with a sinistral movement were also observed in Late Triassic monzogranite (Figures 5.16 c-e).

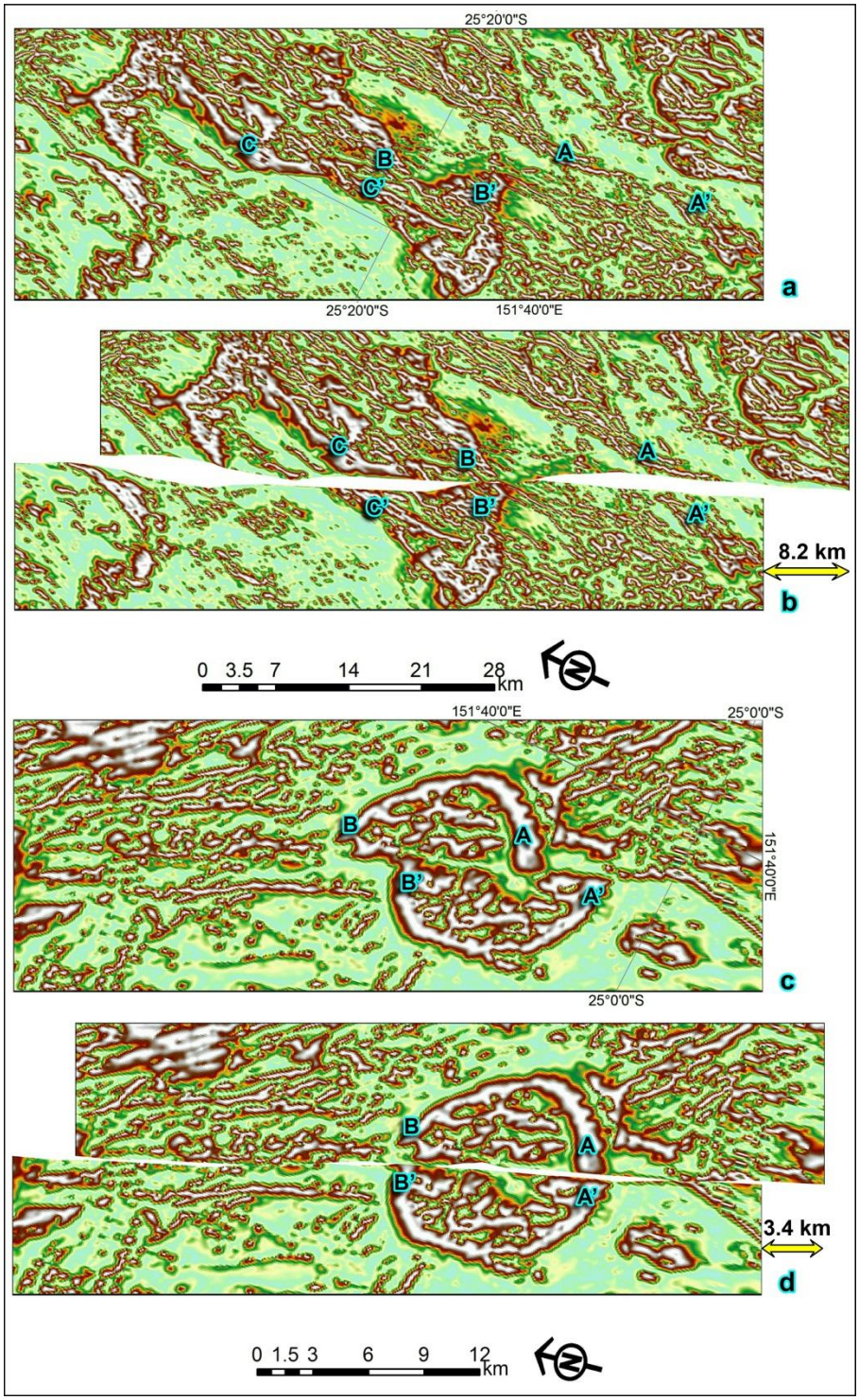

Figure 5.14. Restoration of high anomaly bodies showing ~8.2 and ~3.4 km sinistral offset along NPF7 (a, b) and NPF8 (c, d), respectively (see Figure 5.13b for location).

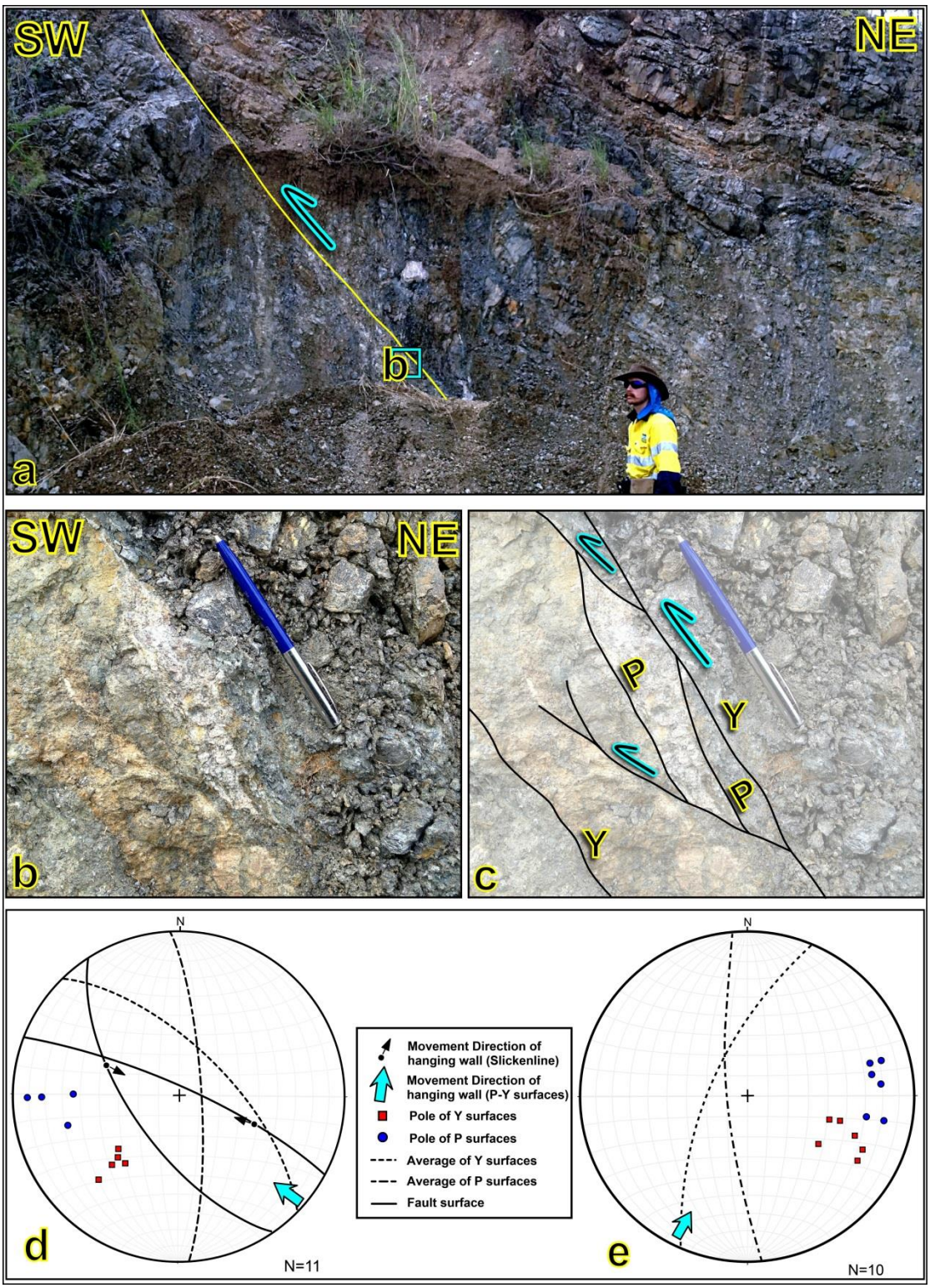

Figure 5.15. (a) Field photograph of the NPF7 segment, deforming intensely folded Paleozoic rocks (see Figure 5.13a for location). (b, c) P-Y surfaces in the fault zone showing a reverse movement of the fault. (d) Lower-hemisphere equal-area stereographic projection of P-Y surfaces and slickenlines in the NPF7 fault zone. (e) Lower-hemisphere equal-area stereographic projection of P-Y surfaces in a NE-striking fault zone (see Figure 5.13a for location).

5.5. Discussion

5.5.1. Kinematics of the North Pine Fault

Field observations of kinematic indicators from different segments of the NPFS indicate that the fault kinematics was predominantly sinistral strike-slip with a minor reverse component. Interpretation of high-resolution gridded aeromagnetic data shows that the NPFS is one of a series of NNW-striking sinistral faults, which displaced Paleozoic and Mesozoic rocks in eastern Queensland.

Based on the aeromagnetic data and the restoration of reliable magnetic markers, I infer that different segments of the NPFS were subjected to different amounts of sinistral displacement. In the southeastern part of the NPFS, the restoration of high anomaly bodies associated with Triassic igneous rocks reveals ~6.5 km sinistral offset (Figures 5.4d, e). In the Central part, the NPF2 and NPF3 have displaced Paleozoic and early Mesozoic rocks sinistrally by ~6.6 km and ~3.8 km, respectively (Figures 5.9, 5.10). In the northeastern part, the NPF7 and NPF8 fault segments displaced late Permian to Late Triassic intrusive and volcanic rocks sinistrally by ~8.2 and ~3.4 km, respectively (Figure 5.10).

Interpretation of aeromagnetic and field data shows that a number of short NE-striking dextral faults, with a maximum length of 40 km, are widespread around the NPFS. I interpret these faults as antithetic dextral faults generated by the sinistral movement along the NPFS.

5.5.2. Timing of faulting

The exact timing of faulting along the NPFS remains unknown. However, the timing of faulting can be constrained indirectly by considering the age of displaced rocks, the deformation history of Mesozoic-Cenozoic sedimentary basins in the region, and the comparison of the results with modeled paleostress maps (Dyksterhuis et al., 2005a; Dyksterhuis and Müller, 2008; Muller et al., 2012). In the following sections, I discuss the deformation and fault reactivation in the NPFS in the context of the three major stages in the Mesozoic and Cenozoic tectonic evolution of eastern Australia.

5.5.2.1. Faulting in the Late Paleozoic to Late Mesozoic

The NPFS has displaced Late Triassic intrusive and volcanic rocks, indicating post-Triassic activity of the fault. Earlier activity, in the Paleozoic to early Mesozoic, is not well constrained. However, previous authors have suggested that the NPF1 segment has acted as a reverse fault during the early stage of the Hunter-Bowen phase at ~260 Ma (Holcombe et al., 1997b). The occurrence of a NNW-striking dyke (Mt Mee Granophyre) parallel to the NPF1 segment, with a possible Late Triassic age, indicates that the fault may have also been active as a normal fault during the Triassic (Figures 5.4c

and 5.5). The occurrence of NNW-striking andesitic dykes with age of ~225 Ma within the North D'Aguilar Block (Holcombe et al., 1997b) (Figure 5.1b) further supports a Late Triassic extension along NNW-striking structures.

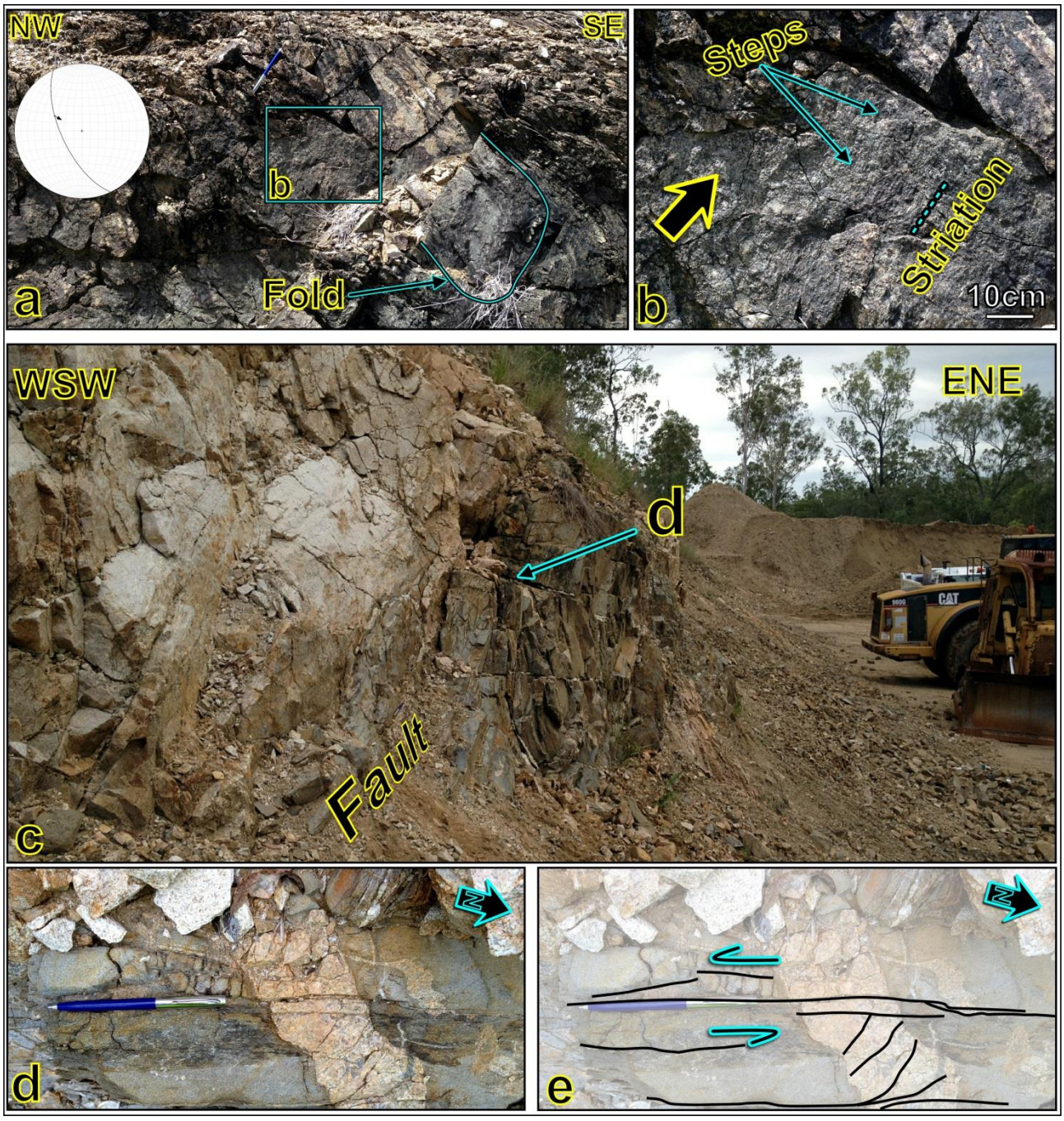

Figure 5.16. (a, b) Field photograph of the NPF7 slickenside with a sinistral reverse movement of missing block displaced the Paleozoic folded metasedimentary rocks (see Figure 5.13a for location). (c-e) Steep fault strands of the NPF8 displacing Late Triassic monzogranite sinistrally (see Figure 5.13a for location).

Table 5.1. Recent contractional reactivation/inversion events in some eastern and southeastern Australian margin sedimentary basins

A number of authors have suggested that the development of sedimentary basins during the Late

Mesozoic-Cenozoic Basins	**Age**	**Contractional Reactivation/Inversion events**
The Capricorn Basin	Early Cretaceous-Cenozoic	NW-striking reverse faulting and folding in Early-Middle Eocene sediments (Hill, 1992)
The Townsville Basin	Late Jurassic-Cenozoic	Minor reactivated faults in Oligocene-present sediments (Struckmeyer et al., 1994; Struckmeyer and Symonds, 1997)
The Hillsborough Basin	Paleogene	Folding and Reactivated Faults in Paleogene sediments (Clarke et al., 1971; Gray, 1976)
The Capel and Faust Basins	Early Cretaceous-Cenozoic	Unconformity in Eocene-Oligocene, Folding and fault reactivation in Paleogene and Neogene sediments (Colwell et al., 2010)
The Clarence-Moreton Basin	Late Triassic-Late Jurassic	Folding, thrusting, and strike-slip faulting in the Late Triassic-Late Jurassic sediments (Korsch et al., 1989; O'Brien et al., 1994)
The Surat Basin	Early Jurassic-Early Cretaceous	Minor reactivated thrusts and gentle folds in Jurassic-Cretaceous sediments (Korsch et al., 2009b)
The Laura Basin	Middle Jurassic-Early Cretaceous	Folded and tilted Jurassic-Cretaceous sediments by reactivated faults (De Keyser, 1963; De Keyser and Lucas, 1968)
The Nambour Basin	Late Triassic-Early Jurassic	Folds and faults due to the North Pine Fault activity (Humphires, 2003)
The Maryborough Basin	Late Triassic-Early Cretaceous	NW-striking folds and reverse faults deformed Early Cretaceous sediments (Hill, 1994)
The Gippsland Basin	Early Cretaceous-Cenozoic	Reactivation and Inversion of faults in the Cenozoic and Quaternary (Dickinson et al., 2001; Sandiford, 2003b; Hillis et al., 2008)

Triassic to Early Cretaceous was associated with strike-slip faulting (Korsch et al., 1989; Babaahmadi and Rosenbaum, 2013). Strike-slip faults within the Maryborough Basin, the closest basin to the NPFS (Figure 5.1a), are parallel to the NPFS. These faults were considered to have been active during the basin development in the Late Triassic to Early Cretaceous (Hill, 1994), suggesting that the NPFS was probably active at that time. However, the exact kinematics of these strike-slip faults at that period is relatively poorly constrained.

5.5.2.2. Transtensional tectonics during the opening of the Tasman and Coral Seas

The opening of the Tasman Sea at ~84-64 Ma was supposedly dominated by sinistral transtension that resulted from the counterclockwise rotation of the Tasman Sea spreading center and its associated change in the spreading direction from NE-SW to NNE-SSW (Gaina et al., 1998a; Gaina et al., 1998b). This transtensional tectonic setting has possibly continued during the Paleocene to early Eocene NNE-SSW opening of the Coral Sea (Weissel and Watts, 1979). There are a number of lines of evidence that suggest that the NPFS and other structures offshore and onshore eastern Australia were possibly active as sinistral normal-oblique faults from the Late Cretaceous to early Eocene.

Firstly, interpretation of gravity and aeromagnetic data indicate that NNW-striking lineaments are predominant within the offshore and onshore eastern margin of Australia (Figure 5.3). These lineaments are parallel or sub-parallel to the Tasman Sea rift axis and are mostly sinistral onshore eastern Australia.

Secondly, NNW-striking strike-slip and normal faults have been reported in offshore basins, such as the Capricorn Basin, which were developed during the Late Cretaceous opening of the Tasman Sea (Hill, 1992). Offshore NNW-striking sinistral strike-slip faults have also displaced Early Cretaceous volcanic rocks in eastern Queensland during the Late Cretaceous to early Cenozoic (Bryan et al., 2000).

Evidence supporting sinistral activity during the early Eocene is the development of Eocene sedimentary basins, such as the Duaringa and Hillsborough Basins, with a maximum depth of 1.3 km (Gray, 1976; Gibson, 1989; Korsch et al., 1998) (Figure 5.1a). The formation of these basins has supposedly involved activity along NNW-striking *en echelon* steep normal faults. In addition, the extremely low-magnitude maximum compressive horizontal stress and a major NNE- to NNW-oriented tensional stress on the modeled paleostress maps of eastern Australia (Dyksterhuis et al., 2005a; Muller et al., 2012) indicates a possible sinistral oblique strike-slip-normal kinematics of NNW-striking faults during the early Eocene opening of the Coral and Tasman Seas (Figure 5.17a).

5.5.2.3. Cenozoic transpression

The results show that the NPFS has a consistent reverse kinematic component, which can be attributed to Cenozoic transpressional tectonics. Evidence for contractional deformation that affected Cenozoic sedimentary rocks is known from the inversion of basement faults and folding in the Capricorn, Townsville, Hillsborough, Capel and Faust Basins in eastern Australia (Clarke et al., 1971; Gray, 1976; Hill, 1992; Struckmeyer and Symonds, 1997; Colwell et al., 2010) and the Gippsland Basin in SE Australia (Dickinson et al., 2001; Sandiford, 2003b; Hillis et al., 2008) (Table 5.1) (Figure 5.1a).

Locally at the NPFS, further support for Cenozoic faulting is the observations of volcanic rocks with an age of ~28 Ma (Cohen et al., 2007) that are offset ~1.5 km by the fault system (Figure 5.5).

The exact tectonic events that led to fault reactivation during the Cenozoic remain relatively poorly constrained. However, a number of possibilities can be raised based on the plate tectonic setting of eastern Australia and modeled paleostress maps (Dyksterhuis et al., 2005a; Muller et al., 2012). Numerous contractional events have been recorded in sedimentary basins in eastern Australia after the cessation of regional extension during the late Eocene to early Oligocene and late Oligocene to Recent events (Tables 5.1 and 5.2). In the late Eocene-early Oligocene (~38-34 Ma), an ophiolite obduction occurred in New Caledonia, perhaps as a result of a major plate reorganization in the SW Pacific (Table 5.2) (Cluzel et al., 2001; Crawford et al., 2003). This significant plate reorganization during the mid-Eocene (~43 Ma) gave rise to the fusion of the Australian and Indian plates, the initiation of new subduction zones in the SW Pacific, and the rapid northward motion of the Australian plate (Veevers, 2000; Cluzel et al., 2001; Crawford et al., 2003; Spandler et al., 2005; Schellart et al., 2006; Knesel et al., 2008). The WSW-directed compressional stresses that resulted from the late Eocene obduction event in New Caledonia (Cluzel et al., 2001) could have possibly been transmitted to the eastern Australian margin, accounting for folding, reverse faulting, and sinistral strike-slip reactivation along NNW-striking faults.

The more recent activity along the NPFS, from Miocene to Recent, could be discussed in the context of the modeled paleostress maps of Australia (Dyksterhuis et al., 2005; Müller et al., 2012). These maps indicate that the sinistral-reverse kinematics of NNW-striking faults, such as the NPFS, and dextral-reverse kinematics of NE-striking faults in SE Queensland are consistent with the maximum horizontal compressive stress directions (Figures 5.17b-d).

According to the modeled stress map, the maximum horizontal stress in the early-middle Miocene (~23-11 Ma) was oriented WNW-ESE (onshore) to ~E-W (offshore), possibly accounting for sinistral-reverse reactivation of the NPFS and other NNW-striking faults (Figure 5.17b). I interpret that the ~E-directed maximum horizontal stress at this time resulted from east-directed highly oblique collision at the NE Australian margin with the Ontong Java Plateau (Petterson et al., 1997; Petterson et al., 1999; Mann and Taira, 2004; Phinney et al., 2004; Knesel et al., 2008) and highly oblique arc-continent collisions at the northern margin of New Guinea (McCaffrey, 1996; Hill and Hall, 2003; Quarles van Ufford and Cloos, 2005; Glen and Meffre, 2009; Baldwin et al., 2012), while WNW-directed maximum horizontal stress occurred as a result of ophiolite obduction and oblique collision in New Zealand (Allis, 1981; Kamp, 1986; Norris et al., 1990) (Table 2).

Table 5.2. Cenozoic collisional/obduction events around eastern Australian boundary after the cessation of the regional extension of eastern Gondwana

Collisional/Obduction Event	Age	Characteristics
Ophiolite obduction in New Caledonia	Late Eocene-Early Oligocene (~38-34 Ma)	Terranes and ophiolite obduction due to a NE-dipping subduction (Cluzel et al., 2001; Crawford et al., 2003)
Collision of the Ontong Java Plateau with the Melanesian arc system	Late Oligocene-Present (~25-0 Ma)	Initiation of highly oblique collision at ~25-20 Ma, polarity reversal in the collisional zone and the onset of a NE-dipping subduction zone at ~12-6 Ma, strong sinistral oblique collision since the Pliocene (Petterson et al., 1997; Petterson et al., 1999; Mann and Taira, 2004; Phinney et al., 2004)
Collisions at the northern margin of New Guinea	Late Oligocene-Pliocene (~25-4 Ma)	Successive oblique arc-continent collisions due to a N-dipping subduction zone between Australian and Pacific plates (Hill and Hall, 2003; Quarles van Ufford and Cloos, 2005; Glen and Meffre, 2009; Baldwin et al., 2012). Sinistral ESE-striking transpression and strain partitioning (McCaffrey, 1996)
Ophiolite obduction in Northland, New Zealand	Late Oligocene-Early Miocene (~25-21 Ma)	Resulted from the final stage of a NE-dipping subduction (Schellart, 2007; Schellart, 2012)
Collision in the South Island of New Zealand	Early Miocene-Present (~23-0 Ma)	Collision between Challenger Plateau on Australian Plate and Chatham Rise-Campbell Plateau, resulting in uplift and creation of the New Zealand Alps (Allis, 1981; Kamp, 1986; Norris et al., 1990). A kinematic change from strike-slip regime to transpression regime since ~6.4 Ma (Walcott, 1998)

For the late Miocene (~11-6 Ma), the Australian paleostress map shows varying orientations of the maximum horizontal stress, from ENE-WSW to WNW-ESE in SE Queensland (Muller et al., 2012). This indicates the possibility of pure reverse to sinistral-reverse oblique kinematics of the NPFS at this time (Figure 5.17c). A NE-directed maximum horizontal stress offshore and north of the study area is normal to the NNW-striking fault lineaments, indicating possible reverse kinematics. I propose that ENE- to ESE-directed maximum horizontal stress at this time resulted from the initiation of sinistral oblique arc-continent collision in the northern margin of Papua New Guinea (Hill and Raza, 1999; Hill and Hall, 2003; Muller et al., 2012).

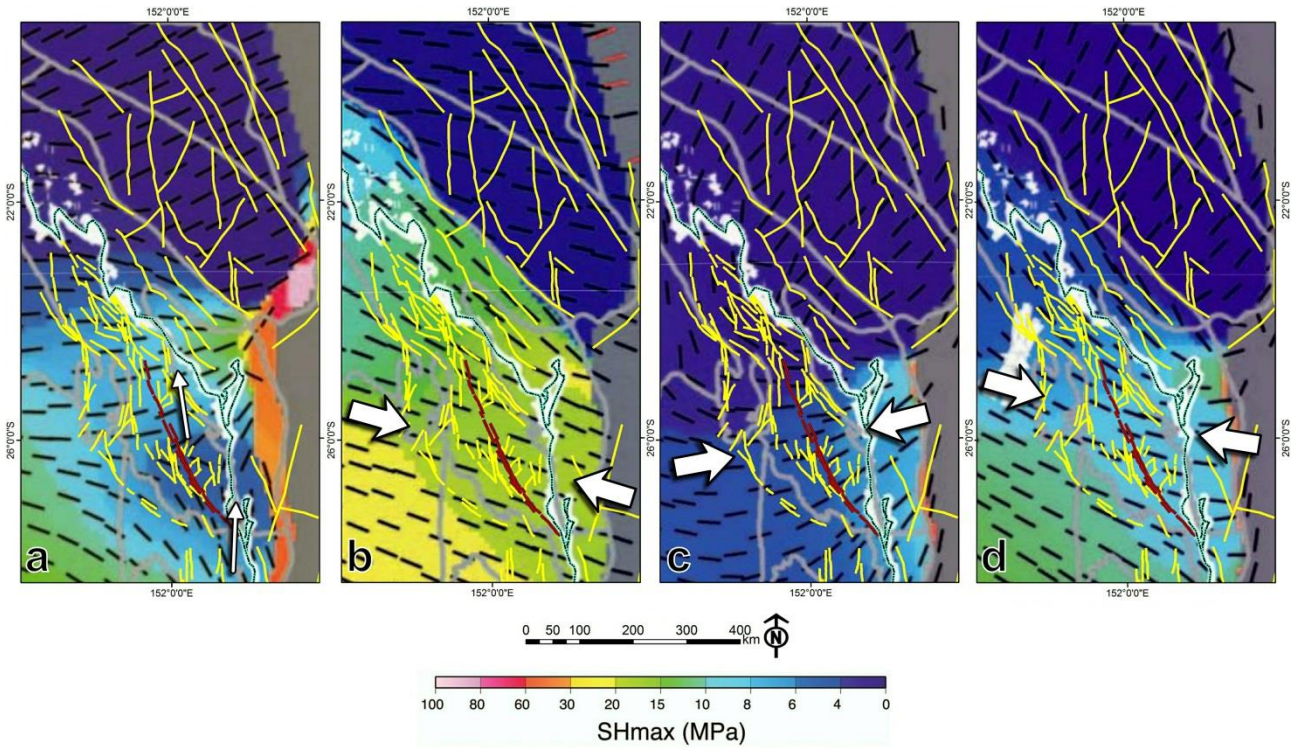

Figure 5.17. Paleostress map of eastern Australia showing the maximum horizontal stress (black lines) (Dyksterhuis et al., 2005a; Muller et al., 2012). (a) Eocene (~55 Ma). The average horizontal tensional stress direction is indicated by white arrows. The amount of onshore extension in Eocene sedimentary basins is ~1.3 km (Gibson, 1989); (b) Early-middle Miocene (~23-11 Ma). ~Maximum 200 meters uplift in west central Queensland has been suggested for this time (Sprigg, 1986; Finlayson et al., 1988; Muller et al., 2012); (c) Late Miocene (~11-6 Ma); (d) Pliocene-Recent (~6-0 Ma). The red lines are the NPFS segments and the yellow lines are interpreted lineaments from gridded aeromagnetic and gravity data. White arrows in b-d show the average trend of maximum horizontal compressive stress.

In the latest Miocene-Quaternary (~6-0 Ma), the observed maximum horizontal stress in SE Queensland is WSW-ESE, in accordance with sinistral-reverse oblique kinematics of the NPFS. A NE-directed maximum horizontal stress is observed offshore north of the study area. This orientation is perpendicular to the NNW-striking fault lineaments, suggesting a possible reverse fault reactivation. There is no evidence of Pliocene-Quaternary deformation on the NPFS, but observations from other localities in SE Australia (Sandiford, 2003b, a) support the idea that deformation in eastern Australia has continued until recently. The Pliocene-Quaternary maximum horizontal stress orientation may have resulted from stress transmitted from collisional events at the NE and SE plate boundaries. A kinematic change from dominantly strike-slip top transpression occurred in the South Island of New Zealand at ~6.4 Ma (Walcott, 1998). At the NE Australian plate boundary, ongoing collision of the Ontong Java Plateau and the Solomon Arc has been taking place since the Pliocene, resulting in a sinistral transpressive regime (Petterson et al., 1997; Petterson et al., 1999; Mann and Taira, 2004; Phinney et al., 2004).

5.6. Conclusions

The North Pine Fault System is one of several NNW-striking sinistral faults in the eastern margin of Australia. I showed that the NPFS is a sinistral high-angle fault system with a minor reverse component. The occurrence of parallel NNW-striking basement faults in the Late Triassic-Early Cretaceous Maryborough Basin in eastern Australia and a possibly Late Triassic granophyre dyke immediately parallel to the NPF1 fault zone indicates that the NPFS was active during the Mesozoic. The NPFS and other NNW-striking faults appear to have been active as sinistral-normal oblique faults during the Late Cretaceous to early Eocene opening of the Tasman and Coral Seas due to an oblique extensional regime. The last activity of the NPFS as a sinistral-reverse oblique fault is interpreted to have resulted from far-field contractional stresses from collisions at the east, SE, and NE boundaries of the Australian Plate during the Cenozoic. Sinistral-reverse oblique kinematics of the NPFS is in line with ESE to ENE orientations of modeled maximum horizontal stress in the mid-Cenozoic to Recent in SE Queensland.

.

Chapter 6

Late Cenozoic intraplate faulting in eastern Australia

Late Cenozoic intraplate faulting in eastern Australia

Abstract

The intensity and tectonic origin of late Cenozoic intraplate deformation in eastern Australia is relatively poorly understood. Here I show that Cenozoic volcanic rocks in southeast Queensland have been deformed by numerous faults. Using gridded aeromagnetic data and field observations, structural investigations were conducted on these faults. Results show that faults have mainly undergone strike-slip movement with a reverse component, displacing Cenozoic volcanic rocks ranging in ages from ~ 31 to ~21 Ma. These ages imply that faulting must have occurred after the late Oligocene. Late Cenozoic deformation has mostly occurred due to the reactivation of major faults, which were active during episodes of basin formation in the Jurassic-Early Cretaceous and later during the opening of the Tasman and Coral Seas from the Late Cretaceous to the early Eocene. The wrench reactivation of major faults in the late Cenozoic also gave rise to the occurrence of brittle subsidiary reverse strike-slip faults that affected Cenozoic volcanic rocks. Intraplate transpressional deformation possibly resulted from far-field stresses transmitted from the collisional zones at the northeast and southeast boundaries of the Australian plate during the late Oligocene-early Miocene and from the late Miocene to the Pliocene. These events have resulted in the hitherto unrecognised reactivation of faults in eastern Australia.

Key words: Cenozoic volcanic rocks, strike-slip reverse faults, far-field stress, eastern Australia, passive margin, intraplate transpressional deformation

6.1. Introduction

Intraplate contractional or transpressional deformation is commonly attributed to compressional horizontal stress fields, which are transmitted from the plate boundaries and reactivating pre-existing faults in the plate interiors (Etheridge et al., 1991; Ziegler et al., 1995). The Australian continent, for example, is situated far from the plate boundaries (Figure 6.1a) and is commonly assumed to be a relatively stable continent. Nonetheless, there is widespread evidence that late Cenozoic intraplate transpressional deformation affected different parts of Australia, mainly through the reactivation of earlier faults (Keep et al., 2000; Dickinson et al., 2001; Sandiford, 2003b, a; Keep et al., 2007; Hillis

et al., 2008). This intraplate deformation has been interpreted to result from the far-field stresses, which were transmitted from the Australian plate boundaries (Hillis et al., 2008; Muller et al., 2012).

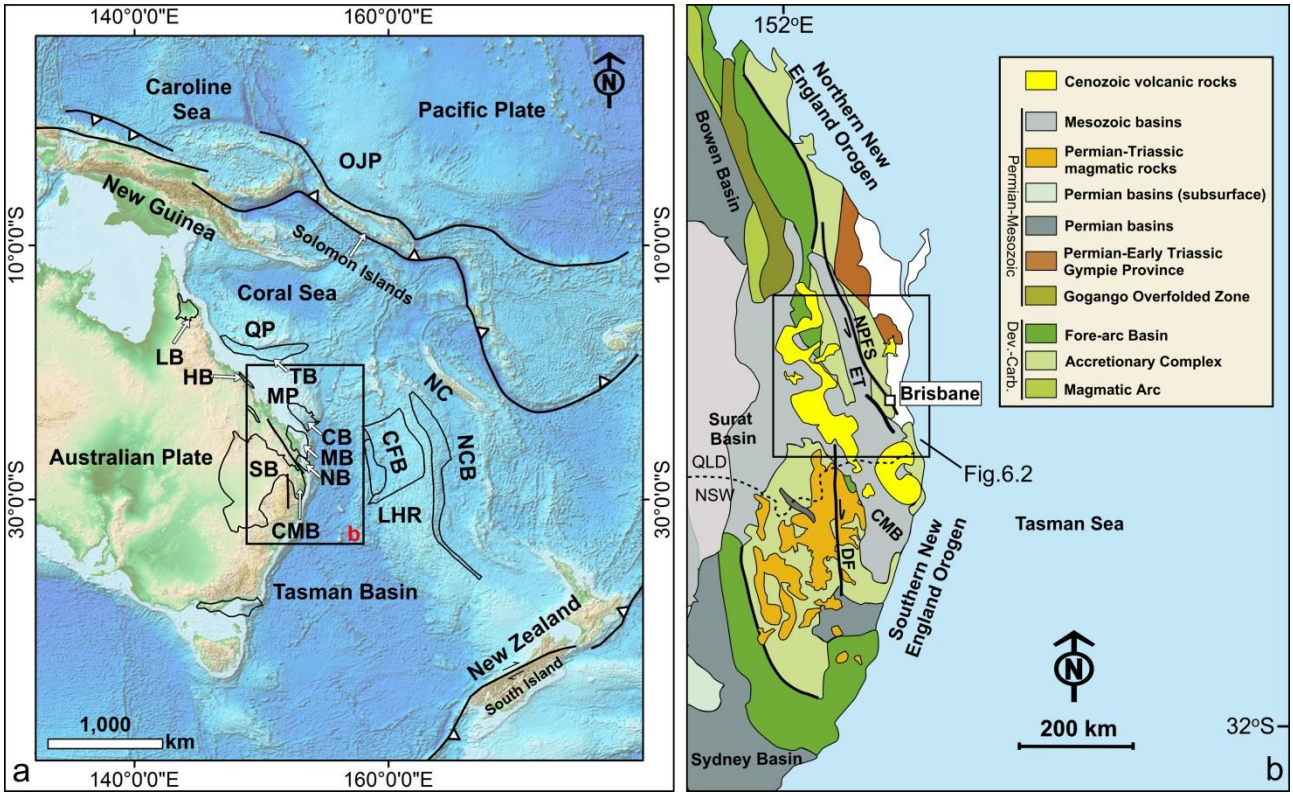

Figure 6.1. (a) ETOPO1 digital elevation model of the Australian and Pacific plates (Amante and Eakins, 2009), and a simplified tectonic framework showing Mesozoic sedimentary basins in eastern Australia. CMB, Clarence-Moreton Basin; CB, Caledonia Basin; CB, Capricorn Basin; CFB, Capel and Faust basins; CT, Cato Trough; DB, Duaringa Basin; HB, Hillsborough Basin; LB, Laura Basin; LHR, Lord Howe Rise; MB, Maryborough Basin; MP, Marion Plateau; NB, Nambour Basin; NCB, New Caledonia Basin; NC, New Caledonia; OJP, Ontong Java Plateau; QP, Queensland Plateau; SB, Surat Basin; TB, Townsville Basin. (b) Simplified regional tectonic elements of eastern Australia. DF, Demon Fault; ET, Esk Trough; NPFS, North Pine Fault System.

One area where the role of late Cenozoic intraplate deformation is less understood is onshore eastern Australia. Major faults in this area have mainly affected late Paleozoic to early Mesozoic rock units (Figure 6.1b) (Holcombe et al., 1997b; Babaahmadi and Rosenbaum, 2014b), but it is possible that a component of the observed deformation has taken place in the late Cenozoic. This problem can be addressed by focusing on mid-late Cenozoic volcanic rocks, which are widely exposed in eastern Australia (Wellman and McDougall, 1974; Cohen et al., 2007; Knesel et al., 2008; Vasconcelos et al., 2008). Therefore, the recognition of structural observations in these rocks provides an opportunity to investigate the kinematics and intensity of late Cenozoic deformation.

The aim of this paper is to investigate whether evidence for intraplate transpressional deformation is recorded in deformational features within Cenozoic volcanic rocks in eastern Australia. I focus on a number of fault systems in southeast Queensland, and use gridded aeromagnetic data and field

observations to analyse the kinematics, magnitude and relative timing of deformation. Finally, I discuss the results in the context of the late Cenozoic geodynamic evolution of the Australian plate.

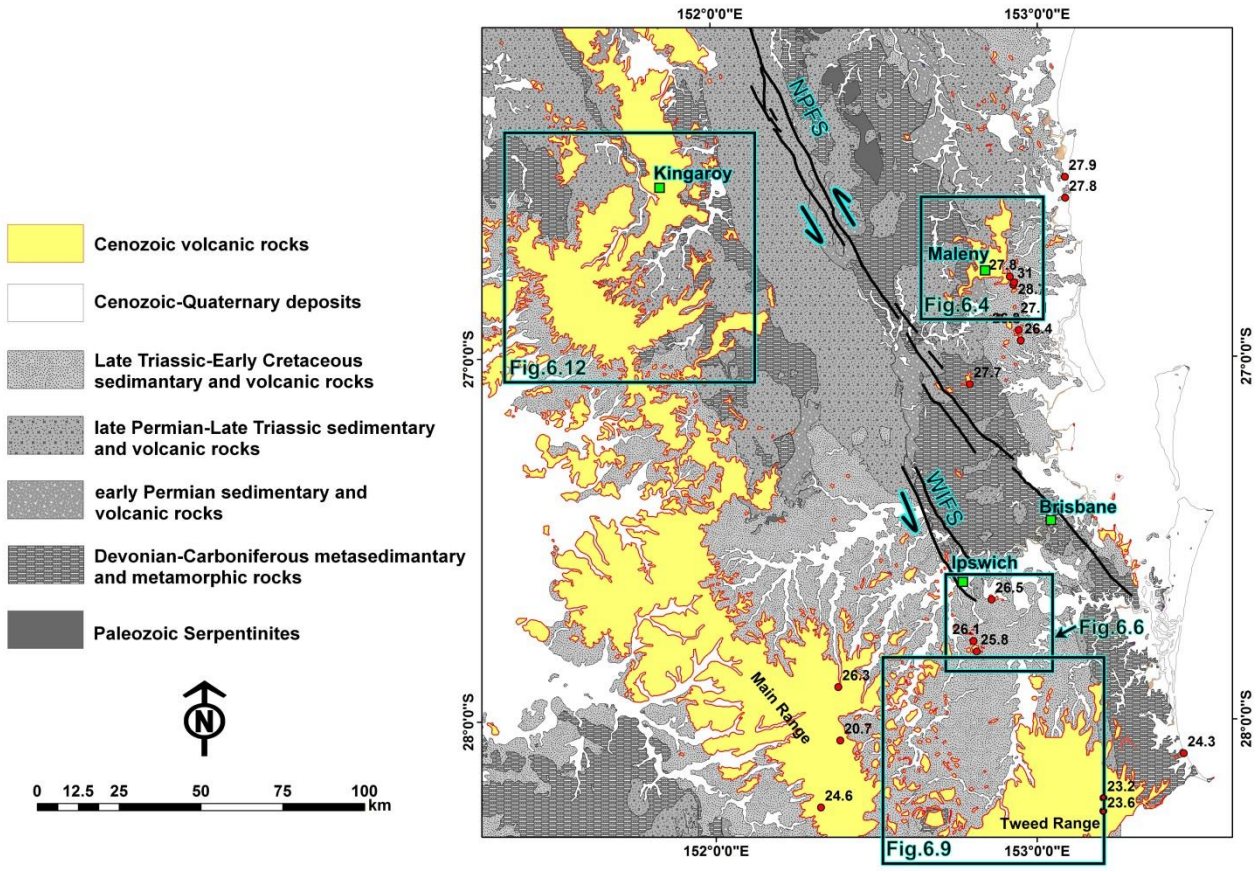

Figure 6.2. Simplified geological map of the study area based on the 1:500,000 Moreton Geology map (Green et al., 1980). Numbers indicate $^{40}Ar/^{39}Ar$ ages of volcanic rocks in Ma (Cohen et al., 2007; Knesel et al., 2008). NPFS, North Pine Fault System; WIFS, Western Ipswich Fault.

6.2. Geological Setting

The surface geology of southeast Queensland is dominated by Paleozoic-Mesozoic rock units, which are overlain by Cenozoic volcanic rocks (Figure 6.1b). The Paleozoic and early Mesozoic rocks belong to the New England Orogen (Figure 6.1b), and mainly consist of (1) Devonian-Carboniferous supra-subduction units (accretionary complex, fore-arc basin and magmatic arc) (Leitch, 1975; Day et al., 1978; Henderson et al., 1993; Holcombe et al., 1997a); (2) early Permian extensional-related sedimentary and magmatic rocks (Korsch et al., 2009a); and (3) Late Permian to Middle Triassic calc-alkaline magmatic rocks. The latter formed during episodic contractional events, collectively referred to as the Hunter-Bowen phase, which was intermitted by an interval of back-arc extension in the Early to Middle Triassic that resulted in the formation of sedimentary basins (e.g., the Esk Trough; Figure 6.1b) (Holcombe et al., 1997b; Li et al., 2012b). Late Triassic and younger sedimentary rocks have supposedly been deposited in post-orogenic localised rift basins (Korsch et al., 1989; Holcombe et

al., 1997b). The Devonian-Carboniferous subduction-related elements are generally characterised by N- to NNW-strike orientations, but in the southern New England Orogen, the orogen is tightly curved forming an oroclinal structure (Cawood et al., 2011b; Rosenbaum, 2012; Rosenbaum et al., 2012).

Late Triassic and younger sedimentary basins have developed in two major episodes. The earlier episode, which occurred in the early Late Triassic, was associated with a major rifting phase that led to the development of the Ipswich and Tarong Basins (Korsch et al., 1989; Holcombe et al., 1997b). Rifting involved bimodal volcanism in southeast Queensland (Holcombe et al., 1997b), accompanied by major normal faults (Babaahmadi and Rosenbaum, 2014b). The second episode of basin formation, from the latest Late Triassic to the Early Cretaceous, was associated with thermal relaxation subsidence that gave rise to the development of the Clarence-Moreton, Surat and Maryborough Basins (Korsch et al., 1989; Hill, 1994; Holcombe et al., 1997b; Korsch and Totterdell, 2009). Subsequently, from the Late Cretaceous to the early Eocene, the eastern Australian margin was subject to continental fragmentation accompanying the opening of the Tasman and Coral Seas (Weissel and Watts, 1979; Gaina et al., 1998a; Gaina et al., 1998b).

Cenozoic intraplate volcanic rocks are distributed over 3000 km throughout the eastern Australian margin (Wellman and McDougall, 1974). This intraplate volcanism is subdivided into three types: central volcanoes, lava field provinces, and high potassium mafic areas (Wellman and McDougall, 1974). The central volcanoes are mostly basaltic but with some felsic lava flows and intrusions, constructing large volcanoes such as Tweed and Main Range (Figure 6.2) (Wellman and McDougall, 1974; Johnson, 1989). These spatio-temporal distribution of the central volcanoes has been attributed to the northward motion of the Australian plate over a stationary hotspot(s) (Knesel et al., 2008). Lava field provinces are mostly composed of extensive and thin basaltic lavas, although in some locations their thickness reaches up to 1000 m (Wellman and McDougall, 1974). High potassium mafic areas are observed in central New South Wales as olivine leucitite (Wellman and McDougall, 1974).

In the study area in southeast Queensland (Figure 6.2), mafic and felsic Cenozoic volcanic rocks are mainly associated with large central volcanoes (Wellman and McDougall, 1974; Johnson, 1989). $^{40}Ar/^{39}Ar$ ages of volcanic rocks from this region range from 31±0.8 Ma at Maleny in the north to 20.7±0.5 Ma at Main Range volcano in the south (Figure 6.2) (Cohen et al., 2007; Knesel et al., 2008).

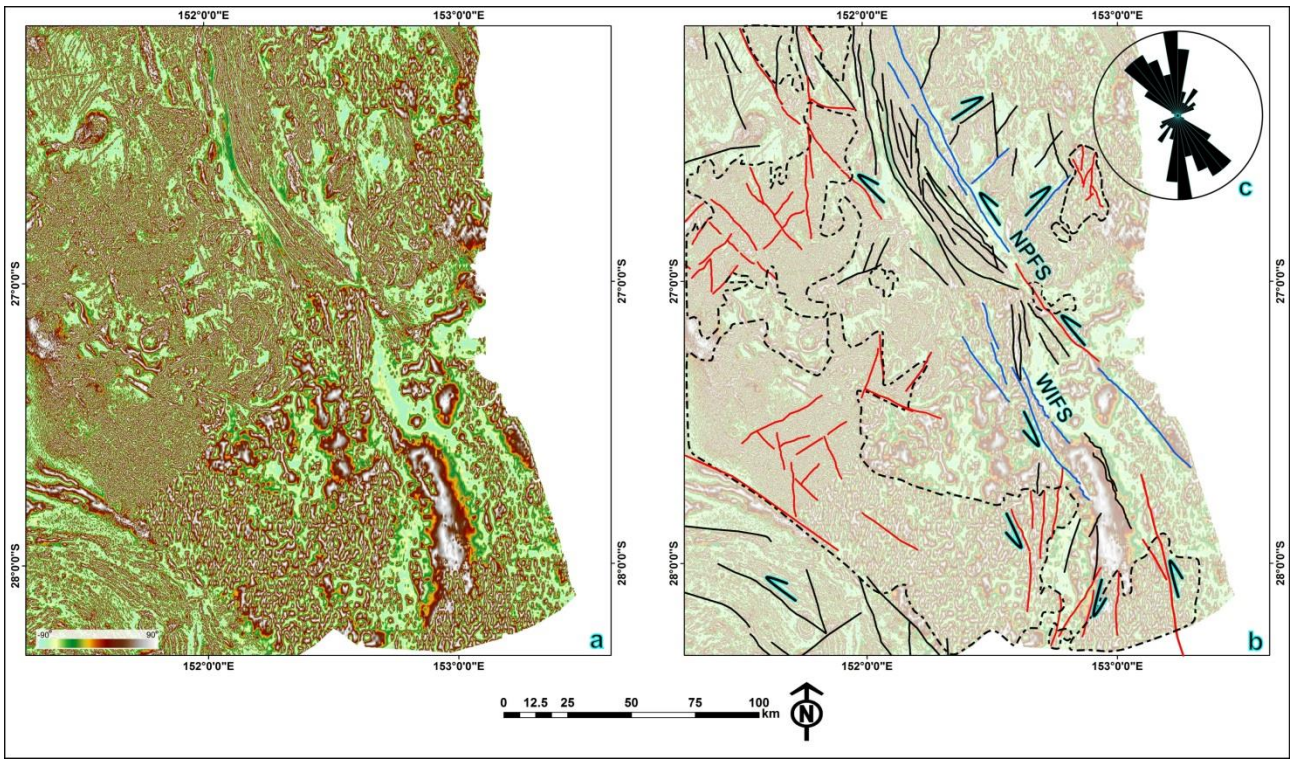

Figure 6.3. (a) Tilt angle derivative of gridded aeromagnetic data of southeast Queensland. (b) Interpreted major faults and their kinematics. Black lineaments are faults on which there is no evidence of Cenozoic activity, whereas blue lineaments are faults that have been inferred to have Cenozoic activity but have not cut Cenozoic volcanic rocks. Red lineaments are faults that have affected Cenozoic volcanic rocks. Dashed lines indicate the magnetic bodies related to Cenozoic volcanic rocks. (c) Rose diagram of fault lineaments in southeast Queensland.

6.3. Methods

Fault traces were detected using reduced-to-pole gridded aeromagnetic data, provided by Geoscience Australia. I operated a variety of filters in the Fourier domain to enhance short-wavelength and shallow sources, and to highlight magnetic lineaments such as the first vertical derivative and tilt angle derivative filters. The first vertical derivative (1VD) was operated to sharpen short-wavelength sources, and especially fault lineaments (Blakely, 1995). In particular, tilt angle derivative (the arc tangent of the ratio of the first vertical derivative to the absolute value of total horizontal derivatives) is a powerful filter for enhancing edges of magnetic sources and fault lineaments (Miller and Singh, 1994; Verduzco et al., 2004). The software Intrepid was used to process aeromagnetic data. The gridded aeromagnetic data allowed us to recognise (1) offset and dragging of magnetic anomalies along faults; (2) pronounced structural lineaments; and (3) lensoid and en-echelon structures.

Field work was conducted in accessible exposures of Cenozoic volcanic rocks with the aim of finding faults and their related kinematic indicators. Kinematic indicators used in this study include slickenlines, offset and dragged structures, and Riedel shears (R, P, and Y shears). In the absence of slickensides, the indicators used to determine the hanging-wall movement in cataclastic fault zones,

were P-Y shears, which are equivalent to S-C fabrics in ductile shear zones (Doblas, 1998; Lin, 1999; Babaahmadi and Rosenbaum, 2013).

6.4. Faulting in Cenozoic volcanic rocks

Interpretation of tilt angle derivative of gridded aeromagnetic data indicates that Cenozoic and basement rocks are displaced by three major sets of faults striking (1) NNW to NW, (2) NNE to NE, and (3) N-S (Figure 6.3). The majority of the faults in southeast Queensland are NNW- to NW-striking sinistral faults, such as the North Pine Fault System (NPFS) and West Ipswich Fault System (WIFS) (Figure 6.3) (Cranfield et al., 1976; Babaahmadi and Rosenbaum, 2014b). NNE- to NE-striking and N-striking faults are dextral (Babaahmadi and Rosenbaum, 2013, 2014b) (Figure 6.3). Faults shown in Figure 6.3b are classified into three groups based on their inferred Cenozoic activity. Faults shown in black (Figure 6.3b) do not show evidence for Cenozoic activity. Faults shown in blue (e.g., WIFS, and several segments of the NPFS) do not cut Cenozoic volcanic rocks but have been inferred to have undergone Cenozoic movement based on geological and kinematic analyses, and geomorphological considerations (Cranfield et al., 1976; Hodgkinson et al., 2007; Babaahmadi and Rosenbaum, 2014b). The distribution of earthquake epicenters along these major faults may also indicate recent faulting (Hodgkinson et al., 2006, 2007). Faults shown in red in Figure 6.3b are those displacing Cenozoic volcanic rocks. Structural observations from these faults are presented below from four areas (Figure 6.2).

6.4.1. The Maleny area

Cenozoic volcanic rocks in the Maleny area comprise a succession of thin layered mafic lavas with a total thickness of 180 m (Cohen et al., 2007) (Figures 6.2, 6.4a). These rocks appear as small high-amplitude short-wavelength bodies in aeromagnetic data (dashed lines in Figure 6.4d). Deeper sources are probably related to Triassic volcanic and intrusive rocks and Paleozoic metasedimentary rocks (Figure 6.4a). Interpretation of the 1VD gridded aeromagnetic data indicates that magnetic anomalies related to Cenozoic volcanic rocks have been displaced by NNW-, NE-, and N-striking faults (Figures 6.4c, d). NNW-striking faults have dragged magnetic anomalies sinistrally, whereas the strike-slip separation of NE- and N-striking faults is dextral (based on dragging and offset of magnetic bodies; Figure 6.4d).

Field observations in the western part of the Maleny area show a number of NE-striking faults displacing Cenozoic mafic volcanic rocks (Figures 6.4a, b, 6.5). Stereographic analyses of P-Y structures indicate a reverse dextral kinematics for these faults (Figure 6.4b). Some of NE-striking

reverse faults in Cenozoic basalts have been displaced by a younger set of reverse faults (red faults in Figure 6.5).

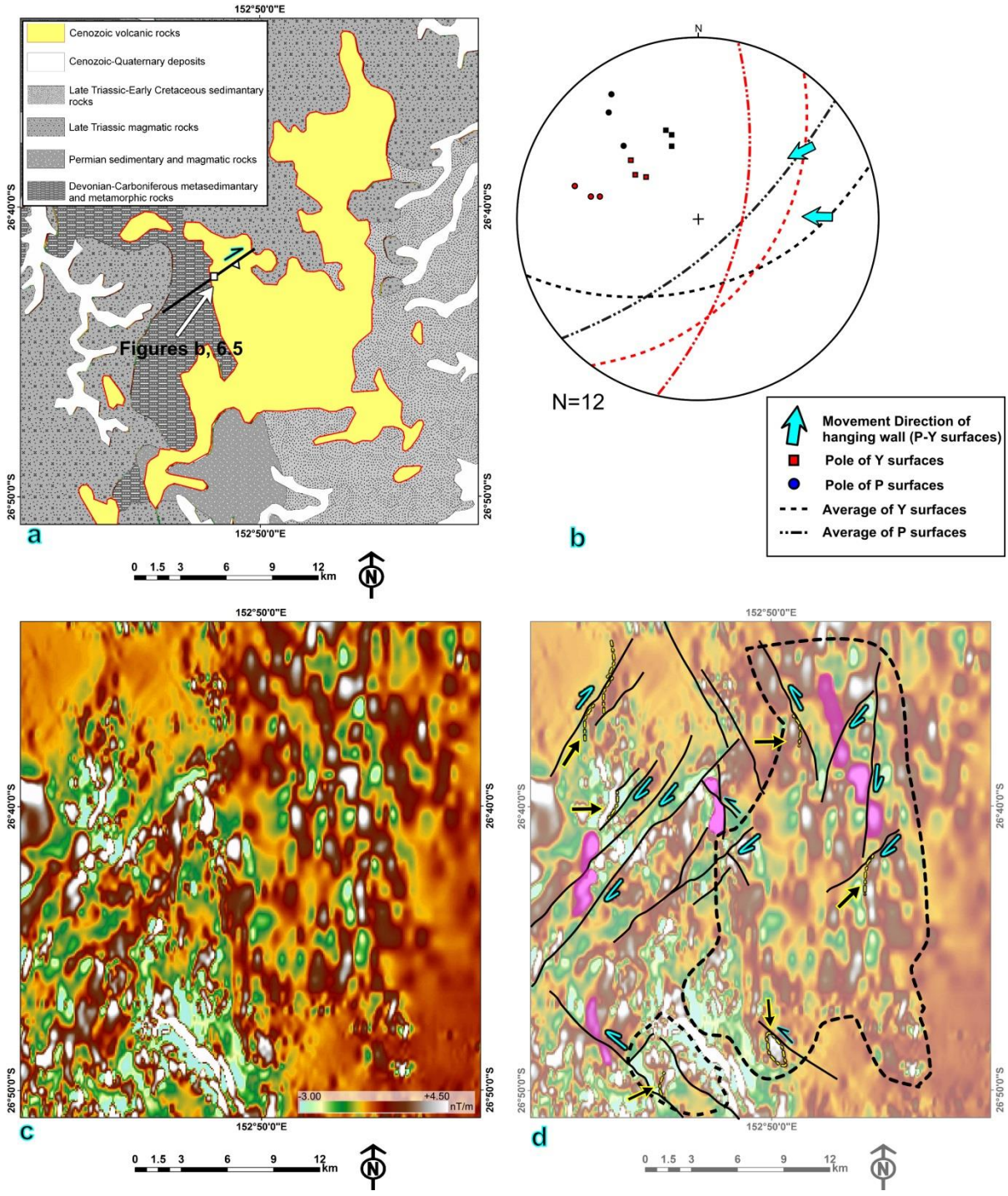

Figure 6.4. (a) Geological map of the Maleny area (after Green et al., 1980) (see Figure 6.2 for location). (b) Lower-hemisphere equal-area stereographic projection of fault surfaces and their kinematics. (c) The 1VD of gridded aeromagnetic data from the Maleny area, and (d) interpreted faults. Black dashed lines indicate magnetic bodies related to Cenozoic volcanic rocks; yellow arrows and pink areas show dragged and separated magnetic bodies, respectively.

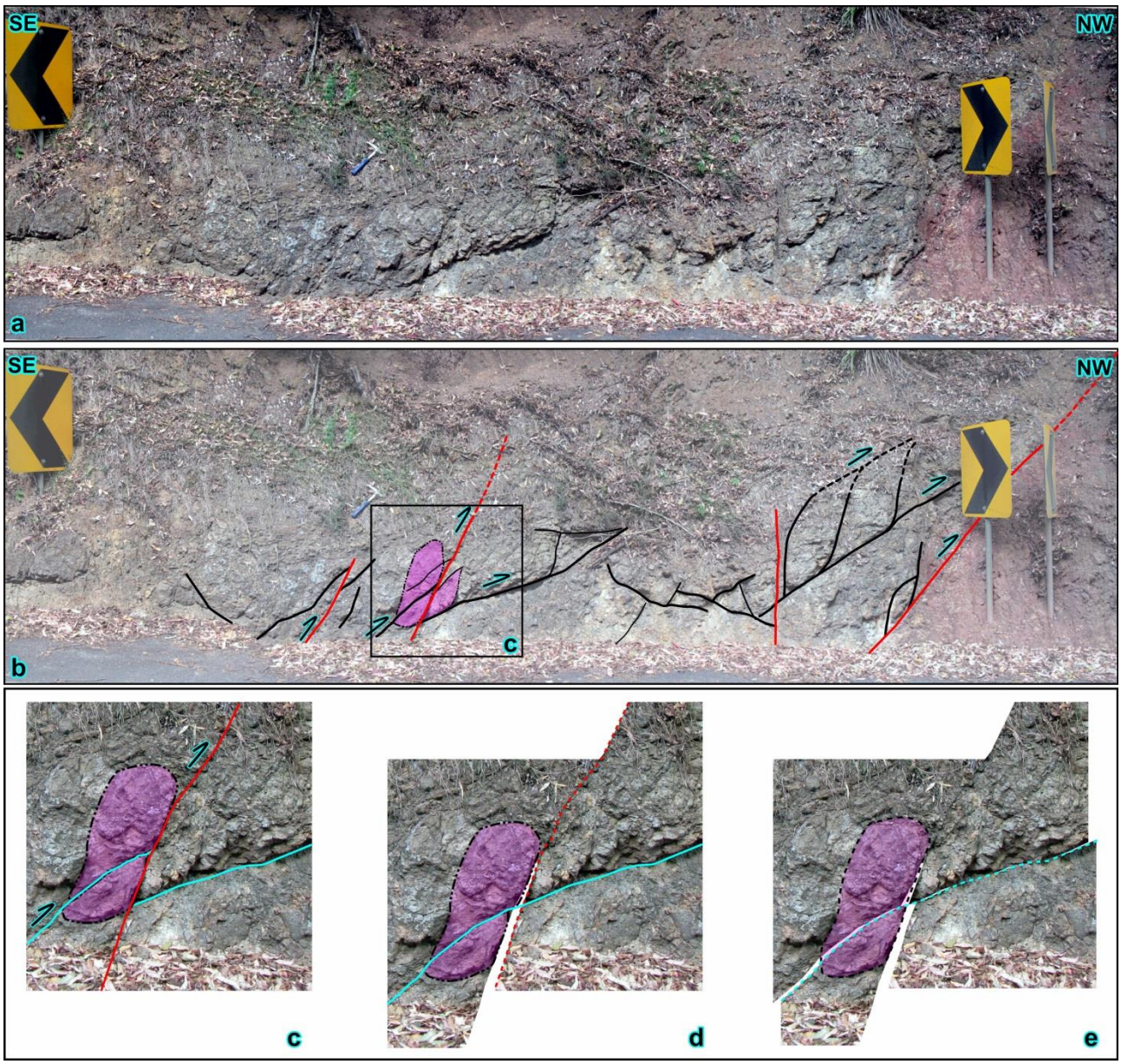

Figure 6.5. (a-b) NE-striking dextral reverse faults, shown in black, displacing Cenozoic basalts. These faults have been displaced by younger NE-striking reverse dextral faults, shown in red (see Figure 6.4a for location); Pink areas mark a large separated volcanic fragment and lensoid structures (X: 152º48', Y: -26º41'). (c-e) Restoration of separated volcanic rocks along two NNE- and NE-striking faults, indicating two possible phases of faulting; Pink areas mark a separated volcanic bomb by older NE-striking thrust fault.

6.4.2. The Ipswich area

Relatively small patches of Cenozoic volcanic rocks are observed in the Ipswich area as some spotted short-wavelength low- and high-amplitude magnetic bodies, overlying Jurassic detrital sedimentary rocks of the Clarence-Moreton Basin (Figures 6.2, 6.3, 6.6a, and black dashed lines in Figure 6.6d). Interpretation of the 1VD of gridded aeromagnetic data shows a NNW-striking high amplitude deep magnetic source interpreted as Paleozoic serpentinites which has been cut by a number of major faults

such as the WIFS (Figures 6.3, 6.6 c, d). Evidence of faulting in Cenozoic volcanic rocks is observed along a NE-striking fault, known in this study as the Redbank Plains Fault (RPF) (Figures 6.6a-d).

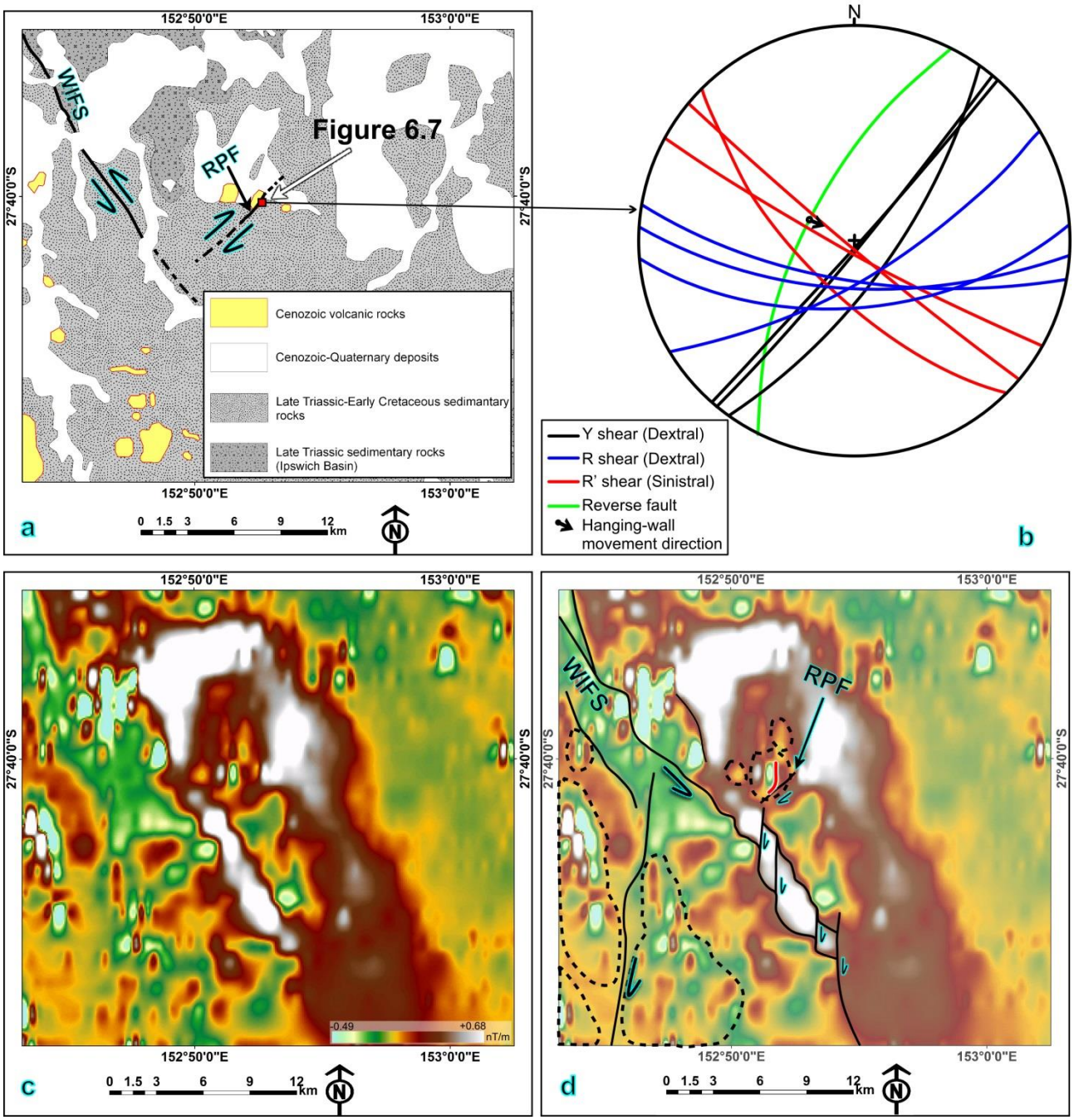

Figure 6.6. (a) Geological map of the Ipswich area showing the location of the RPF (see Figure 6.2 for location). (b) Lower hemisphere equal-area stereographic projection of Riedel shear system within the RPF zone. (c) The 1VD of gridded aeromagnetic data of the Ipswich area. (d) Interpretation of the aeromagnetic data showing the WIFS and RPF. Black dashed lines indicate magnetic bodies related to Cenozoic volcanic rocks. Red line shows dragging of magnetic body along the RPF.

Observations from the RPF show a contact of trachyte overlying basalt, and field evidence that both lithologies have been displaced by a steep, 10 m wide, strike-slip brittle fault zone (Figure 6.7a). Brittle movement along this fault has produced a volume of incohesive fault gouge (Figure 6.7b).

Kinematic indicators, such as dextral Y and R shears and sinistral R' shears in the fault zone; indicate a dextral strike-slip movement (Figures 6.6b, 6.7c, 6.8a-c).

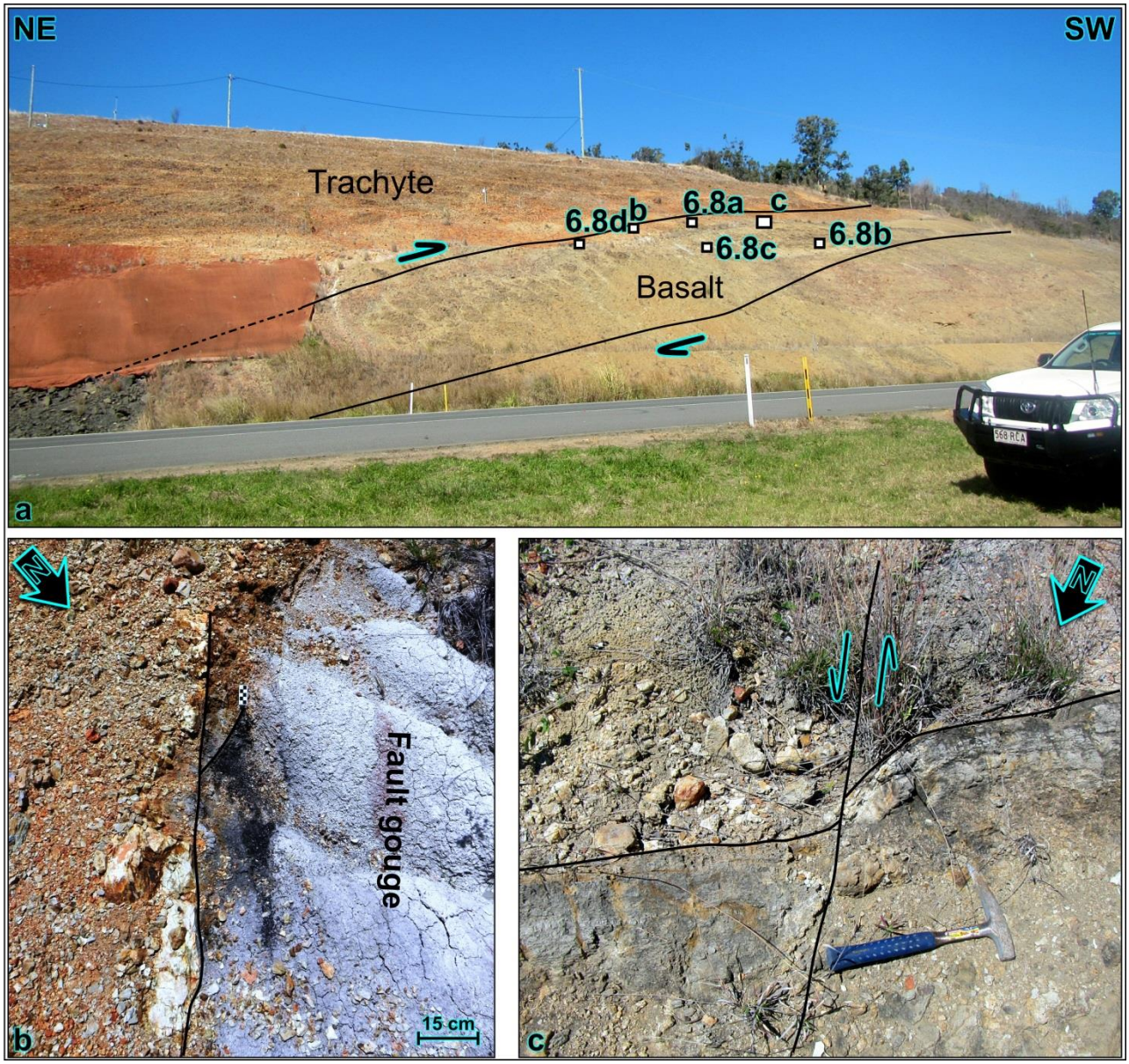

Figure 6.7. (a) The NE-striking dextral RPF, deforming Cenozoic trachyte and basalts (see Figure 6.6a for location) (X: 152º52', Y: -27º39'). (b) Fault gouge developed in the RPF zone. (c) A minor NNW-striking fault (R' shear) that displaced the main fault sinistrally.

A minor steep reverse fault surface observed in the fault zone which is interpreted to be kinematically related to the strike-slip movement of the RPF (Figures 6.6b, 6.8d). I infer that the NE-striking RPF is an antithetic dextral fault associated with the reactivation of the WIFS during the late Cenozoic. The maximum age of deformation is constrained by $^{40}Ar/^{39}Ar$ geochronological data from a nearby outcrop (Figure 6.2), which indicate that the age of the trachyte is ~26.5 Ma (Cohen et al., 2007).

Figure 6.8. Field photographs of the brittle RPF zone (see Figure 6.7a for locations) showing (a) dextral R and Y shears, (b) dextral dragging of a vein in the RPF zone, (c) dextral displacement of Y shears by an R shear, and (d) a small fault slickenside indicating a vertical reverse movement.

6.4.3. The South Ipswich area

In the South Ipswich area, Late Triassic-Jurassic sedimentary rocks are overlain by Cenozoic volcanic rocks (Figures 6.2, 6.9a). $^{40}Ar/^{39}Ar$ ages from the volcanic rocks range from ~26 to ~23 Ma (Cohen et al., 2007; Knesel et al., 2008) (Figure 6.2). In the tilt angle map of the gridded aeromagnetic data, Cenozoic volcanic rocks appear as small irregular, curved, and short-wavelength bodies (black dashed lines in Figure 6.9d), which overlie magnetic bodies related to Paleozoic and Mesozoic rocks (Figures 6.9c, d). Cenozoic volcanic rocks have been displaced by a series of NNW-, N-, and NNE-striking faults (Figures 6.3, 6.9c, d). Dragging and offset of magnetic bodies (red dashed lines in Figure 6.9d), show that the NNW-striking faults are sinistral and the NNE-striking faults are dextral (Figures 6.9c, d). In the west, a N-striking fault has dextrally separated a NNW-striking sinistral fault

by ~4.8 km (Figures 6.9c, d). Another offset is observed to the east where a NE-striking fault has dextrally separated a magnetic body related to Cenozoic volcanic rocks by ~1 km (Figures 6.9c, d).

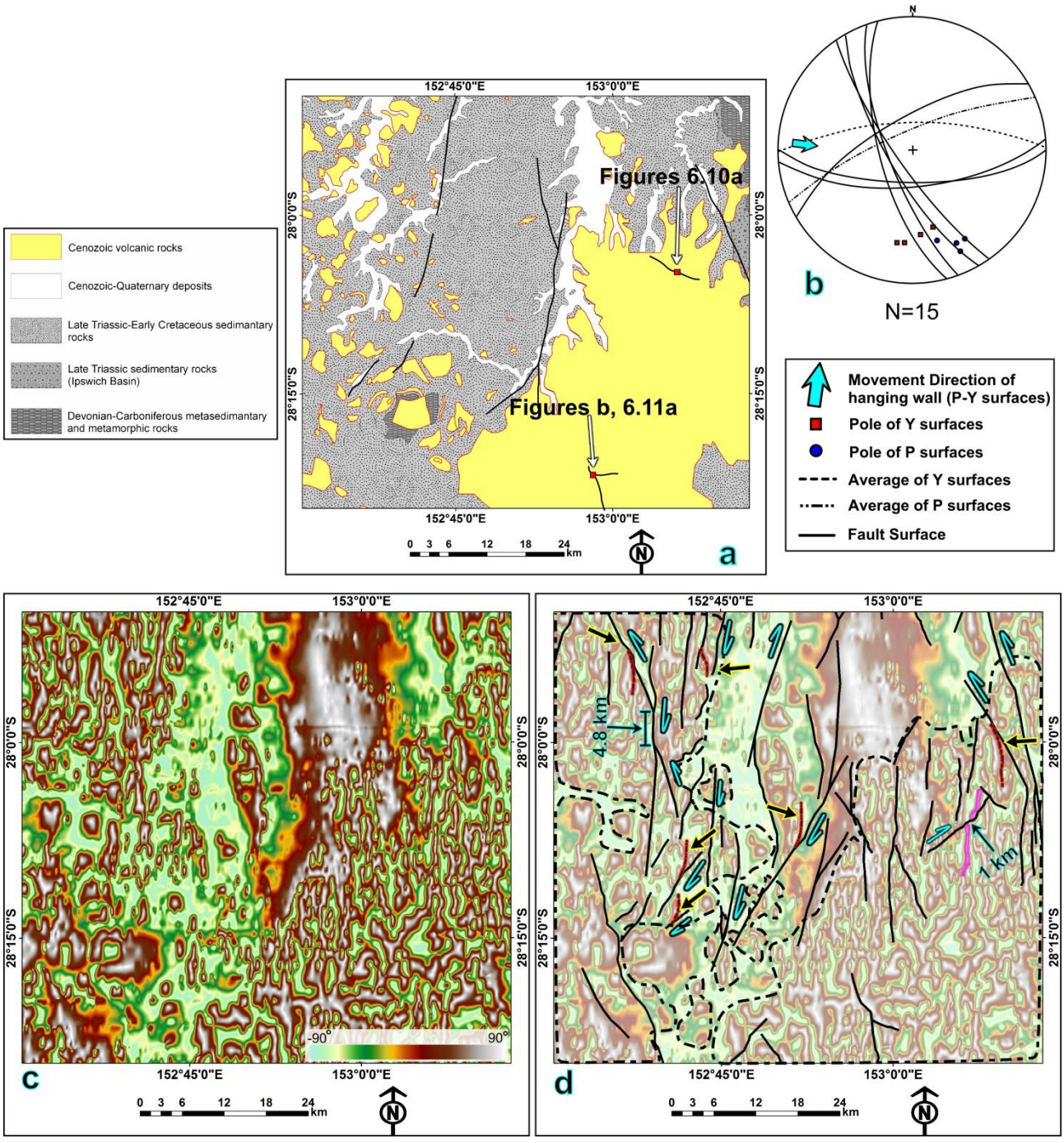

Figure 6.9. (a) Geological map of the south Ipswich area (see Figure 6.2 for location); (b-c) Lower-hemisphere equal-area stereographic projection of fault surfaces and their kinematics. (d) Tilt angle derivative of gridded aeromagnetic data of the South Ipswich area. (e) Interpreted faults. Black dashed line indicates magnetic bodies related to Cenozoic volcanic rocks; red dashed lines and yellow-black arrows show fault-related dragging shapes in magnetic bodies.

Field observations indicate that Cenozoic volcanic rocks have been cut by strike-slip reverse faults (Figures 6.9a-b; 6.10, 6.11a-c). A brittle WNW-striking reverse fault zone, in the eastern part of the

area, was observed affecting volcanic rocks dated at ~23 Ma (Knesel et al., 2008) (Figures 6.9a; 6.10). In the southeastern part of the area, Cenozoic volcanic rocks have been displaced by a series of steep strike-slip reverse brittle faults (Figures 6.9a-b, 6.11a-c).

Figure 6.10. (a-c) Reverse brittle fault zone, displacing Cenozoic basalts (see Figure 6.9a for location) (X: 153º06', Y: -28º04').

6.4.4. The Kingaroy area

In the Kingaroy area, widespread Cenozoic volcanic rocks overlie Paleozoic rocks, Permian-Triassic volcanic and intrusive rocks, and Jurassic sedimentary rocks (Figure 6.12a). Interpretation of a tilt map indicates that the area has mainly been deformed by NW-, N-, and NE-striking faults (Figures 6.12b, c). The NW- and NE-striking faults have dragged and separated Cenozoic volcanic rocks and older rocks sinistrally and dextrally, respectively (Figures 6.12b-c). Outcrop conditions in this area

are relatively poor, and the field observations are limited to one location (in a coal mine), where I observed a series of vertical faults affecting Cenozoic volcanic rocks (Figure 6.11d).

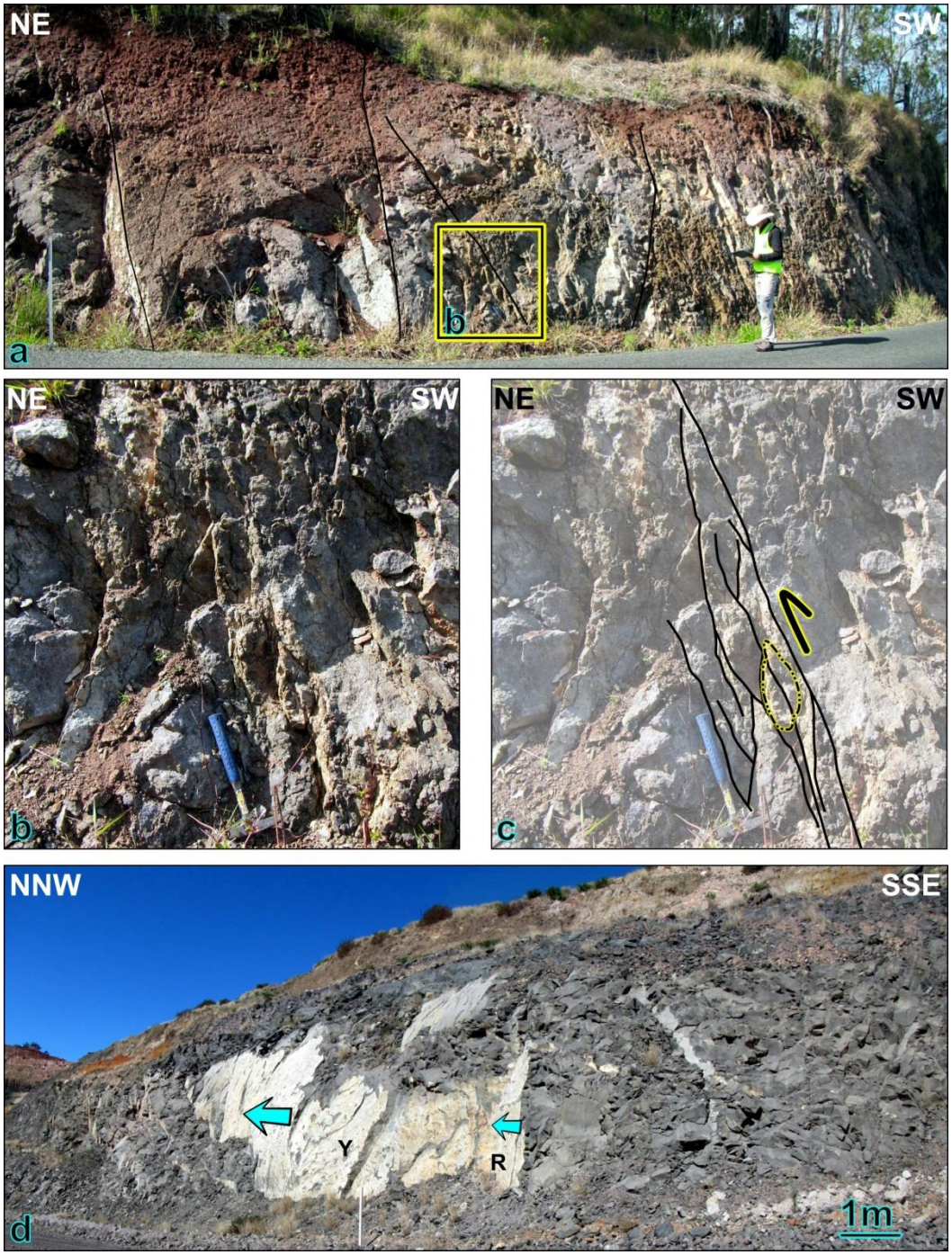

Figure 6.11. (a) Minor faults displacing Cenozoic volcanic rocks (see Figure 6.9a for location) (X: 152º58', Y: -28º20'). (b-c) A steep reverse fault truncating Cenozoic volcanic rocks; (d) A series of parallel N-striking dextral vertical faults displacing Cenozoic basalts (see Figure 6.12a for location) (X: 151º54', Y: -26º54').

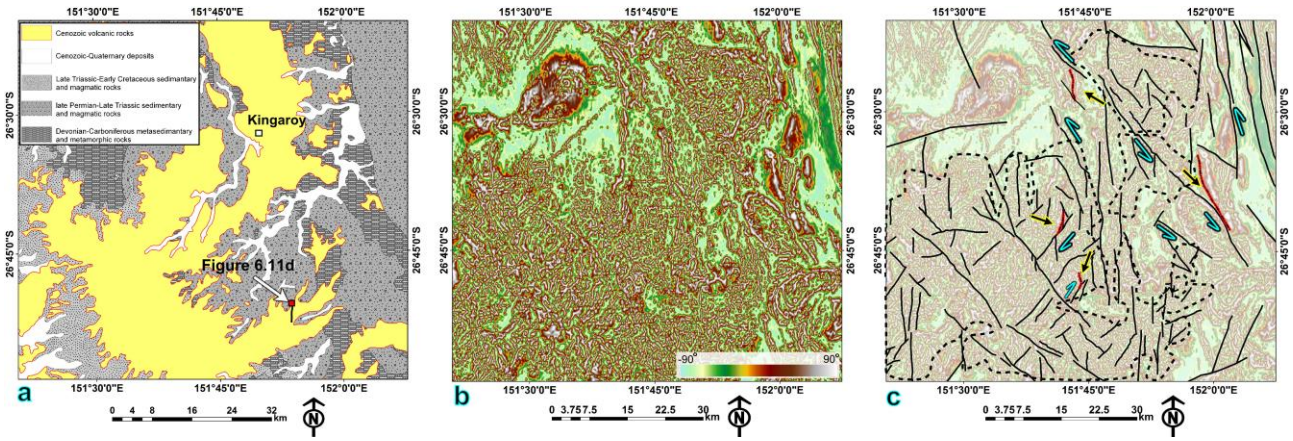

Figure 6.12. (a) Geological map of the Kingaroy area (see Figure 6.2 for location). (b) Tilt angle derivative of gridded aeromagnetic data of the Kingaroy area. (c) Interpreted faults and their kinematics. Black dashed lines indicate magnetic bodies related to Cenozoic volcanic rocks. Red dashed lines and yellow-black arrows show fault-related dragging and lensoid shapes in magnetic bodies.

6.5. Discussion

6.5.1. Late Cenozoic faulting in the eastern Australian passive margin

The observations provide evidence for late Cenozoic deformation in eastern Australia. Within this passive margin, there are a series of major faults that mainly affected Paleozoic and Mesozoic rock units (Babaahmadi and Rosenbaum, 2013, 2014b). Many of these structures operated as major tectonic boundaries during the formation of the New England Orogen (Murray et al., 1987; Holcombe et al., 1997b; Li et al., 2012b). They include NW- and NNW-striking sinistral faults, such as the NPFS and WIFS, and N- and NE-striking dextral faults such as the Demon Fault (Babaahmadi and Rosenbaum, 2013, 2014b) (Figures 6.1, 6.3). Interpretation of aeromagnetic data indicates that some of these faults have been reactivated and also affected Cenozoic volcanic rocks (Figure 6.3). Most faults show evidence for a major strike-slip movement and a minor reverse component (Babaahmadi and Rosenbaum, 2013, 2014b). These faults have possibly had a significant role in shaping the post-Late Triassic crustal structure of eastern Australia. Notable examples of these post-Late Triassic faults are the NPFS and Demon Fault, which record maximum strike-slip separations of ~8.2 km and ~35 km, respectively (Babaahmadi and Rosenbaum, 2013, 2014b).

The major faults discussed above have been reactivated intermittently since the post-Late Triassic. They played an important role in the development of sedimentary basins, such as the Clarence-Moreton and Maryborough Basins, and the geodynamic evolution of eastern Australia during the Jurassic and Early Cretaceous (Hill, 1994; Holcombe et al., 1997b; Babaahmadi and Rosenbaum, 2013, 2014b). Geochronology of fault gouges in the Sydney Basin supports a Jurassic-Early

Cretaceous age of brittle faulting (166-119 Ma), followed by a subsequent thermal event associated with the emplacement of magmas in the early stage of break-up of the eastern Gondawana margin (Och et al., 2014). In addition, it has been suggested that Early Cretaceous extensional faulting occurred simultaneously with volcanic activity in central Queensland (Bryan et al. (2000).

The Jurassic-Early Cretaceous sedimentary rocks in the Clarence-Moreton and Maryborough Basins have been folded and displaced by the reactivation of major faults with reverse components (Hill, 1994; Holcombe et al., 1997b). The origin of these contractional structures was likely related either to a mid-Cretaceous contractional event (Hill, 1994; Korsch et al., 2009b), possibly associated with a lithospheric rebound following subduction cessation (Korsch et al., 2009b), or to the far-field stress fields transmitted from the late Eocene to early Oligocene ophiolite obduction in New Caledonia (Babaahmadi and Rosenbaum, 2014b).

Babaahmadi and Rosenbaum (2014) suggested that major faults in eastern Australia were active as strike-slip normal faults in response to the oblique opening of the Tasman and Coral Seas from the Late Cretaceous to the early Eocene. Evidence of such activity is the development of Eocene sedimentary basins, such as the Duaringa and Hillsborough Basins, which developed over NNW-striking steep normal faults and have a maximum depth of 1.3 km (Gray, 1976; Gibson, 1989). Results of this study and previous studies (Babaahmadi and Rosenbaum, 2013, 2014b) indicate that several major faults have further been reactivated in the late Cenozoic, displacing the Cenozoic volcanic rocks (Figure 6.3). The field observations indicate that the wrench reactivation of major faults in the late Cenozoic gave rise to the occurrence of brittle subsidiary strike-slip and reverse faults (Figures 6.7, 6.8, 6.10, 6.11).

The exact timing of faulting is not precisely constrained, but the fact that brittle faults displaced Cenozoic volcanic rocks can provide a maximum age constraint for deformation. $^{40}Ar/^{39}Ar$ ages of the deformed volcanic rocks in southeast Queensland range from ~31±0.8 Ma at Maleny to ~20.7±0.5 Ma at the Main Range volcano (Cohen et al., 2007; Knesel et al., 2008) (Figure 6.2). Therefore, the timing of faulting in the Maleny area must be younger than ~31 Ma. Moreover, the results show that two phases of faulting have occurred in this area (Figure 6.5). In the Ipswich area, brittle deformation along the RPF affected a ~26.5 Ma trachyte (Figures 6.6-6.8), indicating that the activity of the fault is younger than this age. Similarly, considering that the age of the volcanic rocks at the Main Range volcano is 20.7±0.5 Ma (Figure 6.3), faulting in this area must have occurred after the early Miocene.

6.5.2. Origin of late Cenozoic transpressional deformation

Results of this study and other investigations imply that steeply dipping faults in eastern Australia accommodated intraplate transpressional deformation during the late Cenozoic (Babaahmadi and

Rosenbaum, 2014b). Most of the faults that affected Cenozoic volcanic rocks in the study area have experienced a major strike-slip movement.

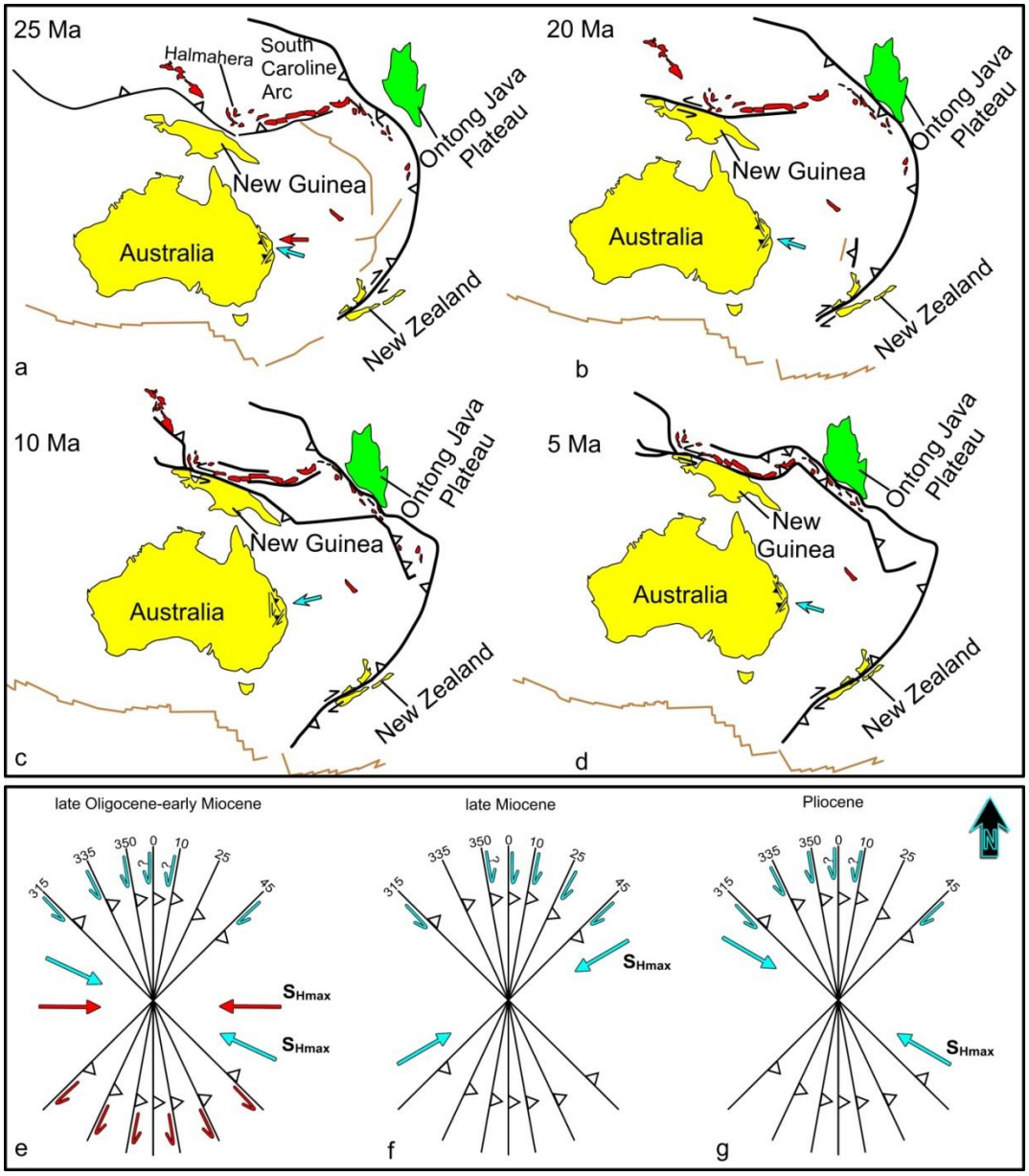

Figure 6.13. (a-d) Schematic tectonic evolution of the northeast and southeast Australian margins based on models by Hall (2002) and Schellart (2006) during the (a) late Oligocene, (b) early Miocene, (c) late Miocene, and (d) the Pliocene. Blue arrows indicate possible S_{Hmax} directions at these times in southeast Queensland (Muller et al., 2012). Red arrow in (a) indicates an inferred E-W S_{Hmax} from collisional zones at the northeast Australian margin; (e-f) Schematic structural model for the reactivation of faults in response to the modeled S_{Hmax} (Muller et al., 2012) since the late Oligocene. Red arrows in (e) indicate an inferred E-W S_{Hmax}. For fault strikes marked by question marks, there is no evidence for such kinematics.

In addition, kinematic analysis of some of these faults shows that they have a reverse component (Figures 6.9, 6.10). Similar reverse strike-slip kinematics is also observed along the NNW-striking NPFS, which displaced Cenozoic volcanic rocks (Babaahmadi and Rosenbaum, 2014b). Moreover,

faulting and folding have been reported in Cenozoic sedimentary rocks of the Hillsborough, Capel and Faust Basins, and central Lord Howe Rise (Figure 6.1a) (Clarke et al., 1971; Gray, 1976; Willcox and Sayers, 2002; Colwell et al., 2010).

I propose that the origin of late Cenozoic intraplate transpressional tectonics in eastern Australia was the far-field compressional horizontal stress fields (S_{Hmax}) transmitted from the plate boundaries. These compressional stress fields were likely intensified during two major collisional events that occurred (1) from the late Oligocene to the early Miocene; and (2) from the late Miocene to the Pliocene.

The earlier phase of deformation, in the late Oligocene-early Miocene, may have been triggered by contractional events along the northeast and southeast boundaries of the Australian plate. These included (1) the initiation of oblique convergence between the Melanesian arc system and the Ontong Java Plateau (OJP) (Petterson et al., 1997; Petterson et al., 1999); (2) arc-continent collision at the northern margin of New Guinea (Hall, 2002; Hill and Hall, 2003); and (3) ophiolite obduction (Schellart, 2007) and the inception of highly oblique convergence in New Zealand (Kamp, 1986; Schellart et al., 2006). The response of the Australian continent to the OJP oblique collision may have resulted in an abrupt deceleration of the Australian plate motion at ~26-23 Ma, as indicated by the spatio-temporal distribution of hotspot-related volcanic rocks in southeast Queensland (Knesel et al., 2008; Cohen et al., 2013). Similarly, the onset of oblique convergence along the northeastern boundary of Australian plate resulted in a westward offset in Cenozoic seamount chains in the Tasman Sea (Knesel et al., 2008; Cohen et al., 2013), possibly due to a possible E-W direction of S_{Hmax}. A numerical paleostress model of the early Miocene shows a dominant ~WNW-ESE direction of S_{Hmax} over southeast Queensland at that time (Dyksterhuis et al., 2005a; Muller et al., 2012), possibly as a result of obduction and collision in New Zealand (Figures 6.13a,b). Consequently, the geometry and kinematics of fault systems in southeast Queensland are generally consistent with both inferred E-W and WNW-ESE S_{Hmax}. In detail, however, the inferred WNW-ESE orientation of S_{Hmax} in southeast Queensland was oblique to major faults during the late Oligocene-early Miocene, and could have produced and reactivated NW- to NNE-striking reverse sinistral faults, and NNE- to NE-striking reverse and reverse dextral faults (Figures 6.13a, e). Nonetheless, there is no evidence for sinistral movements along N- and NNE-striking faults (Figure 6.13e). The inferred E-W S_{Hmax} could account for reverse sinistral movement along NNW- to NW-striking faults, reverse movement along N-striking faults, and reverse dextral kinematics of NNE- to NE-striking faults (Figure 6.13e).

The second stage of compression, from the late Miocene to the Pliocene, could be attributed to a series of successive collisional events that occurred along the northeast and southeast margins of the Australian plate. These events include (1) a sinistral oblique arc-continent collision at the northern margin of New Guinea since the late Miocene (Hill and Raza, 1999; Hill and Hall, 2003); (2) a strong

sinistral oblique collision between the Melanesian arc system and the Ontong Java Plateau (OJP) in the Pliocene (Petterson et al., 1997; Petterson et al., 1999); and (3) the kinematic change from strike-slip to transpression in the South Island of New Zealand since ~6.4 Ma (Walcott, 1998) (Figures 6.13c,d). The modeled paleostress maps show ENE-WSW and WNW-ESE S_{Hmax} directions in southeast Queensland in the late Miocene and the Pliocene, respectively (Muller et al., 2012) (Figures 6.13c,d). The ENE-WSW S_{Hmax} in the late Miocene could possibly result in NW-striking reverse sinistral faults, NNW-striking reverse faults, and N- to NE-striking reverse dextral faults (Figure 6.13f). The WNW-ESE S_{Hmax} during the Pliocene could have reactivated NW- and NNW-striking reverse sinistral faults, and NNE- to NE-striking reverse and reverse dextral faults, respectively (Figure 6.13g).

6.6. Conclusions

I used gridded aeromagnetic data and field observations to study intraplate deformation in Cenozoic volcanic rocks in southeast Queensland. The results indicate that Cenozoic volcanic rocks have been displaced by reverse strike-slip faults. Late Cenozoic deformation has mostly taken place due to the reactivation of major faults, which are interpreted to have been active during episodes of basin formation in the Jurassic-Early Cretaceous and later during the opening of the Tasman and Coral Seas in the Late Cretaceous to early Eocene. Faulted Cenozoic volcanic rocks in southeast Queensland range in ages from 31±0.8 to 20.7±0.5 Ma, indicating that the recent phases of faulting in eastern Australia have occurred since the late Oligocene. This intraplate transpressional deformation is construed to be related to far-field stress fields transmitted from collisional events at the northeast and southeast Australian plate boundaries, which were likely intensified during major collisional events during the late Oligocene-early Miocene and the late Miocene-Pliocene.

Chapter 7

Conclusions and Suggestions

7.1. Conclusions

The main aim of this PhD thesis was to unravel the role of major faults in the tectonic evolution of eastern Australia by studying the geometry, kinematics and reactivation history of fault systems. I used gridded aeromagnetic and gravity data, seismic reflection data, field observations, and remote sensing data in order to achieve this goal. Major conclusions of this study are:

7.1.1. The role of strike-slip faults in the formation of oroclines during the early-mid Permian

The results show that fault systems with a strike-slip separation are parallel to the Texas and Coffs-Harbour oroclines. The observation of orocline-parallel high-angle faults is in line with the idea that oroclinal bending was at least partly facilitated by a flexural slip mechanism. The observed dominant kinematics along the orocline-parallel faults is younger, and was likely associated with reactivation episodes during the Mesozoic and Cenozoic.

7.1.2. The role of faults in the development and inversion of Mesozoic sedimentary basins

The results show that the Triassic tectonic activity in eastern Australia was characterised by two episodes of extension intermitted by a phase of contraction, possibly in response to switches between trench retreat and advance, respectively. An extensional tectonics became dominant during the Early-Middle Triassic, characterised by an early stage of syn-sedimentary normal faults, resulting in the development of the Esk Trough and the Nymboida Coal Measures. The Esk Trough and Nymboida Coal Measures have gently been folded and thrusted due to a contractional event in in the early Late Triassic. After this contractional event, eastward trench retreat recommenced, and gave rise to the development of the Ipswich Basin in the Late Triassic, which is characterised by syn-sedimentary steep normal faults and bimodal volcanism. Since the latest Late Triassic, thermal subsidence led to the deposition of continental sediments in the Clarence-Moreton Basin. A number of strike-slip reverse faults have displaced the Ipswich and Clarence-Moreton Basins. They are construed to be related to the reactivation of basement faults during the mid-Cretaceous or Cenozoic.

7.1.3. The kinematics and timing of the Demon Fault

The results show that the Demon Fault has undergone a dextral strike-slip movement with a minor reverse component. Different displacements have taken place along different parts of the Demon Fault, with a general decrease in displacement towards the south due to either different histories of reactivation along different segments or the partitioning of deformation into minor reverse splays

towards the south. The Demon Fault has displaced NW-striking faults, which deformed Early to Middle Triassic magmatic rocks, indicating that the initiation of faulting along the Demon Fault has occurred after the emplacement of the magmatic rocks and the activity of the NW-striking faults. The presence of sub-parallel structures in Late Triassic to Early Cretaceous basins in eastern Australia suggests that the Demon Fault has been active during the Mesozoic. The last activity of the Demon Fault was associated with a transpressional regime, which is interpreted to be related to a mid-Cretaceous contractional event or to Cenozoic collisional processes at the northern margin of the Australian Plate.

7.1.4. The kinematics and timing of the North Pine Fault System

The North Pine Fault System (NPFS) is a sinistral high-angle fault system with a minor reverse component. The results indicate that the NPFS has had long-lasting periodic activities since the early Mesozoic. A granophyre dyke, which is found parallel to the NPF1 fault zone, has a possible age of Late Triassic, suggesting that the NPFS is construed to have been active with a normal component during the early Mesozoic. The NPFS and other NNW-striking faults appear to have been active as sinistral-normal oblique faults during the Late Cretaceous to Early Eocene opening of the Tasman and Coral seas. The sinistral-reverse oblique movement of the NPFS is interpreted to be driven by far-field contractional stresses from successive collisions at the east, southeast, and northeast boundaries of the Australian Plate since the late Eocene.

7.1.5. Evidence for late Cenozoic intraplate faulting in eastern Australia

The results of this study indicate that Cenozoic volcanic rocks have been displaced by reverse strike-slip faults. The late Cenozoic deformation is interpreted to have resulted from the reactivation of major faults, which have been active during episodes of basin formation in the Jurassic-Early Cretaceous. Faulted Cenozoic volcanic rocks in southeast Queensland range in ages from 31±0.8 to 20.7±0.5 Ma, indicating that recent phases of faulting in eastern Australia are younger than late Oligocene. This intraplate transpressional deformation is construed to be related to far-field stress fields transmitted from collisional events at the northeast and southeast boundaries of the Australian Plate, which were likely intensified during major collisional events during the late Oligocene-early Miocene and the late Miocene-Pliocene.

7.2. Suggestions for future work

7.2.1. Detailed investigation into Quaternary deformation in eastern Australia

There are many instrumentally and historically recorded earthquakes in eastern Australia, indicating that fault systems in eastern Australia are possibly still active. Quaternary deformation can be investigated from structural, geomorphic, and seismotectonic points of view. The geometry and kinematics of faults can be identified by structural analyses, whereas the Quaternary activity of faults can be tested by the study of geomorphic features in response to the activity of faults. A seismotectonic study can be helpful to understand recent deformation in eastern Australia.

7.2.2. The kinematics, timing, and regional influence of the Peel Fault System

The Peel Fault System (PFS) is a steep fault system that is the boundary between the Devonian-Carboniferous forearc basin and accretionary wedge. Although there are some studies on the PFS (e.g., Offler and Williams, 1987; Corbett, 1976), a comprehensive structural and tectonic investigation is required. The geometry and kinematics of the PFS can be studied through detailed geophysical and field observations. The timing and regional tectonic influence of the PFS can be investigated by spatio-temporal analyses of displaced rock units, and direct geochronology of clay gouges from different parts of the fault system.

7.2.3. The geometry and shape of the basement underlying the Triassic-Jurassic basins

Although a detailed structural study has been carried out on the Esk Trough, Nymboida Coal Measures, and Ipswich and Clarence-Moreton Basins in this thesis, the inverse and forward modeling of gravity and aeromagnetic data can be used to determine the depth, shape, geometry and geological characteristics of basement structures of these basins. This study will assist in the better understanding of the role of basement structures in the development of basins.

References

Allis, R.G., 1981. Continental underthrusting beneath the Southern Alps of NewZealand. Geology 9, 303-307.

Amante, C., Eakins, B.W., 2009. ETOPO1 1 Arc-Minute Global Relief Model: Procedures, Data Sources and Analysis. NOAA Technical Memorandum NESDIS NGDC, National Geophysical Data Center-24, NOAA. doi:10.7289/V5C8276M.

ASTER-GDEM-Validation-Team, 2011. ASTER Global Digital Elevation Model Version 2-Summurry of validation results. The Ministry of Economy and Industry of Japan and NASA.

Aubourg, C., Klootwijk, C., Korsch, R.J., 2004. Magnetic fabric constraints on oroclinal bending of the Texas and Coffs Harbour blocks: New England Orogen, eastern Australia, pp. 421-445.

Babaahmadi, A., Mohajjel., M., Eftekhari, A., Davoudian, A., R. , 2012. An investigation into the fault systems in the Chadegan region, West Iran: Evidence for dextral brittle transpression tectonics in the Sanandaj-Sirjan Zone. Journal of Asian Earth Sciences 43 77-88.

Babaahmadi, A., Rosenbaum, G., 2013. Kinematics of the Demon Fault: Implications for Mesozoic strike-slip faulting in eastern Australia. Australian Journal of Earth Sciences 60, 255–269.

Babaahmadi, A., Rosenbaum, G., 2014a. Late Cenozoic intraplate faulting in eastern Australia. Journal of Structural Geology 69, 59-74.

Babaahmadi, A., Rosenbaum, G., 2014b. Late Mesozoic and Cenozoic wrench tectonics in eastern Australia: Insights from the North Pine Fault System (southeast Queensland). Journal of Geodynamics 73, 83-99.

Babaahmadi, A., Rosenbaum, G., Esterle, J., 2015. Alternating episodes of extension and contraction during the Triassic: Evidence from Mesozoic sedimentary basins in eastern Australia. Australian Journal of Earth Sciences 64/5.

Badley, M.E., 1985. Practical seismic interpretation. International Human Resources Development Corporation, Boston, 266 pp.

Baldwin, S.L., Fitzgerald, P.G., Webb, L.E., 2012. Tectonics of the New Guinea Region. Annual Review of Earth and Planetary Sciences 40, 495–520.

Blakely, R.J., 1995. Potential Theory in Gravity and Magnetic Applications. Cambridge University Press, New York, 435pp.

Boisvert, T.H., 1965. Australia Cities Service Inc. Tullymorgan No.1 well completion report, Bureau of Mineral Resources, Australia, File. 65/4147.

Brooke-Barnett, S., Rosenbaum, G., 2015. Structure of the Texas Orocline beneath the sedimentary cover (southeast Queensland, Australia). Australian Journal of Earth Sciences in press.

Brown, R.E., Krynen, J.P., Brownlow, J.W., 1990. Manilla-Narrabri 1:250,000 metallogenic map. . Geological Survey of New South Wales, Sydney.

Brunker, R.L., Offenberg, A.C., Cameron, R.G., 1970. Hastings 1:250 000 Geological Sheet SH/56-14, 1st edition, Geological Survey of New South Wales, Sydney.

Bryan, S.E., Ewart, A., Stephens, C.J., Parianos, J., Downes, P.J., 2000. The Whitsunday Volcanic Province, Central Queensland, Australia: lithological and stratigraphic investigations of a silicic-dominated large igneous province. Journal of Volcanology and Geothermal Research 99, 55–78.

Burmah-Oil, 1963. Burmah Oil Clifden No.3 well completion report. Bureau of Mineral Resources, Australia, File. 62/1310.

Cadman, S.J., Pain, L., Vuckovic, V., 1998. Bowen and Surat Basins, Clarence Morton Basin, Sydney Basin, Gunnedah Basin and other minor onshore basins, Queensland, NSW and NT. Australian Petroleum Accumulations Report 11, Bureau of Resource Sciences, Canberra.

Campbell, J.A., Holcombe, R.J., Fielding, C.R., 1998. The internal structure and sedimentology of the Esk Trough, Southeast Queensland. Geological Society of Australia Abstracts 49, 64.

Campbell, L.M., 2005. Basin Analasis and Tectonic Evolution of the Esk Trough in Southeast Queensland. Unpublished PhD thesis, the University of Queensland, Brisbane.

Campbell, M., 2014. Unraveling the early Permian geodynamics in the Texas Orocline. Unpublished Honours thesis, The University of Queensland.

Caprarelli, G., Leitch, E.C., 1998. Magmatic changes during the stabilisation of a cordilleran fold belt: The Late Carboniferous-Triassic igneous history of eastern New South Wales, Australia. Lithos 45, 413-430.

Cawood, P.A., 1982. Structural relations in the subduction complex of the Paleozoic New England fold belt, eastern Australia. Journal of Geology 90, 381-392.

Cawood, P.A., Leitch, E.C., 1985. Accretion and dispersal ectonics of the southern New England Fold Belt, eastern Australia. Tectonostratigraphic Terranes of the Circum-Pacific Region, 481-492.

Cawood, P.A., Leitch, E.C., Merle, R.E., Nemchin, A.A., 2011a. Orogenesis without collision: Stabilizing the terra australis accretionary Orogen, Eastern Australia. Bulletin of the Geological Society of America 123, 2240-2255.

Cawood, P.A., Pisarevsky, S.A., Leitch, E.C., 2011b. Unraveling the New England orocline, east Gondwana accretionary margin. Tectonics 30.

Clarke, D.E., Paine, A.G.L., Jensen, A.R., 1971. Geology of the Proserpine 1:250,000 Sheet area, Queensland. Bureau of Mineral Resources, Geology & Geophysics, Report 144. 1968/022.

Cluzel, D., Aitchison, J.C., Picard, C., 2001. Tectonic accretion and underplating of mafic terranes in the late Eocene intraoceanic fore-arc of New Caledonia (southwest Pacific): geodynamic implications. Tectonophysics 340, 23–59.

Cohen, B.E., Knesel, K.M., Vasconcelos, P.M., Schellart, W.P., 2013. Tracking the Australian plate motion through the Cenozoic: Constraints from 40Ar/39Ar geochronology. Tectonics 32, 2013TC003352.

Cohen, B.E., Vasconcelos, P.M.D., Knesel, K.M., 2007. 40 Ar/39 Ar constraints on the timing of Oligocene intraplate volcanism in southeast Queensland. Australian Journal of Earth Sciences 54 105-125.

Collins, W.J., 1991. A reassessment of the 'Hunter-Bowen Orogeny': Tectonic implications for the southern New England Fold Belt. Australian Journal of Earth Sciences 38, 409-423.

Colwell, J.B., Hashimoto, T., Rollet, N., Higgins, K., Bernardel, G., McGiveron, S., 2010. Interpretation of Seismic Data, Capel and Faust Basins, Australia's Remote Offshore Eastern Frontier. Geoscience Australia Record, 2010/06.

Cooper, G.R.J., Cowan, D.R., 2005. Differential reduction to the pole. Computers & Geosciences 31 989–999.

Cranfield, L.C., Schwarzbock, H., 1976. Ipswich Basin. In R.B. Leslie, H.J. Evans and C.L. Knight, (Editors), Economic geology of Australia and Papua New Guinea. Volume 3. Petroleum. Australasian Institute of Mining and Metallurgy, Monograph Series 7, 452-454.

Cranfield, L.C., Schwarzbock, H., Day, R.W., 1976. Geology of the Ipswich and Brisbane 1:250000 sheet areas. Geological Survey of Queensland Report 95, 1-176.

Cranfield, L.C., Shorten, G., Scott, M., Barker, R.M., 1997. Geology and mineralisation of the Gympie Province, in Tectonics and metallogenesis of the New England Orogen, edited by P. G. Flood and P. M. Ashley. Geolological Society of Australia Special Publication 19, pp. 128-147.

Crawford, A.J., Meffre, S., Symonds, P., A., 2003. 120 to 0 Ma tectonic evolution of the southwest Pacific and analogous geological evolution of the 600 to 220 Ma Tasman Fold Belt system. Special Publication of Geological Society of America, 372, 383 – 403.

Crook, K.A.W., 1964. Depositional environmental and provenance of Devonian and Carboniferous sediments in the Tamworth Trough, N.S.W. Journal and Proceedings of the Linnean Society of New South Wales 97, 41-53.

Davies, H.L., 2012. The geology of New Guinea: the cordilleran margin of the Australian continent. Episodes 35, 87-102.

Day, R.W., Murray, C.G., Whitaker, W.G., 1978. The eastern part of the Tasman Orogenic Zone. Tectonophysics 48, 327-364.

de Jersey, N.J., 1972. Triassic miospores from the Esk beds, publication no. 357, Geological Survey of Queensland, Brisbane.

de Jersey, N.J., 1973. Triassic miospores from the Bryden Formation. Queensland Government Mining Journal 74, 377-378.

De Keyser, K., 1963. The Palmerville Fault-a 'fundamental' structure in north Queensland. Australian Journal of Earth Sciences 10 273-278.

De Keyser, K., Lucas, K.G., 1968. Geology of the Hodgkinson and Laura Basins, north Queensland. Bureau of Mineral Resources, Geology and Geophysics Australia, Bulletin 84.

DeMets, C., Gordon, R.G., Argus, D.F., Stein, S., 1994. Events of recent revisions to the geomagnetic reversal time scale on estimates of current plate motions. Geophysical Research Letter 21, 2191–2194.

Dickinson, J.A., Wallace, M.W., Holdgate, G., Daniels, J., Gallagher, S.J., Thomas, L., 2001. Neogene tectonics in SE Australia: Implications for petroleum systems. Australian Petroleum Production and Exploration Association Journal 41, 37-51.

Doblas, M., 1998. Slickenside kinematic indicators. Tectonophysics 295, 187–197.

Donchak, P.J.T., Bultitude, R.J., Purdy, D.J., Denaro, T.J., 2007a. Geology and mineralisation of the Texas Region, south-eastern Queensland. Queensland Geology 11, 96 pp.

Donchak, P.J.T., Bultitude, R.J., Purdy, D.J., Pascoe, G.S., 2007b. 100,000 Allora Special Geological Map, Department of Mines and Energy, Queensland.

Dyksterhuis, S., Müller, R.D., 2008. Cause and evolution of intraplate orogeny in Australia. Geology 36, 495-498.

Dyksterhuis, S., Müller, R.D., Albert, R.A., 2005a. Palaeo-stress field evolution of the Australian continent since the Eocene. Journal of Geophysical Research 110, B05102 DOI:10.1029/2003JB002728.

Dyksterhuis, S., Müller, R.D., Albert, R.A., 2005b. Paleostress field evolution of the Australian continent since the Eocene. Journal of Geophysical Research: Solid Earth (1978–2012) 110.

Elliott, L.G., 1993. Post-Carboniferous tectonic evolution of eastern Australia. The APEA Journal 33, 215-236.

Ellis, P.L., 1968. Geology of the Maryborough 1:250,000 Sheet area (SG 56-6) Geological Survey of Queensland, Report 90.

Ellis, P.L., Whitaker, W.G., 1976. Geology of the Bundaberg 1:250,000 sheet area. Queensland Department of Mines, Geological Survey of Queensland.

Etheridge, M., McQueen, H., Lambeck, K., 1991. The role of intraplate stress in Tertiary (and Mesozoic) deformation of the Australian continent and its margins: A key factor in petroleum trap formation. Exploration Geophysics 22, 123–128.

Evans, P.R., Roberts, J., 1980. Evolution of central eastern Australia during the late Palaeozoic and early Mesozoic. Journal of the Geological Society of Australia 26, 325-340.

Faure, M., Lalevée, F., 1987. Bent structural trends of Japan: Flexural-slip folding related to the Neogene opening of the Sea of Japan. Geology 15, 49-52.

Fergusson, C.L., 1982. Structure of the Late Palaeozoic Coffs Harbour Beds, northeastern New South Wales. Journal of the Geological Society of Australia 29, 25-40.

Finlayson, D.M., Leven, J.H., Etheridge, M.A., 1988. Structural Styles and Basin Evolution in Eromanga Region, Eastern Australia. American Association of Petroleum Geologists 72, 33-48.

Flint, J.C.E., Gould, R.E., 1975. A note on the fossil megafloras of the Nymboida and Red Cliff Coal Measures, southern ClarenceMoreton Basin. Journal and Proceedings of the Royal Society of New South Wales 108, 70-74.

Fowler, T.J., 1996. Flexural-slip generated bedding-parallel veins from central Victoria, Australia. Journal of Structural Geology 18, 1399-1415.

Fowler, T.J., Winsor, C.N., 1997. Characteristics and occurrence of bedding-parallel slip surfaces and laminated veins in chevron folds from the Bendigo-Castlemaine goldfields: implications for flexural-slip folding. Journal of Structural Geology 19, 799-815.

Gaina, C., Muller, R.D., Royer, J.-Y., Stock, J., Hardebeck, J., Symonds, P., 1998a. The tectonic history of the Tasman Sea: a puzzle with 13 pieces. Journal of Geophysical Research 103, 12413–12433.

Gaina, C., Muller, R.D., Royer, J.-Y., Symonds, P., 1999. Evolution of Luisiade triple Junction. Journal of Geophysical Research 104, 12927-12939.

Gaina, C., Royer, J.-Y., Muller, R.D., Symonds, P., 1998b. The Opening of the Tasman Sea: A Gravity Anomaly Animation. Earth Interactions 2, 1-22.

Gibert, D., Galdeano, A., 1985. A computer program to perform transformations of gravimetric and aeromagnetic surveys. Computers & Geosciences 11, 553-588.

Gibson, P.J., 1989. Petrology of two Tertiary oil shale deposits from Queensland, Australia. Journal of the Geological Society 146, 319-331.

Gilligan, L.B., Brownlow, J.W., Cameron, R.G., Henley, H.F., 1992. Dorrigo - Coffs Harbour 1:250 000 Metallogenic Map. Geological Survey of New South Wales, Sydney.

Glen, R.A., 2005. The Tasmanides of eastern Australia. In: Vaughan, A.P.M., Leat, P.T., Pankhurst, R.J. (Eds.), Terrane Processes at the Margins of Gondwana. Special Publication of The Geological Society, London 246, 23-96.

Glen, R.A., 2013. Refining accretionary orogen models for the Tasmanides of eastern Australia. Australian Journal of Earth Sciences 60, 315-370.

Glen, R.A., Beckett, J., 1997. Structure and tectonics along the inner edge of a foreland basin: The Hunter Coalfield in the northern Sydney Basin, New South Wales. Australian Journal of Earth Sciences 44, 853-877.

Glen, R.A., Meffre, S., 2009. Styles of Cenozoic collisions in the western and southwestern Pacific and their applications to Palaeozoic collisions in the Tasmanides of eastern Australia. Tecnotophysics 479, 130–149.

Glen, R.A., Roberts, J., 2012. Formation of oroclines in the New England Orogen, eastern Australia. Journal of the Virtual Explorer 43, Paper 3, doi: 10.3809/jvirtex.2012.00305.

Gray, A.R.G., 1976. Hillsborough Basin. In R.B. Leslie, H.J. Evans and C.L. Knight, (Editors), Economic geology of Australia and Papua New Guinea. Volume 3. Petroleum. Australasian Institute of Mining and Metallurgy, Monograph Series, 7, 460-464.

Green, D.C., Webb, A.W., 1974. Geochronology of the northern part of the Tasman Orogenic Zone, in AK Denmead, GW Tweedale & AF Wilson (eds), The Tasman Geosyncline—a symposium,Geological Society of Australia, Queensland Division, Brisbane, pp. 275–93.

Green, P.M., Stephens, R.W., Whitaker, W.G., 1980. Moreton geology, Queensland & New South Wales/Geological Survey of Queensland.

Gross, M.R., Becker, A., Gutiérrez-Alonso, G., 1997. Transfer of displacement from multiple slip zones to a major detachment in an extensional regime: Example from the Dead Sea rift, Israel. Geological Society of America Bulletin 109, 1021-1035.

Gutierrez-Alonso, G., Fernandez-Suarez, J., Weil, A.B., Brendan, M.J., R., D.N., Corfu, F., Johnston, S.T., 2008. Self-subduction of the Pangaean global plate. Nature Geoscience 1, 549-553.

Hall, R., 2002. Cainozoic geological and plate tectonic evolution of SE Asia and the SW Pacific: computer-based reconstructions, model and animations. Journal of Asian Earth Sciences 20, 353-431.

Harrington, H.J., 1983. Correlation of the Permian and Triassic Gympie Terrane of Queensland with the Brook Street and Maitai Terranes of New Zealand.In: Permian geology of Queensland, pp. 431-436. Geological Society of Australia, Queensland Division, Brisbane.

Harrington, H.J., Korsch, R.J., 1985. Late Permian to Cainozoic tectonics of the New England Orogen (USA). Australian Journal of Earth Sciences 32, 181-203.

Henderson, R.A., Fergusson, C.L., Learch, T.L., Morand, V.J., Reinhardt, J.J., Carr, P.F., 1993. Tectonics of the northern New England Fold Belt. . In Flood P.G. and Aitchison J.C., eds New England Orogen, eastern Australia. Department of Geology and Geophysics, University of New England, Armidale,, 505-515.

Henley, H.F., Brown, R.E., Brownlow, J.W., Barnes, R.G., Stroud, W.J., 2001. Grafton-Maclean 1:250 000 Metallogenic Map, 1st edition. Geological Survey of New South Wales, Sydney.

Hensel, H.D., McCulloch, M.T., Chappell, B.W., 1985. The New England Batholith: constraints on its derivation from Nd and Sr isotopic studies of granitoids and country rocks. Geochimica et Cosmochimica Acta 49, 369-384.

Hill, K.C., Hall, R., 2003. Mesozoic-Cenozoic evolution of Australia's New Guinea margin in a west Pacific context. Geological Society of Australia Special Publication 22 and Geological Society of America Special Paper 372, 265–290.

Hill, K.C., Raza, A., 1999. Arc-continent collision in Papua Guinea: Constraints from fission track thermochronology. Tectonics 18, 950-966.

Hill, P.J., 1992. Capricorn and northern Tasman Basins; structure and depositional systems. Exploration Geophysics. 23, 153-161.

Hill, P.J., 1994. Geology and geophysics of the offshore Maryborough, Capricorn and northern Tasman Basins: results of AGSO Survey 91. Canberra, Australian Geological Survey Organisation, Record 1994/1.

Hillis, R.R., Sandiford, M., Reynolds, S.D., Quigley, M.C., 2008. Present-day stresses, seismicity and Neogene-to-Recent tectonics of Australia's 'passive'margins: intraplate deformation controlled by plate boundary forces. Geological Society, London, Special Publications 306, 71-90.

Hodgkinson, J.H., McLoughlin, S., Cox, M.E., 2006. The correlation between physiography and neotectonism in southeast Queensland. Proceedings of the Earthquake Engineering Conference , AEES2006, Canberra, pp. 195 – 202.

Hodgkinson, J.H., McLoughlin, S., Cox, M.E., 2007. Drainage patterns in southeast Queensland: the key to concealed geological structures? Australian Journal of Earth Sciences 54, 1137-1150.

Holcombe, R.J., Stephens, C.J., Fielding, C.R., Gust, D., Little, T.A., Sliwa, R., McPhie, J., Ewart, A., 1997a. Tectonic evolution of the northern New England Fold Belt: Carboniferous to Early Permian transition from active accretion to extension. in: Ashley, P.M., Flood, P.G. (Eds.), Tectonics and metallogenesis of the New England Orogen. Geological Society of Australia special Publication, pp. 66-79.

Holcombe, R.J., Stephens, C.J., Fielding, C.R., Gust, D., Little, T.A., Sliwa, R., McPhie, J., Ewart, A., 1997b. Tectonic evolution of the northern New England Fold Belt: The Permian-Triassic Hunter-Bowen event, in: Ashley, P.M., Flood, P.G. (Eds.), Tectonics and metallogenesis of the New England Orogen. Geological Society of Australia Special Publication, pp. 52-65.

Horne, R., Culshaw, N., 2001. Flexural-slip folding in the Meguma group, Nova Scotia, Canada. Journal of Structural Geology 23, 1631-1652.

Hoy, D., Rosenbaum, G., Wormald, R., Shaanan, U., 2014. Geology and geochronology of the Emu Creek Block (northern New South Wales, Australia) and implications for oroclinal bending in the New England Orogen. Australian Journal of Earth Sciences 61, 1109-1124.

Humphires, D., 2003. An analysis of post-Triassic faulting in southeast Queensland. Honours thesis, The University of Queensland.

Ingram, F.T., Robinson, V.A., 1996. Petroleum Prospectivity of the Clarence-Moreton Basin in New South Wales. New South Wales Department of Mineral Resources, Petroleum Bulletin 3, Sydney, 133pp.

Jenkins, R.B., Landenberger, B., Collins, W.J., 2002. Late Palaeozoic retreating and advancing subduction boundary in the New England Fold Belt, New South Wales. Australian Journal of Earth Sciences, 467-489.

Johnson, R.W., 1989. Intraplate Volcanism in Eastern Australia and New Zealand. Cambridge University Press, Cambridge.

Jorgensen, P.J., 1997. An integrated analysis of the Callide Basin, east-central Queensland. The University of Queensland, unpublished PhD thesis.

Kamp, P.J.J., 1986. The mid-Cenozoic Challenger Rift system of western New Zealand and its implications for the age of Alpine Fault inception. Geological Society of America Bulletin 97, 255-281.

Kassan, J., 1994. Basin analysis of the Triassic succession, Bowen Basin, Queensland. The University of Queensland, unpublished PhD thesis.

Keep, M., Bishop, A., Longley, I., 2000. Neogene wrench reactivation of the Barcoo sub-basin, northwest Australia: implications for Neogene tectonics of the Australian margin. Petroleum Geoscience 6, 211-220.

Keep, M., Harrowfield, M., Crowe, W., 2007. The Neogene tectonic history of the North West Shelf, Australia. Exploration Geophysics 38, 151-174.

Knesel, K.M., Cohen, B.E., Vasconcelos, P.M., Thiede, D.S., 2008. Rapid change in drift of the Australian plate records collision with Ontong Java plateau. Nature 454 754-757.

Korsch, R.J., 1981. Deformational history of the Coffs Harbour Block. Journal and Proceedings of The Royal Society of New South Wales 114, 17-22.

Korsch, R.J., Archer, R., McConachy, G.W., 1978. The Demon Fault. Journal and proceedings, Royal Society of New South Wales 111, 101-106.

Korsch, R.J., Borham, C.J., Totterdell, J.M., Shaw, R.D., Nicoll, M.G., 1998. Development and petroleum resources of the Bowen, Gunnedah and Surat Basins, Eastern Australia. The APPEA Journal 38, 199–237.

Korsch, R.J., Harrington, H.J., 1987. Oroclinal bending, fragmentation and deformation of terranes in the New England Orogen, eastern Australia. inTerrane Accretion and Orogenic Belts, Geodyn. Ser, vol. 19, edited by E. C. Leitch and E. Scheibner, pp. 129–139, AGU, Washington, D. C., doi:110.1029/GD1019p0129.

Korsch, R.J., O'Brien, P.E., Sexton, M.J., Wake-Dyster, K.D., Wells, A.T., 1989. Development of Mesozoic transtensional basins in easternmost Australia. Australian Journal of Earth Sciences 36 13-28.

Korsch, R.J., Totterdell, J.M., 2009. Subsidence history and basin phases of the Bowen, Gunnedah and Surat Basins, eastern Australia. Australian Journal of Earth Sciences 56, 335-353.

Korsch, R.J., Totterdell, J.M., Cathro, D.L., Nicoll, M.G., 2009a. Early Permian East Australian Rift System. Australian Journal of Earth Sciences 56, 381-400.

Korsch, R.J., Totterdell, J.M., Fomin, T., Nicoll, M.G., 2009b. Contractional structures and deformational events in the Bowen, Gunnedah and Surat Basins, eastern Australia. Australian Journal of Earth Sciences 56, 477-499.

Kranendonk, M.J.V., Wardle, R.J., 1997. Crustal-scale flexural slip folding during late tectonic amplification of an orogenic boundary perturbation in the Paleoproterozoic Torngat Orogen, northeastern Canada. Canadian Journal of Earth Sciences 34, 1545-1565.

Leitch, E.C., 1974. The geological development of the southern part of the New England Fold Belt. Australian Journal of Earth Sciences 21, 133-156.

Leitch, E.C., 1975. Plate Tectonic Interpretation of the Paleozoic History of the New England Fold Belt. Geological Society of America Bulletin 86, 141-144.

Leitch, E.C., 1988. The Barnard Basin and the early Permian development of the southern part of the New England Fold Belt, in: Kleeman, J.D. (Ed.), New England Orogen - Tectonics and Metallogenesis. University of New England, Armidale. 61-67.

Leitch, E.C., Fergusson, C.L., Henderson, R.A., 1992. Geological note: The intra-Devonian unconformity at Mt Gelobera, south of Rockhampton, central Queensland. . Australian Journal of Earth Sciences 39, 121-122.

Lennox, P.G., Flood, P.G., 1997. Age and structural characterisation of the Texas megafold, southern New England Orogen, eastern Australia. In: Ashley, P.M., Flood, P.G. (Eds.), Tectonics and Metallogenesis of the New England Orogen: Geological Society of Australia Special Publication, 19. 161-177.

Li, P., Rosenbaum, G., Donchak, P.J.T., 2012a. Structural evolution of the Texas Orocline, eastern Australia. Gondwana Research 29, 279-289.

Li, P., Rosenbaum, G., Rubatto, D., 2012b. Triassic asymmetric subduction rollback in the southern New England Orogen (eastern Australia): the end of the Hunter-Bowen orogeny. Australian Journal of Earth Sciences 59, 965-981.

Li, P., Rosenbaum, G., Yang, J.-H., Hoy, D., 2015. Australian-derived detrital zircons in the Permian-Triassic Gympie terrane (eastern Australia): evidence for an autochthonous origin. Tectonics, DOI: 10.1002/2015TC003829.

Lin, A., 1999. S-C cataclasite in granitic rock. Tectonophysics 304, 257-273.

Mann, P., Taira, A., 2004. Global tectonic significance of the Solomon Islands and Ontong Java Plateau convergent zone. Tectonophysics 389, 137–190.

Marrett, R.A., Allmendinger, R.W., 1990. Kinematic analysis of fault-slip data: Journal of Structural Geology, 12, 973-986.

McCaffrey, R., 1996. Slip partitioning at convergent plate boundaries of SE Asia. Geological Society London Special Publication 106, 3-18.

McElroy, C.T., 1962. The geology of the Clarence-Moreton Basin., Geological Survey of New South Wales. Memoir (Geology), 9, p1-172 + Maps.

McElroy, C.T., 1975. Nymboida Coal Field, NSW, in Traves, D. M. and King, D. (Eds.) Economic Geology of Australia and Papua New Guinea. Australasian Institute of Mining and Metallurgy, Monograph Series 2. Coal, 298-299.

McPhie, J., Fergusson, C.L., 1983. Dextral movement on the Demon Fault, northeastern New South Wales: a reassessment (Australia). Journal & Proceedings - Royal Society of New South Wales 116, 123-127.

Miller, H., G., Singh, V., 1994. Potential field tilt a new concept for location of potential field sources. Journal of Applied Geophysics 32, 213-217.

Mochales, T., Rosenbaum, G., Speranza, F., Pisarevsky, S.A., 2014. Unravelling the geometry of the New England Oroclines (eastern Australia): constraints from magnetic fabrics. Tectonics 33 11: 2261-2282.

Mond, A., Olgers, F., Flood, P.G., 1968. Geological map of Goondiwindi 1:250 000 sheet SH5601, first edition, Bureau of Mineral Resources, Geology & Geophysics, Department of National Development, Canberra, A.C.T.

Morley, C.K., 2002. Evolution of large normal faults: evidence from seismic reflection data. American Association of Petroleum Geologist Bulletin 6, 961–978.

Muller, R.D., Dyksterhuis, S., Rey, P., 2012. Australian paleo-stress fields and tectonic reactivation over the past 100 Ma. Australian Journal of Earth Sciences 59, 13-28.

Murphy, P.R., Schwarzbock, H., Cranfield, L.C., Withnall, I.W., Murray, C.G., 1976. Geology of the Gympie 1:250,000 sheet area. Geological Survey of Queensland Report no.96.

Murray, C.G., Fergusson, C.L., Flood, P.G., Whittaker, W.G., Korsch, R.J., 1987. Plate tectonics model for the Carboniferous evolution of the New England Fold Belt. Australian Journal of Earth Sciences 34, 213-236

Nabighian, M., Grauch, V., Hansen, R., LaFehr, T., Li, Y., Peirce, J., Phillips, J., Ruder, M., 2005. The historical development of the magnetic method in exploration. GEOPHYSICS 70, 33ND-61ND.

Norris, R.J., Koons, P.O., Cooper, A.F., 1990. The obliquely-convergent plate boundary in the South Island of New Zealand: implications for ancient collision zones Journal of Structural Geology 12, 715-725.

O'Brien, P.E., Korsch, R.J., Wells, A.T., Sexton, M.J., Wake- Dyster, K.D., 1994. Structure and Tectonics of the Clarence-Moreton Basin. In: Wells, A.T., O'Brien, P.E. (Eds), Geology and petroleum potential of the Clarence-Morton Basin, New South Wales and Queensland, AGSO Bulletin 241, 117-188.

Och, D.J., Offler, R., Zwingmann, H., 2014. Constraining timing of brittle deformation and fault gouge formation in the Sydney Basin. Australian Journal of Earth Sciences 61, 337-350.

Offenberg, A.C., 1971. Tamworth 1:250 000 Geological Sheet SH/56-13, 1st edition, Geological Survey of New South Wales, Sydney.

Offler, R., Foster, D.A., 2008. Timing and development of oroclines in the southern New England Orogen, New South Wales. Australian Journal of Earth Sciences 55, 331-340.

Offler, R., Williams, A., 1987. Evidence for sinistral movement on the Peel Fault System in serpentinites, Glenrock Station, N.S.W, Terrane Accretion and Orogenic Belts. AGU, Washington, DC, pp. 141-151.

Passchier, C.W., Trouw, R.A.J., 2006. Microtectonics. Springer_Verlog, second edition pp. 366.

Perritt, S., Roberts, M., 2007. Flexural-slip structures in the Bushveld Complex, South Africa? Journal of Structural Geology 29, 1422-1429.

Petit, J.P., 1987. Criteria for the sense of movement on fault surfaces in brittle rocks. journal of Structural Geology 9, 597–608.

Petterson, M.G., Babbs, T., Neal, C.R., Mahoney, J.J., Saunders, A.D., Duncan, R.A., Tolia, D., Magua, R., Qopoto, C., Mahoaa, H., Natogga, D., 1999. Geological–tectonic framework of Solomon Islands, SW Pacific: crustal accretion and growth within an intraoceanic setting. Tectonophysics, 301, 335–360.

Petterson, M.G., Neal, C.R., Mahoney, J.J., Kroenke, L.W., Saunders, A.D., Babbs, T., Duncan, R.A., Tolia, D., McGrail, B.A., 1997. Structure and deformation of north and central Malaita, Solomon Islands: tectonic implications for the Ontong Java Plateau–Solomon arc collision and for the fate of ocean plateaus. Tectonophysics, 283, 281–233.

Phillips, G., Landenberger, B., Belousova, E.A., 2011. Building the New England Batholith, eastern Australia-Linking granite petrogenesis with geodynamic setting using Hf isotopes in zircon. Lithos 122, 1-12.

Phinney, E.J., Mann, P., Coffin, M.F., Shipley, T.H., 2004. Sequence stratigraphy, structural style, and age of deformation of the Malaita accretionary prism (Solomon arc-Ontong Java Plateau convergent zone). Tecnotophysics, 389, 221–246.

Pohl, C., Van Genderen, J.L., 1998. Review article Multisensor image fusion in remote sensing: Concepts, methods and applications. International Journal of Remote Sensing 19, 823-854.

Prost, G.L., 2001. Remote sensing for geologist, 2nd edition. Taylor & Francis, New York, 374 pp.

Purdy, D.J., Cranfield, L.C., 2013. Ipswich Basin (Chapter 5.11), in: Jell, P. A. (Ed), Geology of Queensland. Geological Survey of Queensland, Brisbane, Australia, 391-396.

Purdy, D.J., Cross, A.J., 2013. Triassic volcanic rocks (Chapter 5.13.5), in: Jell, P. A. (Ed), Geology of Queensland. Geological Survey of Queensland, Brisbane, Australia, 433-444.

Quarles van Ufford, A., Cloos, M., 2005. Cenozoic tectonics of New Guinea, AAPG Bulletin, 89, 119-140.

Ramsay, J.G., Huber, M.I., 1987. The tecniques of modern structural geology, Volume 2: Folds and Fractures.

Rasmus, P.L., Rose, D.M., Rose, G., 1969. Singleton 1:250 000 Geological Sheet SI/56-01, 1st edition, Geological Survey of New South Wales, Sydney.

Raza, A., Hill, K.C., Korsch, R.J., 2009. Mid-Cretaceous uplift and denudation of the Bowen and Surat Basins, eastern Australia: relationship to Tasman Sea rifting from apatite fission-track and vitrinite-reflectance data. Australian Journal of Earth Sciences 56, 501-531.

Relph, R.E., 1963. Mid-Eastern Oil N.L. Kyogle No.1 well completion report. Bureau of Mineral Resources, Australia, File. 63/1001.

Retallack, G.J., R., R.P., Kimbrough, D.L., 1993. New radiometric ages for Triassic floras of southeast Gondwana, in Lucas, S. G., Morales, M. (Eds.) The Non-marine Triassic. New Mexico Museum Natural History Science Bulletin 3, 415-418.

Roach, A.F., 1997. Late Triassic volcansim in the Ipswich Basin. Unpublished PhD thesis, Macquarie University, Sydney.

Roberts, J., Engel, B.A., 1987. Depositional and tectonic history of the southern New England orogen. Aust. J. Earth Sci. 34, 1-20.

Rose, G., Jones, W.H., Kennedy, D.R., 1966. Newcastle 1:250 000 Geological Sheet SI/56-02, 1st edition, Geological Survey of New South Wales, Sydney.

Rosenbaum, G., 2012. The oroclines of the southern New England Orogen, eastern Australia. Episodes 35(1), 187-194

Rosenbaum, G., Li, P., Rubatto, D., 2012. The contorted New England Orogen (eastern Australia): new evidence from U-Pb geochronology of early Permian granitoids. Tectonics 31, TC1006, doi:1010.1029/2011TC002960.

Rosenbaum, G., Uysal, I.T., Babaahmadi, A., 2015. The Red Rock Fault Zone (northeast New South Wales): Kinematics, timing of deformation and relationships to the New England oroclines. Australian Journal of Earth Sciences 62, 409-423.

Sandiford, M., 2003a. Geomorphic constraints on the late Neogene tectonics of the Otway Ranges. Australian Journal of Earth Sciences 50, 69-80.

Sandiford, M., 2003b. Neotectonics of southeastern Australia: linking the Quaternary faulting record with seismicity and in situ stress. In: Hillis,R.R.& Muller, D. (eds) Evolution and Dynamics of the Australian Plate. Geological Society of Australia Special Publication of Geological Society of America 22, 101-113.

Schellart, W.P., 2007. North-eastward subduction followed by slab detachment to explain ophiolite obduction and Early Miocene volcanism in Northland, New Zealand. Terra Nova 19, 211-218.

Schellart, W.P., 2012. Comment on"Geochemistry of the Early Miocene volcanic succession of Northland, New Zealand, and implications for the evolution of subduction in the Southwest Pacific"by M.A. Booden, I.E.M. Smith, P.M. Black and J.L. Mauk. Journal of Volcanology and Geothermal Research 211-212, 112–117.

Schellart, W.P., Lister, G.S., Toy, V.G., 2006. A Late Cretaceous and Cenozoic reconstruction of the Southwest Pacific region: Tectonics controlled by subduction and slab rollback processes. Earth-Science Reviews 76 191–233.

Shaanan, U., Rosenbaum, G., Li, P., Vasconcelos, P., 2014. Structural evolution of the early Permian Nambucca Block (New England Orogen, eastern Australia) and implications for oroclinal bending. Tectonics 33, 2013TC003426.

Shaanan, U., Rosenbaum, G., Wormald, R., 2015. Provenance of the Early Permian Nambucca block (eastern Australia) and implications for the role of trench retreat in accretionary orogens. Geological Society of America Bulletin, In press.

Shaw, R.D., 1987. Final report on the 1985 seismic survey (for Claremont Petroleum NL). Geological Survey of New South Walse, seismic file SS149.

Shaw, R.D., Fawckner, J.F., Bultitude, R.J., 1987. The Palmerville fault system: A major imbricate thrust system in the Northern Tasmanides, North Queensland. Australian Journal of Earth Sciences 34, 69-93.

Shaw, S.E., 1969. Granitic rocks from northern portion of the New England Batholite, in Geology of New South Walse. Journal of Geological Society of Australia 16, 285-290.

Shaw, S.E., 1994. Late Permian-Triassic radiometric dates of granitoids and associated volcanics from the southern New England belt, in Permian-Triassic Pangean Basins and Foldbelts Along the Panthalassan Margin of Gondwanaland. edited by J. Veevers and C. M. Powell, Geological Society of America Memoir 184, 147-159.

Shaw, S.E., Flood, R.H., 1981. The New England batholith, eastern Australia: geochemical variations in time and space. Journal of Geophysical Research 86, 10530-10544.

Shaw, S.E., Flood, R.H., 2009. Zircon Hf isotopic evidence for mixing of crustal and silicic mantle-derived magmas in a zoned granite pluton, eastern Australia. Journal of Petrology 50, 47–168.

Spandler, C., Rubatto, D., Hermann, J., 2005. Late Cretaceous–Tertiary tectonics of the southwest Pacific: Insights from U–Pb sensitive, high-resolution ion microprobe (SHRIMP) dating of eclogite facies rocks from New Caledonia. Tectonics 24, TC3003. doi:10.1029/2004TC001709.

Sprigg, R.C., 1986. The Eromanga Basin in the search for commercial hydrocarbons. In: Gravestock D. I., Moore P. S. & Pitt G. M. eds., Contributions to the geology and hydrocarbon potential of the Eromanga Basin Vol. Special Publ. 12, pp. 9–24, Geolological Society of Australia, Sydney.

Struckmeyer, H.I.M., Symonds, P.A., 1997. Tectonostratigraphic evolution of the Townsville Basin, Townsville Trough, offshore northeastern Australia. Australian Journal of Earth Sciences, 44, 799-817.

Struckmeyer, H.I.M., Symonds, P.A., Fellows, M.E., Scott, D.L., 1994. Structural and stratigraphic evolution of the Townsville Basin, Townsville Trough, offshore northeastern Australia. Canberra, Australian Geological Survey Organisation, Record 1994/50.

Swain, C.J., 2000. Reduction-to-the-pole of regional magnetic data with variable field direction, and its stabilisation at low inclinations. Exploration Geophysics 31, 078-083.

Tanner, P.W.G., 1989. The flexural-slip mechanism. Journal of Structural Geology 11, 635-655.

Trompat, H., Boschetti, F., Hornby, P., 2003. Improved downward continuation of potential field data. Exploration Geophysics 34, 249–256.

Twiss, R.J., Moores, E.M., 2007. Structural Geology, 2nd edition. W. H. Freeman and Company, New York.

Vasconcelos, P.M., Knesel, K.M., Cohen, B.E., Heim, J.A., 2008. Geochronology of the Australian Cenozoic: A history of tectonic and igneous activity, weathering, erosion, and sedimentation. Australian Journal of Earth Sciences 55, 865-914.

Veevers, J.J., 2000. Change of tectono-stratigraphic regime in the Australian plate during the 99 Ma (mid-Cretaceous) and 43 ma (mid-Eocene) swerves of the Pacific. Geology, 28, 47–50.

Verduzco, B., Fairhead, J., Green, C., MacKenzie, C., 2004. New insights into magnetic derivatives for structural mapping. The Leading Edge 23, 116-119.

Walcott, R.I., 1998. Modes of oblique compression: late Cainozoic tectonics of the South Island of New Zealand. Reviews of Geophysics 36, 1-26.

Waschbusch, P., Korsch, R.J., Beaumont, C., 2009. Geodynamic modelling of aspects of the Bowen, Gunnedah, Surat and Eromanga Basins from the perspective of convergent margin processes. Australian Journal of Earth Sciences 56, 309-334.

Webb, A.W., Stevens, N.C., McDougall, I., 1967. Isotopic age determination on Tertiary volcanic rocks and intrusives of south-eastern Queensland. Proceedings of the Royal Society of Queensland 79, 79 – 92.

Webb, J.A., 2001. A new Marattialean fern from the Middle Triassic of Eastern Australia. Proceedings of the Linnean Society of New South Wales 123, 215-224.

Webb, J.A., McNaughton, N.J., 1978. Isotopic age of the Sugars Basalt. Queensland Government Mining Journal 79, 591-596.

Weissel, J.K., Watts, A.B., 1979. Tectonic Evolution of the Coral Sea Basin. Journal of Geophysical Research 84, 4572-4582.

Wellman, P., McDougall, I., 1974. Cainozoic igneous activity in eastern australia. Tectonophysics 23, 49-65.

Wells, A.T., O'Brien, P.E., 1994. Lithostratigraphic framework of the Clarence-Moreton Basin. In: Wells, A.T., O'Brien, P.E. (Eds), Geology and petroleum potential of the Clarence-Morton Basin, New South Wales and Queensland, AGSO Bulletin 241, 277-290.

Willcox, J.B., Sayers, J., 2002. Geological framework of the central Lord Howe Rise (Gower Basin) region. Geoscience Australia Record, 2002/11.

Wilson, R.G., 1975. Tarong Coalfield, Q. In Traves, D.M., & King, D. (Editors) - ECONOMIC GEOLOGY OF AUSTRALIA & PAPUA NEW GUINEA, 2. Coal. Australasian Institute of Mining & Metallurgy, Monograph 6, 288-290.

Yassaghi, A., Madanipour, S., 2008. Influence of a transverse basement fault on along-strike variations in the geometry of an inverted normal fault: Case study of the Mosha Fault, Central Alborz Range, Iran. Journal of Structural Geology 30, 1507–1519.

Zhang, Y., 2004. Understanding image fusion. Photogrammetric Engineering & Remote Sensing 70, 657-661.

Ziegler, P., Cloetingh, S., Van Wees, J.D., 1995. Dynamics of intra-plate compressional deformation: the Alpine foreland and other examples. Tecnotophysics 252, 7-59.